



Durham E-Theses

The contemporary distribution of benthic foraminifera in the Pearl River estuary, southeast China, and their use in reconstructing mid to lateHolocene fluvial flux

GARRETT, EDMUND

How to cite:

GARRETT, EDMUND (2010) *The contemporary distribution of benthic foraminifera in the Pearl River estuary, southeast China, and their use in reconstructing mid to lateHolocene fluvial flux*, Durham theses, Durham University. Available at Durham E-Theses Online: <http://etheses.dur.ac.uk/372/>

Use policy

The full-text may be used and/or reproduced, and given to third parties in any format or medium, without prior permission or charge, for personal research or study, educational, or not-for-profit purposes provided that:

- a full bibliographic reference is made to the original source
- a [link](#) is made to the metadata record in Durham E-Theses
- the full-text is not changed in any way

The full-text must not be sold in any format or medium without the formal permission of the copyright holders.

Please consult the [full Durham E-Theses policy](#) for further details.

Academic Support Office, Durham University, University Office, Old Elvet, Durham DH1 3HP
e-mail: e-theses.admin@dur.ac.uk Tel: +44 0191 334 6107
<http://etheses.dur.ac.uk>

**The contemporary distribution of benthic
foraminifera in the Pearl River estuary, southeast
China, and their use in reconstructing mid- to
late-Holocene fluvial flux**

Ed Garrett

Thesis submitted for the degree of Master of Science (by Research)

Department of Geography

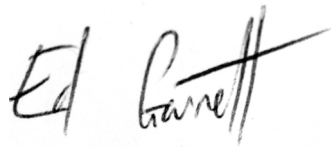
University of Durham

June 2010

Declaration of Copyright

I confirm that no part of the material presented in this thesis has previously been submitted by me or any other person for a degree in this or any other university. In all cases, where it is relevant, material from the work of others has been acknowledged.

The copyright of this thesis rests with the author. No quotation from it should be published without prior written consent and information derived from it should be acknowledged.

A handwritten signature in black ink that reads "Ed Garrett". The signature is written in a cursive style with a long horizontal stroke extending from the end of the name.

Ed Garrett

Department of Geography
University of Durham
June 2010

Abstract

This thesis investigates the contemporary distribution of benthic foraminifera in the Pearl River estuary, southeast China, and establishes a new proxy record of estuarine salinity and fluvial flux over the mid- to late-Holocene. Seventy-six samples from the contemporary estuary yielded 118 benthic taxa. *Ammonia beccarii* dominates a large proportion of the estuary, with contributions from a number of other calcareous taxa, including *Haynesina sp.*, *Elphidium spp.*, *Quinqueloculina spp.* and *Rotalinoides annectens*, and agglutinated taxa, for example *Haplophragmoides sp.* and *Ammobaculites formosensis*. Species distribution maps, cluster analysis and unconstrained ordination suggest a link between foraminiferal assemblages and the magnitude of fluvial influence. Constrained ordination links the faunal data to recognised environmental gradients and highlights salinity as the most important factor in controlling species distributions. Transfer function development enables quantitative estimates of palaeosalinity to be obtained from fossil faunal data.

A radiocarbon dated mid- to late-Holocene sediment core from the same estuary yielded 102 benthic taxa, 83 % of which were also found in contemporary samples. *Ammonia beccarii* and *Quinqueloculina akneriana* dominate fossil assemblages. In light of relative stability in mid- to late-Holocene sea level along the South China coast (Zong, 2004), the long-term increase in taxa indicative of high salinity environments is primarily interpreted in terms of declining fluvial flux. The trends in quantitative palaeosalinity reconstructions are in agreement with qualitative interpretations, however absolute salinity values are subject to large error terms. The inferred decline in fluvial flux is in accord with bulk organic carbon isotope and diatom data from the same core (Zong *et al.*, submitted a; Yu, 2009) and with records of weakening precipitation intensity derived from terrestrial proxies (e.g. An *et al.*, 2000; Y. Wang *et al.*, 2005; Hu *et al.*, 2008). Millennial-scale variability in the East Asian monsoon, linked to precession and obliquity cycles of solar insolation, is the hypothesised cause of these trends. A number of abrupt low discharge events, postulated to reflect northern hemisphere teleconnections, punctuate the Pearl River estuary record.

Contents

Title page		
Declaration of copyright		i
Abstract		ii
Table of contents		iii
List of figures		v
List of tables		x
List of appendices		xii
Acknowledgements		xiii
1. Introduction		1
1.1	Introduction	1
1.2	Research design	2
1.3	Thesis outline	4
2. Context of the research		6
2.1	Dynamics of the contemporary East Asian monsoon	6
2.2	The evolution of the Holocene East Asian monsoon	8
2.3	Reconstructing palaeoenvironments using benthic foraminifera	12
2.4	Chapter summary	16
3. Location: the Pearl River drainage basin and estuary		18
3.1	The Pearl River drainage basin	18
3.2	The Pearl River estuary	20
3.3	Evolution of the Pearl River estuary	25
3.4	Suitability of the Pearl River estuary for palaeodischarge reconstruction	31
4. Methodology		32
4.1	Contemporary surface sample recovery	32
4.2	Core recovery	33
4.3	Procedures for obtaining faunal data	33
4.4	Environmental data	37
5. The contemporary distribution of foraminifera in the Pearl River estuary: results and interpretation		39
5.1	Analysis of contemporary benthic foraminifera	39
5.2	Factors affecting the distribution of contemporary foraminifera	51
5.3	Transfer function development	62
5.4	Chapter summary	67
6. Fossil foraminifera from core UV1: results and palaeoenvironmental interpretation		68
6.1	Lithology of core UV1	68
6.2	Core chronology	70
6.3	Analysis of fossil benthic foraminifera	73
6.4	Quantitative reconstructions of palaeosalinity	82

6.5	Ecological interpretation of faunal data and quantitative palaeosalinity reconstructions	87
6.6	Spectral analysis to investigate cyclicity in foraminiferal time series	92
6.7	Chapter summary	96
7.	Evolution of the Pearl River estuary and the East Asian monsoon: discussion and conclusions	97
7.1	Evolution of the Pearl River estuary	97
7.2	The UV1 record and mechanisms responsible for East Asian monsoon variability	102
7.3	Conclusions	108
	Appendices	111
	Plates	127
	References	132

List of Figures

Chapter 2. Context of the research	Page
Figure 2.1: Maps showing the (a) winter and (b) summer monsoon regimes over East Asia with mean sea-level pressure in January and July respectively (after Xiao and An, 1999). Dominant wind direction and the limits of the contemporary East Asian summer monsoon are also given.	7
Figure 2.2: Location of sites mentioned in text. (A) Wulungu Lake, northwest China (Liu <i>et al.</i> , 2008); (B) Hani bog (Hong <i>et al.</i> , 2005); (C) Yellow Sea (Xiang <i>et al.</i> , 2008); (D) Hulu Cave (Wang <i>et al.</i> , 2001); (E) Hongyang peat research site, eastern Tibetan Plateau (Hong <i>et al.</i> , 2005); (F) Heshang Cave (Hu <i>et al.</i> , 2008); (G) Qixing Cave (Cai <i>et al.</i> , 2001); (H) Dongge Cave (Dykoski <i>et al.</i> , 2005; Y. Wang <i>et al.</i> , 2005); (I) Xiangshui Cave (Zhang <i>et al.</i> , 2004); (J) Toushe Basin, Taiwan (Liew <i>et al.</i> , 2006); (K) Pearl River estuary (Zong <i>et al.</i> , 2006; 2009a; 2009b; submitted a; submitted b; this study); (L) Huguang Maar (Yancheva <i>et al.</i> , 2007); (M) Northern South China Sea (Jian <i>et al.</i> , 1999; Wang <i>et al.</i> , 1999a; 1999b); Inner Mongolian Plateau (Zhang <i>et al.</i> , 1998; Jiang <i>et al.</i> , 2006); Loess Plateau (An <i>et al.</i> , 2000; Maher and Hu, 2006); North China Plain (Cui <i>et al.</i> , 2009).	9
Chapter 3. Location: the Pearl River drainage basin and estuary	
Figure 3.1: Location of the Pearl River drainage basin, southeast China	19
Figure 3.2: The Pearl River estuary, including the three major river branches, the eight distributaries/gates and the Lingdingyang, Modaomen and Huangmohai estuarine bays.	20
Figure 3.3: Faulting in the Pearl River estuary and surrounding area (after Huang, 2000 and references therein).	21
Figure 3.4: Salinity distribution in the Pearl River estuary (a) January 2000 surface water; (b) January 2000 bottom water; (c) July 1999 surface water and (d) July 1999 bottom water (after Dong <i>et al.</i> , 2004).	24
Figure 3.5: Distribution of incised valleys beneath the Pearl River delta with locations of cores mentioned in text (modified from Li <i>et al.</i> , 2006). TOB: Tai O Bay (Bahr <i>et al.</i> , 2005); BWB: Big Wave Bay (Davis <i>et al.</i> , 2000); JT81, ZK83, PK13 (Zong <i>et al.</i> , 2009a); UV1 (Zong <i>et al.</i> , 2009a; this study); V37 (Bahr <i>et al.</i> , 2005; Zong <i>et al.</i> , 2009a); WB7 (Yim, 1994).	27
Figure 3.6: Relative sea-level reconstruction for the Pearl River delta (Zong, 2004)	28
Figure 3.7: The relationship between cumulative sediment load and cumulative fluvial discharge in the Pearl River (excluding the delta area) between 1957 and 2004 (S. Zhang <i>et al.</i> , 2008).	29

Chapter 4. Methodology

Figure 4.1: Location of Pearl River estuary surface samples and core UV1. Samples represented by circles, coloured according to primary source. 33

Figure 4.2: 95 % confidence intervals for species proportions assessed using the binomial distribution (Fatela and Taborda, 2002) for total counts of 50, 100 and 300. 35

Chapter 5. The contemporary distribution of foraminifera in the Pearl River estuary: results and interpretation

Figure 5.1: Pearl River estuary surface sample foraminiferal assemblages. Dominant and common taxa (>10 %) only. Order and clusters according to stratigraphically unconstrained CONISS. 41

Figure 5.2: Scatter plot of sample scores on the first two axes following Correspondence Analysis of an ideal dataset (for each successive sample a previously occurring taxon is no longer present and a new taxon is introduced), showing the arch effect and compression of distances between samples at the extremes of the gradient (after Birks, 1995). 44

Figure 5.3: Detrended Correspondence Analysis sample scores for contemporary samples on (a) axes 1 and 2 and (b) axes 1 and 3. Samples are coloured according to clusters inferred from CONISS. 45

Figure 5.4: Contemporary clusters inferred from results of stratigraphically unconstrained CONISS and Detrended Correspondence Analysis (NI: Neilingding Island; QI: Qi'ao Island; Hu: Humen gate; Ji: Jiaomen gate; Ho: Hongqimen gate). 46

Figure 5.5: Distribution of contemporary sample N_2 scores. 47

Figure 5.6: Maps showing the relative abundance of dominant taxa in contemporary samples: (a) *Ammobaculites formosensis*; (b) *Ammotium salsum*; (c) *Haplophragmoides* sp.; (d) *Ammonia beccarii*; (e) *Haynesina* sp.; (f) *Quinqueloculina akneriana* and (g) *Rotalinoides annectens*. Note: scales vary between graphs to allow better visualisation of data. 48

Figure 5.7: Box plots (minimum, Q_1 , median, Q_3 and maximum values) of (a) mean salinity and (b) depth data for clusters A to E. 52

Figure 5.8: Distribution of environmental variables: (a) mean salinity; (b) depth; (c) total organic carbon; (d) total nitrogen; (e) $\delta^{13}C$; (f) sand; (g) clay; (h) silt. Note: in $\delta^{13}C$ plot, sample PE 60 ($\delta^{13}C = -27\text{‰}$) is not plotted to allow variability in the dataset to be better visualised. 54

Figure 5.9: Pie charts showing the total variation in the contemporary fauna divided into (a) explained and unexplained sectors and (b) the total explained variance divided into sectors representing the individual environmental variables and interactions between variables. 55

Figure 5.10: Relationship between environmental variables analysed using CCA.	56
Figure 5.11: Biplot of Canonical Correspondence Analysis sample scores and the minimum adequate model of environmental variables. Samples are represented by circles coloured according to clusters defined in section 5.1.	58
Figure 5.12: Biplot of Canonical Correspondence Analysis species scores and environmental vectors on axes 1 and 2. See appendix 5.4 for species codes.	59
Figure 5.13: Bootstrapped salinity optima and tolerances of Pearl River estuary foraminifera from Weighted Averaging in C2 (Juggins, 2003). Main diagram shows dominant and common taxa, inset shows full dataset.	61
Figure 5.14 Bootstrapped depth optima and tolerances of Pearl River estuary foraminifera from Weighted Averaging in C2 (Juggins, 2003). Main diagram shows dominant and common taxa, inset shows full dataset.	62
Figure 5.15: Performance of Weighted Averaging - Partial Least Squares component 2 using the reduced modern training set. (a) Observed vs. estimated mean salinity (b) Observed vs. residual (predicted - observed) mean salinity with LOWESS of span 0.45.	66
Figure 5.16: Weighted Averaging – Partial Least Squares residuals plotted against predicted mean salinity (psu) for the reduced dataset, with LOWESS of span 0.45.	66
 Chapter 6. Fossil foraminifera from core UV1: results and palaeoenvironmental interpretation	
Figure 6.1: Sediment description and particle size data (sand, clay and silt fractions) for the M1 unit of core UV1 (after Yu, 2009).	69
Figure 6.2: Comparison of age models based on (a) linear regression, (b) two linear regressions (after Yu, 2009) and (c) second degree polynomial regression.	72
Figure 6.3: Foraminiferal assemblages and environmental variables (Yu, 2009) from core UV1. Dominant, common and accessory taxa (>5%) only. N ₂ measures species diversity (Hill, 1973). Note: <i>Bolivina</i> spp. and <i>Lagena</i> spp. have been classified to species level, but are presented by genus in this figure. $\delta^{13}\text{C}$ values from 1.01 m ($\delta^{13}\text{C} = -18.5 \text{‰}$) and 1.05 m ($\delta^{13}\text{C} = -22.2 \text{‰}$) removed to allow better visualization of trends. Radiocarbon dates quoted as calibrated years before present $\pm 2\sigma$ (Yu, 2009). Dendrogram produced using stratigraphically constrained CONISS (Grimm, 1987).	75
Figure 6.4: Partial Canonical Correspondence Analysis sample scores (black: surface samples; red: fossil samples) rotated in the ordination space defined by the relationship between contemporary assemblages and mean salinity.	79
Figure 6.5: Fossil partial Canonical Correspondence Analysis sample scores on axis 1 after rotation in the ordination space defined by the relationship between contemporary assemblages and mean salinity, plotted against modelled age. Foraminiferal assemblage zones (following constrained clustering in figure 6.3) are also included.	80

Figure 6.6: Pie charts showing the total variation in the fossil dataset divided into (a) explained and unexplained sectors and (b) sectors representing the individual environmental variables and interactions between variables contributing to the total explained variance.	81
Figure 6.7: Biplot of Canonical Correspondence Analysis sample scores and environmental variables for core UV1.	82
Figure 6.8: Calibration of fossil assemblage data using WA-PLS component 2. Bootstrapped estimates of mean salinity within range of radiocarbon dates indicated by black line; sample specific errors of prediction indicated by grey lines.	83
Figure 6.9: Minimum dissimilarity coefficients from the Modern Analogue Technique and analogue statistics for each fossil sample from core UV1. Analogue statistic 1: percentage of the fossil assemblage represented by taxa not found in the training set; analogue statistic 2: percentage of the fossil assemblage that consists of taxa poorly represented by taxa exhibiting (a) <5 % occurrences and (b) <10 % occurrences in the modern training set. Grey box indicates region of greatest dissimilarity between fossil samples and modern training set.	86
Figure 6.10: Canonical Correspondence Analysis sample scores for surface samples (black circles) and core samples (red circles) rotated in the ordination space defined by the surface samples.	87
Figure 6.11: Detrending of (a) transfer function calibration results; (b) Canonical Correspondence Analysis axis 1 sample scores; (c) <i>Ammonia beccarii</i> percentages and (d) the proportion of taxa with contemporary optima exceeding 30 psu. Black line: original data; red line: detrended data with samples above 1.33 m removed. Note: x-axes of (b) and (c) are reversed with respect to figures 6.5 and 6.3 to facilitate comparison of records.	93
Figure 6.12: Periodograms showing results of spectral analysis of (a) detrended transfer function calibration palaeosalinity estimates, (b) detrended partial Canonical Correspondence Analysis sample scores, (c) detrended <i>Ammonia beccarii</i> proportions and (d) detrended high salinity taxa proportions.	94
Figure 6.13: Periodogram showing results of spectral analysis of sand percentages.	95
Figure 6.14: Comparison of spectral analysis derived periodicities in <i>faunal abundances</i> and particle size data. Black line: 830 year <i>Ammonia beccarii</i> percentage sinusoid; red line: 1606 year sand percentage sinusoid.	95

Chapter 7. Evolution of the Pearl River estuary and the East Asian monsoon: discussion

Figure 7.1: Palaeoshoreline of the Pearl River estuary at 6800 cal. years BP (after Zong <i>et al.</i> , 2009a). The positions of the contemporary shoreline and core UV1 are indicated.	98
--	----

Figure 7.2: Compilation of proxy records from core UV1: (a) foraminiferal transfer function calibration palaeosalinity estimates; (b) partial Canonical Correspondence Analysis of foraminiferal data; (c) proportion of *Ammonia beccarii*; (d) proportion of high salinity taxa; (e) bulk organic carbon isotopes (Yu, 2009) and (f) diatom transfer function calibration palaeosalinity estimates (Zong *et al.*, submitted a). Note: $\delta^{13}\text{C}$ and diatom data (Yu, 2009; Zong *et al.*, submitted a) have been replotted using the age model developed in Chapter 6. 101

Figure 7.3: Comparison of (a) Pearl River estuary foraminiferal transfer function calibration palaeosalinity estimates; (b) partial Canonical Correspondence Analysis of foraminiferal data; (c) Dongge cave stable oxygen isotope record (Y. Wang *et al.*, 2005); (d) coeval differences in $\delta^{18}\text{O}$ between Heshang and Dongge Caves, calibrated to annual precipitation (Hu *et al.*, 2008); (e) South China Sea surface salinity estimates (Wang *et al.*, 1999b); (f) modelled June insolation at 30°N (Berger and Loutre, 1991). 103

Figure 7.4: 830 year sinusoid fitted to detrended *Ammonia beccarii* proportions. Grey shading indicates low discharge events inferred from UV1 proxy data (figure 7.2). 105

Figure 7.5: Concurrence of abrupt dry events in (a) Pearl River estuary foraminiferal transfer function calibration palaeosalinity estimates; (b) partial Canonical Correspondence Analysis of foraminiferal data and (c) the Dongge cave stable oxygen isotope record (Y. Wang *et al.*, 2005), along with (d) peaks in drift ice tracers in the North Atlantic (Bond *et al.*, 2001). Bond events 0 to 4 are indicated in grey, with a further weak monsoon event correlated with a drift ice proxy peak indicated in blue. 107

List of Tables

Chapter 2. Context of the research	Page
Table 2.1: Summary of species contributing to assemblages defined by past investigations into the benthic foraminifera of the Pearl River estuary and adjacent inner shelf. Note: The investigations of Li (1988) are only concerned with agglutinated species.	15
Chapter 3. Location: the Pearl River drainage basin and estuary	
Table 3.1: Wet season, dry season and total annual average discharge data for the four Lingdingyang/Pearl River estuary (PRE) gates (Cai <i>et al.</i> , 2004). As noted by Harrison <i>et al.</i> (2008), Chinese literature provides estimates approximately 10% higher (for example see table 2 in Zhou <i>et al.</i> , 2006)).	22
Table 3.2: Classification of Quaternary sediments in Hong Kong (after Yim, 1994; 1999).	26
Chapter 4. Methodology	
Table 4.1: Source of salinity data for Pearl River estuary surface samples.	38
Chapter 5. The contemporary distribution of foraminifera in the Pearl River estuary: results and interpretation	
Table 5.1: Descriptive statistics for contemporary Pearl River estuary foraminifera.	40
Table 5.2: Summary of the characteristic taxa of clusters defined by CONISS.	42
Table 5.3: Average environmental variables for surface sample clusters. Note: missing total organic carbon data affects TOC and C/N averages for clusters A (6/23 samples), C (3/26 samples) and E (4/12 samples). Missing $\delta^{13}\text{C}$ data affects averages for clusters A (6/23 samples), B (1/6 samples) C (3/26 samples) and E (4/12 samples).	51
Table 5.4: Results of partial Canonical Correspondence Analysis (following square root transformation of species data). λ_1 : eigenvalue of axis 1; λ_1/λ_2 : ratio of eigenvalues for axes 1 and 2.	56
Table 5.5: Canonical Correspondence Analysis correlation matrix for environmental variables and the first two extracted CCA axes.	57

Table 5.6: Comparison of transfer function components using the modern training set consisting of all samples with total counts >100, except samples PE 66 and 67. Abbreviations: WA = Weighted Averaging; WATOL = Weighted Averaging with tolerance downweighted; Inv = Inverse deshrinking; Cla = Classical deshrinking; WA-PLS = Weighted Averaging - Partial Least Squares; C = Component. 65

Chapter 6. Fossil foraminifera from core UV1: results and palaeoenvironmental interpretation

Table 6.1: Radiocarbon and optically stimulated luminescence dates obtained for core UV1 (Yu, 2009; Zong *et al.*, 2009a). Calibration of radiocarbon dates was undertaken using CALIB 5.10 (Stuiver *et al.*, 2005) and the marine04 correction (Hughen *et al.*, 2004) with a marine reservoir correction of -128 ± 40 years (Yu, 2009). 70

Table 6.2: Contemporary Pearl River estuary foraminiferal data set descriptive statistics. 74

Table 6.3: Summary of the characteristic taxa of foraminiferal assemblage zones defined by CONISS. Boundaries between zones are stated as the mean depth of the two adjacent samples. 77

Table 6.4: Results of partial Canonical Correspondence Analysis (following square root transformation of species data) and Monte Carlo permutation tests on the fossil dataset (999 permutations). λ_1 : eigenvalue of axis 1; λ_1 / λ_2 : ratio of eigenvalues for axes 1 and 2. 81

Chapter 7: The evolution of the Pearl River estuary and the East Asian monsoon: discussion and conclusions

Table 7.1: Summary of periods characterised by decreased summer monsoon intensity inferred from Chinese proxy records. 104

List of Appendices

Appendices associated with Chapter 5:	Page
5.1: Summary statistics for dominant and common benthic foraminiferal taxa in contemporary surface samples	111
5.2: Relative abundances of contemporary Pearl River estuary foraminifera, ordered by CONISS cluster	112
5.3: Summary surface samples environmental data, grouped by CONISS clusters	118
5.4: Species codes used in Canonical Correspondence Analysis species – environment biplots	120
5.5: Derivation and performance of alternative modern training sets	121
 Appendices associated with Chapter 6:	
6.1: Summary statistics for dominant and common benthic foraminiferal taxa in samples from core UV1	121
6.2: Relative abundance of fossil benthic foraminifera from core UV1	122

Acknowledgements

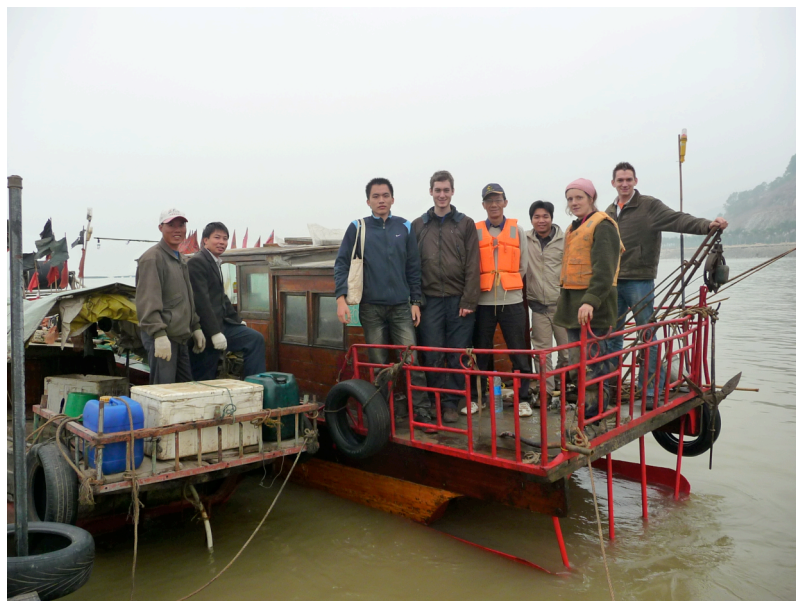
Thanks must first go to Dr Jerry Lloyd and Dr Jamie Casford for their help and advice. Dr Cheng Zong was initially responsible for prompting my interest in the project and provided invaluable assistance in the field. Dave McCarthy, Chris Brodie and others provided thought-provoking conversations throughout the year.

Fieldwork in the Pearl River estuary in March 2009 was undertaken in association with Dave Strong and Dr Rachel Flecker of Bristol University, who provided new insights into the project and were kindly sympathetic to my seasickness! Professor Zheng Zhuo's help in hiring the boat, loaning equipment and providing an opportunity to present initial findings at Sun Yat-sen University was much appreciated. Professor Gordon Huang and Professor Zheng's students, particularly Li Jie, were exceptionally welcoming.

Fieldwork was supported by the Royal Geographical Society (with the Institute of British Geographers) with a Geographical Club Award. Thanks must go to Dr Catherine Souch, Richard Byrne, Michael Palin and the Geographical Club for the award and for making me feel so welcome at the RGS. Presentation of initial results at the QRA International Postgraduate Symposium was possible thanks to the Department of Geography Conference Fund.

The knowledgeable advice of the laboratory staff, in particular Frank Davies, Amanda Hayton, Neil Tunstall and Kathryn Melvin, in the Department of Geography, Durham University, helped immensely. Helen Riggs from Materials Chemistry provided access to the scanning electron microscope.

Finally I must thank Caroline and my family for all the support they have provided throughout the year.



The author, Dr Cheng Zong, Dr Rachel Flecker, Dave Strong, Professor Zheng's students, boat captain and crew on the Pearl River estuary, March 2009.

1. Introduction

1.1 Introduction

East Asian fluvial discharge is closely linked with the intensity of monsoon precipitation (S. Zhang *et al.*, 2008). Perturbations in the intensity, extent and timing of the seasonal advance and retreat of rain-bearing fronts across East Asia are recorded on a range of timescales, from interannual to tectonic (Huang *et al.*, 2003; P. Wang *et al.*, 2005; Wang, 2009). Variability in precipitation can result in periods of severe drought or flood, influencing the lives of the several billion people who live in monsoon Asia (Webster *et al.*, 1998; Ding, 2004). The suggestion of changes in monsoon intensity as a causal factor in the collapse of the Tang, Qin and Shang dynasties (Shi *et al.*, 1994; Yancheva *et al.*, 2007; P. Zhang *et al.*, 2008) highlights the importance of climatic variability to civilization in China. Monsoon driven rainfall and fluvial discharge continues to be important to the prosperity of the region, with prediction of future hydrological trends crucial to agriculture and the management and mitigation of the effects of droughts and floods (Webster, 2006). Consequently, attempts have been made to forecast monsoon intensity on interannual to decadal and centennial timescales (Webster *et al.*, 1998; Lee *et al.*, 2008). While instrumental data provide high-resolution records of interannual changes in the East Asian monsoon, palaeoenvironmental reconstruction using sedimentological,

geochemical and microfossil proxies allows appreciation of changes on longer timescales. Numerous proxies have been proposed to investigate changes in palaeoprecipitation on geological to sub-orbital timescales. Quaternary precipitation records have been developed from the alternating palaeosols and windblown sediments found on the Loess Plateau in northern central China (e.g. An and Xiao, 1990; An *et al.*, 1991; 2000; Ding *et al.*, 1992; Porter and An, 1995; Porter, 2001; Maher and Hu, 2006), stable oxygen isotopes from speleothems (e.g. Wang *et al.*, 2001; Yuan *et al.*, 2004; Dykoski *et al.*, 2005; Y. Wang *et al.*, 2005; Wang *et al.*, 2008), lake cores (e.g. Mingram *et al.*, 2004; Yancheva *et al.*, 2007; Cui *et al.*, 2009) and organic carbon isotopes from plant cellulose (Hong *et al.*, 2001; 2005). The reconstruction of fluvial discharge (e.g. Wang *et al.*, 1999a; 1999b; Xiang *et al.*, 2008) provides further information on past hydrological regimes and is essential in the constraint of boundary conditions of climate models (e.g. Lunt *et al.*, 2008; Strong, in prep.).

Work in the Pearl River estuary, southeastern China, by Yongqiang Zong and colleagues has highlighted the potential for the derivation of new proxy records of Holocene fluvial flux (Zong *et al.*, 2006; submitted a; Yu, 2009). The estuary is highly sensitive to changes in monsoon driven river discharge due to the location of the Pearl River drainage basin in monsoon-dominated southern China. Microfossil and geochemical records are hypothesised to reflect the magnitude of discharge of freshwater into the estuary, in turn providing information on the intensity of precipitation in the drainage basin. Adding to previous work on diatom flora, bulk organic carbon isotopes and selected elements (Zong *et al.*, 2006; submitted a; submitted b; Yu, 2009), this research investigates the potential for benthic foraminifera to provide a further proxy record of changes in Holocene estuarine salinity, influenced at least in part by changes in fluvial discharge.

1.2 Research design

1.2.1 Project rationale

The distribution of contemporary benthic foraminiferal assemblages in the Pearl River estuary is influenced by a range of environmental variables, however spatial variations in bottom water salinity are hypothesised to provide the dominant control. Consequently, changes in faunal assemblages over time are hypothesised to be indicative of temporal changes in salinity. Estuarine salinity is controlled by three primary forcing mechanisms: fluvial flux, sea-level change and shoreline progradation (Zong *et al.*, 2009a). Extraction of a signal of fluvial flux from reconstructions of past

salinity allows inferences to be made on the intensity of precipitation falling in the Pearl River drainage basin.

The link between foraminifera and salinity is well documented (Murray, 1991; 2001; Wang *et al.*, 1992) but must, nevertheless, be tested for the Pearl River estuary. As long-term monitoring of foraminiferal populations and corresponding measurements of changes in salinity are beyond the practical limits of this project, spatial changes in fauna and salinity in contemporary surface samples from a range of locations in the estuary are used as surrogate measurements. Additionally, the influence of a number of supplementary environmental variables on foraminiferal distributions is investigated to assess the importance of other confounding variables. The establishment and quantification of the link between contemporary assemblages and salinity in a modern training set facilitates qualitative and quantitative reconstructions of changes over time, given adequate fossil assemblage data.

Relating reconstructed palaeosalinity to changes in fluvial flux and precipitation over the mid- to late-Holocene requires the a priori knowledge of relative stability in sea level over the same period. This is afforded by well-constrained reconstructions of sea level along the southern Chinese coast (Zong, 2004). The influence of shoreline progradation on the palaeosalinity signal must also be assessed, along with the relationship between fluvial flux and palaeoprecipitation.

1.2.2 Research aims and objectives

The main aims of this research are twofold:

1. Develop benthic foraminifera as a salinity proxy. To achieve this, the contemporary distribution must be assessed and analysed with respect to salinity and a range of other environmental parameters. Quantification of the relationship between assemblage distribution and salinity facilitates their use in palaeoenvironmental reconstruction.
2. Apply the established relationship between foraminifera and salinity to reconstruct palaeosalinity from a mid- to late-Holocene sediment core from the Pearl River estuary.

A number of research objectives are set out to assist in the development of this research. The first three relate to the analysis of contemporary distributions and development of the proxy:

1. Investigate the contemporary distribution of benthic foraminifera in the Pearl River estuary using a modern training set consisting of a large number of surface samples.
2. Analyse the factors controlling the contemporary distribution of estuarine foraminifera. This requires the collection of salinity measurements and other environmental data for each sample in the modern training set.
3. Express the faunal data as a function of the environmental data, allowing quantitative palaeoenvironmental reconstructions.

Once the contemporary faunal distributions have been established and explained, further research objectives apply the knowledge gained to the reconstruction of palaeoenvironmental change:

4. Investigate the benthic foraminiferal assemblages from a Holocene sediment core from the Pearl River estuary.
5. Apply the relationship established between contemporary foraminifera and their environment to the fossil assemblages from the Holocene core to provide quantitative reconstructions of past environmental change.
6. Assess the reliability of quantitative reconstructions of palaeosalinity.
7. Compare the record of palaeosalinity with published records of mid- to late-Holocene East Asian monsoon intensity. This will assist in exploration of the potential mechanisms driving changing monsoon intensity during the mid- to late-Holocene.

1.3 Thesis outline

The following chapters present the context, methodology, results and discussion of the research outlined above. Chapter 2 outlines the climatology of the contemporary East Asian monsoon and reviews literature concerning the reconstruction of palaeomonsoon intensity during the mid- to late-Holocene. The use of benthic foraminifera as indicators of environmental change is also discussed, along with a review of published literature detailing past investigations of foraminiferal assemblages in southeastern China. Chapter 3 provides an overview on the physical environment of the Pearl River estuary. An summary of the geology, climate and morphology of the drainage basin and estuary is presented, followed by discussion of the Holocene evolution of the study area. Chapter 4

introduces the field and laboratory methodology used to obtain the modern training set of samples and environmental data and the fossil core. The process used to obtain faunal assemblage data is also described. Chapters 5 and 6 present the results and analysis of the modern training set and fossil core respectively. Chapter 7 discusses the assemblages from the Holocene core in the context of estuarine evolution, before making comparisons with other proxy records of East Asian monsoon intensity.

2. Context of the research

This chapter introduces the climatology of the contemporary East Asian monsoon before reviewing literature on the evolution of the monsoon over the Holocene, highlighting the major trends and discrepancies between histories inferred from different proxies. Outstanding issues with the use of particular proxies are discussed. The development of a high-resolution record from an estuarine location provides a partial solution to these concerns and benthic foraminifera are introduced as palaeoenvironmental proxies. Previous investigations into the benthic foraminifera of the Pearl River estuary are summarised and the chapter concludes with a brief mention of specific taxonomical issues encountered in the analysis of foraminifera in this location.

2.1 Dynamics of the contemporary East Asian monsoon

Debate is ongoing over the concept of 'the monsoon' (Clift and Plumb, 2008; Berger, 2009). The traditional view suggests the Asian monsoon, subdivided into the Indian or southwest monsoon and the East Asian monsoon, is essentially a large scale land-sea breeze responding to the seasonal reversal of pressure gradients caused by differential heat

capacities of land and sea (Ramage, 1971; Tao and Chen, 1987). During the northern hemisphere winter, cooling of the Asian landmass relative to the adjacent marginal seas and tropical western Pacific results in the formation of a high pressure cell over Siberia and the Tibetan Plateau and low pressure over the western Pacific. Air masses consequently move south and eastwards, forming the cold, dry, dust-laden winter monsoon (figure 2.1a). The higher heat capacity of water results in differential heating of the air overlying land and water in summer, reversing the pressure gradient. Moisture laden air moves onshore from a high-pressure cell located over the Western Pacific Warm Pool around Indonesia and New Guinea, providing seasonal rainfall and increased fluvial discharge in the Philippines, Indochina, China, Korea and Japan (figure 2.1b).

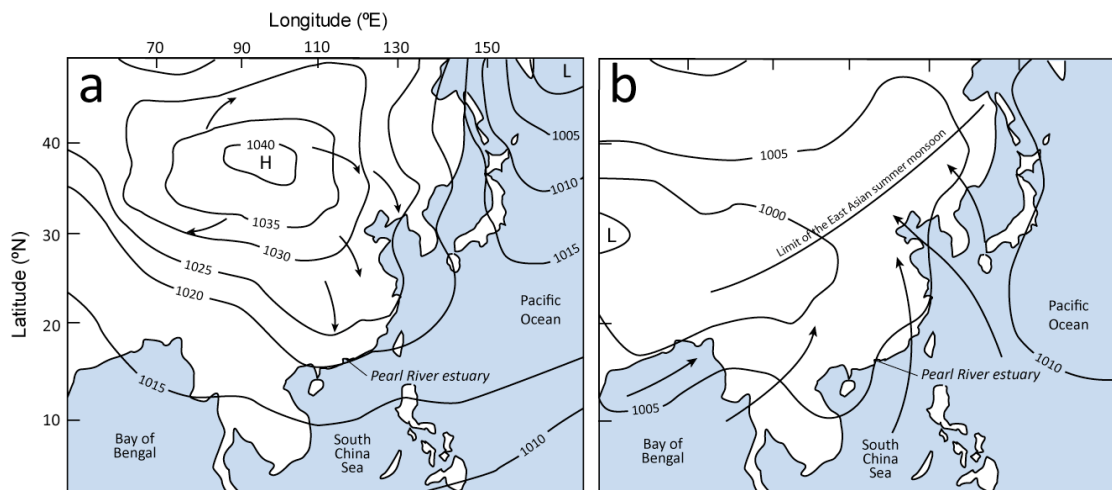


Figure 2.1: Maps showing the (a) winter and (b) summer monsoon regimes over East Asia with mean sea-level pressure in January and July respectively (after Xiao and An, 1999). Dominant wind direction and the limits of the contemporary East Asian summer monsoon are also given.

Trenberth *et al.* (2000), Chao and Chen (2001) and Wang (2009) provide an alternative view, suggesting the 'global monsoon' reflects the seasonal migration of the Intertropical Convergence Zone (ITCZ). Variation in the location of atmospheric overturning allows the expansion of regions of intense precipitation from the tropics towards the summer hemisphere. Within this framework the East Asian monsoon can be divided into two linked zones: the region of the western Pacific under the direct influence of shifts in the position of the ITCZ, analogous with the Western North Pacific monsoon (e.g. Wang *et al.*, 2003), and the subtropical monsoon front, located further north (Wang, 2009).

Whether seasonal variations in precipitation and, consequently, fluvial discharge are seen to result from the migration of the ITCZ, the differential heating of land and sea or a combination of the two, it is the advance and retreat of the subtropical monsoon front, known as the *Meiyu* in China, *Baiu* in Japan and *Changma* in Korea, that is specifically responsible for the extent and intensity of precipitation in China (Qian *et al.*, 2002; Dodson *et al.*, 2004). Approximately 80 % of annual rainfall in the monsoon region falls during the summer months (Zhang *et al.*, 2009). The published literature generally uses the term 'monsoon intensity' as synonymous with precipitation intensity; however, the significant interannual variability in the timing and extent of incursion of the monsoon front creates great spatial variation in the intensity of precipitation (Li *et al.*, 2002). The Philippines, the Indochinese Peninsula and southern China may experience less intense precipitation and decreased fluvial discharge in years when the monsoon front pushes further into the Chinese interior.

2.2 The evolution of the Holocene East Asian monsoon

A wide range of biological, chemical and sedimentological proxies has been established to investigate the nature of variations in Holocene East Asian monsoon precipitation. Figure 2.2 maps the locations of sites mentioned in the text.

Oxygen isotope records from Hulu Cave, eastern China, indicate a rapid transition (< 10 years) at the end of the Younger Dryas from cool, dry conditions to a period of more intense monsoon activity (Wang *et al.*, 2001). Low $\delta^{18}\text{O}$ values from Dongge Cave speleothems suggest elevated precipitation in southern China during the early Holocene (Dykoski *et al.*, 2005; Y. Wang *et al.*, 2005). Expansion of a low salinity surface plume from the Pearl River due to increased fluvial discharge resulted in lowered surface water salinity in the northern South China Sea (Wang *et al.*, 1999b). Warm-temperate and subtropical forests occupied Taiwan during this period (Liew *et al.*, 2006). High lake levels in northeastern China and Inner Mongolia record increased precipitation from 12000 to 10000 cal. years BP (An *et al.*, 2000 and references therein; Jiang *et al.*, 2006; Cui *et al.*, 2009). Northwest China remained beyond the furthest reaches of the East Asian monsoon and was characterised by high temperatures and aridity during the early Holocene (Liu *et al.*, 2008). Multi-proxy records from Lake Huguang Maar, southeast China, may indicate an inverse relationship between

summer and winter monsoons, with the early Holocene characterised by a decline in winter monsoon wind intensity (Yancheva *et al.*, 2007).

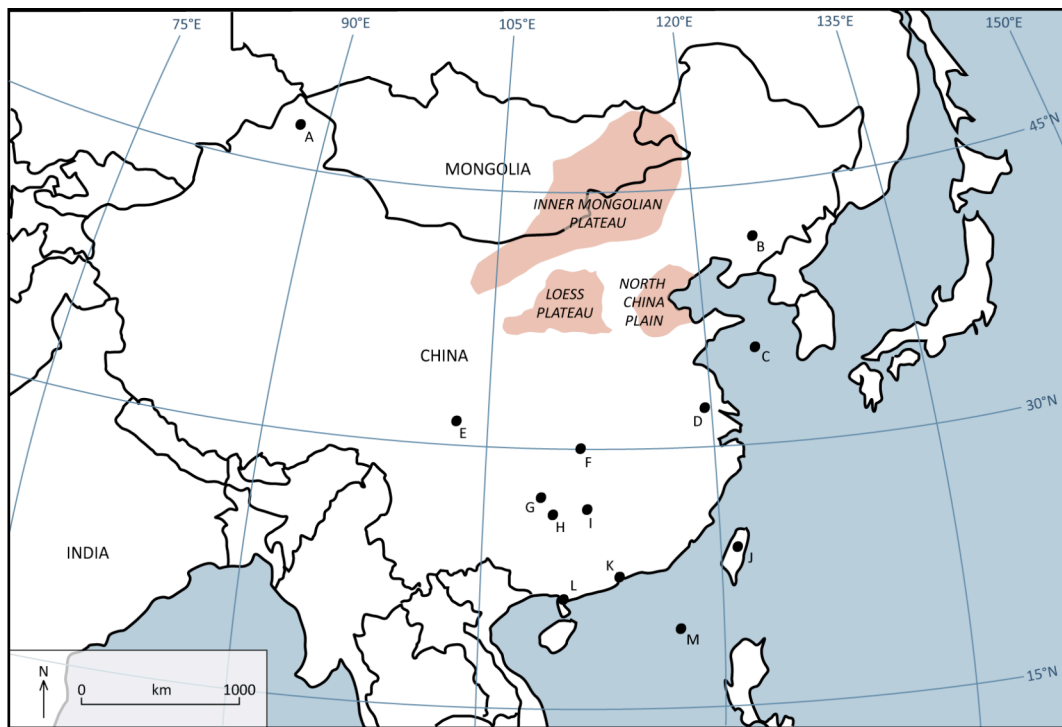


Figure 2.2: Location of sites mentioned in text. (A) Wulungu Lake, northwest China (Liu *et al.*, 2008); (B) Hani bog (Hong *et al.*, 2005); (C) Yellow Sea (Xiang *et al.*, 2008); (D) Hulu Cave (Wang *et al.*, 2001); (E) Hongyang peat research site, eastern Tibetan Plateau (Hong *et al.*, 2005); (F) Heshang Cave (Hu *et al.*, 2008); (G) Qixing Cave (Cai *et al.*, 2001); (H) Dongge Cave (Dykoski *et al.*, 2005; Y. Wang *et al.*, 2005); (I) Xiangshui Cave (Zhang *et al.*, 2004); (J) Toushe Basin, Taiwan (Liew *et al.*, 2006); (K) Pearl River estuary (Zong *et al.*, 2006; 2009a; 2009b; submitted a; submitted b; this study); (L) Huguang Maar (Yancheva *et al.*, 2007); (M) Northern South China Sea (Jian *et al.*, 1999; Wang *et al.*, 1999a; 1999b); Inner Mongolian Plateau (Zhang *et al.*, 1998; Jiang *et al.*, 2006); Loess Plateau (An *et al.*, 2000; Maher and Hu, 2006); North China Plain (Cui *et al.*, 2009).

An *et al.* (2000) suggests declining monsoon intensity was responsible for the southwards migration of the monsoon front during the early- to mid-Holocene. An *et al.* (2006), however, argues for continued humidity in northern and western China, with asynchronous arid intervals in the Loess Plateau and Inner Mongolian Plateau (figure 2.2) cited as explanations for records of lowered monsoon intensity (e.g. An *et al.*, 2000 and references therein; Chen *et al.*, 2003). Zheng *et al.* (1998 and references therein) suggests the northward displacement of the southern limit of boreal coniferous woodland and the presence of forest on the Inner Mongolian steppe indicates intense mid-Holocene summer monsoon activity. Mid-Holocene records from central and southern China also record more intense monsoon precipitation than seen at present. Oxygen isotope records from southern

Chinese caves, including Qixing (figure 2.2, site G; Cai *et al.*, 2001), Xiangshui (figure 2.2, site I; Zhang *et al.*, 2004), Dongge (figure 2.2, site H; Dykoski *et al.*, 2005; Y. Wang *et al.*, 2005) and Heshang (figure 2.2, site F; Hu *et al.*, 2008) all indicate elevated precipitation during the mid-Holocene. Coeval differences between the Dongge and Heshang records, a robust measure of the amount of rainfall falling between the two sites with secondary controls on $\delta^{18}\text{O}$ removed, suggest rainfall totals approximately 8 % higher than present between 6500 and 5000 cal. years BP (Hu *et al.*, 2008). Diatom flora and carbon isotopic records from the Pearl River estuary (figure 2.2, site K) imply increased mid-Holocene fluvial discharge resulting from increased precipitation in the drainage basin (Zong *et al.*, 2006; Yu, 2009) at this time.

Speleothem records almost unanimously show increases in $\delta^{18}\text{O}$, interpreted as indicating declining precipitation intensity, following the mid-Holocene peak (Cai *et al.*, 2001; Zhang *et al.*, 2004; Dykoski *et al.*, 2005; Y. Wang *et al.*, 2005; Cosford *et al.*, 2008; Hu *et al.*, 2008). Sea surface temperature and $\delta^{18}\text{O}$ records from the northern South China Sea (figure 2.2, site M) do not show any significant trend over the mid- to late-Holocene (Wang *et al.*, 1999b), however nearshore records, including diatom flora and bulk organic carbon isotopes from the Pearl River estuary (Zong *et al.*, 2006; Yu, 2009) and foraminiferal assemblages in the southern Yellow Sea (figure 2.2, site C; Xiang *et al.*, 2008) suggest declining fluvial discharge. Increasing titanium counts at Huguang Maar (figure 2.2, site L) during the mid- to late-Holocene provide further evidence for the inverse correlation of summer and winter monsoon intensity (Yancheva *et al.*, 2007). Periods of intense summer monsoon appear to be characterised by weak winter monsoons and vice versa. Zhang and Lu (2007), however, question the correlation between titanium counts and historical records of winter monsoon intensity.

A number of late-Holocene proxy records of precipitation show increased instability, with large fluctuations characterising the last 2000 years (Ge *et al.*, 2007). Speleothem records from Qixing and Xiangshui, south east China, exhibit large shifts in $\delta^{18}\text{O}$, interpreted as reflecting rapid alternation between periods of intensified and diminished precipitation (Cai *et al.*, 2001; Zhang *et al.*, 2004). Wet and dry periods, correlating with the Medieval Warm Period and Little Ice Age respectively, are identified from the Heshang stalagmite (Hu *et al.*, 2008). Large fluctuations in organic carbon isotope values are seen in the last two millennia from Pearl River estuary cores, however these are extensively linked to changing agricultural

activities (Zong *et al.*, 2006; Yu, 2009). No increase in sea surface salinity variability is observed in marine core proxies from the northern South China Sea (Wang *et al.*, 1999b).

While the established pattern of East Asian monsoon intensity, incorporating intense early and mid-Holocene precipitation followed by a progressive decline in moisture, appears to be supported by a wide range of proxy records, a number of issues appear to remain unresolved at present, particularly regarding the use of cave records. Oxygen isotope records have been almost invariably interpreted as reflecting the 'amount effect', where more intense precipitation leads to more negative values (e.g. Wang *et al.*, 2001; Dykoski *et al.*, 2005; Y. Wang *et al.*, 2005). The possibility of the isotopic composition being influenced by changing moisture sources and the length of the water vapour transport path has not been extensively questioned. Less negative $\delta^{18}\text{O}$ values could potentially reflect the declining intensity of isotopically lighter Indian monsoon precipitation, but increasing influence of isotopically heavier East Asian monsoon rainfall (Maher and Hu, 2006; Maher, 2008). A mid- to late-Holocene increase in East Asian monsoon precipitation intensity is supported not only by Loess Plateau soil magnetism transfer functions (Maher and Hu, 2006), but also by peat cellulose $\delta^{13}\text{C}$ records from Hani Bog, northeast China (figure 2.2, site B); a site located beyond the furthest possible extent of the Indian monsoon (Hong *et al.*, 2005). Furthermore, An *et al.*'s (2000) modelling of summer monsoon intensity suggests a precipitation optimum in southern China around 3000 cal. years BP. Comparison of the Hani Bog record with carbon isotope values from the eastern Tibetan Plateau (figure 2.2, site E), a region primarily under the influence of the Indian summer monsoon, provides further support for the inverse phase relationship between the two components of the Asian monsoon system (Hong *et al.*, 2005).

LeGrande and Schmidt (2009) considers the south China speleothem records as solely a reflection of the length of the vapour transport path, with changes in local precipitation having a negligible effect on $\delta^{18}\text{O}$. Comparison of the record from Dongge Cave with that of Heshang Cave, located 600km downwind, supports this hypothesis, with the latter record exhibiting consistently more depleted values. The calculation of coeval differences between high-resolution records from spatially separated records from the same water vapour transport path potentially provides a more robust measure of the amount of rainfall deposited between the selected locations (Hu *et al.*, 2008). This method removes the influence of other controls, including temperature, on the isotopic composition. Hu *et al.* (2008) suggests that the effects of changing moisture source are also circumvented,

however this relies on the assumption that the track of precipitation bearing air masses has not changed through time.

Further questions regarding the source of moisture for cave proxies must also be addressed. If a speleothem draws on precipitation from the immediate vicinity of the cave only, as appears to be the case for the records mentioned above, the resulting $\delta^{18}\text{O}$ may be expected to reflect the microclimate of the surrounding area. Scaling up this microclimate to provide an interpretation of the intensity of precipitation associated with the entire subtropical monsoon front clearly requires a large assumption on the continuity of rainfall patterns over a large area. As spatial variation in the areas of precipitation is a key feature of short- and long-term variability in monsoonal systems (Lau and Yang, 1997; Huang *et al.*, 2003), the analysis of individual cave records is clearly inadequate. The agreement between multiple speleothem records does provide support for the reliability of the inferred trends, although the caveat of the uncertain relationship between the proxy and precipitation intensity remains. A partial solution to the issue of applicability of proxy records from small catchments is to adopt the use of records that average precipitation intensity over larger areas. Estuarine and marine proxies that respond to changes in fluvial flux resulting from precipitation variability in large terrestrial catchments provide a direction for further investigation (Zong *et al.*, 2006).

2.3 Reconstructing palaeoenvironments using benthic foraminifera

The use of estuarine environments as records of precipitation intensity relies on the selection of an appropriate proxy that can be linked to fluvial flux. Diatoms, bulk organic carbon isotopes and selected elements have been investigated (Zong *et al.*, 2006; submitted a; submitted b; Yu, 2009), while this study examines the potential of benthic foraminifera as palaeoenvironmental indicators.

2.3.1 Benthic foraminifera as environmental proxies

Foraminifera are unicellular protists generally characterised by a test made of calcium carbonate or agglutinated particles (Murray, 1991). While the phylum as a whole is found in a wide range of saline environments, the majority of the several thousand currently recorded species of benthic foraminifera are constrained to specific habitats (Scott and

Medioli, 1986; Murray, 2007). Numerous environmental factors have been proposed as important in controlling the distribution of particular species or assemblages, including salinity, water depth, temperature, pH, organic matter flux, dissolved oxygen, predation and competition (Murray, 1991). The restricted distributions of particular species, combined with adaptation of test morphology in response to habitat preference, facilitate their use as proxies for particular environmental variables. Furthermore, their small size and great abundance means that representative assemblages can be determined from small sediment samples.

The reliability of palaeoenvironmental inferences made using foraminiferal proxies is limited by the extent to which the relationship between the environment and assemblage composition is understood (Schafer, 2000). Modelling of this relationship is undertaken through the development of a modern training set, in which known environmental factors are used to explain the distribution of assemblages. The use of foraminifera as a proxy for salinity relies on the variable controlling their distribution to a significant extent. Reconstructing past changes relies on continuity between the contemporary and fossil relationship between foraminifera and salinity (Murray, 2006). With the number of generations reaching the hundreds of thousands in the Holocene alone, evolution of foraminifera in response to a changing environment is to be expected, however the continuity in tolerances to specific environmental variables remains an assumption inherent in this and most other qualitative and quantitative palaeoenvironmental reconstructions.

2.3.2 Contemporary distribution of Pearl River estuary benthic foraminifera

Calcareous microfossils of the Chinese continental shelf have received extensive examination, particularly over the last 30 years, due to petroleum exploration and palaeoceanographic studies (Wang, 1997; Wang and Lipps, 2005). Brady (1884) described a number of species from Hong Kong waters, however the first detailed survey of benthic foraminifera on the northern shelf of the South China Sea was not undertaken until Waller (1960) identified an assemblage in water depths of 54 to 150 ft (16 to 46 m) consisting of *Elphidium advenum*, *E. sagraum* and *Nonion japonicus* (= *Florilus japonicus*).

Wang Pinxian, Min Qiubao, Bian Yunhua and coworkers investigated the distribution of calcareous microfossils in the sediments of the East China Sea, Yellow Sea, South China Sea

and Bo hai (Wang, 1980), later revised, updated and translated into English (Wang, 1985; Wang *et al.*, 1985a; 1985b; 1985c; 1985d). Comparatively low abundance and diversities of foraminifera were encountered in the Pearl River estuary, with <100 tests per gram of sediment and <60 species, compared with >4000 tests and >100 species from samples from the outer shelf (Wang *et al.*, 1985c). Hyaline tests predominate throughout the northern continental shelf of the South China Sea, with trochospiral and planispiral forms abundant on the inner shelf and serial forms more common on or beyond the outer shelf. Agglutinated and porcelaneous foraminifera are widely distributed, with the former most common in water depths of 40 – 60 m. Table 2.1 lists the species contributing to the two assemblages found in the area of interest of this study. Wang *et al.* (1985c) cite water mass distributions as the primary controlling variable on foraminiferal assemblages.

Li (1985 in Huang and Yim, 1998) analysed 209 samples from the Pearl River estuary, identifying three assemblages with strong similarities to Wang *et al.*'s (1985c) estuarine and inner shelf assemblages (table 2.1). Water depth, salinity and sediment type are postulated as key controlling variables. Li and Yim (1988) similarly suggests that variations in salinity, caused by mixing of freshwater from the Pearl River and marine water from the South China Sea, and different energy levels of currents are responsible for the different assemblages found in four areas of Hong Kong territorial water. Li (1985 in Huang and Yim, 1998), Li and Yim (1988) and Wang *et al.* (1985c) concur over the presence of *Hanzawaia nipponica* and *Florilus* sp. on the inner shelf, *Ammonia beccarii* in enclosed estuarine areas with reduced salinity and *Elphidium advenum* in areas of elevated salinity.

Agglutinating foraminifera of the main Pearl River estuary and the smaller estuaries of the Pearl River to the west (the Modaomen and Huangmohai) are the focus of Li (1988). Agglutinated species contribute between 20 and 80 % of the total count of a number of samples from an extensive area of the Pearl River estuary, between Qi'ao Island, Macau and Hong Kong, and the southern Modaomen estuary. In comparison with Wang *et al.*'s (1985c) area of abundant agglutinated species, Li's (1988) zone exhibits significantly higher abundances and is located in an area of shallower water depth and lower salinity. Water depth, salinity, pH and sediment type are suggested as controlling factors for the distribution of agglutinated tests (Li, 1988).

Zheng (1994 in Huang, 2000) subdivides the benthic foraminifera of the northern and eastern areas of the South China Sea into four assemblages, including two within the area of interest of this study (table 2.1). Close agreement is seen with Wang *et al.* (1985c) over outer shelf assemblages.

	Inner estuary	Middle estuary	Outer estuary	Inner shelf
Wang (1980) / Wang <i>et al.</i> (1985c)		<i>Ammonia beccarii</i> <i>Ammonia convexidorsa</i> <i>Elphidium</i> spp. <i>Cribronion vitreum</i>		<i>Hanzawaia nipponica</i> <i>Elphidium hispidulum</i> <i>Ammonia beccarii</i> <i>Ammonia globosa</i>
Li (1985 in Huang and Yim, 1998)	<i>Ammonia beccarii</i> <i>Elphidium nakanokawaense</i>	<i>Ammonia annectens</i> <i>Brizalina striatula</i>		<i>Elphidium advenum</i> <i>Hanzawaia nipponica</i>
Li (1988)	<i>Ammobaculites</i> spp. <i>Haplophragmoides</i> spp. <i>Trochammina</i> spp. <i>Ammotium salsum</i> <i>Miliammina fusca</i>	<i>Ammobaculites</i> spp. <i>Textularia</i> spp. <i>Bigenerina</i> spp.		<i>Textularia</i> spp. <i>Bigenerina</i> spp.
Zheng (1994 in Huang, 2000)		<i>Textularia foliacea</i> <i>Cribronion porisutueralis</i>		<i>Pseudorotalia giamardii</i> <i>Textularia foliacea</i>
Huang and Yim (1998)	<i>Ammonia beccarii</i> <i>Elphidium nakanokawaense</i>	<i>Haplophragmoides canariensis</i> <i>Spiroplectammina biformis</i> <i>Arenoparella asiatica</i> <i>Ammonia beccarii</i> <i>Elphidium nakanokawaense</i>	<i>Ammonia</i> spp. <i>Elphidium magellanicum</i> <i>Quinqueloculina lamarckiana</i> <i>Spiroloculina</i> spp. <i>Ammobaculites</i> spp. <i>Trochammina inflata</i> <i>Brizalina striatula</i>	<i>Elphidium advenum</i> <i>Hanzawaia nipponica</i> <i>Ammonia compressiuscula</i> <i>Florilus japonicus</i> <i>Nonionella</i> spp. <i>Quinqueloculina pseudoreticulata</i> <i>Bigenerina</i> spp. <i>Textularia</i> spp. <i>Fursenkoina schreibersiana</i> <i>Lagena</i> spp. <i>Bulimina marginata</i> <i>Virgulopsis orientalis</i>
Saidova (2007)		Not included in survey		<i>Pseudonion japonicum</i> <i>Hanzawaia nipponica</i> <i>Rotorbinella tepida</i> <i>Elphidium sagrum</i> <i>Elphidium advenum</i> <i>Cellanthus craticulum</i> <i>Cibicides lobatulus</i>

Table 2.1: Summary of species contributing to assemblages defined by past investigations into the benthic foraminifera of the Pearl River estuary and adjacent inner shelf. Note: The investigations of Li (1988) are only concerned with agglutinated species.

Collating the findings of Li (1985), Wang *et al.* (1985c) and Li and Yim (1988), Huang and Yim (1998) identify five foraminiferal assemblages, of which four overlap with the area of this

study (table 2.1). The authors attribute an increase in diversity and abundance with distance from the Pearl River to decreasing seasonal salinity and temperature variation and an increasingly stable environment with lower sedimentation rates. If sedimentation rates have not been taken into account in calculations of the abundance of benthic foraminifera, this may contribute to the lower abundances observed in estuarine environments, with high sedimentation rates effectively diluting the concentration of foraminifera in a given location. Huang and Yim (1998) also cite sea-floor sediment type as a significant controlling variable, with an organic matter-rich flocculent blanket reducing bottom water dissolved oxygen in many areas of the estuary. *Ammonia beccarii* is one of a highly limited number of species that can tolerate the anaerobic environment (Huang and Yim, 1988).

Saidova (2007) provides the most recent review of the foraminiferal assemblages of the northern South China Sea. Compiled from a number of primary sources, including Waller (1960), twelve foraminiferal assemblages are identified from the shelf, continental slope and abyssal region. An inner shelf assemblage, found in water depths of 16 to 45 m characterises the Guangdong coast (table 2.1). With a low sampling resolution and few samples close to the south China coastline, indeed none within the 20m isobath, only large-scale trends in assemblage distribution are observed.

2.3.3 Taxonomic considerations regarding Pearl River estuary foraminifera

The majority of investigations consider *Ammonia beccarii* to represent a single species, however on the basis of molecular evidence, Hayward *et al.* (2004) suggests a number of morphologically distinct species have been classified as *A. beccarii*. Pearl River estuary assemblages contain at least two forms, showing similarities with Hayward *et al.*'s (2004) morphotypes T4 and T6. While distinction between the species is possible for larger specimens, the majority of tests are around 100 µm in diameter and reliable and consistent differentiation is not possible using a binocular microscope. Accordingly, this investigation treats *A. beccarii* as a single species.

2.4 Chapter summary

The majority of proxy records suggest intense monsoon precipitation in the early and mid-Holocene, followed by a progressive decline, with the last two millennia characterised by

alternation of wet and dry periods. Issues remain over the interpretation of speleothem records, however the development of a proxy record drawing on precipitation from a large catchment may resolve at least one of these concerns. The use of benthic foraminifera as a proxy for reconstructing salinity relies on the development of a modern training set, linking the distribution of contemporary foraminifera with environmental variables and the assumption of continuity of these relationships in the fossil record. Past investigations show clear spatial diversity in Pearl River estuary fauna, however the link with salinity must be investigated further.

3. Location: The Pearl River drainage basin and estuary

The Pearl River is a collective term for three southern Chinese rivers – the West River (Xijiang or Si Kiang), the North River (Beijiang) and East River (Dongjiang) – which converge, forming the Zhujiang or Pearl River, close to the city of Guangzhou (figures 3.1, 3.2). The Pearl River estuary provides the link between the drainage basin and the South China Sea. This chapter provides an overview of the contemporary environment and the Holocene evolution of the estuary. The development of the estuary is a history of the interplay between change in accommodation space due to sea-level rise and monsoon driven runoff and sediment supply. The increasing impact of human activities on the basin has exerted a third major control.

3.1 The Pearl River drainage basin

The drainage basin of the West, North and East rivers covers an area of approximately $450 \times 10^3 \text{ km}^2$, incorporating parts of Cao Bằng and Lang Son provinces in Vietnam and Yunan, Guizhou, Guangxi, Hunan and Guangdong provinces in China (figure 3.1). The longest

of the tributaries, the West River, is 2214 km in length. The majority of the drainage basin lies between 22°30'N and 26°00'N.



Figure 3.1: Location of the Pearl River drainage basin (green shaded area), southeast China.

The West River basin predominantly consists of carbonate rocks, providing the Pearl River with the highest specific HCO_3^- flux normalised to basin area of all major rivers in the world (Cai *et al.*, 2008). The East River flows over granites, with the North River overlying more varied geology.

The drainage basin experiences a subtropical climate, controlled primarily by the seasonal advance and retreat of the East Asian monsoon. The year can be divided into two distinct seasons: a wet season (April – October) with increased temperatures and precipitation driven by the southwest monsoon and a dry season (November – March) controlled by the dry and cold northeast monsoon. Annual precipitation in the drainage basin ($1425.8 \text{ mm yr}^{-1}$) exceeds losses through evaporation (1052 mm yr^{-1}) (Kondoh *et al.*, 2004). As the basin lies within the monsoon zone, it is sensitive to variations in monsoon driven precipitation. The annual mean temperature in the drainage basin ranges from 14 to 22 °C, with the temperature at the estuary averaging 22.5 °C (Huang, 2000; S. Zhang *et al.*, 2008).

3.2 The Pearl River estuary

The Pearl River enters the northern South China Sea through a network of distributaries and estuarine bays. A large estuary, the Lingdingyang, separates two main deltaic complexes to the west and northeast. The Lingdingyang occupies an area of approximately 2000 km² and is set within a larger delta plain of 5650 km², not including numerous bedrock hills and islands with a combined area of 2360 km² (Huang, 2000; Cai *et al.*, 2004; Zhou *et al.*, 2006; Wu *et al.*, 2007; Zong *et al.*, 2009a; 2009b). A number of channels of the West, North and East Rivers converge to the southeast of Guangzhou before joining the Lingdingyang estuary through the Humen channel (figure 3.2). A further three channels, or gates, the Jiaomen, Hongqimen or Hongqili and Hengmen, also discharge the West River into the western margin of the Lingdingyang. Four gates, the Yamen, Jitimen, Hutiaomen and Modaomen, discharge the West River into the Modaomen and Huangmaohai estuaries to the west of Macau. Further discussion of the contemporary environment focuses on the Lingdingyang, hereafter referred to as the Pearl River estuary.

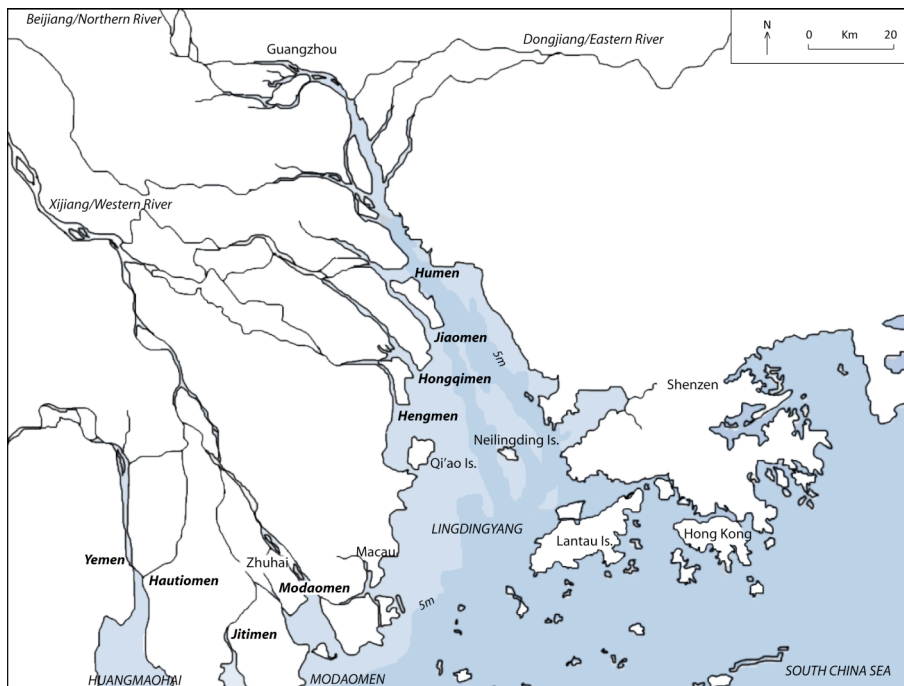


Figure 3.2: The Pearl River estuary, including the three major river branches (*italicised*), the eight distributaries/gates (**emboldened**) and the Lingdingyang, Modaomen and Huangmohai estuarine bays.

The modern Pearl River estuary is predominantly shallow, with depths generally in the region of 2 to 10 m. Two deep water channels, diverging close to the Humen, are separated

by Lantau and Neilingding Islands (Dong *et al.*, 2006). Both channels and areas around the major ports are artificially deepened through dredging. Water depth at the mouth of the Pearl River estuary is approximately 45 m (Zhang *et al.*, 1999).

3.2.1 Geology and tectonics

The majority of the estuary and surrounding delta is underlain by Precambrian granites and Cretaceous-Tertiary sandstones which make up a 9600 km² graben formed by active faulting, basement rifting and subsidence from the upper Cretaceous to the early Oligocene (Lüdmann *et al.*, 2001; Li *et al.*, 2006). Early Triassic to early Cretaceous granite intrusions form the highland areas of Hong Kong, Lantau and numerous smaller islands within the estuary (Yim, 1994). Tertiary sandstones and breccias underlie up to 100 m of Quaternary deposits (Huang, 2000). The Quaternary stratigraphy is closely linked to sea-level change and is examined in more detail in section 3.2.1.

The Pearl River estuary experiences only moderate seismic activity, with few recorded earthquakes exceeding 6 on the Richter scale (Yim, 1994). Faulting divides the area into 12 major blocks (figure 3.3). Huang (2000, and references therein) suggests uplift of the Baiyunshan, Gaohe and Baoan blocks and subsidence of the West River, North River, East River and Lindingyang blocks at a rate of less than 4 mm yr⁻¹. Details on the movement of the Wanshan block, which includes the area around the core used in this study, are not given.

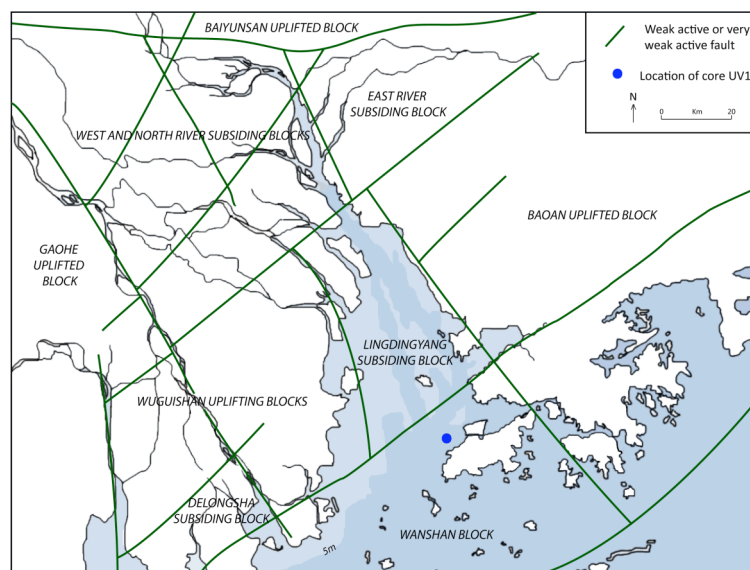


Figure 3.3: Faulting in the Pearl River estuary and surrounding area (after Huang, 2000 and references therein).

3.2.2 Fluvial discharge

The Pearl River's annual discharge of $343 \text{ km}^3 \text{ yr}^{-1}$ is the 14th largest fluvial discharge globally (Cai *et al.*, 2008). Eighty-five percent (approximately $225 \text{ km}^3 \text{ yr}^{-1}$) of the total discharge of the three tributaries of the Pearl River flows through the main Pearl River estuary. Fluvial flux and precipitation are closely linked (S. Zhang *et al.*, 2008) and, with eighty percent of precipitation in the catchment falling during the summer monsoon (Zhang *et al.*, 2009), large differences exist between summer/wet season and winter/dry season discharge (table 3.1)

Gate	Fluvial discharge ($\text{km}^3 \text{ yr}^{-1}$)			Approximate ratio wet : dry season discharge
	Wet season	Dry season	Total	
Humen	76.3	24.8	101.1	3:1
Jiaomen	72.6	21.5	94.1	7:2
Hongqimen	28.1	6.2	34.3	9:2
Hengmen	47.8	13.5	61.3	7:2
PRE Total	224.8	66.1	290.9	7:2

Table 3.1: Wet season, dry season and total annual average discharge data for the four Lingdingyang/Pearl River estuary (PRE) gates (Cai *et al.*, 2004). As noted by Harrison *et al.* (2008), Chinese literature provides estimates approximately 10% higher (for example see table 2 in Zhou *et al.*, 2006)).

3.2.3 Contemporary sediment discharge and deposition

Asian rivers play a key role in the redistribution of sediment on continental and global scales, contributing 40 to 50 % of the total global sediment flux to the oceans (Milliman and Meade, 1983; Milliman, 1991). High precipitation levels under a monsoon climate and the uplift of the Himalayan range are responsible for the large volume of fluvially transported sediment (Saito, 2005). The annual sediment discharge of the Pearl River of $80 \text{ to } 85 \times 10^6 \text{ t}$ is, however, low in comparison with other Asian rivers, including the Yangtze, Mekong and Yellow (Zhang *et al.*, 1999; Zong *et al.*, 2009a; 2009b), and has declined steadily in the last decade (S. Zhang *et al.*, 2008). Approximately 20 % of the sediment is retained within the estuary, with the remaining 80 % discharged into the South China Sea (S. Zhang *et al.*, 2008). Deposition rates are around 0.8 cm yr^{-1} in the upper estuary (north of Neilingding Island) and 2.0 cm yr^{-1} in the lower estuary (Zhang *et al.*, 1999; Zhou *et al.*, 2006). Much higher rates of deposition, in the order of $10 \text{ to } 15 \text{ cm yr}^{-1}$, have been recorded from the deeper channels (Zhou *et al.*, 2006). Lüdmann *et al.* (2001) cites contemporary shoreline progradation rates of $50 \text{ to } 100 \text{ m yr}^{-1}$.

The cities of Hong Kong, Guangzhou, Macau and Zhuhai, amongst others, are located on the delta plain. Domestic, industrial and agricultural effluent discharges have all contributed to considerable pollution of estuarine sediments and degradation of water resources (Li *et al.*, 2000; Zhu *et al.*, 2002).

3.2.4 Estuarine salinity

The wide, shallow estuary of the Pearl River exhibits a strong northwest – southeast salinity gradient resulting from the mixing of low salinity water from the Pearl River and high salinity water from the South China Sea. During the summer, significant freshwater discharge inundates the surface layer of the Pearl River estuary with a buoyant low salinity layer or plume, which extends over the inner shelf of the South China Sea (figure 3.4c; Wong *et al.*, 2003; Dong *et al.*, 2004; Su, 2004). Intrusion of saline water from the South China Sea occurs primarily via two deep water channels in the east of the estuary (figure 3.2). Coriolis forcing deflects water moving into the estuary towards the eastern shore, contributing to increased salinities in the east compared to the west (figure 3.4d; Chao, 1988; Wong *et al.*, 2003). During winter months, the reduced river plume accounts for the displacement of surface isohales to the north and west of their summer positions (figures 3.4a, 3.4b). Northeasterly winds contribute to greater vertical mixing and the formation of a partially mixed estuarine circulation (Wong *et al.*, 2003; Dong *et al.*, 2004). As in summer, gravitational circulation exerts a dominant control on bottom water salinity during the winter, resulting in similar isohale positions (figure 3.4b, d; Wong *et al.*, 2003). Saline intrusions in the east of the estuary and Coriolis forcing contribute to the transformation of the river plume into a coastal current along the western coast in the lower half of the estuary (Su, 2004).

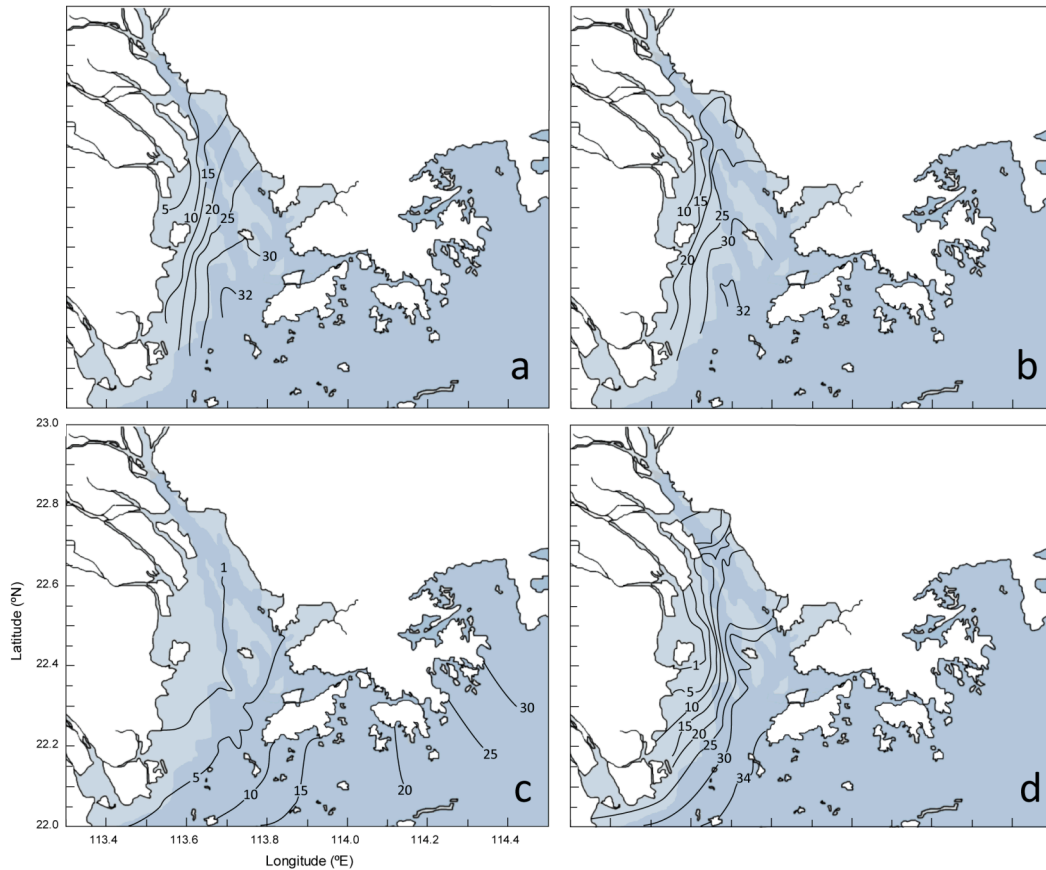


Figure 3.4: Salinity distribution in the Pearl River estuary (a) January 2000 surface water; (b) January 2000 bottom water; (c) July 1999 surface water and (d) July 1999 bottom water (after Dong *et al.*, 2004).

3.2.5 Tides

The South China coastline is micro-tidal, with a mean tidal range of 0.86 m at the mouth of the Pearl River estuary (Huang *et al.*, 2004). The tidal range increases to 1.4 m in the middle reaches and 1.6 m at the Humen gate due to tidal wave amplification in the funnel shaped estuary (Mao *et al.*, 2004). Tidal ranges are greater in the deeper east of the estuary (Xu, 1985 and Zhao, 1990 in Mao *et al.*, 2004; Dong *et al.*, 2006). The relatively low tidal range and reduced energy of waves by protective islands means that, in terms of deltaic and estuarine classifications (Galloway, 1975; Dalrymple, 1992), the Pearl River estuary is fluvially dominated (Li *et al.*, 2006).

3.3 Evolution of the Pearl River estuary

The evolution of the Pearl River estuary and surrounding deltaic lowlands is a history of the interplay between change in accommodation space due to sea-level rise and monsoon driven sediment supply (Zong *et al.*, 2009a; 2009b). More recently, human activities including deforestation and land reclamation have exerted a third major control on deltaic evolution. The significant volume of literature concerning the evolution of the Pearl River delta published in Chinese (including Huang *et al.*, 1982; Huang and Zong, 1982; Li *et al.*, 1990) is not discussed in detail here, however an overview of these works is given by Zong *et al.* (2009a; 2009b).

3.3.1 Sea-level change

Sea-level change is a key parameter in controlling the location, form and development of estuarine and deltaic deposits, both in southern China and worldwide (Stanley and Warne, 1994). The sea-level history of the northern South China Sea has provided a key control on Pearl River basin morphology and the Quaternary sediment sequences (Yim, 1994; 1999; 2001; Bahr *et al.*, 2005; Yang *et al.*, 2008). Well-constrained Holocene sea-level curves provide precise reconstructions of the nature and timing of the postglacial eustatic rise and the magnitude of changes in the mid- to late-Holocene (Zong, 2004).

Rotary boring and cased vibrocoring of boreholes, seismic reflection profiling and side scan sonar data associated with a number of major engineering projects in the estuary, including the airport at Chek Lap Kok and the Hong Kong Mass Transit Railway, have provided a wealth of information on the subsurface stratigraphy of the Pearl River estuary. Cycles of fourth-order sea-level fluctuations, related to changes in global ice volume during glacial-interglacial cycles (Petit *et al.*, 1999), are evoked to explain alternating marine and terrestrial sediments in the south east of the present estuary in the vicinity of Hong Kong and Lantau (Yim, 1994; 1999; 2001; Bahr *et al.*, 2005; Yang *et al.*, 2008). A maximum of ten marine and terrestrial units have been identified, for example in borehole WB7 from the West Lamma channel, interpreted by Yim (1994) as spanning five glacial-interglacial cycles (table 3.2). Uncertainties over the accuracy of pre-Holocene radiocarbon dates and disputes over the use of thermoluminescence or uranium series methods mean that the precise correlation

between stratigraphic units and marine isotope stages remains equivocal (Yim *et al.*, 1990; Bahr *et al.*, 2005; Yim *et al.*, 2008).

Stratigraphic unit	Oxygen-isotope stage	Age
M1	1	Holocene
T1	2	Last glacial
M2	5	Last interglacial
T2	6	Second last glacial
M3	7	Second last interglacial
T3	8	Third last glacial
M4	9	Third last interglacial
T4	10	Fourth last glacial
M5	11	Fourth last interglacial
T5	12 and older	Fifth last glacial

Table 3.2: Classification of Quaternary sediments in Hong Kong (after Yim, 1994; 1999).

Periods of sea level lower than present allowed the deposition of terrestrial sediments in the contemporary estuary area (stratigraphic units T5, T4, T3 etc.), with deltaic sequences deposited on the middle and outer shelf of the northern South China Sea (Yim, 1999; Yang *et al.*, 2008). Subaerial exposure also allowed the incision of elongated valley systems in and seaward of the present estuary (figure 3.5; Lüdmann *et al.*, 2001; Li *et al.*, 2006; Yang *et al.*, 2008). The extent of sub-aerial erosion during lowstands is unclear. Acid-sulphate soils forming palaeo-desiccated crusts at the top of pre-Holocene marine units and the remains of palaeosols may provide evidence for sub-aerial exposure and limited erosion, possibly restricted to shallow channel incision (Yim, 1994; Yim and Tovey, 1995). Few plant remains, however, have been found in forty-four boreholes from Tai O Bay, western Lantau Island (Bahr *et al.*, 2005), suggesting erosion-limiting plant cover may not have been as extensive as previously thought (Yim, 1994). Furthermore, seismic profiles from Tai O Bay suggest the incision of deep valleys into underlying marine deposits (Bahr *et al.*, 2005). Subsequent sea-level rises resulted in the transgression of the estuary and the deposition of marine stratigraphic units (M5, M4, M3 etc.).

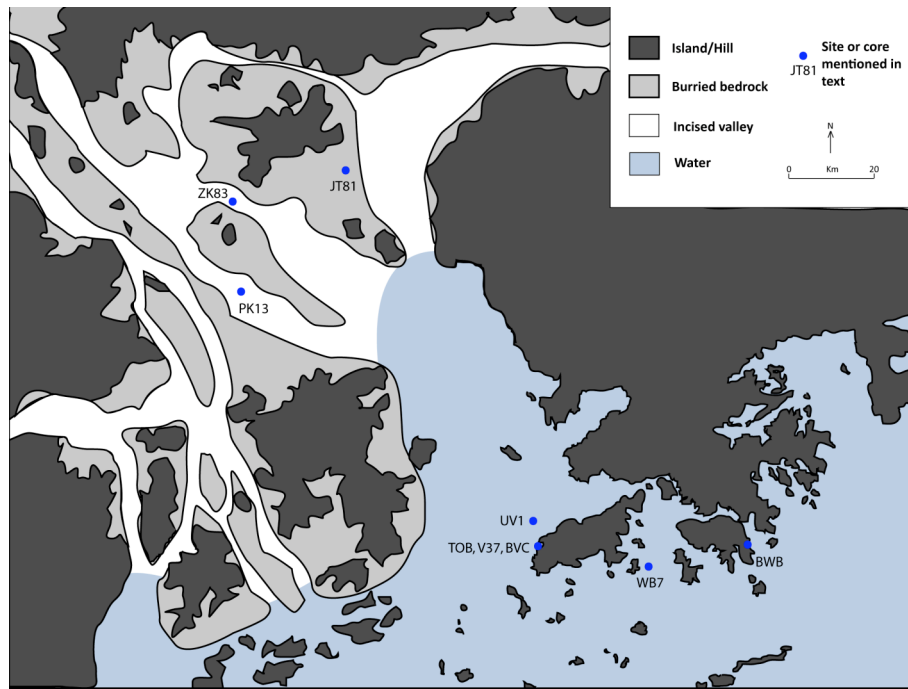


Figure 3.5: Distribution of incised valleys beneath the Pearl River delta with locations of cores mentioned in text (modified from Li *et al.*, 2006). TOB: Tai O Bay (Bahr *et al.*, 2005); BWB: Big Wave Bay (Davis *et al.*, 2000); JT81, ZK83, PK13 (Zong *et al.*, 2009a); UV1 (Zong *et al.*, 2009a; this study); V37 (Bahr *et al.*, 2005; Zong *et al.*, 2009a); WB7 (Yim, 1994).

Reviewing previous literature detailing sea-level index points from numerous locations on the south and east China coastline, Zong (2004) reconstructs Holocene sea-level curves for six distinct sections, including the Pearl River estuary (figure 3.6). Sea level remained more than 20 m below present before 9000 cal. years BP, implying that incised channels in the shallow Pearl River basin remained sub-aerially exposed until after this date. The onset of sedimentation in core JT81, north of the contemporary estuary shoreline, is dated to 8351 – 8157 BP at a depth of 14.4 m below present mean sea level (Zong *et al.*, 2009a). Cores V37 and BVC, located in the southeast of the contemporary estuary, similarly suggest marine inundation by 8800 – 8500 cal. years BP at depths of 11.3 m and 16.4 m below present sea level (Zong *et al.*, 2009a; 2009b). Due to deeper receiving basins, inundation and the deposition of estuarine sequences began at an earlier date in the Yangtze, Mekong and Yellow River mouths (Chen *et al.*, 2000; Ta *et al.*, 2002; Liu *et al.*, 2004).

The southeast China relative sea-level curves (Zong, 2004) do not exhibit the two sharp rises in sea level centred on 8100 and 7250 cal. years BP inferred by Yim *et al.* (2006) and Bird *et al.* (2007) and supported by, for example, intertidal notches surrounding Grand Cayman (Blanchon and Jones, 1995; Blanchon *et al.* 2002). This may be in part due to a relative

paucity of dates before 7ka BP. Zong *et al.* (2009a) suggests that these rapid rises, elevating relative sea-level to 3 m below present, resulted in major transgressions and a change in sedimentation in palaeochannels from tidal sands to deltaic silts and clays, indicating deeper waters and lower energy environments.

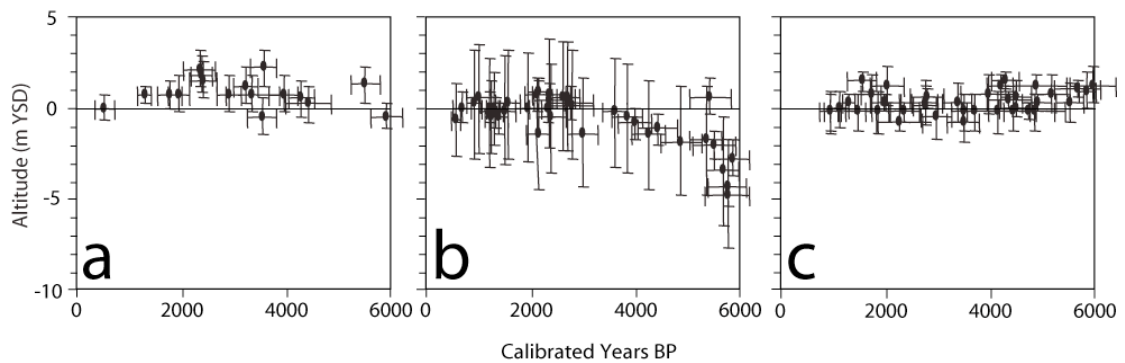


Figure 3.6: Mid- to late-Holocene relative sea-level reconstructions for (a) South China (East Guangdong), (b) the Pearl River delta and (c) South China (West Guangdong and Hainan) (Zong, 2004)

The last six thousand years have been characterised by relative stability in sea level (Zong, 2004). Few sea-level index points relate to elevations above present in the Pearl River delta section of coastline (figure 3.6b), despite mid-Holocene highstands of 1.0 to 1.5 m above present sea level recorded in neighbouring East and West Guangdong (figures 3.6a, 3.6c; Zong, 2004). Davis *et al.* (2000) date a relic oyster encrustation 1.9 m above living conspecifics in Big Wave Bay, Hong Kong, to $5,140 \pm 50$ cal. years BP, however Yim and Huang (2002) and Baker *et al.* (2003) debate its significance. Wave-cut caves and platforms in the Qixing Hill in a suburb of Guangzhou are again proposed as evidence for a highstand above present sea level by 6000 cal. years BP (Fyfe *et al.*, 1999 and references therein; Wu *et al.*, 2007). Sediment compaction and local subsidence may explain the apparent lack of further evidence for a highstand in the Pearl River estuary, while the sea-level index points above present in East Guangdong may be explained by local uplift (Zong, 2004). Overall, sea-level curves from East Guangdong, the Pearl River estuary and the geologically stable area of West Guangdong, including Hainan, suggest changes in relative sea level during the mid- to late-Holocene were minor and probably characterised by a slight sea-level fall. Due to the magnitude of changes, sea level is unlikely to have played a major part in controlling palaeoenvironments in the Pearl River estuary over the studied period.

3.3.2 Sediment discharge

Given stability in relative sea level, sediment discharge and deposition is likely to have provided the main control on estuarine evolution during the mid- to late-Holocene. S. Zhang *et al.* (2008) suggests a clear linear relationship between sediment load and fluvial discharge between 1957 and 1996, although a human-induced deviation from this trend has been observed in the last decade (figure 3.7). Given the link between precipitation in the Pearl River drainage basin and fluvial flux (Zong *et al.*, 2006; S. Zhang *et al.*, 2008), sediment discharge can be seen to reflect precipitation intensity. East Asian monsoon intensity and front position have significant implications for precipitation intensity in southern China, as outlined in section 2.1. The changes in sediment flux arising as a consequence of changes in precipitation intensity are outlined below.

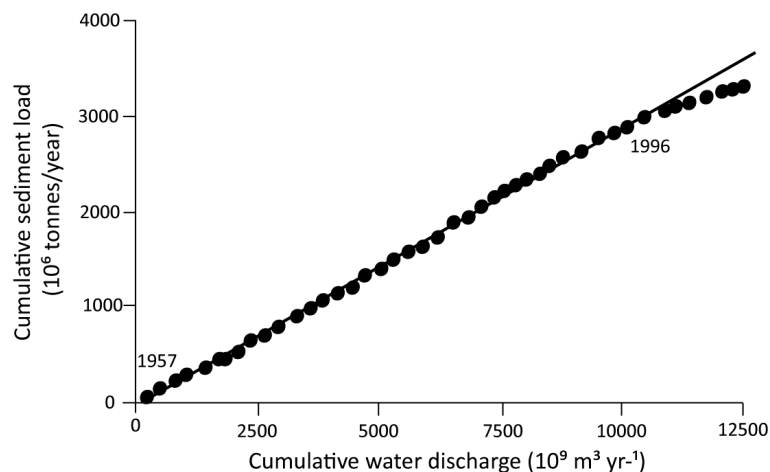


Figure 3.7: The relationship between cumulative sediment load and cumulative fluvial discharge in the Pearl River (excluding the delta area) between 1957 and 2004 (S. Zhang *et al.*, 2008).

A gradual decline in the intensity of the monsoon regime, starting at approximately 7000 – 6000 cal. years BP (Wang *et al.*, 1999b; Y. Wang *et al.*, 2005; Zong *et al.*, 2006), potentially resulted in a progressive decline in sediment supply to the estuary. The diatom flora from cores UV1 and V37 suggest a reversion from delta-front to pro-delta conditions at around 5000 cal. years BP, however delta plain sediments in cores ZK83 and PK13 from the northwest of the delta suggest continued sedimentation and shoreline advance (Zong *et al.*, 2009a). Sediment sequences from Tai O Bay, including core V37, suggest higher than average sedimentation rates at this time (4.4 mm yr^{-1} between 6185 and 4125 cal. years BP, compared to the mid- to late-Holocene average of 2.2 mm yr^{-1}), despite the decline is

sediment supply (Bahr *et al.*, 2005). Bahr *et al.* (2005) suggests high sedimentation rates result from land reclamation, however the lack of a substantial population in the south of China until the Qin and, more significantly, the Sung (= Song) dynasty more than two thousand years later (Lo, 1996; Weng, 2007) hinders their hypothesis.

Continued weakening of monsoon driven discharge throughout the late Holocene (Zhang *et al.*, 2004; Y. Wang *et al.*, 2005; Zong *et al.*, 2006) may have further reduced sediment supply to the estuary. Shoreline progradation continued, however, due to near static relative sea level (Zong *et al.*, 2009a). Shoreline progradation has implications for palaeoenvironmental reconstructions, effectively reducing the distance between the freshwater source and the coring location.

3.3.3 Anthropogenic influences

The widespread settlement of southern China in the centuries leading up to the Qin (221 – 206 BCE) and Han (206 BCE – 220 CE) dynasties marked the start of a third major control on estuarine evolution. Human activity, in both the drainage basin and the estuary itself has led to changes in the discharge and deposition of sediment (Li *et al.*, 2001; S. Zhang *et al.*, 2008; Zong *et al.*, 2009a). Deforestation is likely to have resulted in increased soil erosion and, therefore, greater sediment supply to the Pearl River estuary. Saito *et al.* (2001) suggests that the deforestation and cultivation of the Loess Plateau resulted in a tenfold increase in the sediment discharge of the Yellow River over the last 1000 years. Land reclamation in the Pearl River estuary capitalized on the increase in sediment supply, with farmers accelerating deposition through the creation of lower energy environments with primitive sea walls (Zong *et al.*, 2009a) and later the 'jitang' system of dykes and ponds (Lo, 1996; Weng, 2007). Palaeoshorelines mapped by Zong *et al.* (2009a) suggest an acceleration in the rate of progradation, up to a maximum of 29 m yr⁻¹ in the last millennia. Similar accelerations in shoreline progradation are inferred for the Yangtze, Yellow, Song Hong, Mekong and Chaophraya deltas (Hori *et al.*, 2001; Saito *et al.*, 2001; Saito, 2005; Li *et al.*, 2006).

Over the last 50 years water discharge in the Pearl River estuary has declined and sediment supply increased, although the trends are not significant (S. Zhang *et al.*, 2008; Dai *et al.*, 2008). Land reclamation projects have increased in scale over the same period, with schemes such as the Ai Nan dyke system trapping ever increasing volumes of sediment in

the upper estuary (Chen and Chen, 2004). Chen *et al.* (2005) estimate average land reclamation rates of 5.9 km² per year between 1978 and 1998.

3.4 Suitability of the Pearl River estuary for palaeodischarge reconstruction

Although lower than for other Asian rivers, the volume of fluvially transported sediment entering the Pearl River estuary is considerable. Consequently, many meters of sediment have been deposited over the Holocene, giving the estuary the potential to produce high-resolution palaeoenvironmental records (Zong *et al.*, 2006; 2009a; Yu, 2009). The large bedrock outcrops of Hong Kong to the east and the area north of Macau to the west have restricted the lateral movement of the estuary, ensuring continuous sedimentation over the majority of the Holocene (Zong *et al.*, 2006). The microtidal nature of the estuary and sheltering from excessive wave action by numerous rocky islands has further assisted in the preservation of sediment archives.

The sea-level history of the south China coastline is well constrained, with levels close to present characterising the mid- to late-Holocene (Zong, 2004). Estuarine evolution may, therefore, be interpreted in terms of fluvial flux and shoreline progradation (Zong *et al.*, 2009a). The microtidal nature of the estuary, however, means that small changes in sea level may have a significant impact on salinity. Of several possible processes sea-level rise and declining fluvial discharge may give rise to increases in estuarine salinity. Given knowledge of estuarine evolution and shoreline progradation (Wu *et al.*, 2007; Zong *et al.*, 2009a), declining fluvial flux may be inferred as the primary mechanism resulting in any increases in salinity. A number of other factors may also affect estuarine salinity, including changing tidal amplitude and alterations to estuarine circulation and coastal currents, precluding the possibility for an estuarine salinity record to be interpreted solely in terms of discharge.

The link between precipitation and fluvial discharge and the influence of discharge on estuarine salinity facilitates comparison of environmental reconstructions from the Pearl River estuary with other proxy records of palaeoprecipitation. The size of the drainage basin means that records from the Pearl River estuary may provide a synoptic view of trends in precipitation in southern China, rather than reflecting local precipitation patterns.

4. Methodology

This chapter introduces the basic methods used to provide faunal and environmental data to answer the research objectives set out in Chapter 1. Methods for the recovery of contemporary samples and core UV1 are detailed, alongside the procedures used for extracting faunal data. The potential problems associated with infaunality, taphonomy and bioturbation are discussed. Techniques used to obtain contemporary environmental data are also outlined.

4.1 Contemporary surface sample recovery

A number of expeditions (Zong *et al.*, 2006; Yu, 2009; this study) have contributed to the compilation of a set of 105 samples from the surface sediments of the Pearl River estuary and adjoining river channels, of which 76 yielded significant abundances of foraminifera (figure 4.1). Samples were obtained using a grab sampler, which retrieved approximately 10 cm from the surface of the estuarine sediments at each location. Each sample represents 6 – 10 years of sediment accumulation, assuming a sedimentation rate of between 1.0 and 1.8 cm yr⁻¹ (Li *et al.*, 1991; Owen, 2005). The location of surface sampling sites was recorded using a hand-held Garmin Etrex GPS.

4.2 Core recovery

A vibracore, UV1, was obtained from the northwest of Lantau Island by the Civil Engineering Department, Hong Kong Special Administrative Region Government. The core, located at 22°17'10"N 113°51'49"E (figure 4.1), was recovered from a water depth of 8.6 m. A 30 m sedimentary sequence was obtained, of which the uppermost 10.09 m are analysed in this study. The top 0.35 m of the core was not recovered and sediments between 6.00 and 6.25 m were also lost during sampling (Yu, 2009). Analyses of variation in the organic carbon isotope signature, key metals (Yu, 2009) and diatom assemblages (Zong *et al.*, submitted a) have been undertaken. Core UV1 was sampled at approximately 12 to 14 cm intervals, matching the sampling resolution and depths of previous analyses (Yu, 2009; Zong *et al.*, submitted a). Each sample consisted of a well-mixed 2 cm slice of the core.

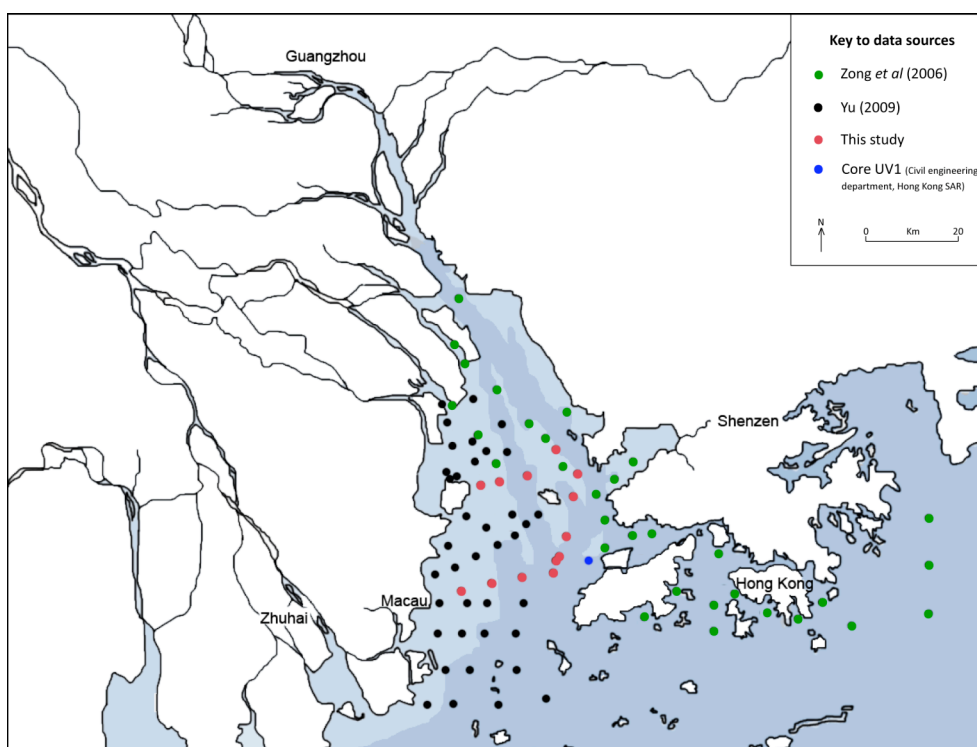


Figure 4.1: Location of Pearl River estuary surface samples and core UV1. Samples represented by circles, coloured according to primary source.

4.3 Faunal data

4.3.1 Procedures for obtaining data

Initially 2 cm³ subsamples from each contemporary grab sample or core sample were washed through 500 µm and 63 µm sieves, with further subsamples processed depending on

test abundance. Analysis of selected >500 µm fractions suggested that few if any foraminifera exceeded this diameter. The <63 µm fraction was also discarded as the small size of foraminifera prevented reliable identification. Wet samples were examined using a Leica binocular microscope at magnifications of 38x to 76x. Taxonomy follows Wang *et al.* (1988), Huang and Yim (1998) Huang (2000), Scott *et al.* (2000) and Saidova (2007). Taxonomical considerations relevant to the location are covered in Chapter 2. Plates of particular specimens have been prepared using a Phillips XL30 environmental scanning electron microscope at magnifications of 80x to 800x. Tests were gold coated and analysed in high vacuum mode with a secondary electron detector. Fatela's (1994) classification of taxa as dominant, common, accessory and rare or accidental are adopted, with slight modification. Specifically taxa attaining a relative abundance of >20 % in one or more sample are classified as dominant; 10 to 20 % common; 5 to 10 % accessory; 1 to 5 % minor and <1 % insignificant.

4.3.2 Total count size

While Phelger (1960) suggests a minimum of 300 tests per sample should be counted, Fatela and Taborda (2002) concludes that, for environmental description based on common species, counts of 100 are sufficient. For any given total count the confidence intervals of a taxon proportion can be calculated using the bimodal distribution (equation 4.1; Fatela and Taborda, 2002) or other, more complex methods (Mosimann, 1965; Maher, 1972).

$$p - 1.96\sqrt{p(1-p)/n} < P < p + 1.96\sqrt{p(1-p)/n} \quad (\text{Equation 4.1})$$

Where p is the species proportion estimate and a 95% confidence interval is sought.

With a total count of 50 tests the 95 % confidence interval for a species contributing 10 % of the assemblage extends from 1.7 to 18.3 % (figure 4.2) and there is a >5 % probability of failure in detecting a species comprising <6 % of the assemblage (Fatela and Taborda, 2002). If the total count is increased to 100 the confidence interval is compressed, ranging from 4.1 to 15.9 %, and the species proportion with a >5 % chance of non-detection falls to <3%. A total count of 300 tests reduces the confidence interval further, to 6.6 to 13.4 %, and the species proportion falls to <1 %. The increase in precision gained by increasing count totals must be weighed against the increase in time devoted to each sample (Woodroffe, 2006). A

flexible approach is adopted here, with counts of 300 or more tests obtained from all fossil and a significant number of contemporary samples. Where test abundances are low, for instance in the northwest of the estuary, lower total counts are accepted. Statistical analyses were based on all samples with total counts exceeding 50. In an attempt to increase the accuracy of the transfer function all samples with total counts of less than 100 were removed. While low abundances meant large volumes of sediment needed to be processed from low salinity environments, by contrast, the high abundance of tests in samples from high salinity areas, combined with the pipetting method of preparing slides (Laws, 1983), meant that counts of more than 300 were needed to avoid a bias in favour of species with large tests.

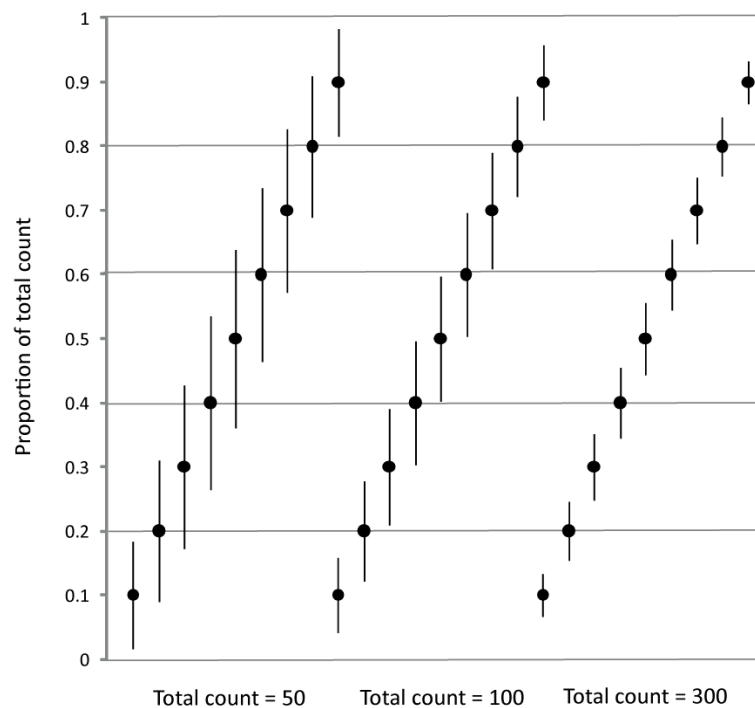


Figure 4.2: 95 % confidence intervals for species proportions assessed using the binomial distribution (Fatela and Taborda, 2002) for total counts of 50, 100 and 300.

4.3.3 Live vs. dead assemblages

Debate is ongoing over the use of live, dead or total (live + dead) assemblages when analysing the distribution of foraminifera in contemporary samples (e.g. Jennings *et al.*, 1995; Murray, 2000; Horton and Murray, 2006; Diz and Francés, 2009). Patterson *et al.* (1999) suggests that inferences based on live and dead assemblages give similar results in a tidal marsh setting, however numerous authors have found significant dissimilarity between the assemblages (e.g. Murray, 2006; Horton and Murray, 2006; Diz and Francés, 2009).

Huang (2000) suggests good agreement between living and total foraminiferal assemblages in the Pearl River estuary. The use of total assemblages may smooth the effects of seasonal and other short-term changes (Jennings *et al.*, 1995; Tobin *et al.*, 2005), while the dead assemblage removes variability inherent in the live component (Horton, 1999; Murray, 2000; Diz and Frances, 2009). Foraminiferal data are consequently expressed here as percentages of the dead assemblage. As each grab sample represents 6 – 10 years of sediment accumulation, foraminiferal assemblages reflect an average of numerous generations.

4.3.4 Issues of infaunality and reworking

The majority of analyses of contemporary foraminiferal distributions in intertidal locations are based on the uppermost 1 cm of sediments (e.g. Alve and Murray, 1994; Horton and Murray, 2006; Fatela *et al.*, 2009), however this method may underrepresent infaunal populations (Duchemin *et al.*, 2005). Due to the sampling technique, this potential source of dissimilarity between surface and fossil samples is not encountered in this project. Infaunal productivity, along with post-mortem taphonomic modification may contribute to the complex process of fossil assemblage development (Berkeley *et al.*, 2007). Loubere and Gary (1990) and Loubere *et al.* (1993) suggest that infaunal taxa may be less at risk from destruction by taphonomic processes and therefore may be overrepresented in fossil record. Taphonomic processes may also result in a change in abundance of individual taxa, decreased diversity, a reduction in the overall number of tests and introduce bias in favour of large, highly calcified tests. Bioturbation may result in mixing of the surface death assemblage with the subsurface fossil assemblage, though the extent to which this may occur is not quantified in the literature. Dissolution may affect the proportion of calcareous tests (Yim, 1994; Murray and Alve, 1999), while oxidation of organic cements may lead to underrepresentation of agglutinated tests in the fossil record (Goldstein and Watkins, 1999; Berkeley *et al.*, 2007).

Both contemporary and fossil samples are a combination of allochthonous and autochthonous tests (Zong *et al.*, submitted b). Wang *et al.* (1992) suggests that in microtidal settings, including the contemporary Pearl River estuary, dead assemblages are primarily controlled by in situ living assemblages, rather than transport due to the hydrodynamic regime. Furthermore, Wang and Murray (1983) suggests that exotic taxa constitute less than 10 % of the contemporary Pearl River estuary fauna. Huang (2000), however, identifies

episodes of extensive reworking of exotic taxa associated with storm events. Visual analysis of the state of preservation of tests may provide information on the possibility of reworking. Abrasion and partial destruction could, however, also result from predation or post-mortem diagenesis.

4.4 Environmental data

4.4.1 Salinity data

Salinity data for samples PE 1 to 20 has been obtained from Zong *et al.* (2006) (Table 4.1). Data for sites in Hong Kong territorial waters (PE 21 to 40) have been obtained from the Environmental Protection Department, Hong Kong SAR government (2007). Bottom water salinity data is available at roughly monthly intervals for the period from February 1998 to December 2007. Due to a water depth of less than 3 m at site PE 40, separate measurements for surface, middle and bottom water salinity are not taken (Hong Kong Environmental Protection Department, 2007) and surface water salinity values are used for this sample. As each grab sample is estimated to include sediments deposited over the last 6 to 10 years, salinity measurements from the last decade are averaged to represent the salinity associated with each given sampling location. Standard deviations in salinity measured at each site average 1.5 psu, with a maximum of 6.1 psu, however variability is almost entirely on an intrannual timescale and no significant trends in salinity are recorded at any of the sites. Due to the lack of sizeable interannual variation over the instrumental record, it is assumed that the stable environment will have been reflected by relatively unchanging foraminiferal communities over the period in which the surface samples accumulated.

Annual average salinity values for sampling sites in Chinese waters have been interpolated from data obtained during cruises in July 1999 and January 2000 (Dong *et al.*, 2004). While the dataset does not account for any interannual variability in freshwater discharge and is limited in spatial extent and number of sampling points, it constitutes the most complete bottom water salinity dataset available. Interannual variability is likely to be lowest in the southeast, where large areas of inner shelf are characterised by relatively stable high salinities (Wong *et al.*, 2003; Dong *et al.*, 2004; HKEPD, 2007). The centre and northwest of the estuary may experience greater variability due to the higher relative contribution of low

salinity water from the river mouths to salinity values. The last 6 to 10 years of sediment accumulation in these areas may be characterised by varying assemblages characteristic of different salinities. Mixing of grab samples, combined with the use of a single salinity values, rather than decadal averages, may mean that samples from the northwest of the estuary are less likely to provide appropriate and dependable modern analogues than samples from the southeast of the estuary.

Sample number	Data source
PE 1 – 20	Zong <i>et al.</i> (2006)
PE 21 – 40	Hong Kong Environmental Protection Department (2007)
PE 41 – 105	Interpolations from Dong <i>et al.</i> (2004)

Table 4.1: Source of salinity data for Pearl River estuary surface samples.

4.4.2 Other environmental data

Depth measurements for Hong Kong samples have been obtained from the Hong Kong Environmental Protection Department (2007). Depths in Chinese territorial waters have been measured using a weighted rope and tape measure and are therefore subject to larger sampling errors, potentially in the order of $\pm 10\%$.

Particle size measurements were obtained using a Beckman L2 13 320 laser coulter following the addition of hydrogen peroxide to remove organic material and sodium hexametaphosphate as a dispersant. Results are categorized into three classes – sand (2 mm – 62.5 μm / -1 – 4 ϕ), silt (62.5 – 3.9 μm / 4.25 – 8 ϕ) and clay (3.9 – 0.061 μm / 8 – 14 ϕ) and expressed in percentage form.

Data on total nitrogen (TN), total organic carbon (TOC) and the ratio of carbon to nitrogen (C/N) has been obtained from Yu (2009) and from further laboratory analysis. Approximately 100 ml of 5 % hydrochloric acid was added to around 2 g of sediment for 24 hours before washing with deionised water, freeze drying and ball milling. 50 mg samples were weighed and processed using a TOC 1200 analyser. $\delta^{13}\text{C}$ values have been obtained from Yu (2009).

5. The contemporary distribution of foraminifera in the Pearl River estuary: results and interpretation

This chapter presents the results of analyses of the contemporary surface sample set. Descriptive statistics, assemblage diagrams, maps and the estimation of optima and tolerances provide information on the distribution of fauna and the environmental preferences of individual taxa. Constrained ordination is employed to link the distribution of foraminifera to environmental parameters. The relationship between foraminifera and salinity is further quantified in the development of a transfer function, facilitating reconstruction of palaeosalinity from fossil assemblages in Chapter 6.

5.1 Analysis of contemporary benthic foraminifera

5.1.1 The foraminiferal assemblages of the Pearl River estuary

The 76 surface samples yielded 112 foraminiferal taxa, of which 18 were agglutinated and 94 calcareous. Planktic species are virtually absent. The majority of surface samples are

dominated by *Ammonia beccarii*, with a number of other calcareous taxa, including *Haynesina sp.*, *Elphidium spp.*, *Quinqueloculina spp.* and *Rotalinoides annectens*, and agglutinated taxa, including *Ammobaculites formosensis* and *Haplophragmoides sp.* contributing. The modern foraminifera are summarised in terms of abundance of taxa according to limits based on Fatela's (1994) classification (>20 % dominant; 10 to 20 % common; 5 to 10 % accessory; 1 to 5 % minor and <1 % insignificant), effective number of taxa per sample and effective number of occurrences per taxon following Hill's (1973) diversity measure (N_2) (table 5.1). Hill's (1973) index of diversity provides an analysis of the number of taxa per sample or occurrences per taxon weighted by their relative abundance. While Debenay and Luan (2006) suggests that diversity indices are of lower value than methods based on the presence or absence of indicator species, they provide useful information in settings where the magnitude of spatial variations in diversity is large. Summary statistics for each of the 20 dominant or common taxa are given in appendix 5.1 and the full contemporary dataset is given in appendix 5.2. Foraminiferal assemblages for the modern dataset are shown in figure 5.1. Key species are illustrated in plates 1 to 4.

Number of taxa	112
dominant (>20%)	7
common (10-20%)	13
accessory (5-10%)	12
rare or accidental (1-5%)	41
negligible (<1%)	39
N_2 for samples	
Minimum	1.4
Median	5.1
Mean	7.3
Maximum	32.2
N_2 for taxa	
Minimum	1.0
Median	5.8
Mean	8.9
Maximum	52.5

Table 5.1: Descriptive statistics for contemporary Pearl River estuary foraminifera.

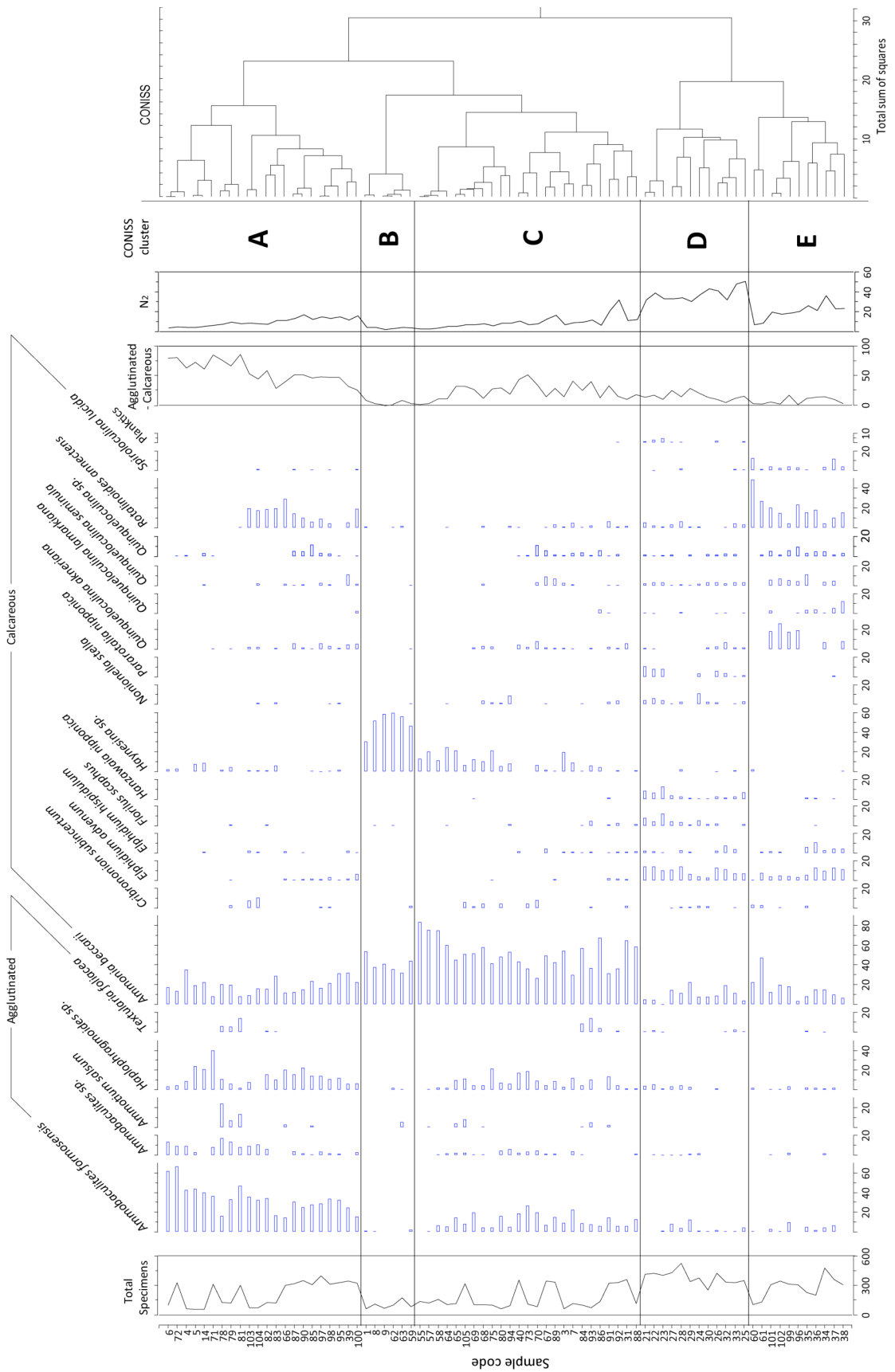


Figure 5.1: Pearl River estuary surface sample foraminiferal assemblages. Dominant and common taxa (>10 %) only. Order and clusters according to stratigraphically unconstrained CONISS.

5.1.2 Cluster analysis

Stratigraphically unconstrained CONISS (CONstrained Incremental Sum of Squares; Grimm, 1987), an agglomerative clustering method within TGVView version 2.0.2 (Grimm, 2004), provides a statistical basis for the identification of groups of similar samples in the contemporary faunal data. Foraminiferal counts were subjected to a square-root transformation before clustering to reduce the influence of dominant species. Five clusters, labeled A to E, were inferred from the dendrogram and foraminiferal assemblage data (figure 5.1). The major division is between clusters A to C, dominated by *Ammonia beccarii*, with some *Haynesina* sp. and agglutinated species, and clusters D and E, which show a more diverse range of species. The principal taxa contributing to the five clusters and average effective number of taxa per sample (N_2) are summarised in table 5.2.

Cluster A is dominated by *Ammobaculites formosensis* and *Ammonia beccarii*, with *Haplophragmoides* sp., *Ammobaculites* sp., *Rotalinoides annectens* and *Ammotium salsum* also reaching common levels. Agglutinated tests contribute the majority of the total count. N_2 values are relatively low and generally in the range of 5 to 15.

CONISS cluster	Number of samples	Characteristic species	Mean N_2
A	22	<i>Ammobaculites formosensis</i> <i>Ammonia beccarii</i> <i>Haplophragmoides</i> sp. (<i>Rotalinoides annectens</i>)	9.7
B	6	<i>Haynesina</i> sp. <i>Ammonia beccarii</i>	3.6
C	25	<i>Ammonia beccarii</i> (<i>Ammobaculites formosensis</i>) (<i>Haynesina</i> sp.) (<i>Haplophragmoides</i> sp.)	9.6
D	12	<i>Ammonia beccarii</i> <i>Elphidium advenum</i> (<i>Florilus scaphus</i>) (<i>Pararotalia nipponica</i>) (<i>Hanzawaia nipponica</i>) <i>Rotalinoides annectens</i>	37.7
E	11	<i>Quinqueloculina</i> spp. <i>Ammonia beccarii</i> (<i>Elphidium advenum</i>)	20.0

Table 5.2: Summary of the characteristic taxa of clusters defined by CONISS.

The proportion of agglutinated species falls to accessory levels in cluster B, with *Ammonia beccarii* and *Haynesina* sp. contributing the majority of the assemblage. No other species

reaches accessory levels in more than a single sample. N_2 scores are correspondingly low, with a cluster average of 3.6.

Cluster C exhibits a similar effective number of species per sample to cluster A, with a mean of 9.6. Again *Ammonia beccarii* dominates, with *Ammobaculites formosensis*, *Haynesina* sp. and *Haplophragmoides* sp. all attaining common levels in more than one sample. Calcareous taxa constitute 60 to 80 % of the total test count.

Cluster D exhibits a wide range of taxa, including *Quinqueloculina* spp., *Elphidium* spp., *Hanzawaia nipponica*, *Florilus scaphus*, *Nonionella stella* and *Pararotalia nipponica*. No single taxon reaches values of greater than 20 % in this area and between 10 and 25 % of the total count for each sample consists of agglutinated taxa (predominantly *Ammobaculites formosensis*, *Sigmoilopsis* spp. and *Trochammina globigeriniformis*). N_2 values are correspondingly high, exceeding 30 effective species per sample for the majority of samples.

Species diversity is slightly lower in cluster E than cluster D, with N_2 averaging 20. *Ammonia beccarii* returns to common or dominant levels, alongside similar abundances of *Rotalinoides annectens*. *Quinqueloculina* spp., particularly *Q. akneriana*, *Q. lamarckiana* and *Q. seminula*, and *Elphidium* spp., including *E. advenum* and *E. hispidulum* attain accessory or common levels. Agglutinated taxa also form a small proportion of the assemblage.

5.1.3 Unconstrained ordination to validate cluster analysis

Ordination methods characterise the major trends in a multidimensional dataset through the extraction of new principal axes which encapsulate the greatest proportion of variability in the data with the minimum distortion to the spatial relationships between data points (Birks, 1995; Legendre and Legendre, 1998; Lepš and Šmilauer, 2003). Describing the data set in such a way can provide information on the relationships between samples and can, in doing so, highlight groupings which occur within the data, supplementing the use of cluster analysis (Kovach, 1995).

Ordination models may be classified as linear or unimodal on the basis of the model of species' response used (Birks, 1995; Lepš and Šmilauer, 2003). While linear models assume a species responds in a linear fashion to an environmental gradient, unimodal models assume

the distribution follows a Gaussian curve, centred on an environmental optimum (Gauch and Whittaker, 1972). Clearly both models are simplified simulations of more complex real distributions. The linear model performs better in situations where the environmental gradient is short in comparison to the species response and the unimodal model in situations where the environmental gradient is long (Birks, 1995; ter Braak, 1996). Choice of model is undertaken after analysis of the gradient of the first axis after Detrended Correspondence Analysis (DCA) of the data set (Birks, 1995; Lepš and Šmilauer, 2003). A threshold of 2 standard deviation (SD) units is used to determine the appropriate model (Birks, 1995). As DCA of the contemporary dataset provides a first axis gradient of 2.97 SD units, Correspondence Analysis (CA; Benzécri, 1973), a unimodal method, is selected over linear Principal Components Analysis (PCA; Pearson, 1901).

Correspondence Analysis is potentially vulnerable to arch effects (figure 5.2); where dissimilar samples at opposite ends of an ecological gradient may be plotted close together and the distances between samples at the extremes of the gradient may be condensed. Detrending the results of CA (Detrended Correspondence Analysis; DCA; Hill and Gauch, 1980) through segmentation of the first axis and equalization of the mean values of samples within each segment rectifies these issues (Kovach, 1995; Hammer *et al.*, 2001).

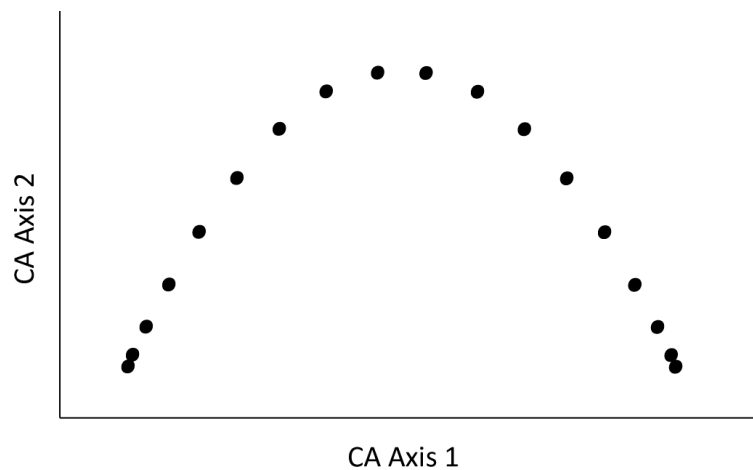


Figure 5.2: Scatter plot of sample scores on the first two axes following Correspondence Analysis of an ideal dataset (for each successive sample a previously occurring taxon is no longer present and a new taxon is introduced), showing the arch effect and compression of distances between samples at the extremes of the gradient (after Birks, 1995).

Division between samples on the basis of sample scores on the first three extracted DCA axes supports the clustering of data suggested by CONISS (figure 5.3). Samples contributing to cluster B are characterised by low DCA axis 1 sample scores, separating them from the

rest of the dataset (figure 5.3a). Clusters D and E are also distinguished by axis 1 sample scores, with cluster E additionally showing higher axis 2 scores. The distribution of scores on axes 1 and 2 does not distinguish between samples classified as clusters A and C, suggesting similarity between the principal components of the clusters. Division between the clusters is seen to some extent in the distribution of sample scores on axis 3 (figure 5.3b).

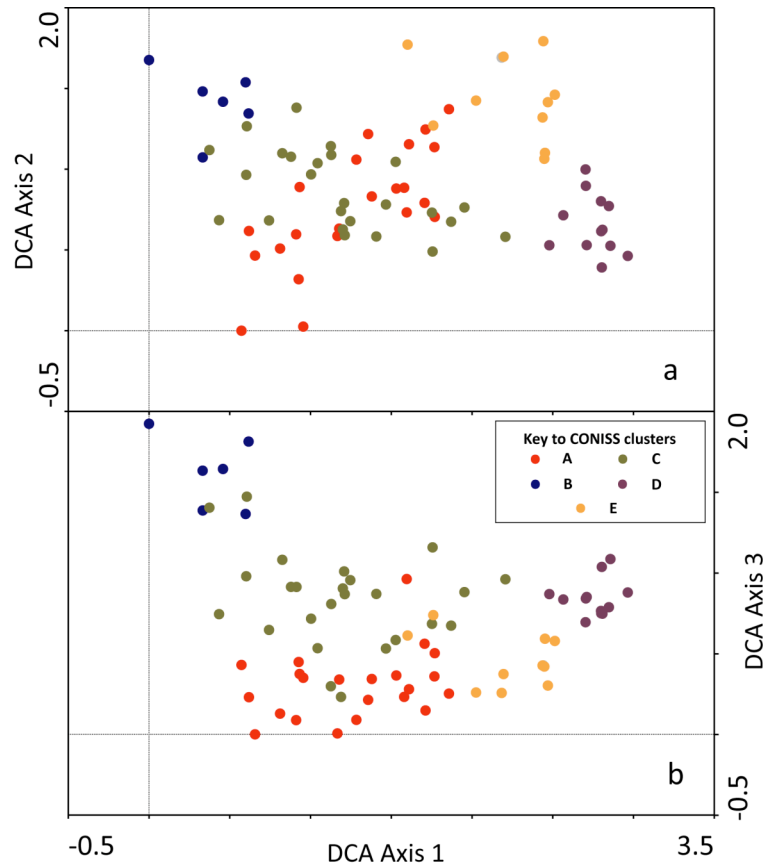


Figure 5.3: Detrended Correspondence Analysis sample scores for contemporary samples on (a) axes 1 and 2 and (b) axes 1 and 3. Samples are coloured according to clusters inferred from CONISS.

Neither method of grouping contemporary samples suggests that truly distinct clusters of samples are seen. Variation between clusters is not discrete and assemblages are characterised by gradual change, rather than complete replacement of their constituent taxa. The five clusters are not defined in terms of specific assemblage zones (c.f. Wang, 1985c; Li and Yim, 1988; Huang and Yim, 1998) due to the gradual changes and shared components, however division of the dataset into five clusters, each with a range of characteristic species (table 5.2), does assist comparison with published literature and interpretation of the fossil dataset.

5.1.4 Spatial distribution of clusters and foraminiferal taxa

While some overlap between areas is seen, particularly in the centre of the estuary, the clusters inferred from CONISS and DCA show a relatively coherent spatial distribution (figure 5.4). Cluster A is relatively widely distributed, with several samples located close to Macau in the southwest of the estuary and a number of samples within 15km of Neilingding Island. A single sample taken from the Humen gate of the Pearl River (PE 14) is also classified as belonging to cluster A. Considerable overlap is seen between cluster A and cluster C, which occupies much of the western half of the estuary. Samples from cluster C are found to both the north and south of Qi'ao Island, with four samples located to the south of or level with Macau. In the north of the estuary there is some overlap between clusters C and B. Samples contributing to the latter are generally located close to the Jiaomen and Hongqimen gates of the Pearl River, with one sample close to the northern shoreline of Qi'ao Island. Cluster E is located in an area to the north of Lantau, with four samples north of Neilingding Island. Overlap is again seen with cluster A. Cluster D represents the most spatially distinct group, with little overlap with other clusters. Samples are located to the south and east of Hong Kong and between Hong Kong and Lantau.

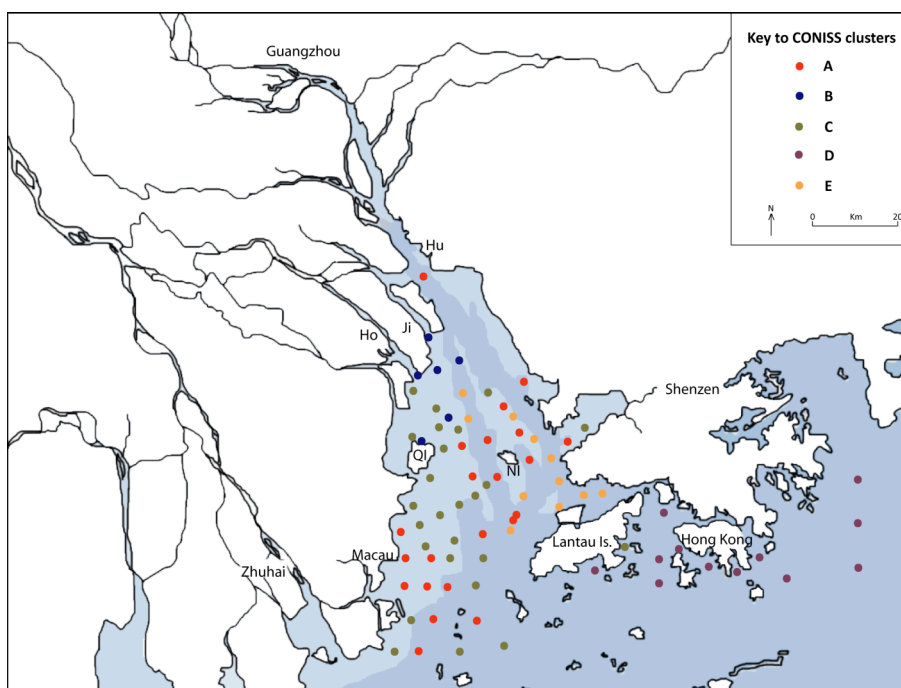


Figure 5.4: Contemporary clusters inferred from results of stratigraphically unconstrained CONISS and Detrended Correspondence Analysis (NI: Neilingding Island; QI: Qi'ao Island; Hu: Humen gate; Ji: Jiaomen gate; Ho: Hongqimen gate).

The overall trend in species diversity, as measured by N_2 , is an increase from the inner to the outer estuary. The lowest diversities are found in the shallow, low salinity waters of the inner estuary, suggesting that few species can occupy this specialist niche. Increasing water depth and salinity with distance from the gates of the Pearl River is accompanied by increasing N_2 . The highest species diversities are found to the west and east of Hong Kong in samples PE 25 and 33 (figure 5.5). A slight decline is seen to the east in samples PE 21 to 23.

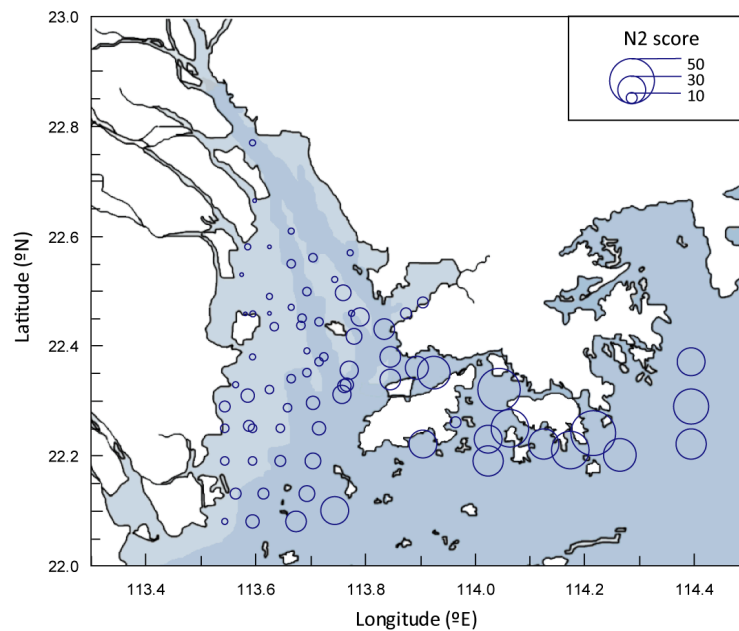
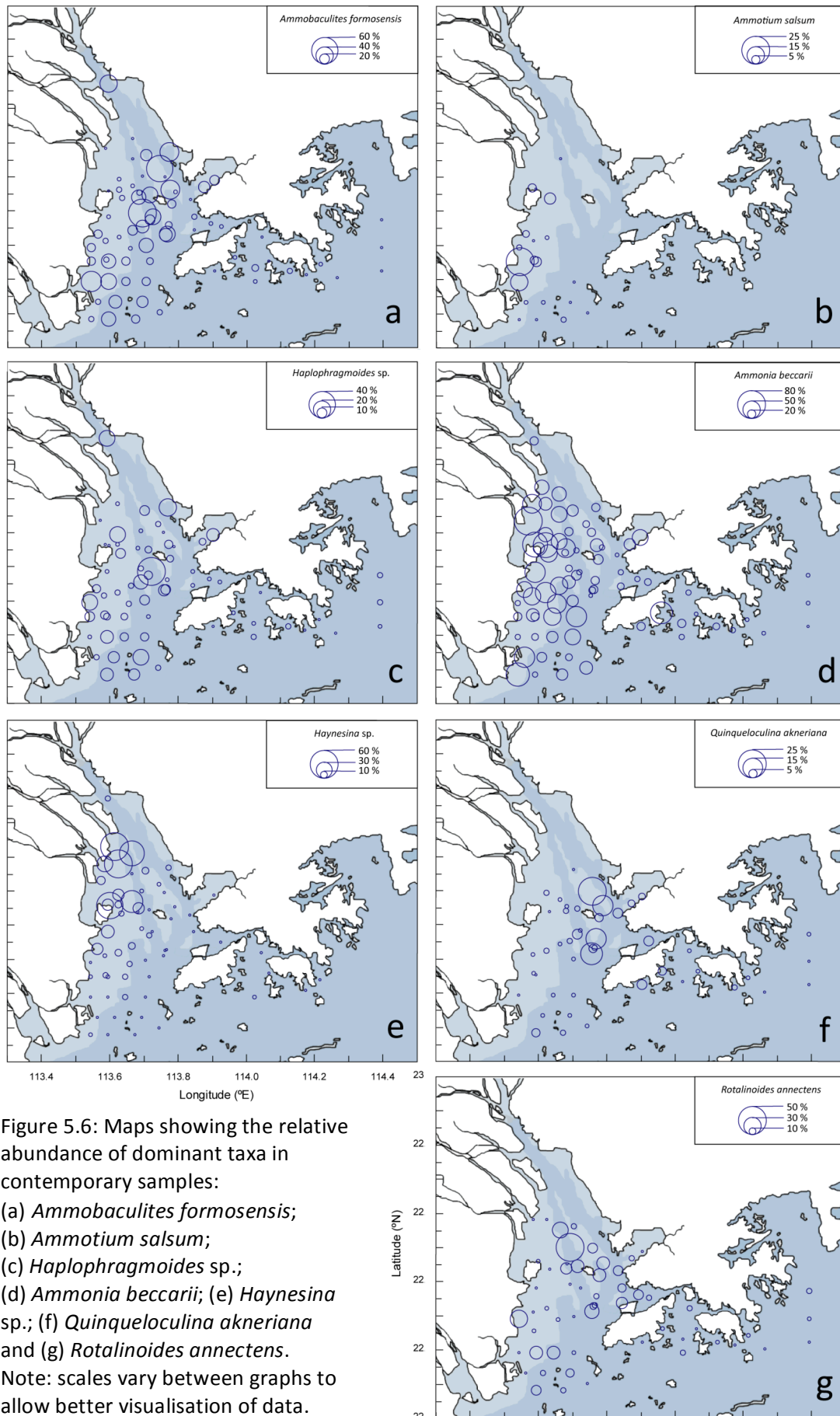


Figure 5.5: Distribution of contemporary sample N_2 scores.

Further information on the distribution of contemporary foraminifera can be gained through mapping relative abundances of individual taxa (figure 5.6). The highest proportions of agglutinated taxa, including *Ammobaculites formosensis* (figure 5.6a), *Ammotium salsum* (figure 5.6b) and *Haplophragmoides* sp. (figure 5.6c) are found in the centre of the estuary between the northeast of Neilingding Island and Macau. Relative abundances are lower in the shallow, low salinity waters of the northwest and the deep, saline waters of the southeast. Debenay and Luan (2006) suggests that, as a consequence of low salinity, low pH and reduced availability of calcium carbonate, agglutinated taxa are generally indicative of higher fluvial influence than calcareous taxa. Furthermore, the authors list *A. formosensis*, *Haplophragmoides wilberti* and *Ammotium* cf. *salsum* as indicative of very high fluvial influence in the Mekong delta, Vietnam. Wang *et al.* (1985a) similarly suggest an optimum for *Haplophragmoides canariensis* of below 10 psu in estuaries of the East China and Yellow Seas. The distribution of agglutinated and calcareous tests does not follow as simple a pattern in the Pearl River estuary, with a number of hyaline species, including *Haynesina* sp. and *Ammonia beccarii*, characterising the most brackish locations in the estuary.



The most abundant species in the estuary, *Ammonia beccarii*, shows a generally cosmopolitan distribution, although proportions are noticeably lower in the deep, high salinity areas of the inner shelf to the south and east of Hong Kong (figure 5.6d). The high relative abundances in the west of the estuary suggest a tolerance to low salinity environments. Murray (1991) identifies *A. beccarii* as the most widespread species in the western Pacific due to its broad tolerances to temperature and salinity. The species has been reported from a range of contemporary environments, from saltmarsh (e.g. Horton, 1999) and mangrove (e.g. Haslett, 2001; Horton *et al.*, 2003) to lagoon (e.g. Javaux and Scott, 2003; Serandrei Barbero *et al.*, 2004), estuarine (Yim and He, 1988; Huang and Yim, 1998) and shelf settings (Wang *et al.*, 1985a; Kumar and Manivannan, 2001) at numerous locations in the western Pacific and worldwide. The perceived near-global distribution of the species may result from the misidentification of a number of *Ammonia* spp. as *A. beccarii* (Hayward *et al.*, 2004). While it may provide some indication of the presence of brackish inner and middle estuary environments, the euryhaline nature of *A. beccarii* and broad tolerances to environmental variables may mean other species provide more constructive ecological information when fossil foraminifera are used to reconstruct past environments.

Haynesina sp. exhibits perhaps the most spatially distinct distribution, concentrated in the northwest of the estuary around the Jiaomen and Hongqimen gates of the Pearl River (figure 5.6e). The strong preference for low salinity environments observed here is supported by contemporary samples from brackish locations in the Yellow Sea (Xiang *et al.*, 2008), Nanlijiang estuary (Wang *et al.*, 1985d) and estuaries of the Bo hai (Wang *et al.*, 1985d; Wang and Bian, 1985).

Quinqueloculina akneriana constitutes a minor or accessory species in the majority of contemporary samples. Common or dominant levels are, however, reached in four samples from around Neilingding Island (figure 5.6f), suggesting a preference for intermediate salinities and water depths. Abundances are highly variable, with adjacent samples characterised by widely different proportions of the species. Huang (2000) identifies a similar area of the estuary as characterised by between 5 and 50 % porcelaneous forms and, although *Q. akneriana* is not recognised, *Q. lamarckiana* and *Q. seminulum* are listed as common components. While porcelaneous taxa are not frequently encountered in the northern South China Sea (Waller, 1960; Wang *et al.*, 1985c; Saidova, 2007) or Bo hai (Wang and Bian, 1985), Wang *et al.* (1985b) and Xue *et al.* (1995) identify a *Quinqueloculina*

akneriana rotunda assemblage, with significant *A. beccarii*, as characteristic of the subaqueous delta of the Yellow river, with annual average salinities of less than 31 psu.

The highest proportions of *Rotalinoides annectens* are found in the centre of the estuary, particularly around Neilingding Island (figure 5.6g). A second cluster of samples exhibiting higher than average abundances is seen in the southwest of the estuary, close to Macau. The species is not encountered extensively in the published literature, however Huang (2000) also identifies *Rotalidium annectens* (= *Rotalinoides annectens*) as an estuarine to marine species in the Pearl River estuary. Although the species shares morphological similarities with *Pseudorotalia gaimardii*, the distribution of *R. annectens* found here suggests a greater affinity for estuarine environments than the more marine distribution of *P. gaimardii* (Zheng, 1994, in Huang, 2000).

The distributions of a number of other common taxa show links with fluvial discharge. The proportions of *Hanzawaia nipponica*, *Pararotalia nipponica*, *Florilus scaphus* and *Elphidium advenum* are observed to increase with increasing distance from the gates of the Pearl River. Huang and Yim (1998) attribute a broad range to the latter species, suggesting a distribution from the middle estuary to the outer shelf adjacent to the Pearl River estuary. While *E. advenum* exhibits a generally marine distribution, *E. hispidulum* constitutes the majority of the total *Elphidium* count in the inner and middle estuary, suggesting a greater tolerance to brackish conditions. Huang (2000) suggests *E. hispidulum* is found between 17 and 30 psu in estuarine to marine settings of the Pearl River estuary. Similarly Wang *et al.* (1985a) lists the species as characteristic of littoral areas of Zhejiang province, with salinities in the region of 24 to 33 psu.

5.1.5 Comparison with published studies on Pearl River estuary foraminifera

Literature detailing the contemporary distribution of foraminifera in the Pearl River is reviewed in section 2.3.2 and summarised in table 2.1. General consensus is seen between the literature and data reported here. As Wang (1980) and Huang and Yim (1998) suggest, the sediments of the Pearl River estuary are dominated by hyaline planispiral and trochospiral forms, with *Ammonia beccarii* contributing significantly to assemblages. The occurrence of an area of agglutinated taxa in the centre of the estuary is supported by Li (1988), Huang and Yim (1998) and by data presented here. *Ammobaculites formosensis*, *A.*

sp. and *Haplophragmoides* spp. are the dominant species, with *Ammotium salsum* and *Textularia* spp. frequently occurring (Li, 1988; this study) and *Bigenerina* spp. and *Spiroplectammina biformis* also present (Li, 1988; Huang and Yim, 1998; Huang, 2000 and references therein). Outer estuary assemblages show extensive similarities with those reported by Wang (1980), Huang and Yim (1998) and Saidova (2007), with *Ammonia* spp., *Hanzawaia nipponica*, *Textularia foliacea*, *Quinqueloculina* spp. and *Elphidium* spp. significant components of assemblages.

A number of differences are apparent, as would be expected between studies of differing spatial resolution and sample location. *Elphidium nakanokawaense*, a major inner estuary species in the investigations of Huang and Yim (1998) and references therein, was not encountered in this study. Conversely *Haynesina* sp., identified as abundant in the same inner estuary setting, was not mentioned in the cited literature. Differences between the datasets are thought to arise from a wide range of sources including sample location, sampling resolution, depth of sediment recovered, time of year, changes in assemblages between investigations, laboratory methods for foraminiferal preparation and taxonomy.

5.2 Factors affecting the distribution of contemporary foraminifera

5.2.1 Environmental variables

A range of environmental variables was measured for each of the modern sampling locations. Summary environmental data for the 5 clusters are presented in table 5.3. Appendix 5.3 provides data for all 76 surface samples with greater than 50 tests counted.

Cluster	Mean salinity (psu)	Water depth (m)	TOC (%)	TN (%)	C/N	$\delta^{13}\text{C}$ (‰)	Sand (%)	Clay (%)	Silt (%)
A	24.3	7.2	1.07	0.10	10.27	-23.13	18.08	29.14	52.78
B	10.5	6.3	1.05	0.09	12.23	-23.76	22.77	20.38	56.83
C	20.1	9.0	1.17	0.11	10.88	-23.16	17.63	27.14	55.23
D	33.0	20.0	0.82	0.10	8.01	-21.87	15.15	22.10	62.73
E	28.3	10.7	0.71	0.05	11.77	-23.76	27.54	23.31	49.12

Table 5.3: Average environmental variables for surface sample clusters. Note: missing total organic carbon data affects TOC and C/N averages for clusters A (6/23 samples), C (3/26 samples) and E (4/12 samples). Missing $\delta^{13}\text{C}$ data affects averages for clusters A (6/23 samples), B (1/6 samples) C (3/26 samples) and E (4/12 samples).

Clear differences can be seen in the mean salinities of each cluster (figure 5.7a). Cluster B, located closest to the gates of the Pearl River, exhibits the lowest salinity values. An increase in mean salinity is seen with increasing distance from the freshwater source, with clusters C and A averaging 20.1 and 24.3 psu respectively. The highest salinity values are found in clusters D and E, with the former showing a relatively small range of mean salinity values around an average of 33.0 psu. The spatial variation in salinity values (figure 5.8a) provides further support for the salinity of sample sites being strongly controlled by their location with respect to the gates of the Pearl River.

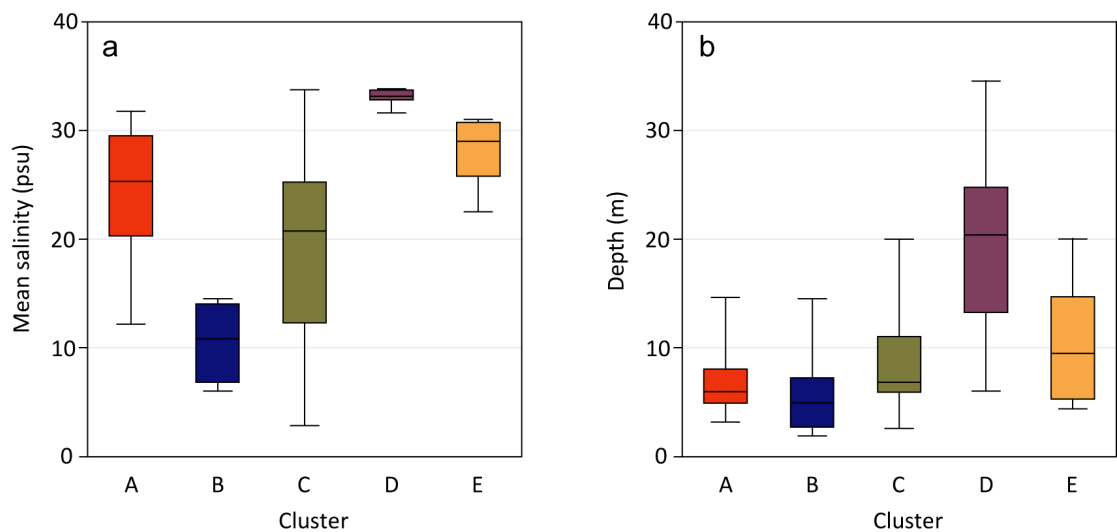


Figure 5.7: Box plots (minimum, Q₁, median, Q₃ and maximum values) of (a) mean salinity and (b) depth data for clusters A to E.

Depth measurements show a similar pattern to mean salinity measurements, with a general increase from the northwest to the southeast (figure 5.8b). Cluster D exhibits the greatest median and maximum depths (figure 5.7b), with clusters E and C intermediate and A and B shallowest. The correlation between depth and mean salinity and between other environmental variables is analysed in section 5.2.2.

Total organic carbon and total nitrogen show a more complex pattern which cannot be attributed to fluvial influence alone (figures 5.8c, d). The percentage of total organic carbon does exhibit a decline with distance from the terrestrial source, however a number of samples from the northwest show relatively low percentages, while one sample from southwest of Hong Kong exhibits a much higher value. Total nitrogen is relatively stable between clusters, with the exception of cluster E, which is characterised by significantly lower values. If this was related to the reduced input of nitrogen from fibrous plants due to

distance from the freshwater source, cluster D would be expected to show similarly low or even lower values. $\delta^{13}\text{C}$ values (Yu, 2009) are generally less negative with increasing distance from the Pearl River (figure 5.8e). Cluster E does not conform with this trend, with the average value suggesting significant terrestrial influence (Bender, 1971; Lamb *et al.*, 2006). This may be explained by a localised area of low aquatic productivity or discharge of terrestrial C_3 plants and freshwater plankton from streams in the east of the estuary.

Particle size data again appears to be linked to proximity to the Pearl River. The sand sized fraction is highest in abundance in the northwest (figure 5.8f), with cluster B exhibiting a high average proportion. Cluster E, however, is characterised by the highest proportion of sand, perhaps suggesting increased current velocity through the restricted channels around Lantau and Neilingding Islands. Clusters A and C, located further from the source of fluvially transported sediment than cluster B, show decreased sand and elevated clay percentages, while cluster D, furthest removed from the Pearl River, exhibits the highest fraction of silt.

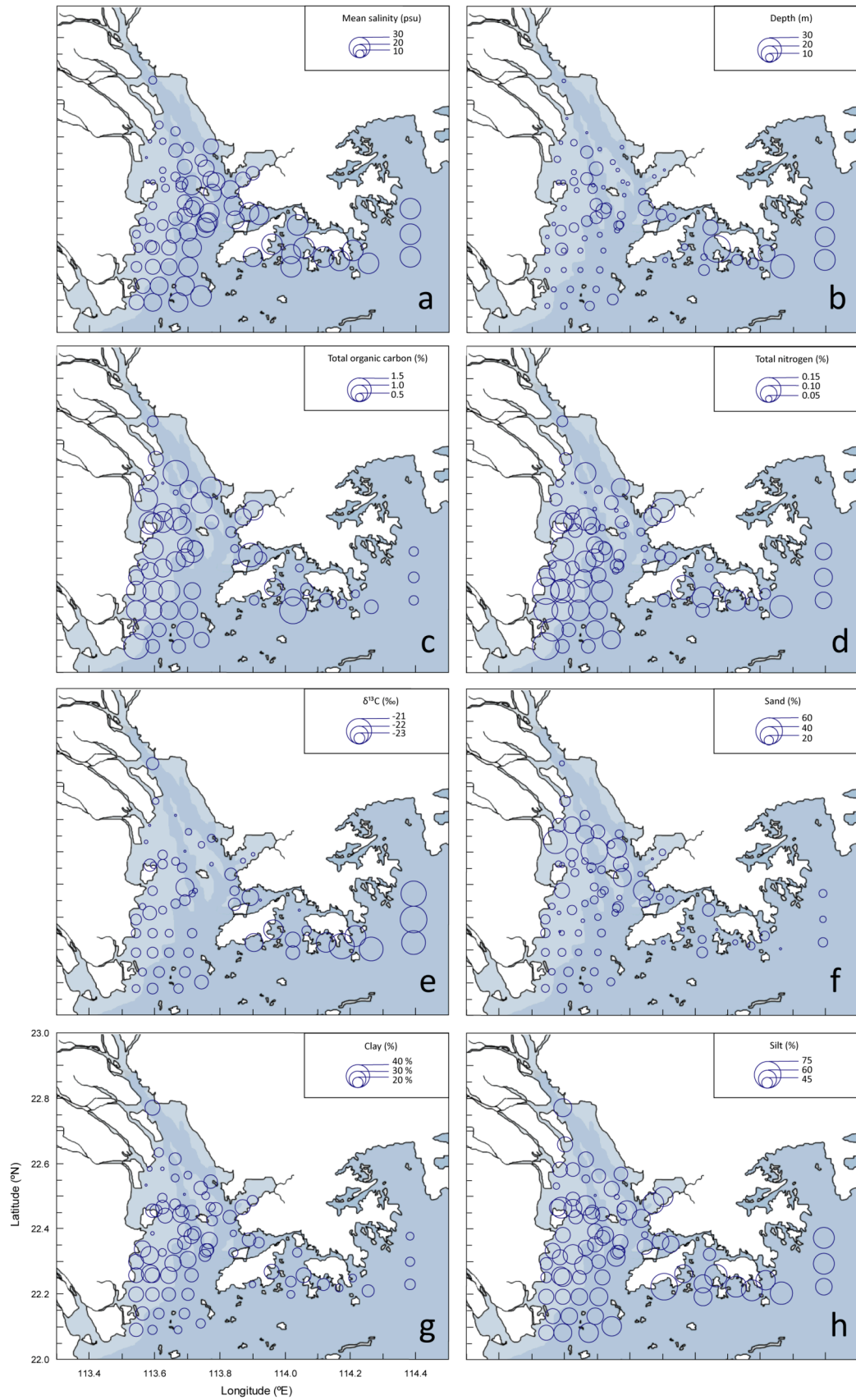


Figure 5.8: Distribution of environmental variables: (a) mean salinity; (b) depth; (c) total organic carbon; (d) total nitrogen; (e) $\delta^{13}\text{C}$; (f) sand; (g) clay; (h) silt. Note: in $\delta^{13}\text{C}$ plot, sample PE 60 ($\delta^{13}\text{C} = -27\text{‰}$) is not plotted to allow variability in the dataset to be better visualised.

5.2.2 Constrained ordination to investigate the influence of environmental variables

While indirect ordination methods (section 5.1.3) optimize the variance explained by each axis, direct ordination methods are constrained to linear combinations of environmental variables, maximizing variance on given environmental gradients (Legendre and Legendre, 1998). Canonical Correspondence Analysis (CCA; ter Braak, 1986), a constrained version of Correspondence Analysis, allows simultaneous analysis of the faunal and environmental data. CCA is chosen over linear methods, such as Redundancy Analysis, as the gradient of the first DCCA axis suggests unimodal methods best describe the response of species to environmental gradients. Partial CCAs, obtained in CANOCO version 4.55 (ter Braak, 2006) by constraining the ordination by a single environmental variable, describe the variance in the dataset explained by the chosen variable.

The nine environmental variables outlined in section 5.2.1 explain 37.9 % of the variance in the contemporary foraminiferal dataset (figure 5.9a). Partial CCAs suggests mean salinity alone accounts for 16.9 % of the variance, equivalent to 20.5 % of the total explained variance when autocorrelation between variables is taken into account (table 5.4; figure 5.9b). The length of each vector is proportional to the explained variance along each given axis. The close alignment of the salinity vector with the first extracted axis (figure 5.10) and the correspondingly high correlation between salinity and axis 1 ($r = -0.90$; table 5.5) confirm mean salinity as the most important variable in explaining variability in the faunal data.

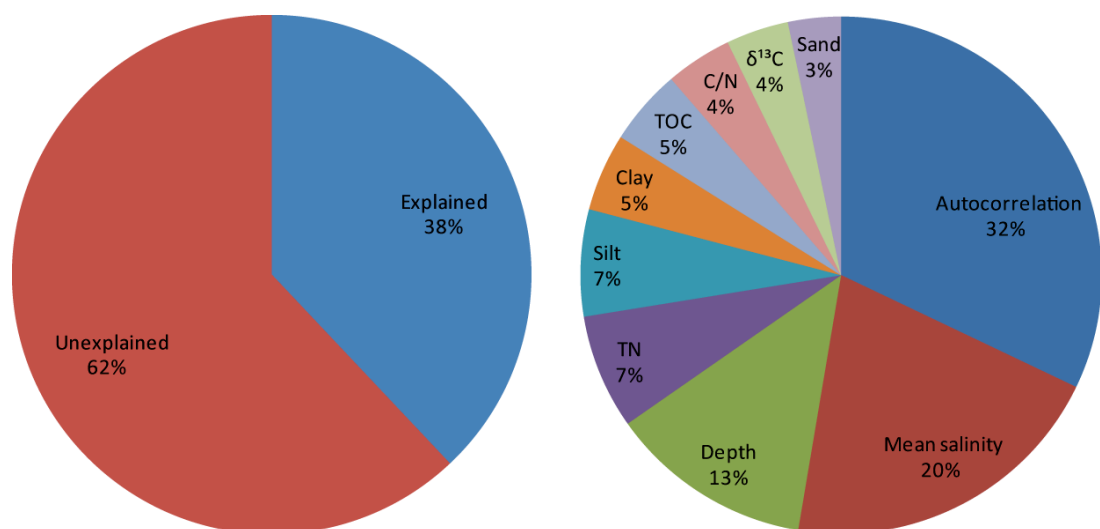


Figure 5.9: Pie charts showing the total variation in the contemporary fauna divided into (a) explained and unexplained sectors and (b) the total explained variance divided into sectors representing the individual environmental variables and interactions between variables.

Environmental variable	% of variance in species data explained	Estimated p value	λ_1	λ_1/λ_2
Mean salinity (psu)	16.9	0.001	0.290	1.429
Depth (m)	10.4	0.001	0.179	0.617
Total Nitrogen (%)	5.9	0.001	0.101	0.262
Silt (%)	5.5	0.001	0.094	0.263
Clay (%)	4.0	0.002	0.068	0.183
Total Organic Carbon (%)	3.9	0.003	0.067	0.176
Carbon / Nitrogen	3.4	0.005	0.058	0.151
$\delta^{13}\text{C}$ (‰)	3.2	0.008	0.054	0.136
Sand (%)	2.7	0.022	0.046	0.117

Table 5.4: Results of partial Canonical Correspondence Analysis (following square root transformation of species data). λ_1 : eigenvalue of axis 1; λ_1/λ_2 : ratio of eigenvalues for axes 1 and 2.

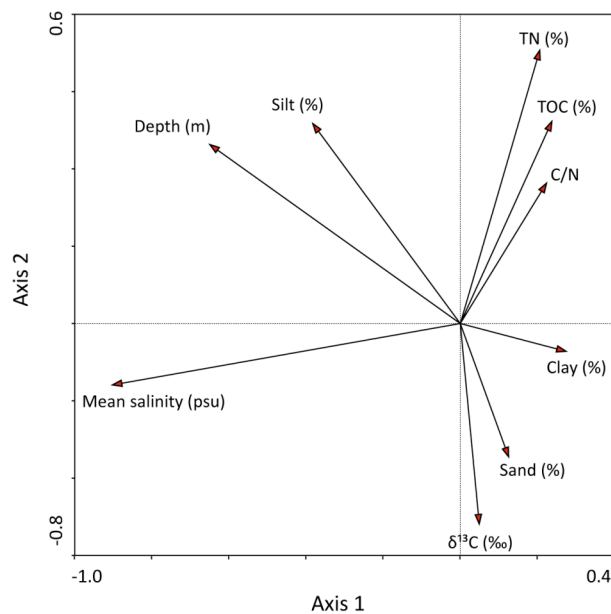


Figure 5.10: Relationship between environmental variables analysed using CCA.

While mean salinity explains a significant proportion of the variability on axis 1, total nitrogen is most important in explaining variation on the second axis, with $\delta^{13}\text{C}$, total organic carbon and depth also contributing. The correlation between mean salinity and depth ($r = 0.46$; table 5.5) suggests that, as expected, the variables do not vary independently. Mean salinity and depth both increase with increasing distance from the Pearl River. The correlation between silt and depth ($r = 0.24$) conforms with the mapped distributions of the variables (figure 5.8) in suggesting a decrease in particle size with distance from the Pearl River. A negative relationship between salinity and C/N ($r = -0.28$) suggests decreasing C/N with increasing marine influence.

	Salinity (psu)	Depth (m)	TOC (%)	TN (%)	C/N	$\delta^{13}\text{C}$ (‰)	Sand (%)	Clay (%)	Silt (%)
CCA Axis 1	-0.90	-0.65	0.24	0.21	0.22	0.05	0.13	0.27	-0.38
CCA Axis 2	0.16	-0.46	-0.52	-0.71	-0.36	0.52	0.34	0.07	-0.52
Mean Salinity (psu)	1								
Depth (m)	0.46	1							
TOC (%)	-0.21	-0.01	1						
TN (%)	-0.10	0.02	0.59	1					
C/N	-0.28	0.03	0.78	0.13	1				
$\delta^{13}\text{C}$ (‰)	0.04	-0.19	-0.82	-0.34	-0.90	1			
Sand (%)	-0.15	-0.10	-0.10	-0.51	0.22	-0.02	1		
Clay (%)	-0.11	-0.14	-0.08	0.39	-0.37	0.28	-0.67	1	
Silt (%)	0.28	0.24	0.20	0.38	0.00	-0.20	-0.81	0.10	1

Table 5.5: Canonical Correspondence Analysis correlation matrix for environmental variables and the first two extracted CCA axes.

When analysed individually the significance level of all nine variables exceeds $p = 0.05$ (table 5.4), however if manual forward selection is applied using Bonferroni corrections only five variables are needed to form the minimum significant model (figure 5.11). The addition of further variables does not significantly contribute to the description of species variability. Together mean salinity, total nitrogen, depth, clay percentage and sand percentage explain 30.8 % of the variance in the species data.

The biplot of sample scores and environmental vectors (figure 5.11) supports the environmental cluster averages in suggesting that samples from cluster D are characterised by the highest salinities and deepest water depths, followed by cluster E, then clusters A and C, with cluster B the least saline and shallowest. The high proportion of sand and low total nitrogen in samples from cluster E account for their relatively low axis 2 scores, at the positive end of the sand vector and the negative end of the total nitrogen vector. Low sand percentages explain the positive axis 2 scores shown by cluster D.

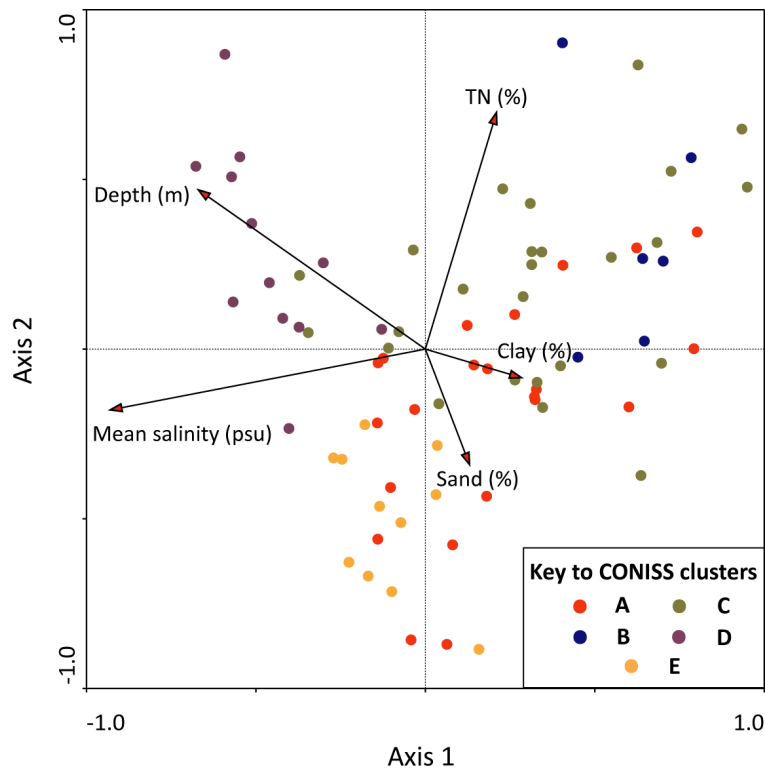


Figure 5.11: Biplot of Canonical Correspondence Analysis sample scores and the minimum adequate model of environmental variables. Samples are represented by circles coloured according to clusters defined in section 5.1.

A biplot of species scores and environmental vectors (figure 5.12) allows the ecological preferences of individual taxa to be interpreted (Kovach, 1995; ter Braak and Šmilauer, 2002). The distribution of species scores along the first axis principally shows their tolerance to salinity and water depth. Negative axis 1 sample scores suggest *Pararotalia nipponica*, *Hanzawaia nipponica*, and *Elphidium advenum* are found in high salinity areas. A range of taxa, including *Quinqueloculina* spp., *Rotalinoides annectens* and *Spiroloculina lucida*, prefer intermediate salinity areas, with *Cribrononion subincertum*, agglutinated taxa, *Ammonia beccarii* and *Haynesina* sp. found in progressively less saline areas. The agglutinated species *Ammobaculites formosensis*, *Ammobaculites* sp. and *Haplophragmoides* sp. show a close affinity to the clay vector, suggesting a preference for substrates of intermediate particle size.

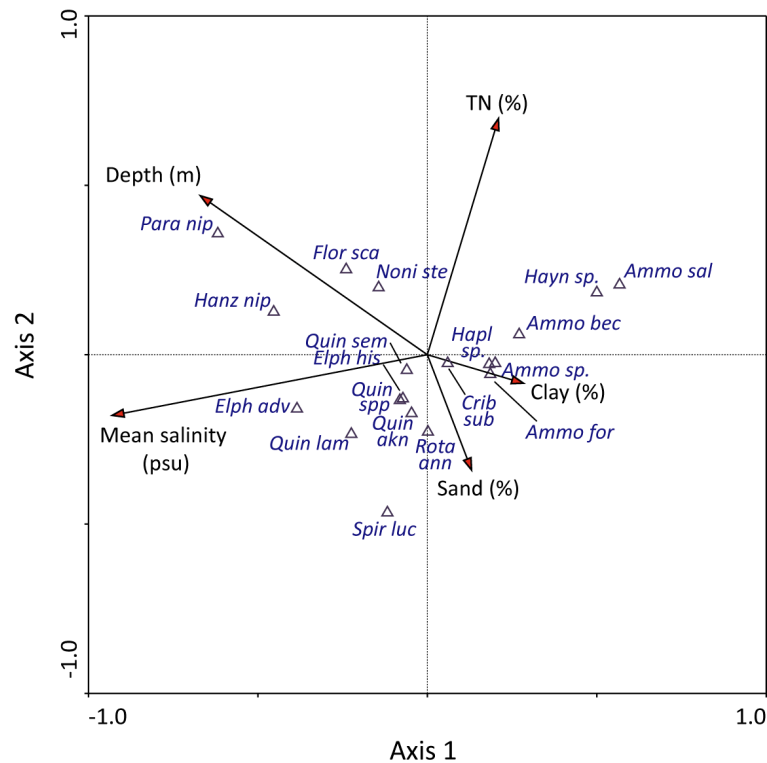


Figure 5.12: Biplot of Canonical Correspondence Analysis species scores and environmental vectors on axes 1 and 2. See appendix 5.4 for species codes.

While the recorded environmental variables explain 38% of the total variation in the contemporary data, 62 % remains unaccounted for (figure 5.9a). This percentage is in line with a number of other investigations into factors affecting the contemporary distribution of marine microfossils (e.g. Zong and Horton, 1999; Zong *et al.*, submitted b) and substantially better than for some other ecological datasets with a large number of samples with many zero values (e.g. Gasse *et al.*, 1995). This unexplained variance may arise from a combination of the contribution of other environmental factors not quantified here, issues inherent in the sampling and counting method resulting in inaccuracies in the recorded assemblages and stochastic processes affecting foraminiferal distributions. Environmental variables not quantified include temperature, calcium carbonate availability, pH and dissolved oxygen concentration, as well as ecological factors such as competition and predation.

In this study the use of a sampling strategy incorporating multiple samples from areas of similar mean salinity captures variation in assemblages across as well as along the main observed gradient. Sampling strategies based on transects have been widely adopted in reconstructions of palaeoenvironments, particularly in investigations of sea level (e.g. Horton *et al.*, 1999; Edwards *et al.*, 2004; Hamilton and Shennan, 2005), but also in studies

of estuarine salinity (e.g. Hassan *et al.*, 2009). These strategies serve to artificially reduce variation in assemblage composition independent of the main environmental gradient of interest. Consequently the importance of particular environmental variables in controlling species distributions may be exaggerated and, when contemporary data are used in the reconstruction of past environmental change from microfossil data, the magnitude of errors may be underestimated.

5.2.3 Modelling species' response to the environment

The estimation of optimum environmental conditions for particular species, an essential component of quantitative reconstructions, is also valuable for qualitative palaeoenvironmental inferences. As ecological information on a large number of species found in Pearl River estuary samples is limited, establishing their ecological preferences assists in interpretation of the fossil record. While constrained ordination orders species along environmental gradients, precise estimates of their optima and tolerances cannot easily be extracted. They are, however, produced as part of Weighted Averaging in C2 version 1.5.0 (Juggins, 2003) and are presented for the 20 dominant or common species (figures 5.13, 5.14). Optima and tolerances are only presented for salinity and depth as other environmental variables do not exert as great an influence on foraminiferal assemblages.

Figure 5.13 suggests that the majority of species have relatively broad distributions with respect to salinity, with average tolerances of ± 6.0 psu for the 20 dominant or common taxa and 3.6 psu for the full dataset. Taxa with optima over 29 psu have an average tolerance of ± 2.5 psu, compared to ± 6.3 psu for species with optima less than 29 psu. These tolerances reflect a plateauing of salinity at approximately 34.5 psu for the open South China Sea (Su, 2004), decreased fluctuation in salinity and potentially the dominance of other factors in influencing the distribution of foraminifera in highly saline environments. At the low end of the gradient, species may exhibit wider tolerances to salinity due to more variable conditions in the inner estuary, both on daily and seasonal timescales. The possibility of species opportunistically migrating into areas while salinity conditions are favourable may also increase the perceived tolerance to salinity. A species could potentially contribute to the dead assemblage of a location not appropriately reflected by the corresponding mean salinity value. The broad tolerance to salinity has implications for quantitative

reconstructions, effectively increasing the error term associated with any reconstruction using the surface samples as a modern training set (Birks, 1995; 1998).

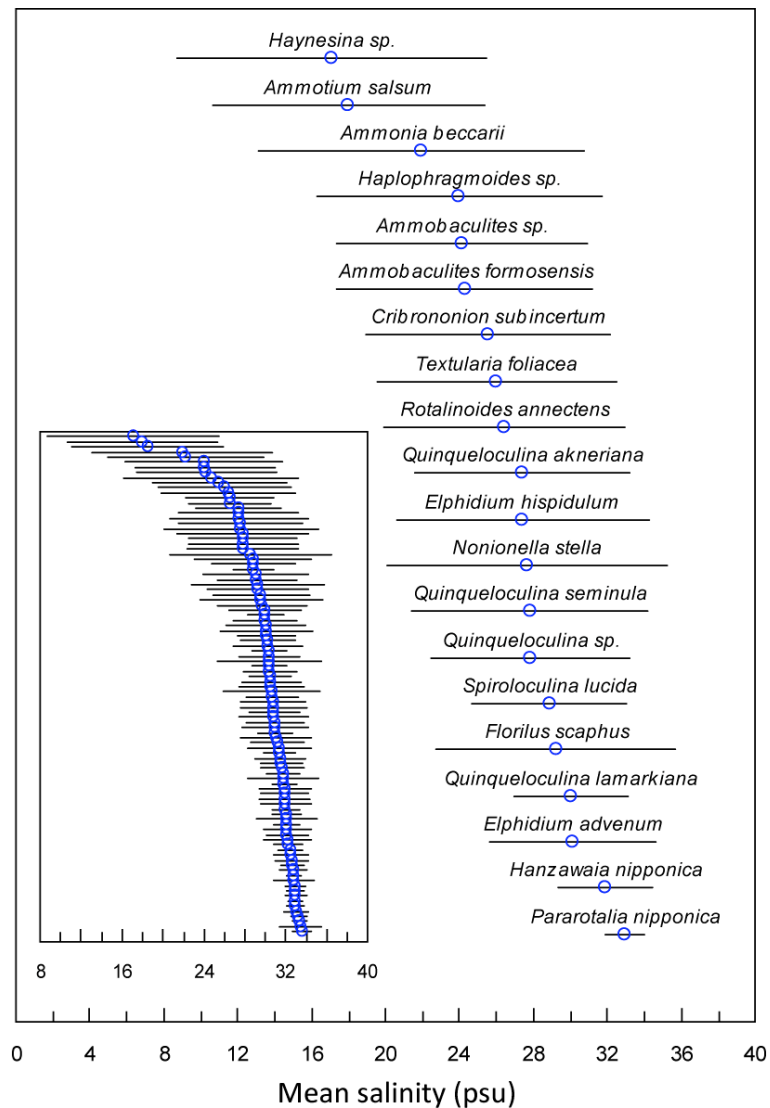


Figure 5.13: Bootstrapped salinity optima and tolerances of Pearl River estuary foraminifera from Weighted Averaging in C2 (Juggins, 2003). Main diagram shows dominant and common taxa, inset shows full dataset.

The depth optima and tolerance data (figure 5.14) suggests that the majority of species inhabit a wide range of depths, with an average tolerance of ± 7.4 m. A slight increase in average tolerance with increasing depth is observed. It must be stated that WA-derived optima and tolerances are estimates of real distributions and, as they are based on a unimodal model, may be biased if the entire range is not sampled. Weighted Averaging also assumes an equal distribution of samples with respect to the environmental parameter, a prerequisite not met by this or most other biological datasets.

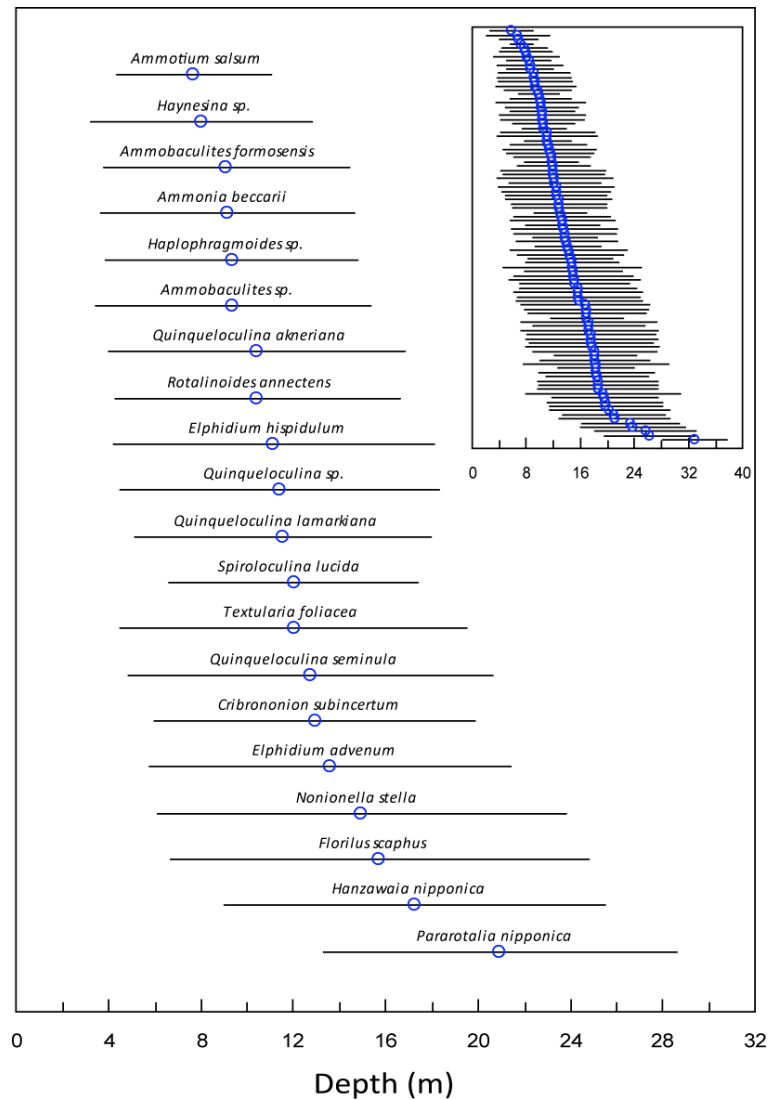


Figure 5.14 Bootstrapped depth optima and tolerances of Pearl River estuary foraminifera from Weighted Averaging in C2 (Juggins, 2003). Main diagram shows dominant and common taxa, inset shows full dataset.

5.3 Transfer function development

Rossi and Horton (2009) suggests that quantitative reconstructions of specific environmental variables have replaced qualitative palaeoenvironmental inferences. While this is clearly an overstatement, quantitative methods can, in certain circumstances, provide additional information inaccessible by qualitative investigations alone. Quantitative reconstructions of palaeoenvironmental variables from fossil assemblages rely on a comprehensive understanding of the contemporary relationship between foraminifera and the environmental variable of interest. Fossil assemblage data can then be transformed, using this modern training set, into quantitative estimates of past values of the selected variable. As mean salinity explains a significant amount of the variability in contemporary

foraminiferal assemblages and as the ratio of CCA eigenvalues for axes 1 and 2 is high (>0.5 ; table 5.4; Ng and Sin, 2003), salinity is the most suitable variable for the development of a transfer function. Autocorrelation between environmental variables accounts for 32% of the explained variance and it is assumed that the joint distribution of the variables with mean salinity is the same in the modern and fossil datasets (Birks, 1995).

Transfer functions use regression to express an environmental parameter as a function of a modern training set of biological data. A number of transfer function techniques have been developed, based on either linear or unimodal models of species response to the environment (see Birks, 1995; 1998; ter Braak, 1995 for reviews of techniques). Discrimination between linear and unimodal techniques is undertaken using the same criteria as for constrained ordination methods. As the eigenvalue of the first DCCA axis suggests that foraminifera are ordered along relatively long environmental gradients (Birks, 1998; section 5.2.2), unimodal models of species' response were selected. Transfer functions were consequently developed using Weighted Averaging (WA; ter Braak, 1987) and Weighted Averaging Partial Least Squares (WA-PLS; ter Braak and Juggins, 1993; ter Braak *et al.*, 1993).

WA regression uses the theory that a given sample will be characterised by taxa with an environmental optima close to the sample's environmental variable value. The taxon's environmental optimum is estimated through averaging the environmental values of all sites with the particular taxon, weighted by their relative abundances. WA calibration averages the relative abundance weighted optima of all taxa found in a sample to provide a quantitative estimate of the environmental variable (ter Braak and Juggins, 1993; Birks, 1995). Ter Braak and Juggins (1993) suggests that WA represents a modification of the first component of WA-PLS, with further components in the latter method extracted using residual structure in the species data to improve optima estimates. This not only improves the performance of calibration, but may also better represent the true nature of the dataset, where factors other than the primary variable of interest influence the distribution of species (ter Braak and Juggins, 1993; ter Braak *et al.*, 1993). The advantages of WA-PLS over WA are most significant in datasets with low noise (ter Braak and Juggins, 1993). WA-PLS also reduces, though does not eliminate, the influence of the edge effect (overestimation of optima at the low end of the gradient and underestimation at the high end) that affects WA (Birks, 1998).

5.3.1 Formation of the modern training set

Due to the increase in the magnitude of errors with decreasing total count size (Fatela and Taborda, 2002), all samples with total counts of less than 100 are removed from the modern training set, leaving a total of 63 samples. Following Jones and Juggins (1995) samples with a residual (predicted minus observed value) greater than the standard deviation of the training set mean salinity data are removed. Samples PE 66 and 67 exceed the threshold of 9.0 psu and are not included in the modern training set. Their high proportions of large tests of *Elphidium* spp., *Rotalinoides annectens* (PE 66) and *Quinqueloculina* spp. (PE 67) may suggest winnowing of smaller components of the assemblage. While a number of investigations remove rare taxa (e.g. <2 %; Jian *et al.*, 1999; Kim and Kucera, 2000; Hassan *et al.*, 2009; Zong *et al.*, submitted b), Birks (1998) argues that they contribute coherent information to the model, rather than having a negative effect by introducing random variation. Accordingly all taxa are included in transfer function development.

Two alternative modern training sets, consisting of (a) a transect of 25 samples and (b) 14 pseudosamples created by combining samples into 2.5 psu intervals, were also investigated (appendix 5.5). The transect was rejected as it resulted in reduced predictive ability. The pseudosamples increased predictive ability, however effective estimation of optima and tolerances depends on the use of a large modern training set (Birks, 1995; 1998), a demand not met by this training set. Consequently calibration of fossil assemblages is based on the full modern training set.

5.3.2 Transfer function performance

The predictive ability of WA and WA-PLS regression is assessed using the Root Mean Square Error of Prediction (RMSEP), the coefficient of determination (r^2), mean and maximum bias. These measures of the similarity between observed and predicted salinity values are obtained by bootstrapping, a method of resampling the original dataset to produce pseudoreplicate training sets. Regression and calibration of these bootstrapped training sets provides estimates of the environmental variable of interest for any samples not selected during bootstrapping (Manly and Chotkowski, 2006). Bootstrapping is chosen over jack-knifing as the preferred method of cross-validation as the latter does not provide sample

specific errors of prediction for each fossil sample and is more prone to bias (Birks, 1995). The cross validated coefficient of determination (r^2), mean and maximum bias and errors of prediction (RMSE components and RMSEP) for WA and WA-PLS are compared in table 5.6.

Name	r^2_{boot}	Average bias _{boot}	Max bias _{boot}	RMSE s_1	RMSE s_2	RMSEP
WA_Inv	0.82	-0.31	6.35	0.90	3.68	3.79
WA_Cla	0.82	-0.35	5.44	1.01	3.77	3.90
WATOL_Inv	0.78	-2.21	7.77	1.74	4.62	4.94
WATOL_Cla	0.78	-2.47	6.83	1.97	4.65	5.05
WA-PLS C1	0.82	-0.37	6.78	0.84	3.79	3.89
WA-PLS C2	0.88	-0.25	4.42	1.04	3.01	3.18
WA-PLS C3	0.88	-0.15	4.26	1.27	2.99	3.25
WA-PLS C4	0.87	-0.07	4.01	1.48	3.08	3.42
WA-PLS C5	0.87	0.01	4.10	1.60	3.14	3.52

Table 5.6: Comparison of transfer function components using the modern training set consisting of all samples with total counts >100, except samples PE 66 and 67. Abbreviations: WA = Weighted Averaging; WATOL = Weighted Averaging with tolerance downweighted; Inv = Inverse deshrinking; Cla = Classical deshrinking; WA-PLS = Weighted Averaging - Partial Least Squares; C = Component.

WA-PLS component 2 provides the best performance, with the lowest RMSEP, high r^2_{boot} and low average and maximum bias (figures 5.15a, 5.15b). A plot of residuals against observed mean salinity with a locally weighted scatterplot smooth (LOWESS; figure 5.15b), suggests the transfer function systematically overestimates by an average of 1 to 4 psu at observed mean salinities of less than 21 psu, with slight underestimation of mean salinity above 28 psu. This bias, a relatively common feature of WA-PLS (Jones and Birks, 2004), may be an artifact of the procedure by which model performance is assessed (Racca and Prairie, 2004). A scatterplot of residuals against predicted values (figure 5.16), as advocated by Racca and Prairie (2004), suggests overestimation between 10 and 24 psu and underestimation between 24 and 30 psu.

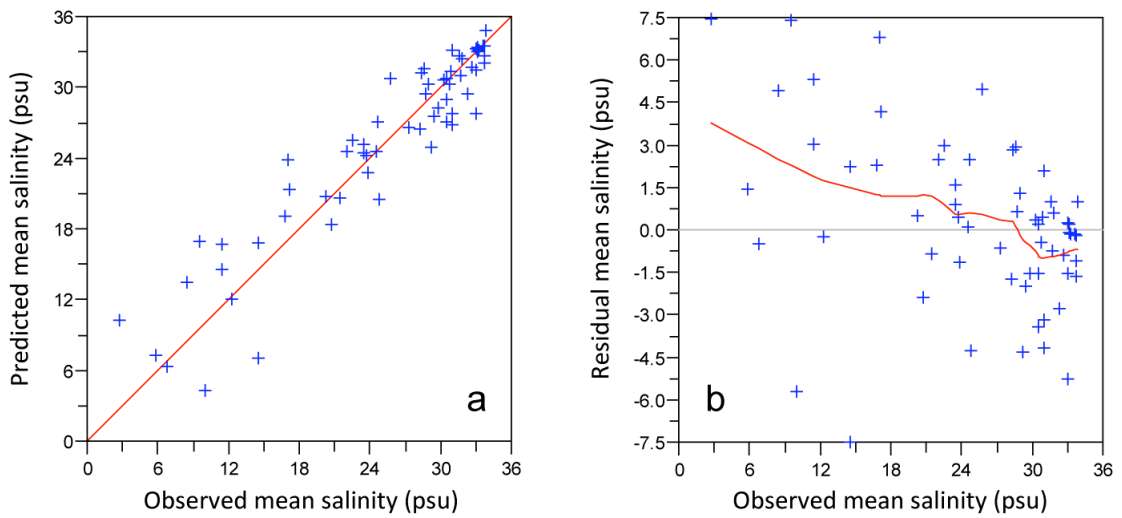


Figure 5.15: Performance of Weighted Averaging - Partial Least Squares component 2 using the reduced modern training set. (a) Observed vs. estimated mean salinity (b) Observed vs. residual (predicted - observed) mean salinity with LOWESS of span 0.45.

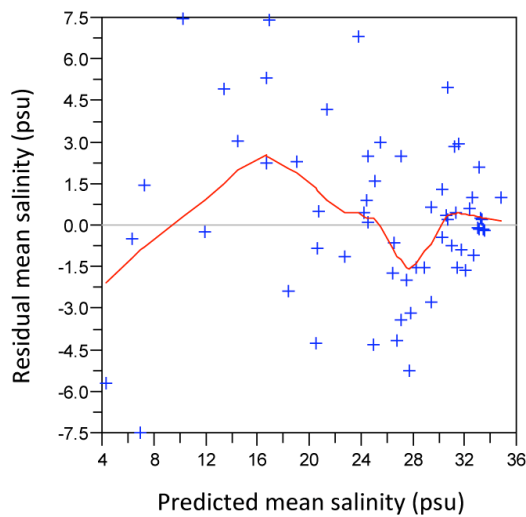


Figure 5.16: Weighted Averaging – Partial Least Squares residuals plotted against predicted mean salinity (psu) for the reduced dataset, with LOWESS of span 0.45.

5.3.3 Discussion of transfer function performance

Positive spatial autocorrelation, the tendency for proximal sites to resemble one another more than randomly selected sites, may result in over-optimistic evaluation of the predictive performance of the transfer function and may be exacerbated by the nature of the sampling strategy used in this investigation (Telford *et al.*, 2004; Telford and Birks, 2005; Zong *et al.*, submitted b). The RMSEP of 3.01 is, however, comparable with other estuarine salinity transfer functions (e.g. Hassan *et al.*, 2009; Zong *et al.*, submitted b), but must be compared

to the range of the reconstructed salinity values to provide meaningful analysis of the predictive potential of the transfer function.

Analysis of RMSE components may assist in explaining the magnitude of prediction errors (Birks, 1995). Estimation error in the optima and tolerances of taxa (RMSE s_1) contributes 10.7 % of the RMSEP of WA-PLS component 2, while the remaining 89.3 % is explained by variations in taxa abundance at a given environmental value (RMSE s_2). Optima and tolerance estimations may be biased if the sampling scheme does not incorporate the complete range of the species' distribution, with a shift away from the truncated tail (Lepš and Šmilauer, 2003). While the contribution of the s_1 component might be reduced through the use of more complex model of species' responses to the environment, possibly implemented using Artificial Neural Networks (e.g. Malmgren and Nordlund, 1997; Giraudel and Lek, 2001; Racca *et al.*, 2004), the majority of the prediction error is accounted for by the RMSE s_2 component. Variations in abundance of taxa at given environmental values are unsurprising given the nature of the sampling strategy. Multiple transects parallel with salinity isohales are likely to capture variability in assemblages independent of mean salinity.

5.4 Chapter summary

Contemporary foraminiferal assemblages in the Pearl River estuary show clear spatial variation, linked primarily to the magnitude of fluvial influence on the sample location. Mapping the distribution of assemblages and individual taxa along with estimating optima and tolerances provides valuable baseline data, essential for accurate reconstruction of palaeoenvironments. Constrained ordination suggests mean salinity explains the largest proportion of the variability in contemporary assemblages and is the most appropriate environmental variable for the development of transfer functions. Transfer function prediction errors arise from variation in assemblages at a given salinity value, in part resulting from the sampling strategy, and inadequacies of unimodal models for representation of the response of taxa to environmental variables.

6. Fossil foraminifera from core UV1: results and palaeoenvironmental interpretation

The uppermost 10.09 m of core UV1, recovered from an area to the northwest of Lantau Island in the southeast of the Pearl River estuary, has been sampled at 12 to 14 cm intervals. While previous investigations have focused on the diatom flora and organic carbon isotopes (Zong *et al.*, submitted a; Yu, 2009), this chapter investigates the benthic foraminiferal assemblages of these samples. Trends in the faunal data are highlighted using constrained ordination within a temporal framework developed using radiocarbon dating. Constrained ordination is also used to investigate the variance in assemblage data explained by known factors. Calibration applies the transfer function developed in Chapter 5 to provide quantitative reconstructions of palaeosalinity. An ecological interpretation is then constructed from the faunal data and supporting quantitative reconstructions.

6.1 Lithology of core UV1

The 30.0 m long core – UV1 – consists of two marine units separated by a terrestrial unit. Deposits below 10.6 m, dominated by silts and clays, date to MIS 5 and are assigned to Yim's

(1994) M2 unit (Yu, 2009; Zong *et al.*, 2009a, b). The uppermost section of the M2 unit was subaerially exposed and weathered during a period of lowered sea level (MIS 4-2; Zong *et al.*, 2009b). During the last interglacial a terrestrial unit, occurring between 10.6 and 10.09 m core depth, was deposited in palaeo-channels (Zong *et al.*, 2009b). This unit, analogous to Yim's (1994) T1 deposit, is characterised by firm silt and clay with gravel and coarse sand. A second marine deposit, M1, consisting of silts and clays with some sand and shell rich layers, unconformably overlies the T1 unit (Yu, 2009). Two sections, from 6.25 to 6.00 m and from 0.35 m to the present sediment surface, were lost during sampling. The M1 unit, Holocene in age (Yu, 2009; Zong *et al.*, 2009a), is the focus of analyses in this chapter. Particle size data (figure 6.1) shows a decline in clay content through the Holocene, accompanied by a slight increase in the proportion of silt and variable percentages of sand. A notably sand rich layer, with a high shell content occurs between 1.04 and 0.98 m.

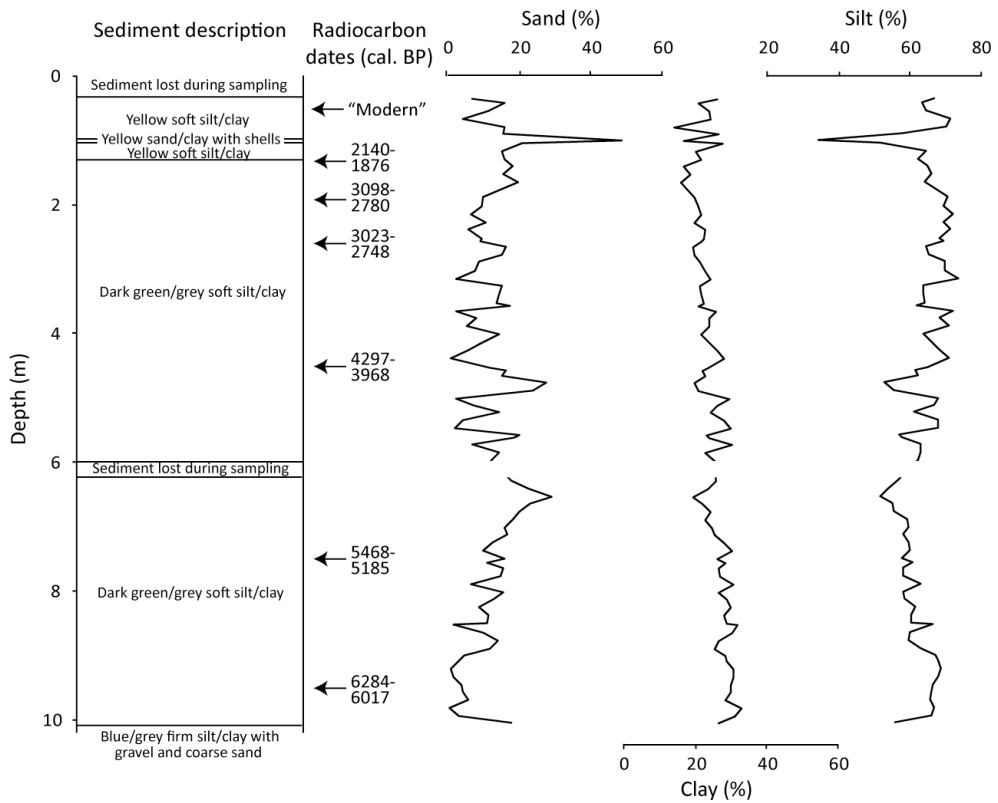


Figure 6.1: Sediment description, radiocarbon (see section 6.2) and particle size data (sand, clay and silt fractions) for the M1 unit of core UV1 (after Yu, 2009).

6.2 Core chronology

Seven radiocarbon dates have been obtained from benthic foraminifera and marine bivalves, in addition to a single optically stimulated luminescence date from a marine shell at 12.5 m (table 6.1; figure 6.2; Zong *et al.*, 2009a; Yu, 2009).

Depth (m)	Median depth (m)	Sample code	Material	¹⁴ C enrichment (% modern $\pm 1\sigma$)	¹⁴ C age	Cal. year BP ($\pm 2\sigma$)	Median (cal. yr BP)
0.50-0.54	0.52	GZ2211	Shell	108.19 \pm 0.42	"Modern" (Yu, 2009: 124)		
1.32-1.34	1.33	GZ2212	Foraminifera	-	2254 \pm 30	2140-1876	2011
1.90-1.94	1.92	SUERC-9602	Foraminifera	66.67 \pm 0.30	3019 \pm 35	3098-2780	2935
2.60-2.62	2.61	GZ2213	Foraminifera	-	2974 \pm 33	3023-2748	2878
4.50-4.54	4.52	SUERC-9605	Foraminifera	61.06 \pm 0.27	3963 \pm 35	4297-3968	4137
7.50-7.54	7.52	SUERC-9606	Foraminifera	54.69 \pm 0.24	4847 \pm 35	5468-5185	5331
9.50-9.54	9.52	SUERC-9607	Foraminifera	49.60 \pm 0.22	5633 \pm 36	6284-6017	6184
12.50	12.50	OS-51226	Shell	NA	37900 \pm 320	41220-40900	41600

Table 6.1: Radiocarbon and optically stimulated luminescence dates obtained for core UV1 (Yu, 2009; Zong *et al.*, 2009a). Calibration of radiocarbon dates was undertaken using CALIB 5.10 (Stuiver *et al.*, 2005) and the marine04 correction (Hughen *et al.*, 2004) with a marine reservoir correction of -128 ± 40 years (Yu, 2009).

The six radiocarbon dates indicating Holocene ages suggest a relatively constant sedimentation rate throughout the core. Yu (2009) excludes the date at 1.92m to resolve a minor age reversal involving samples at 2.60 m (3023 – 2748 cal. years BP) and 1.92 m (dated to 3098 – 2780 cal. years BP). Reworking of older foraminifera at 1.92 m is provided as justification for the exclusion, however the contributions of bioturbation, infaunality and the use of mixed 2 or 4 cm core slices to the actual dating errors are not quantified. The depth of bioturbation in microtidal subtropical estuaries is not well documented in the literature and the depth of infaunal activity of benthic taxa found in the Pearl River estuary is not known, however either factor could potentially increase the overlap between the actual error terms of the two dates. Sedimentation rates suggest the range of depths used for each radiocarbon sample may contribute a further ± 10 to 20 years to the error term. As insufficient data is available to provide justification for the exclusion of the date at 1.92 m, age models are developed using the full set of dates.

The sample from 0.52 m shows relative enrichment of ^{14}C in comparison to the modern value and, therefore, a modern age is inferred (Yu, 2009). This may result from the use of wood grown in 1890 as the “modern” standard. Saliège and Fontes (1984) also suggests atmospheric CO_2 is enriched by 4.3 % with respect to wood due to the fractionation of ^{14}C during photosynthesis. Furthermore, the use of nuclear weapons and fossil fuels has resulted in significant increases in atmospheric and, consequently estuarine ^{14}C subsequent to 1890 (Reimer *et al.*, 2004). ^{14}C enrichment of more than 4.3 % may suggest that the marine reservoir correction used by Yu (2009) is too large, with the delay between the transfer of carbon from the atmosphere to estuary and the death of the marine bivalve less than 128 ± 40 years. The modern age inferred for 0.52 m and the date of 2140 – 1876 cal. years BP at 1.33 m suggests either a substantial decline in the sedimentation rate within the last two millennia or a hiatus in deposition. Consequently the date at 0.52 m is excluded from age model development and samples above 1.33 m core depth are highlighted in or removed from analyses.

Three age models are considered, incorporating a single linear regression (figure 6.2a), two linear regressions (figure 6.2b; Yu, 2009) or a second degree polynomial regression (6.2c). While R^2 values suggest that all are highly significant, the polynomial model is adopted. This model outperforms the simple linear regression in terms of R^2 and there is no evidence for the rapid decline in sedimentation rate suggested by Yu’s (2009) model (Zong *et al.*, 2009a). Additionally the perceived gradual decline in sedimentation rate may better model the possible differential compaction of the core by overlying sediments through the Holocene and during the vibracoring process (Finkl and Khalil, 2005). No attempt is made to correct for compression during coring as the depth of core penetration is not known.

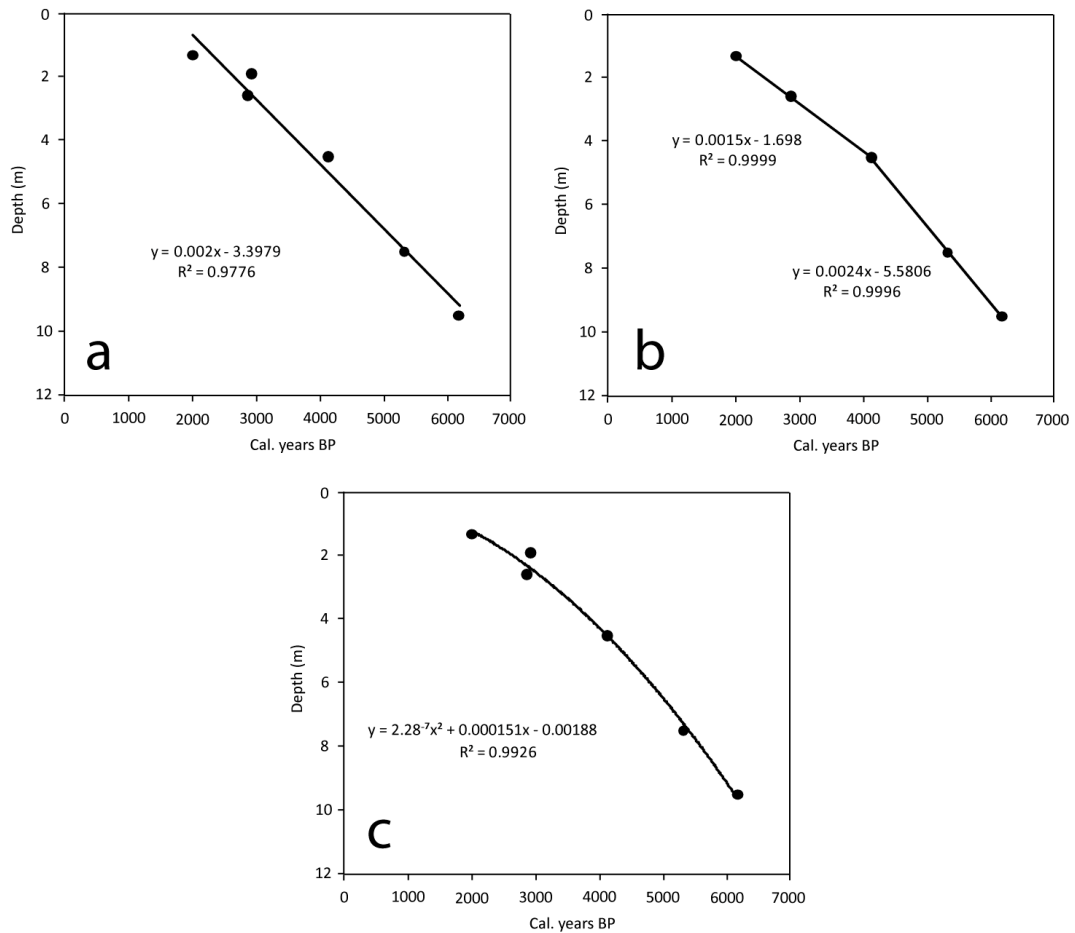


Figure 6.2: Comparison of age models based on (a) linear regression, (b) two linear regressions (after Yu, 2009) and (c) second degree polynomial regression.

The quadratic formula is used to estimate the ages of each sample (equation 6.1). This age model is valid from 1.33 to 9.52 m and is also tentatively extrapolated to the base of Holocene sedimentation at 10.09 m. Modelled ages are cited as exact dates but are subject to errors in radiocarbon dating, reservoir correction and variations in the sedimentation rate between dated samples.

$$x = \frac{-1.51 \cdot 10^{-4} + \sqrt{((1.51 \cdot 10^{-4})^2 - 4 \cdot (2.28 \cdot 10^{-7}) \cdot (-0.00188 - y))}}{4.56 \cdot 10^{-7}} \quad (\text{Equation 6.1})$$

Where x = age (cal. years BP) and y = depth (m).

The age model suggests sediments from 10.09 m to 1.33 m relate to the period between 6330 and 2090 cal. years BP. Modelled ages are generally older than those proposed by Yu (2009), with a maximum difference of 202 years and an average of 84 years. Modelled ages for sediments below 9.04 m are younger than those calculated by Yu (2009), with a difference in the base of the M1 unit of 73 years. Sedimentation rates at the base of the core

are approximately 0.30 cm/year, declining progressively to 0.11 cm/year by 1.33 m and averaging 0.21 cm/year. The resolution of foraminiferal data averages 57 years. Each 2 cm slice of the core relates to 10.3 years of sediment accumulation on average, although this varies from 6.6 years at the base of the Holocene sequence to 18.0 years at 1.33 – 1.31 m.

The radiocarbon date at 9.52 m and the optically stimulated luminescence date at 12.50 m core depth (6284 – 6017 and 41220 – 40900 cal. years BP respectively) suggest that early Holocene sediments are not preserved in core UV1 (Yu, 2009). Extrapolation of the age model provides a date of 6330 cal. years BP for the onset of Holocene sedimentation, at a core depth of 10.09 m, equivalent to 19.09 m below present sea level. Subaerial exposure due to sea level lower than present during the early Holocene is proposed by Yu (2009) for the absence of older sediments. The sea-level reconstructions of Zong (2004) include a sea-level index point with a corrected altitude of 18.50 m below present sea level, dated to 9396 – 8347 cal. years BP, perhaps suggesting an earlier inundation of the coring location of UV1 than the extrapolated age model date. Furthermore, by 6300 cal. years BP, the majority of index points from the eastern south China region suggest sea level was within 5 m of the present level (Zong, 2004). This evidence, combined with an unrealistically low sedimentation rate (in the order of 0.03 cm/year) if continuous deposition was assumed from 8000 cal. years BP, may suggest inundation of the core location before 6300 cal. years BP and a hiatus in sedimentation before the deposition of the first radiocarbon dated sample. Cores V37 and BVC, located in close proximity to UV1, further support an earlier inundation, with radiocarbon dates suggesting strong marine influence by 8600 – 8500 cal. years BP and 8800 – 8600 cal. years BP at depths of 11.3 m and 16.4 m below present sea level respectively (Zong *et al.*, 2009b). The inferred hiatus in sedimentation may have resulted from higher energy water movement in a channel in the coring location preventing deposition. Subsequent channel shifting or abandonment may have then led to the initiation of sedimentation.

6.3 Analysis of fossil benthic foraminifera

6.3.1 The foraminiferal assemblages of core UV1

Core UV1 yielded 102 species of foraminifera, of which 85 (83%) were also found in contemporary surface samples. Assemblages are dominated by *Ammonia beccarii* and

Quinqueloculina akneriana, with contributions from a number of other calcareous taxa including *Cribrononion subincertum*, *Elphidium advenum*, *E. hispidulum*, *Quinqueloculina* spp. and *Rotalinoides annectens*. The combined proportions of the 9 agglutinated taxa reach accessory levels (>5 %) only in samples between 0.67 and 1.17 m. Fossil foraminifera are summarised in terms of number of samples, abundance of taxa according to limits based of Fatela's (1994) classification (>20 % dominant; 10 to 20 % common; 5 to 10 % accessory; 1 to 5 % minor and <1 % insignificant) and effective number of taxa per sample following Hill's (1973) diversity measure (N_2) (table 6.2). The distribution of dominant, common and accessory species is shown in figure 6.3. The included summary plot of low, intermediate and high salinity taxa is based on the modelled contemporary salinity optima, with boundaries set at 26 and 30 psu. Summary statistics for dominant and common taxa are given in appendix 6.1 and the full fossil dataset in appendix 6.2.

Number of samples	84
Total test count >300	84
Number of taxa	102
dominant (>20%)	4
common (10-20%)	2
accessory (5-10%)	9
minor (1-5%)	38
insignificant (<1%)	49
N_2 for samples	
Minimum	10.9
Median	19.0
Mean	20.1
Maximum	31.9

Table 6.2: Contemporary Pearl River estuary foraminiferal data set descriptive statistics.

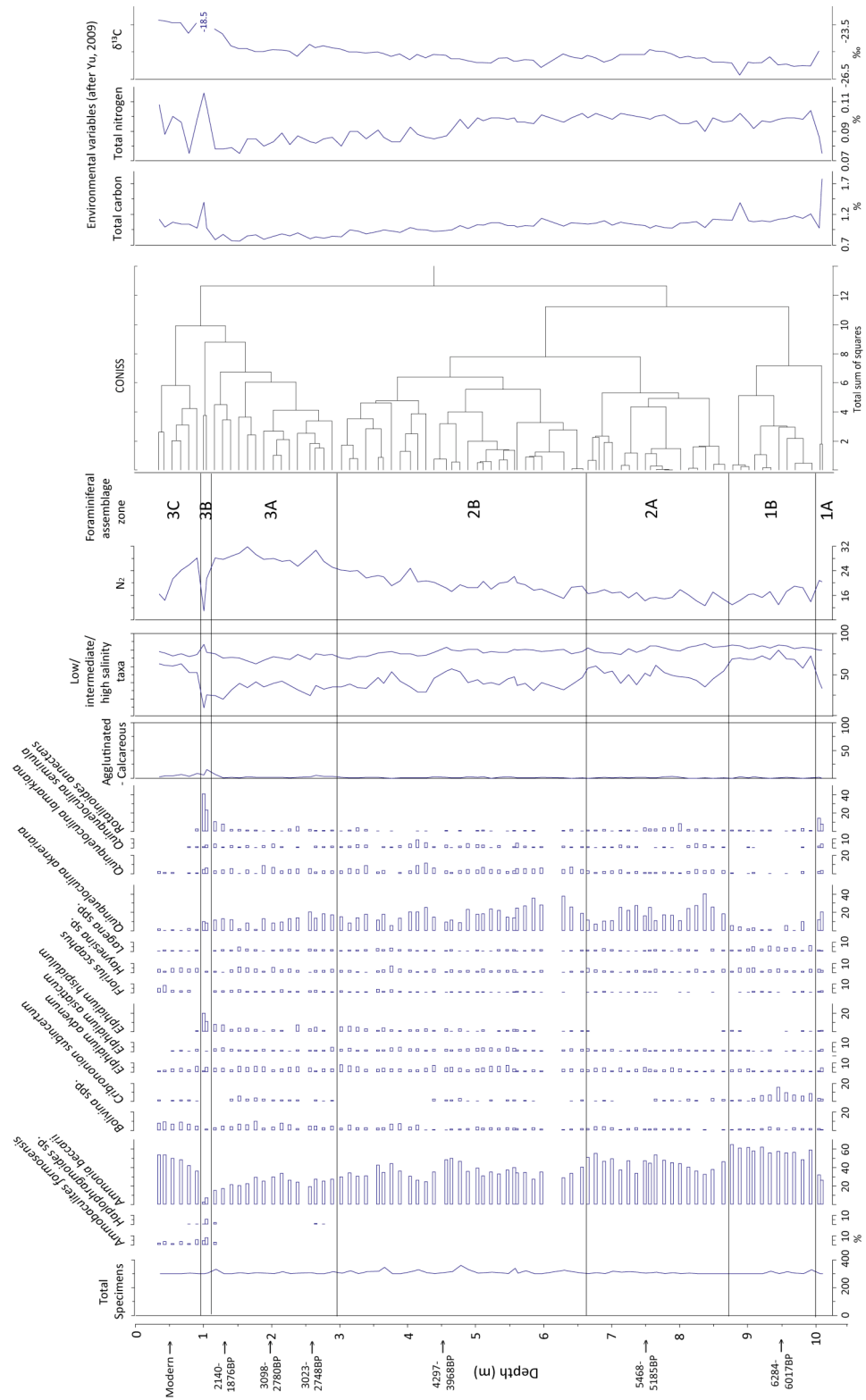


Figure 6.3: Foraminiferal assemblages and environmental variables (Yu, 2009) from core UV1. Dominant, common and accessory taxa (>5%) only. N₂ measures species diversity (Hill, 1973). Note: *Bolivina* spp. and *Lagena* spp. have been classified to species level, but are presented by genus in this figure. δ¹³C values from 1.01 m (δ¹³C = -18.5 ‰) and 1.05 m (δ¹³C = -22.2 ‰) removed to allow better visualization of trends. Radiocarbon dates quoted as calibrated years before present ±2σ (Yu, 2009). Dendrogram produced using stratigraphically constrained CONISS (Grimm, 1987).

6.3.2 Cluster analysis and description of foraminiferal assemblage zones

Stratigraphically constrained CONISS within TGView version 2.0.2 (Grimm, 2004) was used to divide the faunal record into groups of similar samples and to highlight changes in assemblages. A square root transformation was applied before analysis to downweight the influence of dominant species. Three major groups of samples are inferred from the dendrogram and foraminiferal assemblage data: group 1, ranging from the base of the Holocene marine unit at 10.09 m to 8.71m; group 2, spanning the largest section of the core up to 2.96 m and group 3, consisting of samples from 2.96 m to 0.35 m. The three groups are subdivided into seven foraminiferal assemblage zones (FAZ), labeled 1A, 1B, 2A, 2B, 3A, 3B and 3C (figure 6.3; table 6.3).

The most significant division occurs between assemblage zones 1A to 2B and 3A to 3C. This division is not reflected by the characteristic species, which FAZ 2B and 3A share (table 6.3). This apparent contradiction reflects the agglomerative nature of CONISS and the square root transformation of species data before clustering. The dendrogram is constructed by first grouping the two most similar samples, then treating this group as a single sample before pairing the next most similar samples. Consequently relatively similar samples can appear to be significantly different due to the influence of more dissimilar samples in previously selected groups. The square root transformation applied to species data before clustering reduces the influence of major species and is used here to prevent CONISS primarily identifying changes in the abundance of *Ammonia beccarii* and, to a lesser extent, *Quinqueloculina akneriana*.

FAZ 1A is characterised by *Ammonia beccarii*, *Quinqueloculina akneriana* and *Rotalinoides annectens*, with N_2 values of around 20. *Q. akneriana* and *R. annectens* rapidly fall from common (10 to 20 %) to minor (1 to 5 %) levels in FAZ 1B, accompanied by an increase in *A. beccarii*, *Lagena* spp. and *Cribronion subincertum*. *A. beccarii* contributes approximately 60 % of the total counts between 9.93 and 8.77 m core depth, forming the main component of the low salinity taxa group (species with contemporary optima of less than 26 psu). Effective species numbers, as measured by N_2 , are low and fluctuating (12 to 20).

Foraminiferal assemblage zone	Core depth	Number of samples	Characteristic species	Mean N ₂
1A	10.09 – 9.99	2	<i>Ammonia beccarii</i> <i>Quinqueloculina akneriana</i> <i>Rotalinoides annectens</i>	20.6
1B	9.99 – 8.71	11	<i>Ammonia beccarii</i> (<i>Cribrononion subincertum</i>)	15.8
2A	8.71 – 6.61	18	<i>Ammonia beccarii</i> <i>Quinqueloculina akneriana</i>	15.8
2B	6.61 – 2.96	29	<i>Ammonia beccarii</i> <i>Quinqueloculina akneriana</i> (<i>Elphidium</i> spp.)	20.2
3A	2.96 – 1.11	15	<i>Ammonia beccarii</i> <i>Quinqueloculina akneriana</i> (<i>Elphidium</i> spp.)	28.2
3B	1.11 – 0.96	2	<i>Rotalinoides annectens</i> <i>Elphidium hispidulum</i>	16.2
3C	0.96 – 0.35	6	<i>Ammonia beccarii</i> <i>Bolivina</i> spp.	21.8

Table 6.3: Summary of the characteristic taxa of foraminiferal assemblage zones defined by CONISS. Boundaries between zones are stated as the mean depth of the two adjacent samples.

A decline in *A. beccarii*, *Cribrononion subincertum* and *Lagena* spp. and corresponding increase in *Q. akneriana* is observed in FAZ 2A. The proportion of intermediate salinity taxa (contemporary optima of 26 to 30 psu) increases with the decline in low salinity taxa. *Q. akneriana* exceeds 40 % of the total count at a depth of 8.37 m. A number of other porcelaneous taxa, including *Q. lamarckiana* and *Q. seminula*, are also seen to increase in relative abundance. The assemblage zone is characterised by fluctuating *A. beccarii* and *Q. akneriana*, with no other species exceeding 10 % and only *Q. seminula*, *Q. lamarckiana* and *Rotalinoides annectens* reaching accessory levels. N₂ scores suggest an increase in the effective number of species per sample through FAZs 2A and 2B, from 14.7 at 8.65 m to 24.2 at 3.03 m. *Q. akneriana* exhibits a decline in relative abundance in FAZ 2B. *Elphidium* spp. are seen to increase in relative abundance from approximately 5.60 m, with the introduction of *E. hispidulum* and increases in relative importance of *E. advenum* and *E. asiaticum*. A gradual increase in the proportion of high salinity taxa (contemporary optima of greater than 30 psu) characterises zone 2B, with *Bolivina* spp., particularly *B. spathulata* and *B. robusta*, show increased relative percentages towards the boundary with assemblage zone 3A.

While there is no major change in assemblages, FAZ 3A continues the trend for declining proportions of *Q. akneriana* and *A. beccarii* established in zone 2B, although both are still

found at dominant or common levels. *Bolivina* spp. continue to contribute to the assemblage, with the genus supplying 3 to 11 % of the assemblage. *Cribronion subincertum* increases in abundance, reaching over 6 % at a depth of 1.53 m. N₂ scores reach their highest values in this section of the core, reaching 30.7 at 2.65 m and 31.9 at 1.65 m.

Agglutinated taxa, mainly *Ammobaculites formosensis* and *Haplophragmoides* sp., peak in abundance in FAZ 3B, immediately below the sand and shell rich layer between 0.98 and 1.04 m. The sand layer itself, also included in zone 3B, is characterised by intermediate salinity taxa, including *Rotalinoides annectens* and *Elphidium hispidulum*, with some *Quinqueloculina akneriana*. *Ammonia beccarii* is found at its lowest relative abundance in the core, with its contribution classed as minor at 1.01 m. The size of tests is notably larger than in immediately underlying and overlying sediments, with the majority of *R. annectens* and *E. hispidulum* tests measuring over 250 µm in diameter. The significant change in assemblage composition is accompanied by a sharp decline in assemblage diversity, with N₂ reaching its lowest value, 10.9, at 1.01 m.

The assemblages of FAZ 3C are substantially different to both FAZ 3B and FAZ 3A, with low salinity taxa once again dominating. *Ammonia beccarii* exceeds 50 % of the total count. *Bolivina* spp., predominantly *B. pseudopunctata* and *B. spathulata*, contribute the second largest proportion of the assemblage, reaching 7 – 10 %, however low salinity taxa are also observed to increase in abundance. *Elphidium hispidulum* and *Quinqueloculina* spp. fall to insignificant or minor levels. N₂ values, although initially high, decline progressively from 28.2 at 0.91 m to 14.3 at 0.43 m.

6.3.3 Constrained ordination to analyse trends in faunal data

Canonical Correspondence Analysis of surface samples (section 5.2.2) shows a significant ratio between the eigenvalues of the first and second axes and a close correlation between mean salinity and the first axis. A partial CCA, involving rotation of the fossil data in the ordination space defined by the relationship between contemporary assemblages and mean salinity (figure 6.4), provides an illustration of the magnitude and direction of compositional change (figure 6.5). Aligning axis 1 with salinity means that the change in CCA sample scores can be interpreted primarily in terms of changes in salinity. Quantitative estimates are not

extracted from this method as transfer function calibration provides more appropriate estimates with associated error terms (Birks, 1995).

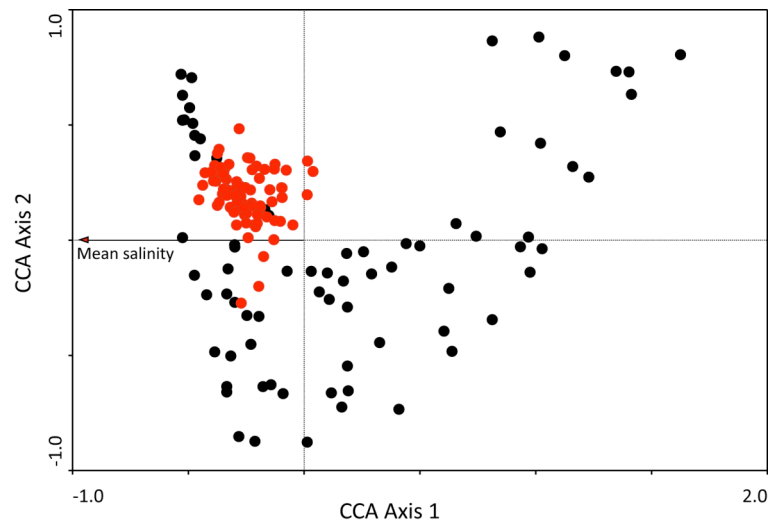


Figure 6.4: Partial Canonical Correspondence Analysis sample scores (black: surface samples; red: fossil samples) rotated in the ordination space defined by the relationship between contemporary assemblages and mean salinity.

Fossil sample scores plot towards the more saline end of the range of contemporary sample scores. When plotted stratigraphically (figure 6.5) partial CCA sample scores show a general trend of increasing salinity through time, with substantial short-term variability. Low, but fluctuating initial salinities are observed to give way to increased salinity, with less variability from around 5000 cal. years BP. A substantial decrease in sample scores (increase in salinity) is observed from around 4000 cal. years BP, interrupted by a reversion to a higher sample score at 3750 cal. years BP. CCA sample scores reach their lowest value immediately prior to 2000 cal. years BP, with subsequent samples suggesting a return to lower mean salinities.

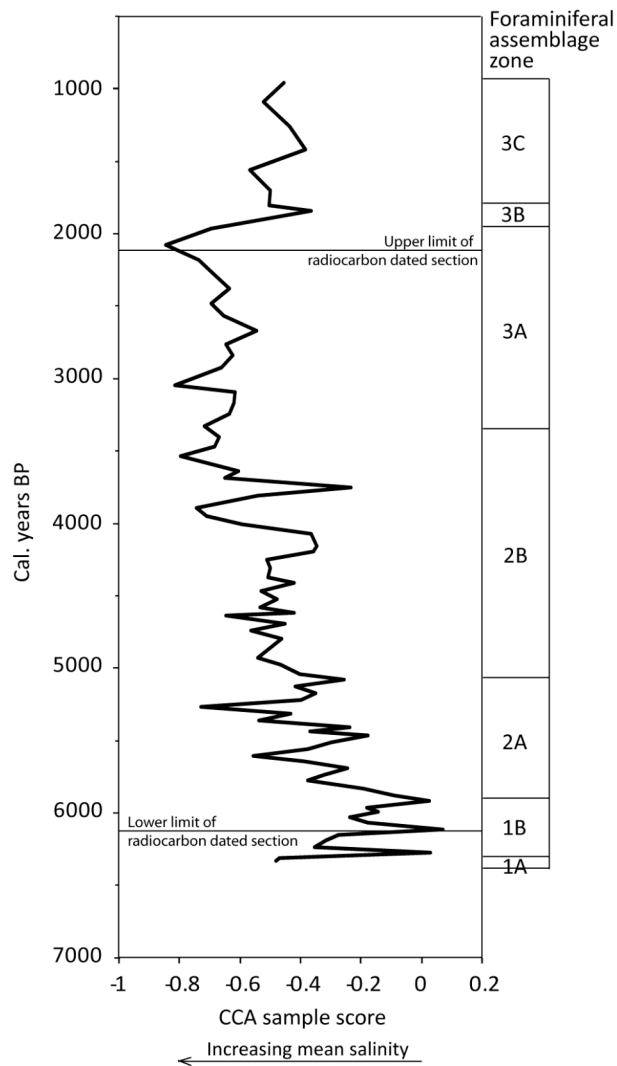


Figure 6.5: Fossil partial Canonical Correspondence Analysis sample scores on axis 1 after rotation in the ordination space defined by the relationship between contemporary assemblages and mean salinity, plotted against modelled age. Foraminiferal assemblage zones (following constrained clustering in figure 6.3) are also included.

6.3.4 Constrained ordination to investigate the influence of environmental variables

Canonical Correspondence Analysis also provides information on the relationship between variability in fossil assemblages and the available environmental data. If a large proportion of fossil assemblage variability was attributable to known variables, taphonomic processes might be viewed as more significant than unknown variables such as bottom water salinity and depth. CCA was undertaken using three classes of particle size (sand, clay and silt), total carbon, total nitrogen, carbon – nitrogen ratio and $\delta^{13}\text{C}$, obtained from Yu (2009). The methodology for the extraction of partial CCAs is discussed in section 5.2.2.

The seven variables together account for 26.0 % of the variance in the fossil foraminiferal dataset (figure 6.6a). Partial CCAs, including results of Monte Carlo permutation tests (table 6.4) show that all of the environmental variables are significant ($p > 0.05$) in explaining the variability in the dataset. Variables associated with the productivity of the environment, including $\delta^{13}\text{C}$ and total nitrogen, account for approximately 47 % of the explained variance, with particle size classes, potentially reflecting the energy regime of the environment, account for a further 34 % (figure 6.6b). The remaining 18 % of the explained variability is contributed by autocorrelation between variables. The distribution of sample scores with respect to the environmental variables is shown in figure 6.7.

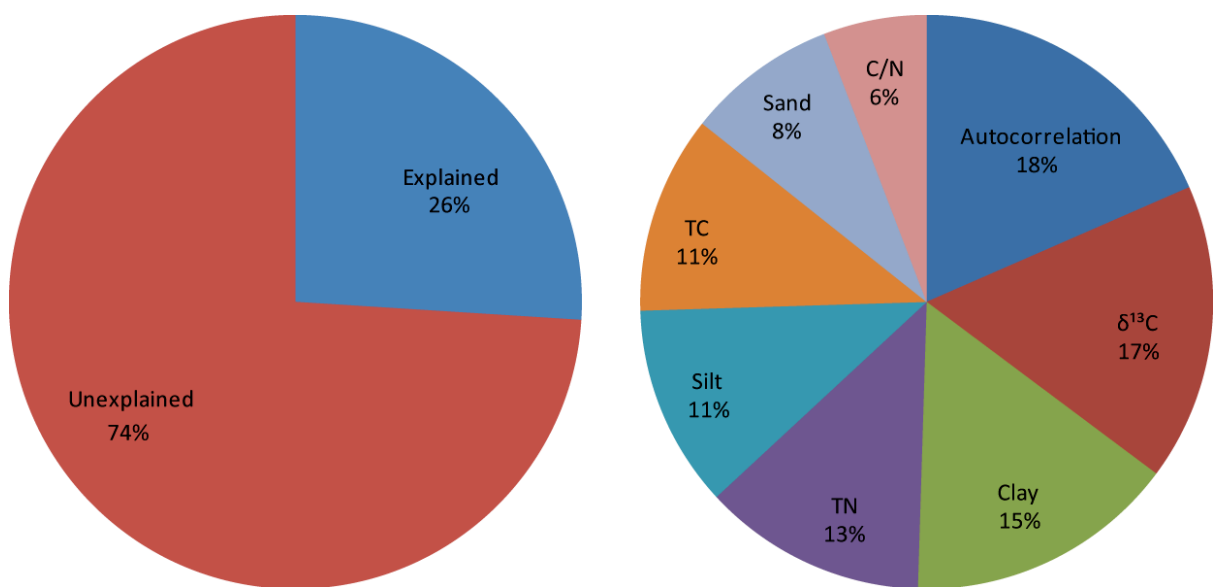


Figure 6.6: Pie charts showing the total variation in the fossil dataset divided into (a) explained and unexplained sectors and (b) sectors representing the individual environmental variables and interactions between variables contributing to the total explained variance.

Environmental variable	% of variance in species data explained	Estimated p value	λ_1	λ_1 / λ_2
$\delta^{13}\text{C}$ (‰)	6.9	0.001	0.048	0.600
Clay (%)	6.3	0.001	0.044	0.564
Total Nitrogen (%)	5.2	0.001	0.036	0.404
Silt (%)	4.7	0.001	0.033	0.355
Total Carbon (%)	4.6	0.001	0.032	0.348
Sand (%)	3.5	0.002	0.024	0.261
Carbon / Nitrogen	2.4	0.045	0.017	0.181

Table 6.4: Results of partial Canonical Correspondence Analysis (following square root transformation of species data) and Monte Carlo permutation tests on the fossil dataset (999 permutations). λ_1 : eigenvalue of axis 1; λ_1 / λ_2 : ratio of eigenvalues for axes 1 and 2.

The extent to which each environmental variable explains variability in the fossil dataset is in line with the corresponding variables influence on the contemporary dataset. This supports the assumption that foraminiferal assemblages are uniform in their past and present responses to environmental variables.

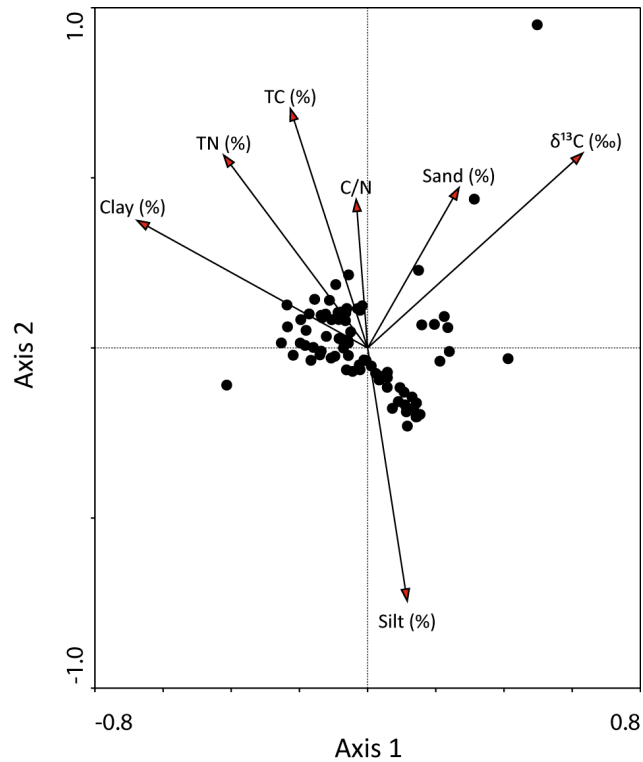


Figure 6.7: Biplot of Canonical Correspondence Analysis sample scores and environmental variables for core UV1.

Approximately 74% of the variance in the fossil assemblage dataset remains unaccounted for. Canonical Correspondence Analysis of contemporary assemblages suggests that mean salinity and water depth are likely to explain part, though not all of the unexplained variance. A number of other factors, including water temperature, dissolved oxygen and stochastic processes are also likely to influence the faunal assemblages of core UV1.

6.4 Quantitative reconstructions of palaeosalinity

6.4.1 Calibration of fossil assemblage data

The transfer function developed in section 5.3 is used to calibrate foraminiferal assemblage data from core UV1 and provide a quantitative reconstruction of palaeosalinity (figure 6.8).

Before trends in the record are discussed it must be observed that the cross validated sample-specific error term is larger than the changes in reconstructed salinity. The predictive power of the transfer function is, in part, compromised by the magnitude of the error term with respect to the range of reconstructed values (c.f. Hassan *et al.*, 2009; Zong *et al.*, submitted a). While the absolute values of palaeosalinity may not be reliable, the coherence of trends of increase or decrease over a number of data points may increase confidence in interpretations of relative changes in salinity.

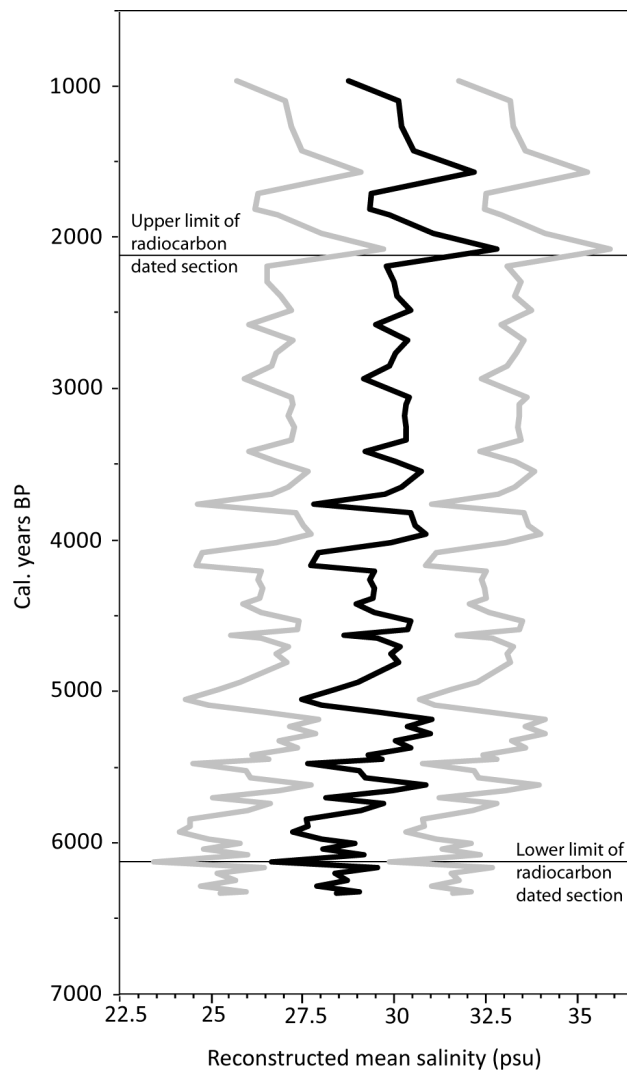


Figure 6.8: Calibration of fossil assemblage data using WA-PLS component 2. Bootstrapped estimates of mean salinity within range of radiocarbon dates indicated by black line; sample specific errors of prediction indicated by grey lines.

Mean salinity estimates within the radiocarbon dated section of the core range from 26.8 ± 3.3 psu at 9.45 m (6116 cal. years BP) to 31.2 ± 3.2 psu at 6.89 m (5177 cal. years BP). Reconstructed mean salinity shows a slight increase over the record, from approximately

28±3.2 psu at the start of the record to 30±3.2 psu between 4000 and 2200 cal. years BP. Assemblages above 1.33m (2140 – 1876 cal. years BP) suggest two further peaks in salinity, up to a maximum of 33.0±3.5 psu at 0.79 m (1562 cal. years BP). A number of fluctuations in the order of 2 to 3 psu are superimposed on the long-term trend, especially in the lower half of the core. Fluctuations appear to decrease in magnitude over time, with the period between 3500 and 2200 cal. years BP showing particular environmental stability.

6.4.2 Assessing transfer function reliability

Whether or not they are statistically or ecologically sound, all transfer function techniques will produce results (Birks, 1998). Consequently further analysis is needed to provide information on the reliability of the results. Woodroffe (2009) suggests current measures of discrimination of good and bad fit are insufficient and the use of complimentary methods is, at present, the most appropriate technique for analysis of the similarity of contemporary and fossil samples. Consequently several statistical measures have been undertaken (after Woodroffe, 2006, 2009):

1. Modern Analogue Technique (MAT) dissimilarity coefficients (MinDC)
2. Analogue statistics (Birks, 1998)
3. Constrained ordination in a mutual ordination space.

These methods determine the similarity between modern and fossil assemblages and can suggest whether the modern training set adequately encompasses the environments suggested by foraminiferal assemblages from the Holocene core. There is an inherent assumption that if modern and fossil foraminiferal assemblages show extensive similarities, their inferred environments can similarly be matched. Erroneous false positive matches could possibly occur through convergence of assemblages representing different environmental conditions (Jackson and Williams, 2004).

Minimum dissimilarity coefficients (MinDC) between individual fossil samples and the modern training set are obtained through Modern Analogue Technique (MAT) in C2 version 1.5.0 (Juggins, 2003). The MinDC of each sample in the modern training set is also calculated and used to provide thresholds for “good”, “close” and “poor” modern analogues. Various percentiles of the range of modern MinDC have been proposed for the threshold of a good

modern analogue, ranging from the extreme value to the 20th percentile (Birks, 1995; Horton, 1997; Hamilton and Shennan, 2005; Horton and Edwards, 2005; Woodroffe, 2006; Simpson, 2007; Rossi and Horton, 2009). The use of the extreme MinDC suggests that all modern samples are good analogues for one another, a situation that is unlikely given the range of environments sampled here. Consequently the 5th percentile is used as the threshold between good and close modern analogues, with the 2.5th percentile the thresholds between close and poor modern analogues.

Minimum dissimilarity thresholds of 50.2 (5th percentile of the modern range) and 52.4 (2.5th percentile) are not exceeded by any of the 83 fossil samples (figure 6.9). Adopting these thresholds, all fossil samples can be said to have good modern analogues. A total of 19 samples, almost exclusively located between 1.41 and 4.04 m, exceed the extreme 20th percentile (minimum dissimilarity coefficient of 34.8). Samples from the shell rich layer between 0.98 and 1.04 m exhibit the lowest MinDC (17.2 and 23.0 respectively) and are therefore interpreted as having the closest modern analogues.

Birks (1998) proposes two 'analogue statistics' to measure reconstruction reliability:

1. The percentage of the fossil assemblage represented by taxa not found in the training set. No explicit threshold for good modern analogues is made.
2. The percentage of the fossil assemblage that consists of taxa poorly represented in the modern training set.

The application of analogue statistic 1 to the Pearl River estuary datasets suggests that a maximum of 3% of any fossil assemblage consists of taxa not found in the modern training set (figure 6.9). While the statistic suggests that modern and fossil assemblages are generally comprised of the same species, it does not provide an effective means of discriminating between fossil samples. The definition of poor representation for analogue statistic 2 is not explicit and two thresholds are adopted: the proportion of the fossil assemblage represented by taxa exhibiting (a) less than 5% occurrences and (b) less than 10% occurrences in the modern training set (figure 6.9). Analogue statistics 2a and 2b show very similar trends to each other and to MAT MinDC. Taxa failing to reach common levels (>10%) contribute more than 25% to each of 16 samples between 3.15 and 1.17 m. The peaks in analogue statistics 2a, 2b and MinDC occur synchronously at 1.77 m, indicating the region of

the core with the poorest modern analogues. Similarly analogue statistics 2a and 2b reach their lowest values alongside MinDC at 1.01 m. Analogue statistics may suggest a high degree of similarity between the fossil and modern dataset in situations where taxa are shared, though at widely different relative abundances.

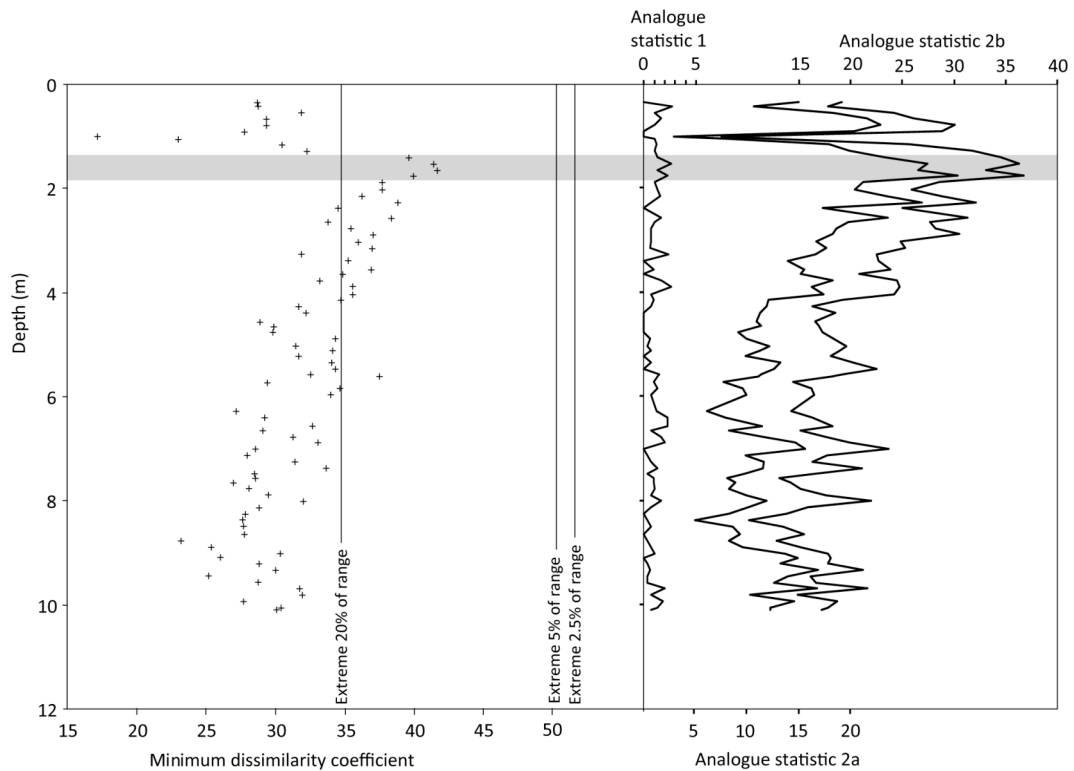


Figure 6.9: Minimum dissimilarity coefficients from the Modern Analogue Technique and analogue statistics for each fossil sample from core UV1. Analogue statistic 1: percentage of the fossil assemblage represented by taxa not found in the training set; analogue statistic 2: percentage of the fossil assemblage that consists of taxa poorly represented by taxa exhibiting (a) <5 % occurrences and (b) <10 % occurrences in the modern training set. Grey box indicates region of greatest dissimilarity between fossil samples and modern training set.

A number of authors use Canonical Correspondence Analysis to provide a measure of the similarity between fossil and contemporary samples (e.g. Hassan *et al.*, 2009; Woodroffe, 2009). CCA is performed on contemporary data, with supplementary fossil assemblage data transformed in the same ordination space. The data are subjected to a square root transformation and rare species are downweighted before performing a partial CCA, constrained by mean salinity only. Sample scores for the contemporary and fossil datasets are compared using scatter plots of the first and second axes (figure 6.10). There is no strict threshold for what constitute similar samples using this method so interpretation is visual and subjective. Fossil and contemporary CCA sample scores show generally overlapping

distributions. The similarity of scores on the first two axes suggests analogous assemblages in the modern and fossil datasets. While overlap is seen, a number of the fossil samples are characterised by higher axis 2 scores than modern samples with similar axis 1 scores (alternatively higher axis 1 scores than samples with similar axis 2 scores). These samples, identified as at the less saline end of the range of fossil samples due to the fact that the CCA is constrained by salinity only, are not those identified by analogue statistics and MAT MinDC as having poorer than average modern analogues. Instead they are generally from the base of the core, particularly from below 8.77 m core depth.

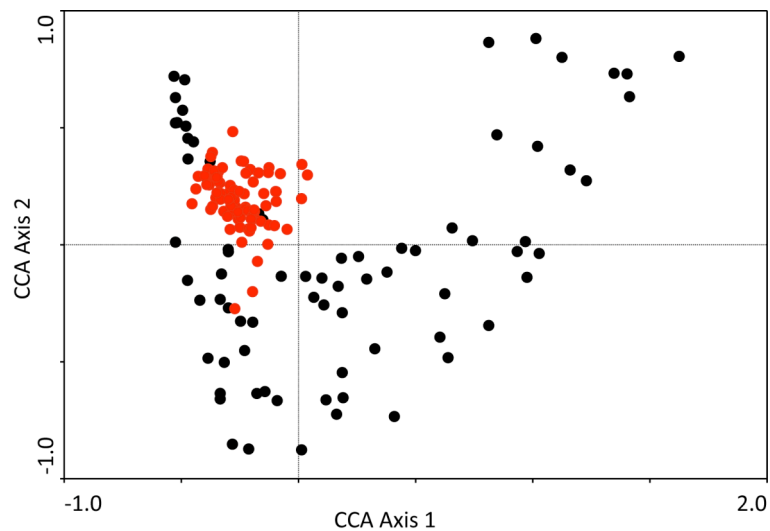


Figure 6.10: Canonical Correspondence Analysis sample scores for surface samples (black circles) and core samples (red circles) rotated in the ordination space defined by the surface samples.

Minimum dissimilarity coefficients, analogue statistics and constrained ordination are generally in agreement that the contemporary foraminiferal dataset provides good modern analogues for the fossil assemblages found in core UV1, supporting the reliability of transfer function calibration.

6.5 Ecological interpretation of faunal data and quantitative palaeosalinity reconstructions

A comprehensive view of the palaeoecological information provided by the foraminiferal assemblages of core UV1 is obtained through the combination of qualitative interpretations of faunal data and quantitative reconstructions of palaeosalinity. A number of changes in assemblage composition are identified and their potential environmental implications are discussed below. Changes in faunal composition may arise from one or more living or

postmortem processes. The magnitude of fluvial influence, controlled by changes in sea level, fluvial discharge or delta progradation is proposed as the most important factor in controlling mean salinity and, consequently foraminiferal assemblages. A number of other linked factors, including water depth, particle size and nutrient availability may explain some of the variation. Postmortem factors, including reworking and redeposition by tidal and storm forces, are also likely to influence the relationship between the foraminiferal assemblages and their depositional environment. It must be remembered that the majority of contemporary assemblage variability cannot be attributed to recorded variables and, accordingly, much of the variability in fossil assemblages may relate to changes in other factors.

6.5.1 Palaeoenvironments of assemblage zones 1A and 1B: 6330 to 5880 cal. years BP

Foraminiferal assemblage zone 1A shares characteristic species, particularly *Ammonia beccarii*, *Quinqueloculina akneriana* and *Rotalinoides annectens*, with samples from contemporary cluster E, particularly samples PE 101 and 102 (figure 5.4). These modern samples are characterised by mean salinities of 25 to 30 psu, suggesting that basal samples from core UV1 were deposited in a saline estuarine environment. Transfer function calibration estimates concur, suggesting mean salinities for the earliest Holocene marine deposits of 28.6 ± 3.2 and 29.3 ± 3.1 psu.

The low abundance of taxa with small tests, the frequency of test damage and the high sand content (figure 6.1) suggest that FAZ 1A relates to a relatively high energy environment. This concurs with the suggestion that a channel may have occupied the coring location in the early Holocene. Declining discharge may have allowed the deposition of the first Holocene marine deposits. Extensive test damage could also be indicative of reworking of the basal assemblage. While Wang and Murray (1983) and Wang *et al.* (1992) suggest the microtidal nature of the Pearl River estuary means that tidal reworking is minimal, the palaeo-tidal regime of the estuary is not well understood and past basin configurations may have resulted in a tidally dominated estuary, with implications for increased test redistribution (Li *et al.*, 2001). Reworking of allochthonous forms or the selective non-deposition of small tests in a high energy environment could result in assemblages not providing an accurate reflection of the salinity of their depositional environment.

Cluster analysis identifies a significant change in fauna with the transition from FAZ 1A to FAZ 1B (figure 6.3). Taxa indicative of a range of different salinities are observed to increase, from the mesohaline *Cribronion subincertum* and *Ammonia beccarii* to the polyhaline *Lagena* spp. and *Florilus scaphus*. While the optima and tolerances of the former pair of species might suggest a decrease in mean salinity when compared to the *A. beccarii* – *Quinqueloculina akneriana* – *Rotalinoides annectens* assemblage of FAZ 1A, *Lagena* spp. and *F. scaphus* exhibit more saline optima. This combination of species may reflect an environment not adequately represented in the modern sample set. Calibration estimates average 28.3 ± 3.2 psu for FAZ 1B, suggesting a slight decline in salinity, a trend supported by the increase in low salinity taxa and the decline in species diversity, as measured by N_2 . The potential for the assemblage to not accurately reflect the depositional environment is again not discounted. The possibility of reworking of tests under an enhanced tidal regime has been considered in relation to zone 1A. Bioturbation and infaunality could also contribute to smoothing of downcore trends, resulting in the combination of assemblages indicative of higher and lower mean salinities (Martin, 1999).

6.5.2 Palaeoenvironments of assemblage zones 2A and 2B: 5838 to 3330 cal. years BP

FAZ 2A is characterised by the establishment of *Quinqueloculina akneriana* as a major component of assemblages alongside *Ammonia beccarii*. *Q. akneriana* exceeds 15 % of the total assemblage in only four contemporary samples. These samples are all located to the north of the coring location and are characterised by water depths of between 4.8 and 9.6 m, with salinities in the range of 25.7 to 31.0 psu. Given a sea level close to present (Zong, 2004), the assemblages of zone 2A are likely to have been deposited in water depths of between 15.5 and 17.5 m, suggesting *Q. akneriana* may have a broader tolerance to depth than contemporary distributions suggest. The decline in the relative abundance of low salinity taxa, including *A. beccarii*, *Cribronion subincertum* and *Haynesina* sp., with the rise of *Q. akneriana* and other intermediate salinity taxa in zone 2A may suggest an increase in salinity with respect to the potential contemporary analogues of FAZ 1B. CCA sample scores and calibration estimates concur, suggesting a rapid increase in mean salinity from around 6000 cal. years BP. In keeping with the salinity values of the potential modern analogues, calibration estimates for the assemblage zone range from 27.8 ± 3.2 to 31.2 ± 3.2 psu.

The progressive increase in high salinity taxa, including *Elphidium* spp. and *Bolivina* spp., coincident with the decline of *Ammonia beccarii* and *Quinqueloculina akneriana*, suggests a further decrease in fluvial influence in FAZ 2B. Assemblages show similarities with contemporary cluster D, although *A. beccarii* and *Haynesina* sp. form a larger part of the fossil assemblage. The increase in N₂ scores and decrease in total carbon and total nitrogen also suggest a more marine environment with respect to zone 2A (figure 6.3). Calibration estimates show a slight trend for increasing salinity, overlain by substantial fluctuations including three notable troughs at 5048, 4159 and 3750 cal. years BP. Cluster analysis (figure 6.3) suggests the sample at 3.77 m, dating to 3750 cal. years BP, shows extensive differences from adjacent samples. CCA sample scores and calibration estimates also suggest a substantially lower salinity than the zone average. The increase in *A. beccarii* and *Haynesina* sp. at the expense of *Q. akneriana*, lasting for a single sample only, suggests a brief period of increased fluvial influence, perhaps resulting from a period of increased discharge. Events centred on 5048 and 4159 cal. years BP are characterised by lowered estimates for more than a single sample, suggesting more prolonged changes in fluvial influence.

6.5.3 Palaeoenvironments of assemblage zones 3A, 3B and 3C: after 3246 cal. years BP

The trend for decreasing abundances of *Quinqueloculina akneriana* and *Ammonia beccarii* and increasing abundances of a range of minor high salinity species continues in FAZ 3A, suggesting increasing marine influence. The brackish taxa *Haynesina* sp. and *Cribronion subincertum* are observed to increase alongside species indicative of higher salinities, including *Bolivina* spp.. Calibration estimates suggest an increase in salinity, averaging 30.5 ± 3.3 psu for the assemblage zone. CCA sample scores and calibration estimates identify the sample at 1.29 m as indicative of the highest salinity in any core sample. High relative abundances of *Elphidium* spp. and *Bolivina* spp. at the expense of *A. beccarii*, *C. subincertum* and *Haynesina* spp. contribute to the calibration estimate of 33.0 ± 3.5 psu.

Foraminiferal assemblage zone 3B, relating to two samples from immediately below and within a sand and shell rich layer (1.04 to 0.98 m), is dominated by large *Rotalinoides annectens* and *Elphidium hispidulum* tests. The link between the abundance of *R. annectens* and the concentration of sand suggested by constrained ordination of the contemporary data is supported by this fossil assemblage (figure 5.12, chapter 5), however the concurrence of an increase in particle size and test diameter may be more suggestive of

postmortem reworking or winnowing of smaller specimens than any ecological preference (Wang and Murray, 1983; Huang, 2000). Huang and Yim (1998) and Huang (2000) identify sand rich layers exhibiting a significant change in assemblage composition in cores NL and VB1, located to the north of Lantau, and attribute them to storm deposition. The same process is proposed for the occurrence of the sand layer in core UV1. Changes in particle size (figure 6.1), total carbon, total nitrogen and $\delta^{13}\text{C}$ (Yu, 2009; figure 6.3) associated with the sand layer are rapid and short-lived, however foraminiferal data suggests a more gradual change, with increases in *R. annectens* and *E. advenum* and a corresponding decline in *Ammonia beccarii* from at least 1.17 m core depth. A similar pattern is observed in cores NL and VB1 (Huang, 2000). Bioturbation could result in the smoothing of an otherwise sharp faunal transition, however this modification would be expected to also affect the environmental variable datasets. Murray (2006) lists a number of species of *Elphidium* as infaunal, however the frequency of abrasion and breakage in the sand layer suggests that tests, rather than live foraminifera may have been deposited. Furthermore increases in *E. hispidulum* and *R. annectens* are seen at least 13 cm below the sand layer, a depth requiring a high degree of vertical movement following deposition. Storm-driven reworking of in situ foraminifera is therefore seen as one possible explanation for the trends in assemblage data. Calibration estimates of 30.1 ± 3.1 and 29.5 ± 3.2 psu for samples at 1.05 m (1842 cal. years BP) and 1.01 m (1801 cal. years BP) respectively are in keeping with the salinity range of cluster D, which includes the closest modern analogues of the fossil assemblages.

The replacement of *Quinqueloculina akneriana* by *Bolivina* spp. as the second largest component of assemblages could suggest a decrease in fluvial influence in FAZ 3C, with the latter genus exhibiting a more marine distribution in the contemporary dataset. Increases in the proportion of low salinity taxa, particularly *Ammonia beccarii*, and declining *Elphidium* spp., *Rotalinoides annectens* and N_2 values, however, suggest increasing fluvial influence compared to zones 3A and 3B. Calibration estimates average 30.4 ± 3.1 psu, with the maximum of 32.4 ± 3.1 psu immediately prior to 2000 cal. years BP exceeding the present annual average salinity of the coring location.

6.6 Spectral analysis to investigate cyclicity in foraminiferal time series

Repeated quantitative estimates of palaeosalinity through core UV1 form a time series, potentially comprised of a long term trend, cyclic changes and residual irregular movements (Chatfield, 1989; Diggle, 1990). Spectral analysis is used to determine the magnitude and significance of cyclic oscillations (Priestley, 1981) and is chosen over autocorrelation analysis due to the variation in the time interval between samples. Analysis has been undertaken on partial CCA sample scores constrained by mean salinity (figure 6.5), transfer function calibration estimates (figure 6.8), the abundances of *Ammonia beccarii* and the percentage of taxa with contemporary salinity optima exceeding 30 psu (figure 6.3). As spectral analysis is only applicable to stationary time series (Diggle, 1990), data are first detrended using either linear or low degree polynomial models to remove any long term trend (figure 6.11). Spectral analysis of detrended data is undertaken using PAST (Hammer *et al.*, 2001) and presented in the form of periodograms (figure 6.12). Samples with ages younger than the youngest radiocarbon date (1.33 m core depth) are not included in analysis due to the magnitude of uncertainties over their ages. Conclusions drawn from analysis of palaeosalinity estimates are limited by substantial uncertainties in both salinity and the dating of samples.

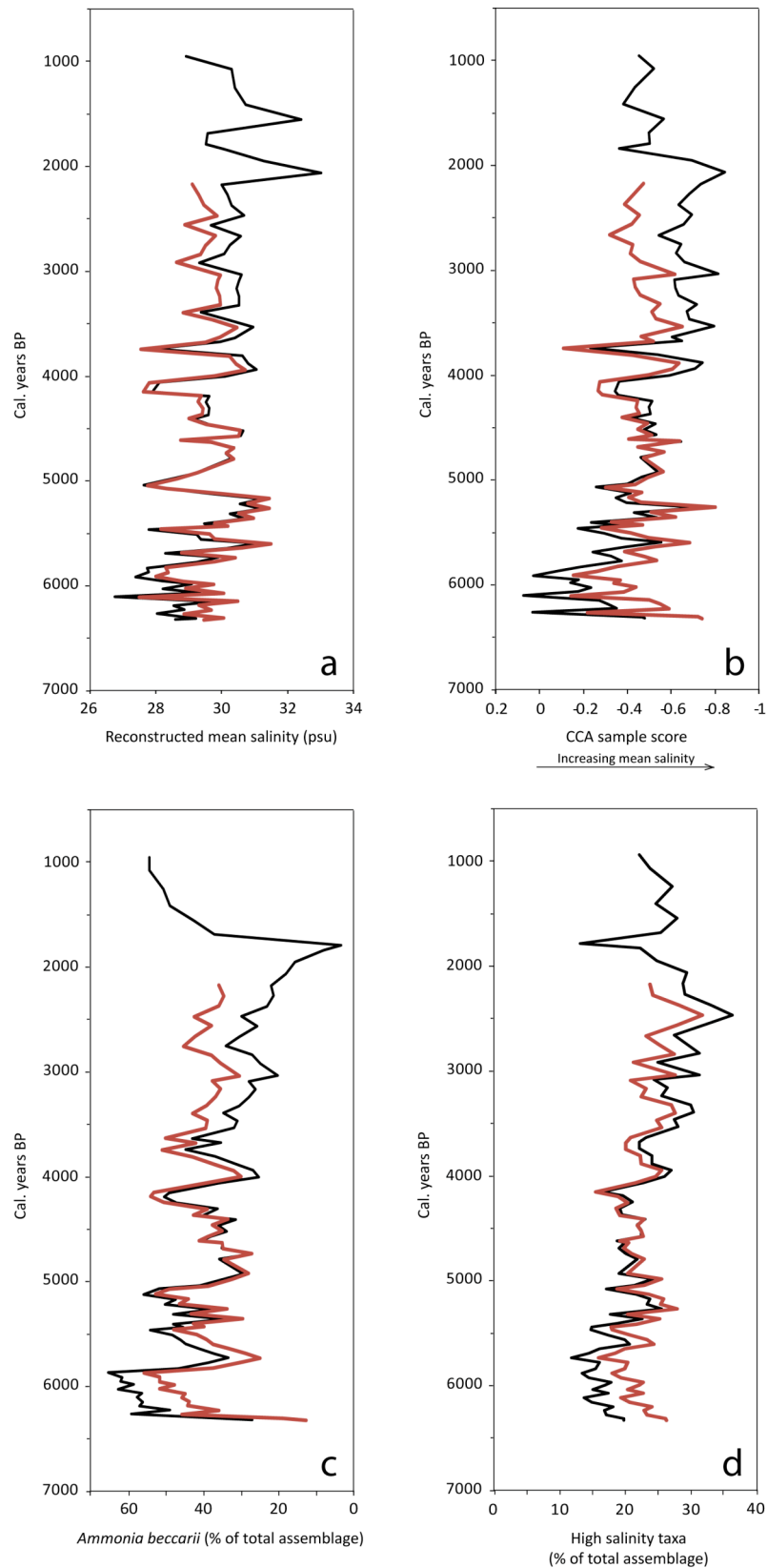


Figure 6.11: Detrending of (a) transfer function calibration results; (b) Canonical Correspondence Analysis axis 1 sample scores; (c) *Ammonia beccarii* percentages and (d) the proportion of taxa with contemporary optima exceeding 30 psu. Black line: original data; red line: detrended data with samples above 1.33 m removed. Note: x-axes of (b) and (c) are reversed with respect to figures 6.5 and 6.3 to facilitate comparison of records.

Periodograms showing the results of spectral analysis suggest that no periodicities are significant at $p < 0.05$ in the detrended calibration estimates (figure 6.12a), detrended CCA sample scores (figure 6.12b) or high salinity taxa data (figure 6.12d). An 830 year cycle in the *Ammonia beccarii* time series is, however, significant at $p < 0.01$ (figure 6.12c). Insignificant, but notable cycles of 426 and 461 years are also seen in the transfer function calibration and *A. beccarii* records respectively.

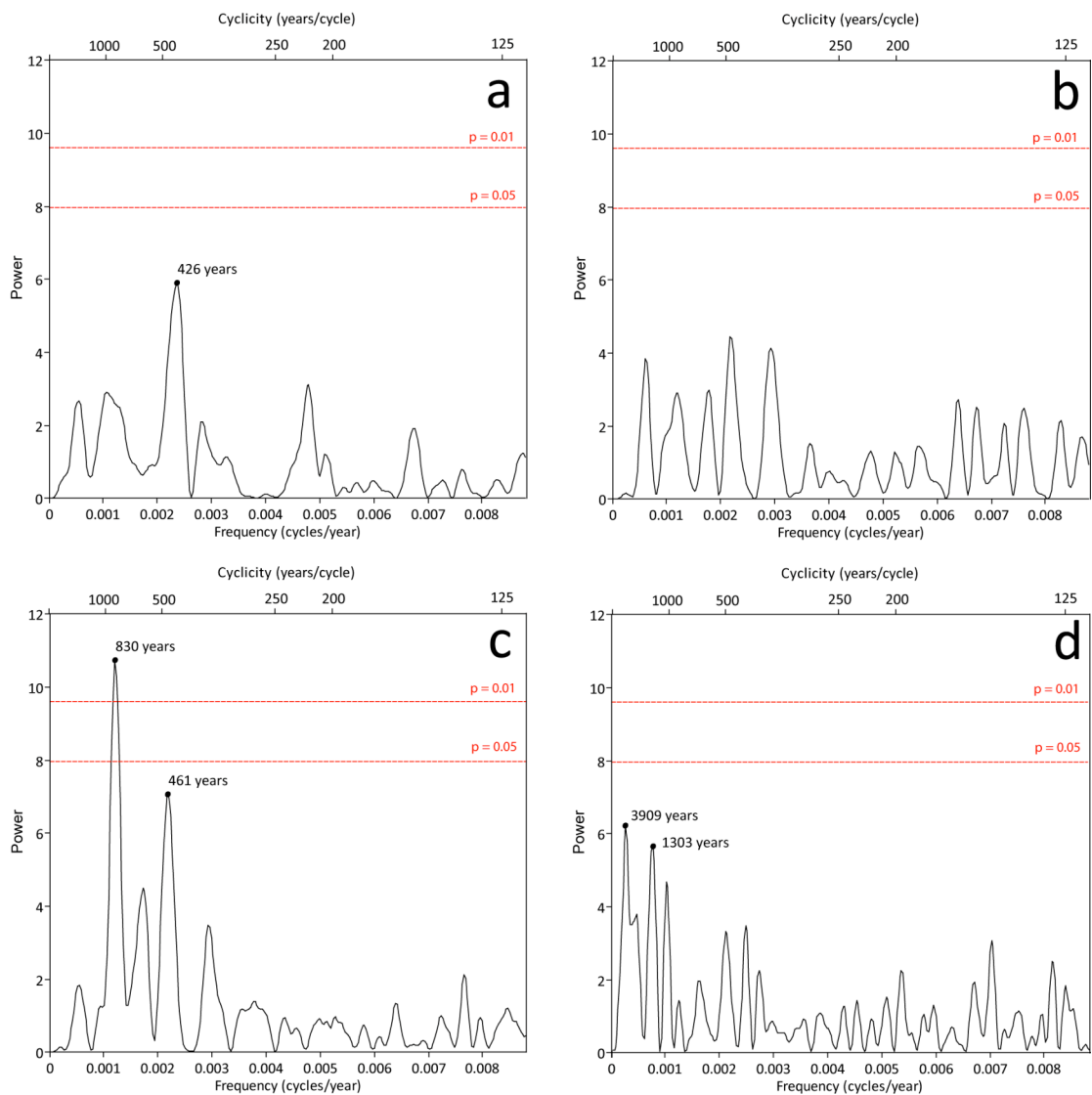


Figure 6.12: Periodograms showing results of spectral analysis of (a) detrended transfer function calibration palaeosalinity estimates, (b) detrended partial Canonical Correspondence Analysis sample scores, (c) detrended *Ammonia beccarii* proportions and (d) detrended high salinity taxa proportions.

While *Ammonia beccarii* favours brackish locations in the contemporary Pearl River estuary, its broad tolerance to salinity means that relating the observed cyclicity directly to fluvially driven changes in palaeosalinity is assumptive at best. Spectral analysis of detrended sand

percentages suggests an insignificant cycle of 1606 years (figure 6.13). Comparison of the corresponding sinusoid with the 830 year cycle in the detrended *A. beccarii* proportions suggests an in-phase relationship (figure 6.14). Given an infaunal habitat preference (Murray, 1991), particle size may play an important role in defining the niche of the taxa. Sand percentages may, in turn, reflect the magnitude of fluvial discharge. As evidenced by contemporary particle size data (section 5.2.1; figure 5.8), sand percentages are linked to fluvial influence. Periods of more intense discharge are hypothesised to lead to greater input of sand to the coring location and, consequently, influence the proportion of *A. beccarii* in benthic assemblages.

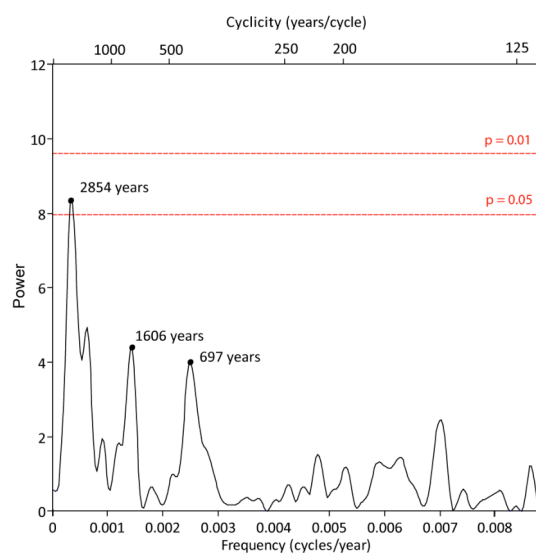


Figure 6.13: Periodogram showing results of spectral analysis of sand percentages.

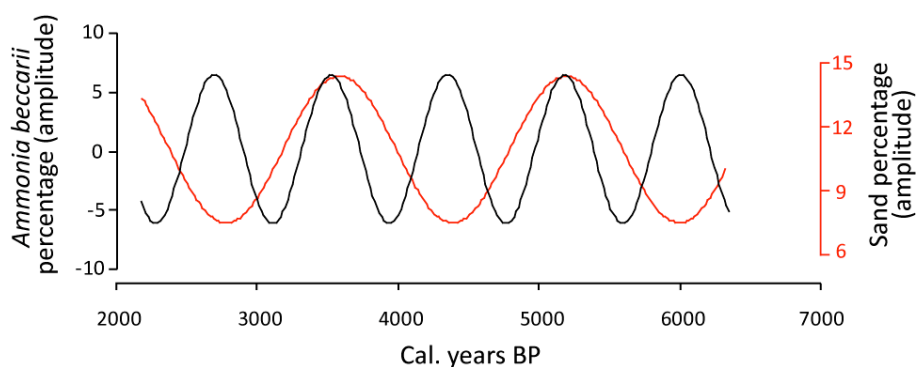


Figure 6.14: Comparison of spectral analysis derived periodicities in *faunal abundances and* particle size data. Black line: 830 year *Ammonia beccarii* percentage sinusoid; red line: 1606 year sand percentage sinusoid.

6.7 Chapter summary

Core UV1 provides a 4250 year record of foraminiferal assemblages with a temporal resolution of between 0.15 and 0.24 cm/year. One-hundred and two benthic taxa have been identified from 83 fossil samples, with *Ammonia beccarii* and *Quinqueloculina akneriana* dominant throughout much of the core. Constrained ordination suggests that fluctuations in particle size, total carbon, total nitrogen, carbon – nitrogen ratio and $\delta^{13}\text{C}$ together explain 26 % of the variability in fossil assemblages, with salinity and depth hypothesised to contribute to the unexplained variance. CCA is also used to provide an initial reconstruction of the relative trends in salinity through core UV1. Transfer function calibration provides quantitative estimates of palaeosalinity, but its predictive power is compromised by error terms larger than the reconstructed changes in salinity. Spectral analysis suggests a significant periodicity of 830 years in foraminiferal data, with further insignificant but noteworthy cycles of 426 and 461 years in transfer function calibration palaeosalinity estimates and *Ammonia beccarii* data.

7. The evolution of the Pearl River estuary and the East Asian monsoon: discussion and conclusions

This chapter discusses the evolutionary history of the Pearl River estuary, based on proxy records from core UV1 (this study; Zong *et al.*, 2009a; 2009b; submitted a; Yu, 2009). The foraminiferal record is interpreted primarily in terms of changes in fluvial discharge from the Pearl River and comparisons are made with other proxy records of fluvial flux and monsoon precipitation. This significance of cyclic variation in the UV1 and other records is examined and the potential mechanisms driving change in the East Asian monsoon are discussed.

7.1 Evolution of the Pearl River estuary

The Holocene evolution of the Pearl River estuary reflects the changing influences of sea level, fluvial discharge and delta progradation. Inundation of the shallow basin of the palaeo-Pearl River occurred during a period of rapid early-Holocene sea-level rise (Zong, 2004). Transgression resulted in the formation of a ria, with the northern coast at least as far inland as Guangzhou (figure 7.1; Wu *et al.*, 2007; Zong *et al.*, 2009a). Sedimentation in core UV1

does not appear to have been initiated until after the marked slowdown in sea-level rise at around 6800 cal. years BP. Wu *et al.* (2007) and Zong *et al.*'s (2009a) reconstructions indicate that the rate of infilling of the estuary outstripped further rises in sea-level, resulting in progradation of palaeoshorelines. The seawards migration of the palaeoshoreline through the mid Holocene effectively brought the source of freshwater into the estuary closer to the coring location, mitigating any possible increases in salinity due to sea-level rise. Furthermore the rate of sedimentation recorded in core UV1 suggests infilling of the southeast of the estuary at $0.30 \text{ cm year}^{-1}$, approximately three times the rate of sea-level rise between 6000 and 3000 cal. years BP suggested by Zong (2004). Any possible late-Holocene decline in sea level from a highstand, as suggested by relative sea-level reconstructions from adjacent regions (Zong, 2004), would have contributed further to seawards shoreline migration and decreases in salinity in the southeast of the estuary. Consequently the decrease in low salinity foraminiferal taxa in favour of intermediate and high salinity taxa recorded in core UV1 can be attributed primarily to reductions in the volume of freshwater discharged from the Pearl River, rather than sea-level rise. Indeed, increasing salinity concurrent with a possible fall in sea level and shoreline progradation is suggestive of an even more marked decline in fluvial discharge.

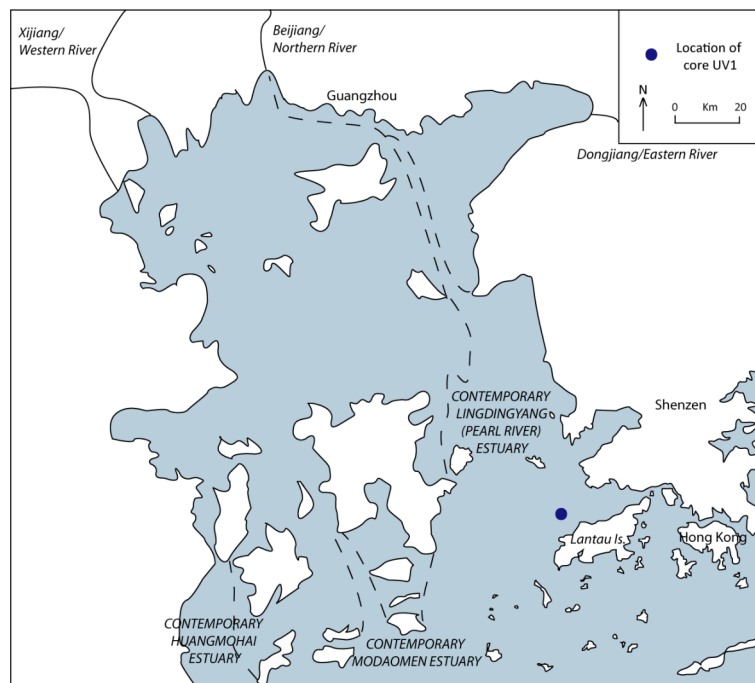


Figure 7.1: Palaeoshoreline of the Pearl River estuary at 6800 cal. years BP (after Zong *et al.*, 2009a). The positions of the contemporary shoreline and core UV1 are indicated.

Although the precise date of the earliest marine Holocene deposits in core UV1 is unclear, Zong's (2004) sea-level reconstruction suggests that water depths at the coring location may have exceeded 14 m during the deposition of foraminiferal assemblage zone 1A. The location of the palaeoshoreline, 120 km to the northwest (figure 7.1; Wu *et al.*, 2007; Zong *et al.*, 2009a), suggests that fluvial influence on the coring site was limited. Furthermore, Coriolis deflection would have resulted in the movement of freshwater from the Lingdingyang gates of the Pearl River, along the western coast of the estuary, towards the region presently occupied by the Modaomen and Huangmohai estuaries (Yim and He, 1988). The proposed mid-Holocene configuration of the estuary (Wu *et al.*, 2007; Zong *et al.*, 2009a) and inferred movement of freshwater would promote greater saline intrusion from the South China Sea through the channels around Hong Kong and Lantau. Foraminiferal assemblages from sites in the southeast of the palaeo-estuary would consequently be expected to reflect a highly saline environment. The fauna of assemblage zones 1A and 1B are not, however, suggestive of a more saline environment than that which is presently found in the coring location. Increased fluvial discharge is a potential explanatory mechanism, resulting from a greater intensity of monsoonal precipitation in the Pearl River catchment. The diatom (Zong *et al.*, submitted a) and $\delta^{13}\text{C}$ (Yu, 2009) records from core UV1 provide support for this hypothesis, suggesting that surface water salinities were markedly lower before 6000 cal. years BP than at present (figure 7.2).

Despite the progradation of palaeoshorelines (Wu *et al.*, 2007; Zong *et al.*, 2009a), foraminiferal data suggest a significant increase in mean salinity between 6000 and 3000 cal. years BP (figure 7.2). As previously mentioned, the rate of shoreline progradation suggests that increasing salinity cannot be attributed to rising sea level. The trend for increasing salinity is again extensively supported by diatom and $\delta^{13}\text{C}$ data from core UV1 (figure 7.2; Yu, 2009; Zong *et al.*, submitted a) and by diatom and $\delta^{13}\text{C}$ data from core V37 (Zong *et al.*, 2006; submitted a). Increasing proportions of taxa with high contemporary salinity optima (figure 7.2d) and falling percentages of *Ammonia beccarii* cannot be explained by sea-level rise; therefore declining fluvial discharge is speculated as the primary cause of increasing salinity through the majority of the UV1 record. Outstanding issues over defining the morphology and hydrography of the estuary mean that long-term changes in estuarine circulation or tides cannot be discounted as possible contributing factors.

A number of brief, but significant events are identified in the $\delta^{13}\text{C}$, diatom and foraminiferal data. The coincidence of increases in fluvial flux interpreted from foraminifera, $\delta^{13}\text{C}$ and diatom proxies is highlighted in blue in figure 7.2, with samples suggesting lowered fluvial discharge highlighted in grey. Proxy data from core UV1 suggests periods of elevated discharge centred on 5923 and 3750 cal. years BP, with lower discharge estimates around 5738, 5272 and 3044 cal. years BP. Further correlations between the foraminiferal and $\delta^{13}\text{C}$ data are observed at the base of the Holocene section of the core, at approximately 4159 cal. years BP and immediately following the final radiocarbon date at 2140 – 1876 cal. years BP. The agreement between the three separate proxies provides support for the records reflecting real changes in fluvial flux. Rapid increases or decreases in salinity, affecting both surface and bottom water salinity may reflect flood or drought events. The lower resolution of the diatom and foraminiferal sampling strategy may explain the lack of peaks or troughs coinciding with further events identified in the $\delta^{13}\text{C}$ data. The identification of high or low discharge events from the microfossil datasets may be, in part, compromised by the sampling resolution, which results in a large number of data points appearing as peaks or troughs.

The fluctuations in foraminiferal palaeosalinity estimates in the poorly age-constrained section of the core (after 2140 – 1876 cal. years BP) are replicated in the $\delta^{13}\text{C}$ data (figure 7.2). Anthropogenic activity may have exerted an additional major control on estuarine evolution during this period. $\delta^{13}\text{C}$ is influenced by the changing proportions of C_3 and C_4 plants with the development of agriculture (Yu, 2009). The combination of increased sediment discharge resulting from deforestation of the Pearl River drainage basin and land reclamation for agriculture increased the volume of sediment retained in the estuary (Li *et al.*, 2001; S. Zhang *et al.*, 2008; Zong *et al.*, 2009a). Consequent shoreline progradation, exceeding 29 m year^{-1} (Zong *et al.*, 2009a) and supported by a possible sea-level fall from a high-stand marginally above present (Zong *et al.*, 2004), would have brought the freshwater source closer to the coring location and may explain the slight decrease in foraminiferal palaeosalinity estimates at the top of the core.

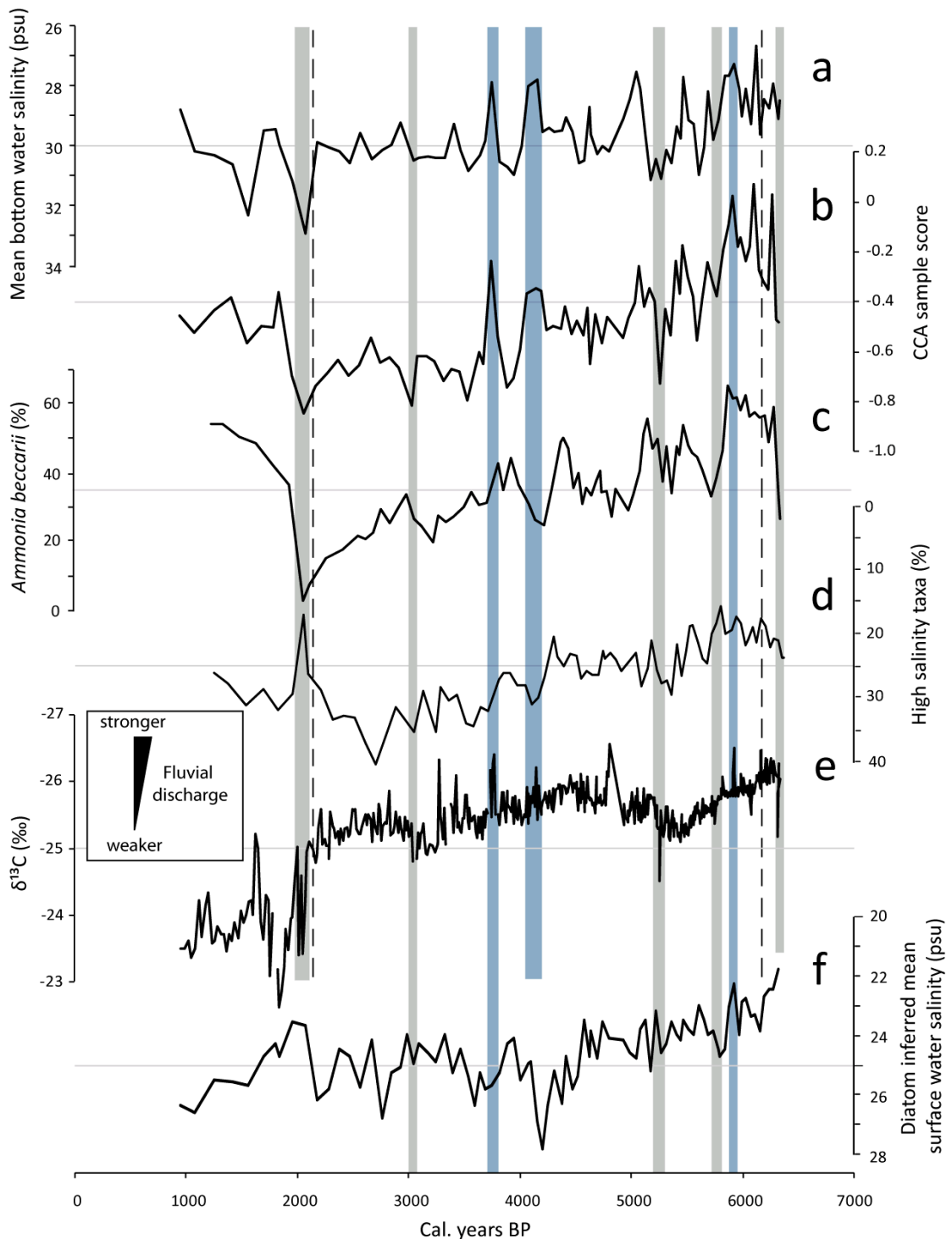


Figure 7.2: Compilation of proxy records from core UV1: (a) foraminiferal transfer function calibration palaeosalinity estimates; (b) partial Canonical Correspondence Analysis of foraminiferal data; (c) proportion of *Ammonia beccarii*; (d) proportion of high salinity taxa; (e) bulk organic carbon isotopes (Yu, 2009) and (f) diatom transfer function calibration palaeosalinity estimates (Zong *et al.*, submitted a). Note: $\delta^{13}\text{C}$ and diatom data (Yu, 2009; Zong *et al.*, submitted a) have been replotted using the age model developed in Chapter 6.

7.2 The UV1 record and mechanisms responsible for East Asian monsoon variability

7.2.1 Long term trends in Holocene monsoon intensity

While salinity estimates from the foraminifera from core UV1 are subject to errors larger than the magnitude of changes, a slight long-term trend towards increasing salinity values is observed. It is speculated that this trend is related to declining fluvial discharge. If genuine, this trend supports various proxy records of precipitation in the East Asian monsoon region (figure 7.3). Intense mid-Holocene rainfall, as suggested by more negative $\delta^{18}\text{O}$ values in Dongge Cave speleothems (figure 7.3c; Y. Wang *et al.*, 2005), is proposed as the cause of high fluvial discharge and correspondingly low salinity at the start of the UV1 record (6300 to 5900 cal. years BP). Elevated mid-Holocene precipitation proxies are recorded from numerous other speleothems (e.g. Cai *et al.*, 2001; Zhang *et al.*, 2004; Cosford *et al.*, 2008; Hu *et al.*, 2008), while increased Pearl River discharge is also seen as responsible for lowered sea surface salinity in the northern South China Sea (figure 7.3e; Wang *et al.*, 1999b).

The Dongge Cave record suggests a post-peak decline in precipitation from around 7000 cal. years BP (figure 7.3c; Y. Wang *et al.*, 2005), with coeval differences in $\delta^{18}\text{O}$ between Heshang and Dongge Caves declining from around 6000 cal. years BP (figure 7.3d; Hu *et al.*, 2008). Pearl River estuary foraminiferal data exhibits an increase in estimated salinity beginning between 6000 and 5500 cal. years BP, which may relate to declining fluvial discharge. Declining monsoon intensity is postulated as responsible for these trends and for increasing sea surface salinity in the South China Sea (figure 7.3e; Wang *et al.*, 1999b) and the Yellow Sea (Xiang *et al.*, 2008). The coherent mid- to late-Holocene decline has been linked to declining summer insolation (Dykoski *et al.*, 2005), a function of the earth's precession and obliquity cycles (figure 7.3g; Berger and Loutre, 1991). This may reflect both the direct influence of reductions in the thermal contrast between land – sea, resulting in reduced onshore movement of moisture bearing summer winds, and the southwards migration of the Intertropical Convergence Zone (ITCZ; Yancheva *et al.*, 2007). The movement of the ITCZ has also been used to explain the declining intensity of the Indian monsoon, as recorded by speleothems from Oman (Neff *et al.*, 2001; Fleitmann *et al.*, 2003), over the same period. Furthermore, the global southwards shift in ITCZ position is supported by proxy records for declining summer precipitation from the Cariaco Basin, Venezuela (Haug *et al.*, 2001) and increasing effective moisture in the Amazon basin (Maslin and Burns, 2000).

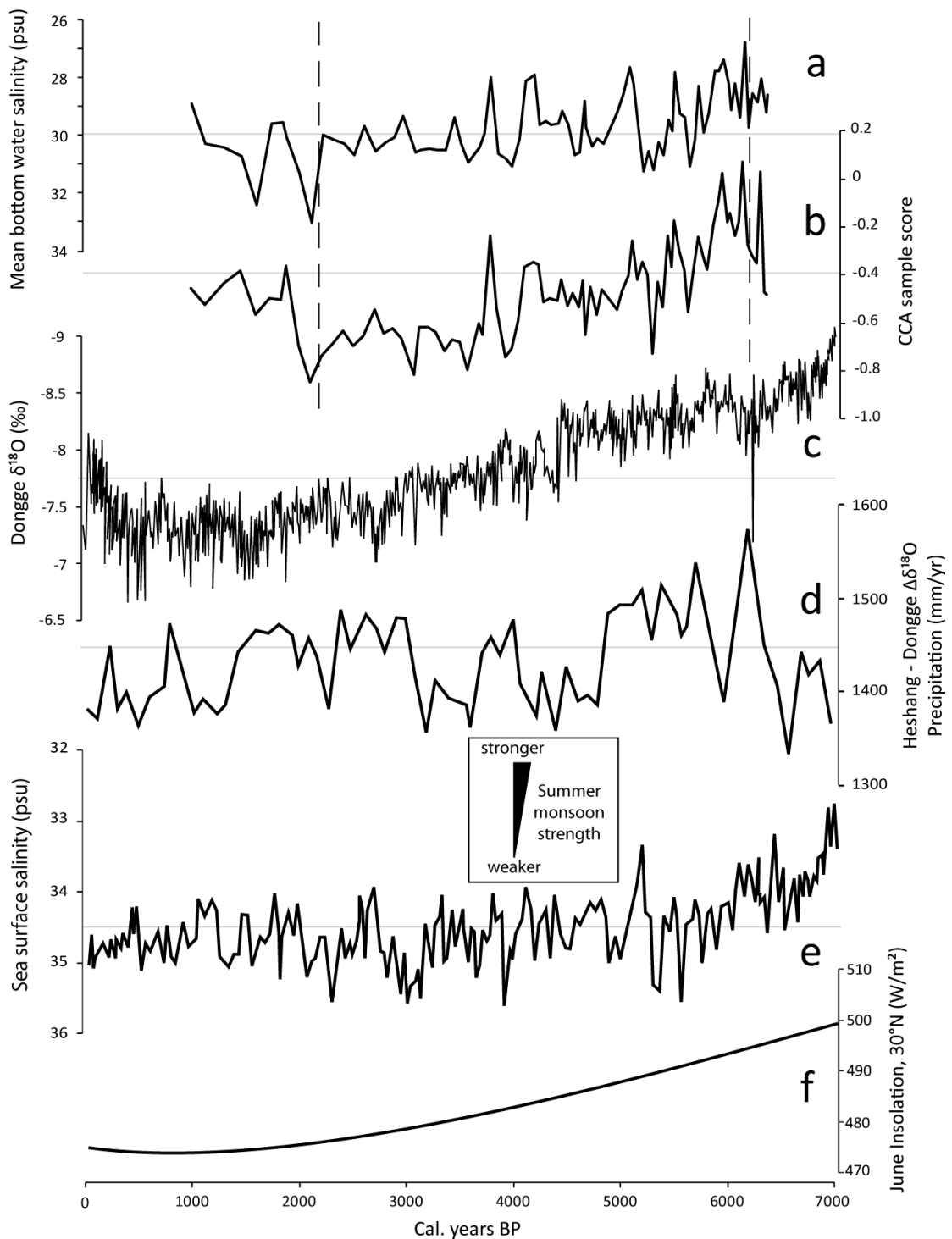


Figure 7.3: Comparison of (a) Pearl River estuary foraminiferal transfer function calibration palaeosalinity estimates; (b) partial Canonical Correspondence Analysis of foraminiferal data; (c) Dongge cave stable oxygen isotope record (Y. Wang *et al.*, 2005); (d) coeval differences in $\delta^{18}O$ between Heshang and Dongge Caves, calibrated to annual precipitation (Hu *et al.*, 2008); (e) South China Sea surface salinity estimates (Wang *et al.*, 1999b); (f) modelled June insolation at 30°N (Berger and Loutre, 1991).

As outlined in Chapter 2, there are a range of outstanding issues over the interpretation of speleothem $\delta^{18}\text{O}$ – the most widely cited proxy for Holocene monsoon intensity – as solely a record of precipitation amount. Nevertheless, declining monsoon intensity has been recorded by various other proxies, as outlined above. The increase in precipitation after 4000 cal. years BP inferred by Hong *et al.* (2005) from peat cellulose organic carbon isotopes from Hani bog, northeast China, does not, however, conform with the majority of precipitation intensity records. Furthermore, the record from Hani bog does not exhibit the same trends as a similar peat cellulose $\delta^{13}\text{C}$ record from Jinchuan, northeast China, published by the same authors (Hong *et al.*, 2001). This discrepancy suggests other processes may affect the $\delta^{13}\text{C}$ values of peat cellulose in addition to monsoon precipitation.

7.2.2 Abrupt changes in monsoon intensity

A number of abrupt events indicative of decreased monsoon precipitation have been identified from a variety of proxies. Literature suggesting dry periods and reduced monsoon intensity is summarised in table 7.1.

Age range (cal. years BP)	Location
~6300	Pearl River estuary (this study; Yu, 2009) Dongge Cave (Y. Wang <i>et al.</i> , 2005) Hani peat bog (Hong <i>et al.</i> , 2005)
5700 – 5500	Pearl River estuary (this study; Yu, 2009; Zong <i>et al.</i> , submitted a) Dongge Cave (Y. Wang <i>et al.</i> , 2005)
~5300	Pearl River estuary (this study; Yu, 2009; Zong <i>et al.</i> , submitted a) Dongge Cave (Y. Wang <i>et al.</i> , 2005)
4400 – 4000	Pearl River estuary (this study) Jinchuan (Hong <i>et al.</i> , 2001) Dongge Cave (Y. Wang <i>et al.</i> , 2005) Loess Plateau (Porter and Zhou, 2006) Heshang and Dongge Caves (Hu <i>et al.</i> , 2008)
3000 – 2700	Pearl River estuary (this study; Yu, 2009; Zong <i>et al.</i> , submitted a) Jinchuan (Hong <i>et al.</i> , 2001) Dongge Cave (Y. Wang <i>et al.</i> , 2005) Loess Plateau (Porter and Zhou, 2006)
1600 – 1400	Qixing Cave (Cai <i>et al.</i> , 2001) Jinchuan (Hong <i>et al.</i> , 2001) Dongge Cave (Y. Wang <i>et al.</i> , 2005) Loess Plateau (Porter and Zhou, 2006) Heshang and Dongge Caves (Hu <i>et al.</i> , 2008)

Table 7.1: Summary of periods characterised by decreased summer monsoon intensity inferred from Chinese proxy records.

Some differences in the timing of events are apparent, however it appears plausible that these derive from age model inaccuracies. Liu *et al.* (in press) suggests cycles of 1606 years in the Dongge Cave $\delta^{18}\text{O}$ data, incorporating these weak monsoon events, while Wang *et al.* (1999b) identifies 775 year cyclicality in South China Sea surface salinity. Spectral analysis of the Pearl River estuary foraminiferal data suggests a single significant period of around 830 years, found in the relative abundances of *Ammonia beccarii* (figure 7.4), although not in the calibration estimates, constrained ordination sample scores or the proportion of high salinity taxa. Issues over inaccuracies in the age model and the low resolution of sampling mean the equivalence of these cycles with published periodicities is uncertain. The 830 year cycle could conceivably match the 775 year cycle or represent a subharmonic of the 1606 year cycle. While the low discharge events at approximately 6300 and 5700 cal. years BP coincide with *A. beccarii* minima, further events are more easily identified from transfer function palaeosalinity estimates, constrained ordination sample scores and other proxy data from core UV1 (figures 7.2; 7.4).

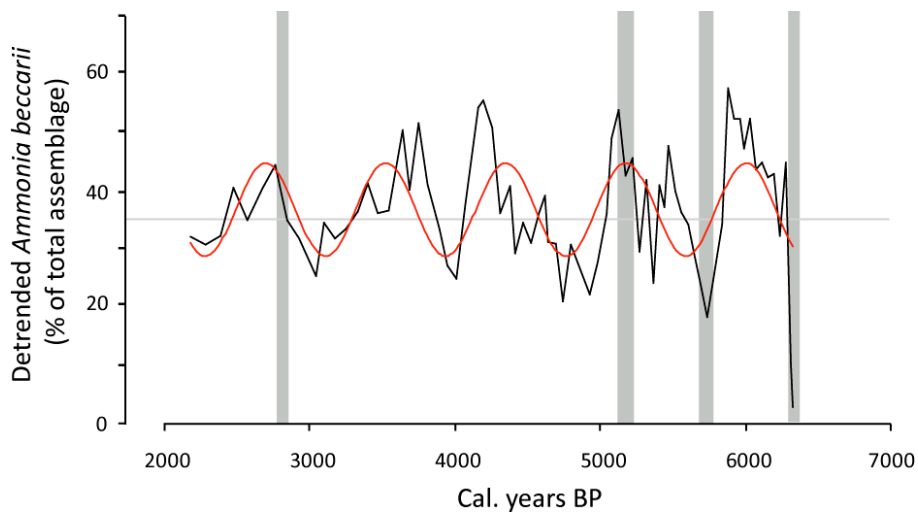


Figure 7.4: 830 year sinusoid fitted to detrended *Ammonia beccarii* proportions. Grey shading indicates low discharge events inferred from UV1 proxy data (figure 7.2).

Correlations have been proposed between the timing of weak East Asian summer monsoon events and episodic increases in ice rafting in the North Atlantic (Y. Wang *et al.*, 2005; Porter and Zhou, 2006). Noting the synchronicity between peaks in drift ice proxies and five periods of reduced rainfall inferred from Oman stalagmites, Bond *et al.* (2001) suggests a 1500 year cycle in solar variability as the forcing mechanism for changes in both ice rafting and low latitude precipitation. Decreased solar insolation, resulting in expansion of northern hemisphere ice cover, may also have led to a reduction in the intensity of the Western

Pacific Warm Pool high pressure cell and, consequently, the thermal contrast between land and sea and ultimately the intensity of East Asian precipitation. Potential synchronicity can be seen between Bond events 4 and 3 in the North Atlantic and declines in Pearl River discharge inferred from foraminiferal, $\delta^{13}\text{C}$ and diatom proxies (figure 7.5). A further low discharge episode at around 6300 cal. years BP observed in the foraminiferal data corresponds with a positive shift in the oxygen isotope record from Dongge Cave (figure 7.5c) and with an additional peak in ice rafted debris.

Alternative mechanisms for the generation of abrupt precipitation anomalies have been proposed, advocating North Atlantic events as the cause of reductions in East Asian rainfall (Porter and An, 1995; An, 2000; Zhao *et al.*, 2003). Increasing northern hemisphere ice extent may have resulted in the intensification and southward migration of the Siberian high pressure cell in winter, increasing the thermal contrast between land and sea and strengthening the East Asian winter monsoon (Porter and An, 1995; An, 2000; Y. Wang *et al.*, 2005). A reduced summer thermal gradient between land and sea, further suppressed by lower Western Pacific sea surface temperatures, would have contributed to less intense summer precipitation (Zhao *et al.*, 2003). A further hypothesis focuses on oceanic, rather than atmospheric teleconnections, with intense North Atlantic iceberg calving resulting in perturbations of global oceanic circulation and cooling in the western Pacific (Broecker, 1994; Clift and Plumb, 2008).

While the majority of East Asian proxy records suggest periodic abrupt weakening of precipitation intensity, the Hani peat bog record suggests in-phase abrupt strengthening, particularly at around 4200 cal. years BP (Hong *et al.*, 2005). While increased precipitation is supported by Shi *et al.*'s (1994) suggestion that a legendary catastrophic flood at around 4000 cal. years BP led to the demise of the Longshan and Lianzhu cultures, Y. Wang *et al.* (2005) suggests droughts characterised the period, resulting in the collapse of Neolithic cultures. Again the peat cellulose $\delta^{13}\text{C}$ record from Jinchuan is at odds with the Hani record, with the former suggesting decreased humidity or precipitation around 4150 – 3800 cal. years BP (Hong *et al.*, 2001).

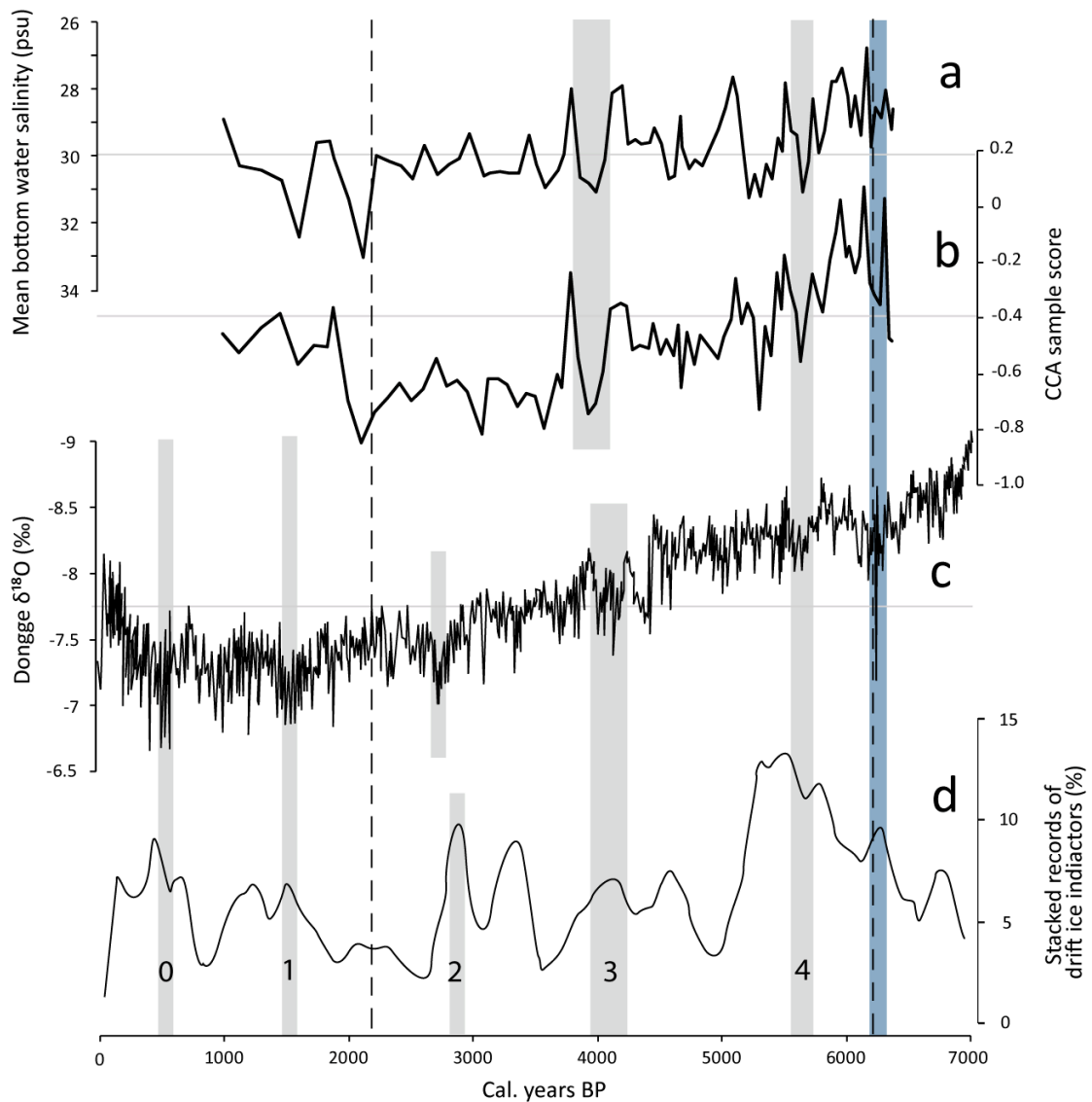


Figure 7.5: Concurrence of abrupt dry events in (a) Pearl River estuary foraminiferal transfer function calibration palaeosalinity estimates; (b) partial Canonical Correspondence Analysis of foraminiferal data and (c) the Dongge cave stable oxygen isotope record (Y. Wang *et al.*, 2005), along with (d) peaks in drift ice tracers in the North Atlantic (Bond *et al.*, 2001). Bond events 0 to 4 are indicated in grey, with a further weak monsoon event correlated with a drift ice proxy peak indicated in blue.

As previously mentioned, solar variability has been proposed for the 1500 year cycles in North Atlantic ice rafting and monsoon intensity. Numerous shorter cycles have also been attributed to changes in solar activity, with significant periods of around 11 – 13, 22 – 25 years (P. Wang *et al.*, 2005; Liu *et al.*, in press), 84 – 88 years (Wang *et al.*, 1999a; Hong *et al.*, 2001; Y. Wang *et al.*, 2005; Hu *et al.*, 2008; Liu *et al.*, in press), ~110 and ~210 years (Hong *et al.*, 2001; Y. Wang *et al.*, 2005; Hu *et al.*, 2008; Liu *et al.*, in press). The sampling resolution of foraminiferal data presented here negates the possibility of detecting any of these decadal and centennial scale cycles. High resolution studies have additionally

identified sub-decadal cycles that have been attributed to El Niño (e.g. Peng *et al.*, 2003; Dykoski *et al.*, 2005; Hong *et al.*, 2005).

7.3 Conclusions

7.3.1 Benthic foraminifera as proxies for salinity

Analysis of 76 grab samples from the Pearl River estuary suggests that foraminiferal assemblages show clear spatial variation. Cluster analysis and unconstrained ordination delineate five contemporary clusters of samples. Mapping the distributions of clusters, individual species and environmental data suggests a link between sample composition and distance from the gates of the Pearl River. Ordination provides a valuable and frequently overlooked stage in the analysis of contemporary distributions for transfer function development. Constrained ordination suggests 38 % of the variance in the species data can be accounted for by the recorded variables, with the remaining 62 % attributed to environmental factors not quantified in this investigation and stochastic processes. Mean annual bottom water salinity explains 16.9 % of the variance and is deemed significant in controlling the distribution of foraminifera, consequently allowing transfer function development. Unimodal models of species' response to the environment express salinity as a function of the contemporary faunal data. The use of a sampling strategy based on a single transect along the environmental gradient of interest, as adopted by a significant number of quantitative palaeoenvironmental studies, minimizes variation in assemblages at a given environmental value and, consequently, leads to an underestimation of the error term. The multiple transect strategy used here better quantifies variability independent of the desired parameter, providing larger, but more realistic prediction errors.

7.3.2 Reconstructing palaeosalinity and the evolution of the East Asian monsoon

Eighty-three fossil samples from core UV1 provide a record of palaeoenvironmental change spanning approximately 6330 to 2090 cal. years BP. Cluster analysis divides the stratigraphic data into seven foraminiferal assemblage zones. While the precise estimates of palaeosalinity provided by transfer function calibration are compromised by the size of the sample specific error term with respect to the magnitude of recorded changes, relative trends are reliable and concur with qualitative assessments based on the preferred habitats

of key indicator species. Foraminiferal assemblages suggest a long-term trend for increasing salinity during the mid- to late-Holocene in the southeast of the Pearl River estuary. Given the a priori knowledge of relative stability in sea level (Zong, 2004), palaeosalinity is interpreted primarily as a record of fluvial influence. Despite shoreline progradation bringing the source of freshwater closer to the coring location, I propose that the decline in fluvial discharge during the mid- to late-Holocene was significant enough to result in increasing salinity. The interpretation of the foraminiferal data in terms of changing fluvial discharge is, however, subject to a number of caveats, with the exact relationship between palaeosalinity and palaeodischarge unknown and a number of other factors potentially giving rise to salinity variations. A long-term increase in salinity, if related to declining fluvial flux, is in accord with the majority of records of changing precipitation intensity derived from biological, sedimentological and chemical proxies from across China. Declining insolation due to the earth's obliquity and precession cycles is hypothesised to have resulted in the southwards migration of the ITCZ and reduction of the thermal contrast between land and sea. While issues remain over the interpretation of speleothem records as indicative of regional precipitation intensity, the Pearl River estuary record is thought to document average changes in precipitation over the entire drainage basin.

The progressive increase in Pearl River estuary salinity is punctuated by a number of short-lived high and low salinity events. Foraminiferal evidence for these events shows synchronicity with bulk organic carbon isotope data from core UV1 (Yu, 2009) and with southeastern Chinese speleothem oxygen isotope records (Y. Wang *et al.*, 2005; Hu *et al.*, 2008). The coincidence of ice-rafting events in the North Atlantic and weak monsoon intervals in East Asia is proposed to reflect forcing by solar variability or the rapid propagation of atmospheric or oceanic circulation disturbances following iceberg calving events (Broecker, 1994; Bond *et al.*, 2001; Zhao *et al.*, 2003; Porter and Zhou, 2006).

Holocene sedimentation in core UV1 is inferred to have commenced at approximately 6300 cal. years BP. Subaerial exposure of the shallow basin due to lowered sea level explains the lack of Last Glacial Maximum or early-Holocene estuarine deposits. With significant changes in monsoon precipitation intensity inferred for these periods from terrestrial and marine proxies (e.g. Wang *et al.*, 1999a; Y. Wang *et al.*, 2005; Yancheva *et al.*, 2007), it is clearly desirable for further work to be focused on obtaining a corresponding nearshore record. While cores taken from further offshore contain lowstand sediments, the rise in sea level

during the early Holocene is likely to have had a profound effect on faunal assemblages. Furthermore changes in fluvial flux are unlikely to have had as great an influence on the salinity of locations further removed from the contemporary coastline.

7.3.3 Final thesis conclusions

This thesis reports the distribution of benthic foraminifera from the Pearl River estuary, southeast China and their development as a proxy for salinity. Qualitative and quantitative analyses are used to produce a high resolution, precisely dated record of a relative stable estuarine environment over the mid- to late-Holocene. The slight increase in salinity in the face of shoreline progradation observed over the course of the record is primarily attributed to decreasing fluvial discharge, supporting previous terrestrial, lacustrine and marine reconstructions of Holocene East Asian monsoon intensity. Further work would be required to establish the precise link between salinity estimates derived from foraminiferal proxies and palaeodischarge. A recent, well dated sediment record, with a corresponding instrumental record of fluvial discharge could indicate the extent to which variability in salinity in the southeast of the estuary is dependant on fluvial flux. This research has provided extensive and hitherto unavailable baseline data on the ecology of foraminifera in an estuarine environment. While the magnitude of the sample specific errors to some extent negate the use of transfer functions to reconstruct Pearl River estuary palaeosalinity, the modern dataset may potentially provide a basis for the analysis of other cores in the Pearl River estuary and vicinity. Areas of the contemporary delta plain and inner estuary may have experienced greater changes in salinity and cores from these locations could provide further information on fluvial flux and the evolution of the estuary.

Appendices

Appendix 5.1: Summary statistics for dominant and common benthic foraminiferal taxa in contemporary surface samples

Taxa	Number of occurrences	N ₂	Maximum %	Sample with maximum %	Mean %	Number of samples >5%
<i>Ammobaculites formosensis</i>	71	35.8	66.8	72	14.5	49
<i>Ammobaculites</i> sp.	54	23.7	17.3	78	2.5	11
<i>Ammotium salsum</i>	20	6.9	24.4	78	1.1	6
<i>Haplophragmoides</i> sp.	66	34.0	40.4	71	6.8	31
<i>Textularia foliacea</i>	27	8.8	14.5	93	1.0	5
<i>Ammonia beccarii</i>	76	52.5	83.8	55	29.7	72
<i>Cibrononion subincertum</i>	34	16.8	11.0	104	1.1	4
<i>Elphidium advenum</i>	40	24.2	14.4	28	3.0	18
<i>Elphidium hispidulum</i>	41	22.7	10.9	36	1.3	3
<i>Florilus scaphus</i>	29	13.7	12.6	23	1.0	4
<i>Hanzawaia nipponica</i>	25	10.6	13.1	23	0.9	4
<i>Haynesina</i> sp.	62	17.2	60.0	62	7.6	25
<i>Nonionella stella</i>	35	15.7	11.1	24	1.0	3
<i>Pararotalia nipponica</i>	13	6.9	11.1	21	0.6	4
<i>Quinqueloculina akneriana</i>	46	18.2	26.2	102	2.7	13
<i>Quinqueloculina lamarkiana</i>	26	8.7	12.7	38	0.6	2
<i>Quinqueloculina seminula</i>	40	24.2	11.5	39	1.8	8
<i>Quinqueloculina</i> sp.	47	27.3	12.0	85	2.0	11
<i>Rotalinoides annectens</i>	56	23.4	49.1	60	6.0	24
<i>Spiroloculina lucida</i>	30	10.6	13.2	60	0.9	2

Appendix 5.2: Relative abundances of contemporary Pearl River estuary foraminifera, ordered by CONISS cluster

Sample	Total Specimens	<i>Ammobaculites formosensis</i>	<i>Ammobaculites</i> sp.	<i>Ammotium salsum</i>	<i>Haplophragmoides</i> sp.	<i>Millammina fusca</i>	<i>Reophax</i> sp.	<i>Sigmollina tenuis</i>	<i>Sigmoilopsis asperula</i>	<i>Sigmoilopsis schlumbergeri</i>	<i>Siphonaperta</i> cf. <i>agglutinans</i>	<i>Siphonotularia watoana</i>	<i>Spirolectamina bififormis</i>	<i>Textularia conica</i>	<i>Textularia earlandi</i>	<i>Textularia foliacea</i>	<i>Textularia valentula</i>	<i>Trochammina globigeriniformis</i>
6	103	62.14	13.59		3.88													
72	331	66.77	9.37		4.53		0.3											
4	65	43.08	9.23		9.23	1.54												
5	61	44.26	3.28		24.59													
14	57	40.35			21.05													
71	312	36.54	8.33		40.38													
78	127	16.54	17.32	24.41	11.02	0.79										6.3		
79	123	33.33	13.82	7.32	6.5											5.69		
81	303	47.19	8.58	13.86	1.98											14.19	0.33	
103	75	36	9.33		8													
104	73	32.88	10.96															
82	125	34.4	6.4		16											1.6		
83	124	16.94			10.48											0.81		
66	305	14.75	0.66	3.28	20.98													
87	321	30.84	4.05	0.62	15.89													
90	349	25.21	2.01	0.29	22.64			0.29									0.31	
85	308	27.92	0.97	2.27	14.61												0.86	
97	399	29.32	3.76		14.29												0.65	
98	312	33.97	1.92		11.22													
95	328	32.62	1.83		12.2		0.3											
39	347	25.07	0.58		6.34													0.29
100	322	15.84	3.11		6.83	0.31												
1	65	1.54			6.15													
8	110	0.91			1.82													
9	68																	
62	100				2													
63	176		0.57	5.68	1.14													0.57
59	83	2.41																
55	136				0.74													
57	124	0.81		0.81	0.81													
58	157	7.01	1.27		2.55													
64	104	5.77	1.92		1.92													0.96
65	116	14.66	2.59	4.31	10.34													
105	318	8.49	2.83	8.49	11.64													
69	104	20.19	0.96		4.81									0.96				
68	105	4.76	0.95	0.95	4.76													
75	100	5			22													
80	66	16.67	4.55		7.58													
94	97	5.15	6.19		6.19												1.03	
40	354	19.21	2.82		17.51	1.13		0.28						0.56				1.98
73	110	27.27	3.64		19.09									0.91				
70	85	20	4.71		9.41													
67	343	7.29	1.46	0.58	4.66													
89	334	15.57	1.8	0.3	9.28			0.9				0.3						0.6
3	64	9.38			3.13	1.56												
7	115	22.61	4.35		12.17	1.74												
84	101	8.91	0.99	0.99	4.95													
93	76	7.89		5.26	10.53	1.32												
86	140	6.43	0.71															
91	324	14.81	0.62	2.78	13.89									0.31				
92	327	6.42	0.31	0.31	4.59		0.92	0.61								1.53		0.31
31	359	6.13	0.28		1.67		1.67	0.28										
88	115	13.28	1.56		1.56	0.78										0.78		
21	416	0.72	0.72		4.33			1.92	2.4	0.96	0.72					1.2		
22	426	0.7	0.94		5.87		0.47	0.47	0.7	0.47						2.11		4.69
23	404	1.49	0.25		1.73		0.5	0.99	1.24							0.25		3.22
27	430	8.37	0.23		3.95		0.23	5.81	5.12		0.47					0.47		
28	527	3.98	0.19		4.55		0.38	2.66	1.14							0.76		
29	340	12.65	1.47		2.94		3.53	1.76			4.71			0.19	0.88			
24	377	1.59	1.86		0.53		5.04	1.33	1.33		3.71		0.27	0.27	0.27			3.45
30	257	1.17	0.39				1.95	4.28	3.5					0.78	0.39			0.78
26	427	2.34	0.7		1.41			1.87	2.81					0.23	0.7			
32	334	0.9			0.6		0.3	0.9	0.9				0.3		0.9			
33	331	1.21			0.6		0.6	2.42	2.11				0.6	0.6	2.72			0.3
25	349	4.87	0.57		0.57		0.57	1.15	1.15		1.15		0.86	1.72	1.15			2.01
60	106	0.94			1.89													
61	135	0.74		0.74														
101	308	3.25	0.97		1.3													
102	347	1.15			0.86													
99	312	10.26	2.56		3.53												0.64	
96	307							0.98										
35	229	5.24			2.62		0.44				0.44		0.44		1.75			
36	202	1.98	0.5		1.98		0.5	1.49	1.98	0.99					0.5			0.99
34	476	4.83	2.31		1.68	0.21	0.42	1.89	1.47						0.21			0.84
37	359	6.96			1.95			0.28			0.56				0.28			
38	308	0.65							0.97	0.32					0.32			

Appendix 5.2 (continued):

Sample	Trochammina squamata	Ammonia ariakensis	Ammonia beccarii	Ammonia ketenziensis angulata	Ammonia luqiataensis	Ammonia spp.	Astrononion sp.	Bolivina pseudoplicata	Bolivina pseudopunctata	Bolivina robusta	Bolivina spathulata	Bolivina striatula	Brizalina c.f. canvallaria	Buccella frigida	Bulimina elongata	Bulimina marginata	Buliminella elegantissima	Cassidulina cf. teretis
6		17.48																
72		13.6				0.91												
4		35.38																
5		19.67																
14		22.81																
71		8.65				1.6												
78		20.47				0.79												
79		20.33				0.81		0.81										
81		8.58				1.98												
103		9.33			1.33	1.33												
104		16.44																
82		16				1.6												
83		29.03		0.81		0.81						3.23				0.81	1.61	
66		12.13				3.28												
87		12.77		0.62				0.31			0.31				0.31			
90		15.47		0.29						0.29	2.58	0.86					0.57	
85		24.03				1.95		0.32										
97		16.79			0.5	1.75												
98		21.79				3.85												
95		32.01				3.05	0.3				0.3	0.61				0.3		
39		32.28				3.46			0.58									
100		22.98				0.62												
1		53.85				6.15												
8		38.18				3.64												
9		41.18																
62		36																
63		32.39		0.57														
59		44.58																
55		83.82				1.47												
57		75.81				0.81												
58		75.16				2.55												
64		60.58																
65		45.69				0.86												
105		51.57				2.52												
69		51.92	2			2.88												
68		58.1				2.86												
75		42				3												
80		48.48								1.52	3.03	1.52		1.52	3.03			
94		53.61				2.06					1.03							
40	0.28	43.22				1.69						0.28						
73		36.36				2.73												
70		27.06																
67		49.85				3.5		0.29										
89		43.11		0.6		2.1		0.6		0.6	1.2	1.8	0.3				0.3	
3		54.69																
7		30.43				6.09												
84		57.43				2.97		0.99								0.99		
93		36.84				1.32												
86		67.86				2.86				0.71								
91		31.79		0.31		1.85		1.54			0.31	0.93			0.62		0.62	
92		36.39		0.61		3.67		3.06		0.31	1.53	0.92	0.31		0.31		0.92	
31		64.9				0.84					1.95	2.51				0.84		0.28
88		58.59		0.78		1.56				0.78	0.78	2.34				1.56		
21	0.24	5.05				1.68		0.48	0.48	0.48	1.44	0.96	0.48	0.24	0.48	0.96		
22	0.23	0.47	4.69		0.23	1.64		1.64	0.47	0.94	0.7	0.7				1.17		0.47
23	0.5		0.25	0.74		2.23		0.74	0.5	1.98	1.49	0.25				0.99	0.25	0.74
27	0.23		14.88			1.63		0.93	0.47	0.47	3.26	0.7	0.23			2.09		
28			11.76			2.85				1.71	1.33	0.57	0.76		0.95	0.76		
29		2.65	22.65			1.76	0.59			0.57	2.35	3.82		0.88		0.59		
24		0.8	7.96	1.06		3.98					4.77	2.12	0.27		0.53	1.59		0.53
30		2.33	7.78	0.78	0.39	4.67			0.8		3.89	2.33	2.72		0.39	5.06	0.78	
26			9.13			2.58					2.11	2.34	0.47			1.17		
32			19.76		1.2	2.4			0.3	1.2		3.29				0.3		
33		1.21	11.48	1.51	0.6	4.83						1.51	0.6			1.21		
25		0.57	4.01	1.43	0.29	1.15			0.86		1.72	1.43	0.57			2.01	0.29	
60			22.64	0.94														
61			47.41			1.48					0.74							
101			12.66		0.65	2.27												
102			20.17		0.86	1.15												
99			18.59			3.85					0.32							
96			3.91			0.33					0.33				0.98			
35	0.44		8.3		0.44				0.44			0.44						
36	1.98		15.35		1.49									1.49				
34		1.26	15.13		0.84	3.78			0.63		0.42	0.63	0.42	0.42				
37		0.84	10.31		0.28	3.62						0.56						
38			7.14			4.55						0.32				0.32		

Appendix 5.2 (continued):

Sample	<i>Cibicides lobatulus</i>	<i>Cibicides pseudoemgerianus</i>	<i>Cibicides</i> sp.	<i>Cribronion subincertum</i>	<i>Dentalina</i> spp.	<i>Edentostomina cultrata</i>	<i>Elphidium advenum</i>	<i>Elphidium asiaticum</i>	<i>Elphidium crispum</i>	<i>Elphidium etigoense</i>	<i>Elphidium hispidulum</i>	<i>Elphidium incertum</i>	<i>Elphidium magellanicum</i>	<i>Elphidium</i> spp.	<i>Elphidium williamsoni</i>	<i>Fissurina lucida</i>	<i>Fissurina marginata</i>
6																	
72																	
4																	
5																	
14											1.75						
71								0.32									
78																	
79				3.25			0.81										
81																0.33	
103				8							2.67						
104				10.96							1.37						
82																0.8	
83	1.61															1.61	
66	0.33						1.97	6.23			1.97			0.66			
87							0.93				0.31					0.31	
90				0.57			1.43	0.86			1.15					0.57	
85							1.95	0.32								0.65	0.32
97	0.5	0.25		1.5			1.5	1	0.75		0.5						
98	1.28			1.6			3.85	0.32			0.32						
95	1.22		0.3				0.91	0.91								0.3	
39				0.29			2.02	0.86	0.29		2.59	0.58				0.29	
100	0.62	0.31		0.31			6.83	1.55	3.11		1.24	0.31					
1																	
8																	
9																	
62																	
63									0.57								
59				2.41													
55											0.74						
57																	
58																	
64																	
65																	
105				6.29													
69				1.92				0.96									
68				4.76													
75							1										
80				4.55													
94								2.06								1.03	
40								0.28			1.98	1.13		0.28		0.28	
73	0.91			4.55													
70				8.24													
67	0.58			0.58			0.58				4.96			0.29			
89							1.5	0.3			0.3		0.3			0.3	
3											1.56						
7											1.74						
84	1.98										0.99						
93	1.32			1.32							1.32						
86																	
91							2.78	0.31			0.93		0.31			0.93	
92	2.75						2.14	0.61			1.83	0.61	0.31	1.83		0.92	
31				2.51			1.39	0.84	0.28		1.39		0.84			1.11	
88	0.78						0.78	1.56			2.34		0.78			1.56	
21			0.24				14.42	0.48	1.2		2.4						
22	0.7		0.23	0.47		0.47	14.32	0.94	1.17		2.11					0.7	
23	0.99						10.64	0.74	0.99		1.24	0.5			0.74	0.5	
27	0.7			0.23			10.93	0.7	1.4		0.47	0.23		1.86		1.16	
28	0.95			1.33			14.42	3.42	3.23		3.42	0.57		2.85			
29			0.29	1.76			6.76	2.65			1.76	1.76		2.06		0.88	
24	0.27			2.39			4.24	1.86	0.27			1.86		1.06		1.86	
30	0.39		0.78	1.95			3.11	0.78			0.78	4.28		0.78		0.39	
26			0.7	0.47	0.23		13.11	3.28	1.17		2.81	0.47		1.17			
32	0.6			0.6	0.3		11.68	3.29	0.6		8.08	2.1		0.9		0.3	
33	1.51		1.21	1.21			7.55	1.81	2.42		4.23	0.6		1.51	0.3	0.91	
25	0.57						7.16	0.29	2.58		0.57	0.57		0.57		0.29	0.57
60				3.77			0.94										
61				2.96			8.15	2.96	0.74		1.48						
101	0.65	0.65					4.22	0.65	2.27		2.27	0.65			0.32		
102		0.86		0.86		0.29	5.19	0.29	3.46		1.73	1.15	0.58				
99	1.6	0.32		0.64			4.81	1.28	0.96								
96	3.91						3.58	0.98	2.93							0.33	
35	1.75			2.62	0.44	0.44	5.68		7.42		6.11	0.87					
36	1.49			0.5			13.37	1.98	2.97		10.89						
34	0.21		0.84	0.42			9.87	1.05	3.99		3.36	1.89		0.63		0.84	
37			0.56				13.37	2.79	6.13		4.74			2.51			
38							11.36	2.27	0.97		4.87	0.32		2.27		0.32	

Appendix 5.2 (continued):

Sample	<i>Florilus decorus</i>	<i>Florilus japonicus</i>	<i>Florilus scaphus</i>	<i>Fursenkoina compactiformis</i>	<i>Fursenkoina fusiformis</i>	<i>Fursenkoina schreibersiana</i>	<i>Glandulina laevigata</i>	<i>Guttalina</i> sp.	<i>Hanzawaia nipponica</i>	<i>Haynesina</i> sp.	<i>Heterolepa haidingeria</i>	<i>Hopkinsina pacifica</i>	<i>Hyalinonetricion gracillima</i>	<i>Lagena distoma</i>	<i>Lagena elongata</i>	<i>Lagena hispidula</i>	<i>Lagena perlucida</i>
6									2.91								
72									3.02								
4																	
5									8.2								
14									8.77								
71			0.32						0.32								
78									2.36								
79			1.63						4.88								
81					0.33				0.33								
103									1.33								
104									1.37								
82			1.6						1.6								
83	0.81								6.45								
66		0.33							0.66								
87								0.31	0.31					0.31			
90	0.57		0.29	0.86		0.29			0.57							0.29	
85						0.32			1.3								
97			0.5						0.25								
98									0.96								
95	0.3		0.3		0.3			0.3	2.13							0.3	
39																	
100			0.31					0.31	0.62								
1									30.77								
8			0.91						51.82								
9									58.82								
62			1						60								
63									56.25								
59									46.99								
55									13.24								
57									20.97								
58									11.46								
64			0.96						25								
65									21.55								
105									6.92								
69								0.96	12.5								
68									10.48								
75									22								
80									6.06								
94			2.06						8.25								
40									0.56								
73																	
70									7.06								
67		0.58				0.29			2.33							0.29	
89		0.3		0.3					1.2								
3									20.31								
7									9.57								
84			0.99						0.99								
93			5.26						6.58								
86									5								
91			1.54	0.31				2.16	0.62					0.62	0.31		
92	0.92		3.36	0.61	0.31	0.61		0.31	1.53						0.61		
31				0.84													
88			2.34	0.78					1.56								
21	2.16		8.41	2.16				9.13									
22	3.05		4.69	3.76			0.47	6.81									
23	7.43		12.62	1.73				13.12		0.74							
27	4.19		4.65	2.33				3.95									
28	4.36		4.17	1.52				3.04	2.66								
29	2.35		1.76	0.88	0.88			1.47						0.29			
24	1.86		5.57	7.96				1.06									
30	2.72		2.33	1.17				1.17	0.39		0.78						
26	4.22		2.81	1.87				3.28	0.23								
32	1.5		0.6	0.3				2.1									
33	1.81		0.3	0.91	0.6			3.32	1.81								0.3
25	2.87		2.29	2.58			0.57	7.16	0.57		0.29						
60									2.83								
61									0.74								
101				0.32				0.32	0.32								
102				0.58				0.58	0.58								
99					0.32			0.64	0.64								
96		0.65							0.65								
35								2.18									
36			0.99					1.49									
34					0.42			0.63	0.63	0.63							
37								1.11	0.28								
38									0.97								

Appendix 5.2 (continued):

Sample	Lagena piscata	Lagena substriata	Milliolina circularis	Milliolina sp.	Milliolina subrotunda	Neoponides mira	Nonion pauperata	Nonionella stella	Oolina striata	Orphomorphina perversa	Pararotalia nipponica	Planorbulina mediterraneensis	Quinqueloculina akneriana	Quinqueloculina akneriana rotunda	Quinqueloculina bicostata	Quinqueloculina contorta	Quinqueloculina donghaiensis
6																	
72																	
4																	
5																	
14																	
71								0.32					0.96				
78																	
79													0.81				
81													0.66				
103													2.67				
104								1.37					2.74				
82																	
83								2.42					1.61			0.81	
66								0.33									
87								0.31					6.23				
90													2.01			0.29	
85													0.97				
97								0.5					6.52				
98								0.96					3.85	0.32			
95								1.52					1.52	0.3			
39													5.19	0.58	0.29		
100													5.9				
1																	
8																	
9																	
62																	
63																	
59								1.2					1.2				
55																	
57																	
58																	
64								0.96						0.96			
65																	
105								0.63					0.31				
69													1.92				
68								3.81					3.81				
75								2					3				
80								1.52									
94								9.28									
40													4.52				
73													2.73				
70													8.24				
67								1.17					2.33				
89		0.3			0.3								1.5				
3													1.56			1.56	
7													0.87				
84								0.99						1.98			
93													1.32				
86																	
91		0.31						2.47			0.62		2.78				
92		0.31						3.67			0.31		1.83			0.92	
31								0.56					6.41				
88																2.34	
21	0.48	0.48						4.09			11.06		1.44				
22	0.23	1.64			0.23			6.34		0.23	8.45		0.94				
23		0.5						4.46			8.42		0.5				
27	1.16							0.93								0.23	
28	0.57	0.57						2.66				0.23					
29		0.59										0.38					
24		1.06										0.59	0.59	0.29			
30		3.11						11.14	0.27		3.45		0.27				
26		1.87			0.47		1.17	2.72	0.39		0.39		2.33			0.78	
32		0.6			0.3			2.11			6.32	0.23	3.28	0.47		0.47	
33		0.91				0.91	0.6	0.91			4.19		7.19	0.3			
25		2.01			0.57		0.29	3.15			1.21		2.11	0.3	0.3	0.6	
60											2.29	0.57	2.29	0.57			
61													0.94				
101								0.65					18.18	0.97		0.74	
102								0.29					26.22			0.29	
99								0.32					17.95	0.64			
96						0.33		0.65					19.54	2.28		0.33	0.33
35															0.87	0.87	
36															3.47		
34					0.84			0.42			0.63		7.14	1.05		0.21	
37					0.56						1.39				0.84	0.56	
38			0.32	0.97	1.95								8.44	1.62			

Appendix 5.2 (continued):

Sample	Quinqueloculina elongata	Quinqueloculina granulocostata	Quinqueloculina lamarkiana	Quinqueloculina poeyana	Quinqueloculina pseudoreticulata	Quinqueloculina sabulosa	Quinqueloculina seminula	Quinqueloculina sp.	Quinqueloculina stalkerii	Quinqueloculina tiktoensis	Quinqueloculina venusta	Reussella aculeata	Reussella pacifica	Rosalina australis	Rosalina globularis	Rosalina spp.	Rotalioidea annectens
6																	
72								0.91									0.3
4								1.54									
5																	
14							1.75	3.51									
71			0.32				0.32	0.96									0.64
78																	
79																	
81								0.66									0.99
103																	20
104							2.74										17.81
82						0.8											19.2
83																	20.16
66							2.3	0.33									29.51
87	0.31						1.25	5.61							0.31		14.95
90			0.57				1.43	5.16									10.6
85	0.97					0.32		12.01									6.49
97	0.5						3.01	3.51									9.52
98	1.6						1.6	3.21									4.81
95	1.83		0.3				0.3	1.22									0.61
39			0.29				11.53		0.29			0.29					6.05
100			2.48		0.31		2.17	1.24									19.57
1																	1.54
8																2.73	
9																	
62																	1
63																	2.27
59							1.2										
55																	
57																	
58																	
64																	0.96
65																	
105																	0.31
69																	
68							1.9								0.95		1.9
75																	
80																	
94																	2.06
40							0.28	0.85									0.85
73								1.82									
70							3.53	11.76									
67	1.17		0.29				9.62	6.41									0.87
89	0.3						7.19	2.1									3.59
3							3.13	1.56									1.56
7							1.74	3.48									5.22
84								3.96									0.99
93								1.32		1.32							2.63
86	0.71		4.29					6.43									
91	1.23		1.23				0.93	0.93		0.31					0.62		6.79
92	1.53		0.61				1.22	2.75	0.31						0.31		1.53
31								0.56									1.95
88																	
21	0.24		0.96				2.64	2.16			0.96				1.44	0.72	5.53
22	0.47		0.23				3.52	1.17			0.47			0.23	1.41	0.23	2.58
23	0.5						3.71	1.73					0.5	0.99	2.97	1.24	1.49
27	3.02		0.7				0.93	1.86				0.23			1.86	1.4	3.49
28	0.76	0.19	1.33				1.33								1.14		6.64
29	0.88		0.29				1.18	2.06				0.88				2.06	1.47
24	1.86		0.27				1.86	0.27	1.06						0.27	1.59	1.06
30	2.33					0.78	3.89	2.72	3.89				0.78	1.95	2.72	3.5	0.39
26	3.98		0.23		0.23		3.75	1.87		0.94	0.94		0.23	1.17	1.64	1.41	0.7
32	5.99		0.9				2.69	2.99		0.3	1.2				2.4	1.2	1.2
33	4.23	0.3	0.6		0.3		3.63	2.42			0.91			2.11	1.21	1.51	4.83
25	3.44		0.86	0.29			3.72	0.57	2.01		4.3		0.29	0.57	3.72	0.57	3.72
60						2.83											49.06
61								2.22									27.41
101	1.3		3.25		0.32		6.17	5.84									20.45
102	1.44				0.29		7.49	2.02	0.58								15.27
99	3.85						5.77	6.09		0.32							4.81
96	5.21		0.98		0.98		4.89	9.77		0.65							23.45
35	0.87		3.93		2.18		11.35	3.93		0.87			0.87			0.44	15.72
36			3.96					5.45							0.5		18.32
34	3.15		1.26		0.42		4.2	5.46								1.26	4.83
37	0.56		5.85		1.11		5.29	2.23		0.28							10.58
38	5.19		12.66					3.57	2.6	0.97				0.97	0.65		15.58

Appendix 5.2 (continued):

Sample	Spirillina sp.	Spiroculina aescata	Spiroculina communis	Spiroculina laevigata	Spiroculina luccia	Stainforthia complanata	Triloculina rotunda	Triloculina tricarinata	Triloculina trigonula	Planktic foraminifera
6										
72					0.3					
4										
5										
14										
71										
78										
79										
81										
103										
104					1.37					
82										
83										
66					0.33					
87					1.87		0.62			
90					0.57	0.29	0.29			
85					1.3			0.32		
97				1.5	0.75				1	
98	0.32			1.28	0.96					
95				0.3	0.61		0.61			
39										
100				0.93	1.86				0.31	
1										
8										
9										
62										
63										
59										
55										
57										
58										
64										
65										
105										
69										
68										
75										
80										
94										
40										
73										
70										
67										
89	0.3							0.6		
3										
7										
84										
93										
86										
91					0.62					0.31
92				0.92	0.31		0.92	0.31		0.92
31										
88									0.78	
21	0.24							1.2	0.24	1.92
22					0.23			1.17	0.47	3.29
23								0.74		4.95
27		0.23			0.7			0.7		1.16
28	0.19	0.19	0.57		1.9			0.57		0.95
29					0.29					
24										
30										0.78
26	0.7	0.23			0.7			1.41	0.7	2.34
32				0.6	0.3			0.3	1.2	0.3
33	0.3				1.51			0.6	1.21	
25			1.72		1.15			1.15	1.72	1.43
60					13.21					
61					1.48					
101				4.22	4.22				0.65	
102				2.88	2.59			0.29		
99	0.32			4.81	4.17				0.64	
96			0.65	3.58	3.26			1.63	1.95	
35				5.24	0.87		1.75	1.75		
36				0.99			1.98	0.5		
34	0.21	0.84			3.99			1.26		
37					12.26		0.28	1.11		
38				0.65	4.55			0.65	0.65	

Appendix 5.3: Summary surface samples environmental data, grouped by CONISS clusters

Cluster	Sample	Longitude (°E)	Latitude (°N)	Mean salinity (psu)	Water depth (m)	TOC (%)	TN (%)	C/N	δ13C (‰)	Sand (%)	Clay (%)	Silt (%)
A	6	113.80	22.52	20.30	5.8	1.27	0.09	14.60	-23.50	16.8	28.2	55.0
	72	113.75	22.39	23.85	15.0	0.96	0.10	9.90	-22.00	16.8	30.5	52.8
	4	113.83	22.46	26.00	4.8	0.90	0.08	11.10	-23.90	35.7	21.5	42.8
	5	113.83	22.54	23.45	4.0	1.32	0.11	12.30	-23.30	18.9	29.1	52.0
	14	113.65	22.77	12.15	3.8	0.74	0.07	11.40	-22.70	8.4	32.4	59.2
	71	113.78	22.38	29.25	13.0	0.95	0.08	11.60	-23.80	15.8	28.4	55.8
	78	113.60	22.25	14.50	6.2	1.24	0.15	8.40	-23.10	20.3	33.2	46.5
	79	113.65	22.25	21.50	5.3	1.25	0.14	9.10	-23.10	9.0	32.5	58.6
	81	113.60	22.19	17.00	5.3	1.24	0.14	8.80	-23.10	16.1	31.3	52.6
	103	113.77	22.44	30.25	5.0	...	0.06	18.5	31.3	50.1
	104	113.74	22.44	17.50	12.0	...	0.07	7.1	35.5	57.3
	82	113.65	22.19	23.50	7.0	1.13	0.12	9.40	-22.90	16.9	28.2	54.9
	83	113.70	22.19	27.25	6.0	1.16	0.12	9.60	-23.20	14.7	29.7	55.6
	66	113.60	22.29	12.75	3.5	0.94	0.11	8.90	-22.90	22.0	31.1	46.9
	87	113.65	22.08	28.75	8.5	0.93	0.09	10.30	-23.00	20.9	20.2	58.9
	90	113.75	22.13	31.75	8.5	1.09	0.11	9.90	-22.90	18.6	24.3	57.1
	85	113.67	22.13	28.25	8.5	0.90	0.09	9.70	-22.90	19.6	25.2	55.2
	97	113.82	22.33	31.00	11.3	...	0.08	18.7	30.7	50.5
	98	113.82	22.33	31.00	10.5	...	0.07	24.5	27.1	48.4
	95	113.76	22.30	29.75	5.3	...	0.09	13.1	35.6	51.3
39	113.93	22.46	24.63	4.0	1.05	0.11	9.30	-23.80	4.0	32.3	63.8	
100	113.83	22.42	29.50	5.2	...	0.06	41.4	22.7	35.9	
Average		113.74	22.34	24.27	7.2	1.07	0.10	10.27	-23.13	18.1	29.1	52.8
B	1	113.64	22.58	6.00	4.4	1.02	0.06	17.50	-24.20	32.9	12.8	54.3
	8	113.72	22.61	14.50	2.8	1.51	0.12	12.70	-24.10	19.9	25.4	54.7
	9	113.67	22.63	11.60	2.1	0.99	0.08	13.00	-23.60	24.0	22.0	53.9
	62	113.68	22.58	10.00	8.0	0.25	0.03	8.50	...	37.8	11.2	51.0
	63	113.66	22.45	6.80	5.5	1.21	0.11	11.20	-23.50	9.3	27.0	63.7
	59	113.72	22.47	14.00	15.0	1.34	0.13	10.50	-23.40	12.7	23.9	63.4
Average		113.68	22.55	10.48	6.3	1.05	0.09	12.23	-23.76	22.8	20.4	56.8
C	55	113.63	22.53	2.80	8.0	1.40	0.08	17.10	-23.90	55.8	7.3	37.0
	57	113.65	22.45	5.85	7.0	1.35	0.13	10.70	-22.70	13.3	29.8	57.0
	58	113.68	22.46	8.50	10.0	1.26	0.11	11.40	-23.20	12.5	29.2	58.3
	64	113.65	22.38	11.50	7.0	1.27	0.13	9.90	-23.20	36.0	11.1	53.0
	65	113.62	22.33	12.25	5.0	0.71	0.06	11.30	-23.50	12.8	34.5	52.7
	105	113.69	22.43	11.40	7.0	...	0.09	16.7	32.2	51.0
	69	113.72	22.34	20.75	13.5	1.23	0.12	9.90	-23.10	12.5	33.3	54.1
	68	113.68	22.32	16.75	12.0	1.13	0.09	12.20	-23.40	19.9	18.4	61.6
	75	113.68	22.49	9.50	7.0	1.11	0.09	11.80	-23.10	26.9	20.8	52.3
	80	113.70	22.25	25.25	5.8	1.26	0.13	9.70	-23.40	13.7	35.2	51.1
	94	113.71	22.29	23.55	5.8	...	0.11	6.3	34.7	59.0
	40	113.96	22.48	22.00	3.0	1.23	0.14	9.00	-23.90	13.8	23.3	62.9
	73	113.75	22.35	24.50	15.0	1.13	0.11	10.30	-22.90	18.4	28.9	52.7
	70	113.77	22.37	27.50	20.0	1.38	0.12	12.00	-23.60	15.7	31.3	53.0
	67	113.64	22.31	15.50	13.0	1.07	0.12	8.90	-22.60	7.1	38.3	54.6
	89	113.76	22.19	30.50	8.5	1.10	0.11	9.70	-23.20	14.8	25.6	59.6
	3	113.74	22.45	19.85	5.0	1.17	0.10	11.50	-23.10	22.3	26.1	51.6
	7	113.76	22.56	17.20	4.8	1.13	0.06	17.70	-23.50	30.8	17.8	51.4
	84	113.62	22.13	23.75	6.8	1.23	0.13	9.40	-23.30	15.4	29.5	55.1
	93	113.64	22.25	19.00	15.0	...	0.12	3.4	38.1	58.4
	86	113.60	22.08	24.75	6.0	1.50	0.15	10.30	-23.40	17.1	28.7	54.2
	91	113.73	22.08	32.25	11.5	0.91	0.09	10.60	-23.10	16.9	19.8	63.3
	92	113.80	22.10	33.75	14.0	0.98	0.11	8.80	-22.50	15.9	21.5	62.6
	31	114.02	22.26	33.01	8.0	1.13	0.14	7.80	-21.80	6.8	32.8	60.4
88	113.77	22.25	30.50	6.3	1.09	0.12	9.40	-23.20	16.0	30.2	53.8	
Average		113.72	22.33	20.09	9.0	1.17	0.11	10.88	-23.16	17.6	27.1	55.2

Appendix 5.3 (continued):

Cluster	Sample	Longitude (°E)	Latitude (°N)	Mean salinity (psu)	Water depth (m)	TOC (%)	TN (%)	C/N	δ13C (‰)	Sand (%)	Clay (%)	Silt (%)	
D	21	114.45	22.37	33.64	24.0	0.68	0.10	6.80	-21.00	17.3	18.8	63.9	
	22	114.45	22.29	33.75	25.0	0.75	0.11	6.80	-20.80	14.4	21.6	63.9	
	23	114.45	22.22	33.84	28.0	0.63	0.10	6.50	-21.20	19.8	24.6	55.6	
	27	114.18	22.22	32.99	14.0	0.92	0.12	7.70	-21.80	9.9	26.0	64.1	
	28	114.08	22.19	32.98	14.0	1.60	0.09	10.00	-22.50	23.5	18.1	58.4	
	29	114.08	22.23	31.78	8.0	1.02	0.12	8.80	-22.30	15.8	24.8	59.4	
	24	114.32	22.20	33.75	31.0	0.92	0.13	7.10	-21.10	3.4	27.8	68.7	
	30	114.12	22.25	33.18	35.0	0.83	0.09	9.00	-23.20	2.6	31.0	66.5	
	26	114.23	22.21	33.11	14.0	0.68	0.09	7.10	-21.00	16.5	17.4	66.1	
	32	113.96	22.22	31.62	6.0	0.62	0.08	8.00	-21.90	8.3	15.8	75.9	
	33	114.10	22.32	32.64	20.0	0.59	0.06	10.30	-24.10	29.0	21.7	49.2	
	25	114.27	22.24	33.31	21.0	0.57	0.07	8.00	-21.50	21.3	17.6	61.1	
	Average		114.22	22.25	33.05	20.0	0.82	0.10	8.01	-21.87	15.2	22.1	62.7
	E	60	113.75	22.50	23.50	18.0	0.66	0.04	14.90	-24.20	63.2	8.6	28.2
61		113.72	22.55	22.50	16.0	0.38	0.03	15.10	-27.00	42.5	17.9	39.5	
101		113.85	22.45	29.00	5.2	...	0.04	8.9	28.6	62.5	
102		113.81	22.50	25.75	4.8	...	0.04	46.8	19.0	34.1	
99		113.83	22.36	30.75	9.5	...	0.08	11.9	34.6	53.5	
96		113.81	22.31	31.00	6.5	...	0.05	12.2	27.7	60.0	
35		113.95	22.36	30.92	14.0	1.45	0.07	10.60	-22.20	13.9	29.3	56.8	
36		113.90	22.32	28.38	5.0	0.39	0.04	9.00	-22.80	24.9	22.4	52.6	
34		113.98	22.35	30.24	11.0	0.78	0.08	10.10	-24.10	18.9	24.9	56.2	
37		113.90	22.38	30.51	20.0	0.56	0.05	10.40	-23.20	47.8	15.2	37.0	
38		113.89	22.43	28.63	8.0	0.75	0.06	12.30	-22.80	11.9	28.2	59.9	
Average			113.85	22.41	28.29	10.7	0.71	0.05	11.77	-23.76	27.5	23.3	49.1

Appendix 5.4: Species codes used in Canonical Correspondence Analysis species – environment biplots

<i>Ammo for</i>	<i>Ammobaculites formosensis</i>
<i>Ammo sp.</i>	<i>Ammobaculites sp.</i>
<i>Ammo sal</i>	<i>Ammotium salsum</i>
<i>Hapl sp.</i>	<i>Haplophragmoides sp.</i>
<i>Text fol</i>	<i>Textularia foliacea</i>
<i>Ammo bec</i>	<i>Ammonia beccarii</i>
<i>Crib sub</i>	<i>Cribrononion subincertum</i>
<i>Elph adv</i>	<i>Elphidium advenum</i>
<i>Elph his</i>	<i>Elphidium hispidulum</i>
<i>Flor sca</i>	<i>Florilus scaphus</i>
<i>Hanz nip</i>	<i>Hanzawaia nipponica</i>
<i>Hayn sp.</i>	<i>Haynesina sp.</i>
<i>Noni ste</i>	<i>Nonionella stella</i>
<i>Para nip</i>	<i>Pararotalia nipponica</i>
<i>Quin akn</i>	<i>Quinqueloculina akneriana</i>
<i>Quin lam</i>	<i>Quinqueloculina lamarckiana</i>
<i>Quin sem</i>	<i>Quinqueloculina seminula</i>
<i>Quin sp.</i>	<i>Quinqueloculina sp.</i>
<i>Rota ann</i>	<i>Rotalinoides annectens</i>
<i>Spir luc</i>	<i>Spiroloculina lucida</i>

Appendix 5.5: Derivation and performance of alternative modern training sets

Two potential solutions to reducing the influence of the RMSEP s_2 component are proposed:

- Select a subset of samples, minimising the number of samples at any given mean salinity value (samples PE 6, 22, 26, 33, 37, 39, 40, 55, 57, 58, 62, 63, 66, 67, 72, 75, 78, 79, 81, 85, 87, 97, 100, 102 and 105)
- Combine assemblages from samples with similar mean salinities, forming a reduced number of assemblages with recalculated percentage values (c.f. Woodroffe, 2006)

Analysis of transfer function performance for solution a:

Name	r^2_{boot}	Average bias _{boot}	Max bias _{boot}	RMSE s_1	RMSE s_2	RMSEP
WA_Inv	0.76	-0.57	5.54	1.51	4.73	4.96
WA_Cla	0.77	-0.65	5.65	1.68	4.73	5.02
WATOL_Inv	0.76	-3.85	8.20	3.88	6.05	7.19
WATOL_Cla	0.77	-4.36	8.67	4.34	6.33	7.68
WA-PLS C1	0.76	-0.47	5.73	1.58	4.85	5.10
WA-PLS C2	0.80	-0.10	6.68	1.68	4.25	4.57
WA-PLS C3	0.82	-0.27	5.87	1.90	4.06	4.48
WA-PLS C4	0.83	-0.24	5.54	1.92	3.97	4.41
WA-PLS C5	0.83	-0.24	5.65	1.93	3.95	4.40

Analysis of transfer function performance for solution b:

Name	r^2_{boot}	Average bias _{boot}	Max bias _{boot}	RMSE s_1	RMSE s_2	RMSEP
WA_Inv	0.96	-1.00	4.23	1.32	2.63	2.94
WA_Cla	0.96	-1.04	3.85	1.32	2.47	2.80
WATOL_Inv	0.95	-3.30	7.49	2.32	4.53	5.08
WATOL_Cla	0.95	-3.46	7.55	2.41	4.45	5.07
WA-PLS C1	0.96	-0.83	4.51	1.47	2.84	3.20
WA-PLS C2	0.96	-0.52	4.01	1.31	2.41	2.75
WA-PLS C3	0.96	-0.53	3.61	1.32	2.38	2.72
WA-PLS C4	0.96	-0.54	3.47	1.33	2.35	2.70
WA-PLS C5	0.96	-0.53	3.44	1.33	2.34	2.69

Appendix 6.1: Summary statistics for dominant and common benthic foraminiferal taxa in samples from core UV1

Taxa	Number of occurrences	Maximum %	Depth with maximum %	Mean %	Number of samples >5%
<i>Ammonia beccarii</i>	83	65.5	8.77	39.0	82
<i>Cribronion subincertum</i>	66	16.3	9.45	2.2	8
<i>Elphidium hispidulum</i>	74	20.7	1.01	2.3	9
<i>Quinqueloculina akneriana</i>	82	41.0	8.37	14.7	67
<i>Quinqueloculina lamarckiana</i>	78	12.0	4.27	3.9	25
<i>Rotalinoides annectens</i>	76	41.7	1.01	3.0	8

Appendix 6.2: Relative abundance of fossil benthic foraminifera from core UV1

Depth	Total specimens	<i>Ammobaculites formosensis</i>	<i>Ammobaculites</i> sp.	<i>Ammotium salsum</i>	<i>Bigenerina nodosaria</i>	<i>Cellanthus craticulus</i>	<i>Haplophragmoides</i> sp.	<i>Sigmollina tenuis</i>	<i>Spirolectamina bifurcata</i>	<i>Textularia foliacea</i>	<i>Ammonia ariakensis</i>	<i>Ammonia beccarii</i>	<i>Ammonia equitoriana</i>	<i>Ammonia ketenziensis angulata</i>	<i>Amphicoryna scalaris</i>	<i>Astronionion</i> sp.	<i>Boilvina marginata</i>
0.35	300	2.67										54.33					
0.43	300	4.33					0.33					54.33		1			2.67
0.55	300	2.33		0.33		0.67	0.33	0.33				50.67		0.67		0.67	0.33
0.67	301	4.32	0.33	0.33		0.33	0.66	0.33		0.33	0.33	48.84		1			0.66
0.79	305	1.97	0.33			0.33	1.31				0.33	42.62		2.62			0.66
0.91	300	6.33	0.67				1	1			0.33	37		1.67			
1.01	300	5					1					3.33					
1.05	307	8.47	0.33	0.33		0.65	6.19					7.82		0.33			0.33
1.17	333	3.9				0.6	2.4					15.62		1.5			0.6
1.29	301					0.33	0.66					17.94		1.33			0.66
1.41	300							1.33				22		0.67			1.33
1.53	310							1.29				21.29		1.61			2.58
1.65	301			0.33		0.33		1.66				22.92		2.66			0.33
1.77	309					0.65	0.32	0.65				29.77		3.24			1.62
1.89	307			0.33		0.33		0.98				25.73		2.61			
2.03	303		0.33			0.33		1.32				30.36		2.64			0.66
2.15	315					0.95	0.32	0.63				33.97		1.27			0.32
2.27	301		0.33					0.33				26.91		1.99			0.33
2.39	306							1.63			0.65	24.84		1.31			
2.57	308					0.32	0.32	1.62				20.13		0.97			0.65
2.65	302	0.33	0.66			0.66	1.66	1.66		0.66		27.81		1.32			0.33
2.77	300		0.33		0.33		1	1.67				26		0.67			0.33
2.89	317		0.32					3.47				27.76		0.95			0.32
3.03	305							1.64				30.49					0.66
3.15	323							0.62				34.67		0.62			0.31
3.27	300							1				31		1.67			1.67
3.39	315							1.9				31.75		0.95			
3.57	321							1.87				42.99		0.93			0.31
3.65	348							1.15				35.34		0.29			
3.77	300											44.67					1.67
3.89	301							0.66				36.88		1			2.66
4.04	317							1.26				31.23		0.95			0.63
4.15	330							0.61		0.3		26.67		0.61			0.91
4.27	309							0.65				25.24		1.94			0.32
4.39	300		1					2				35.67					
4.57	311		0.32					1.61				49.2		1.29			
4.65	317		0.63									50.47		0.95			
4.77	362							0.83				47.24		0.28			
4.89	330		0.3					2.12				36.06		0.91			0.61
5.03	304							1.32				40.13		0.66			0.33
5.11	309		1.29					0.97				31.39		1.29			0.65
5.23	312							0.32				35.9		0.32			
5.35	309		0.65					0.97				33.66		1.29			0.65
5.47	300		1.33					1				38		1.33			
5.57	339		0.88			0.59		0.59				40.71		1.47			0.88
5.61	307					0.33		0.98			0.33	34.85		0.33		0.33	0.98
5.73	322		0.31			0.31						35.09		0.31			0.31
5.85	300							0.67				27.67		0.67			1.33
5.97	300		0.33			0.33	0.33	0.67				35.67		0.67			
6.29	327					0.31		0.61				29.36					0.92
6.41	316					0.32						34.18			0.32		0.63
6.57	305					0.33		0.33				40.98		0.33	0.33		1.31
6.65	300		0.33									51.67					0.67
6.77	310					0.32	0.32	0.32				55.81					1.29
6.89	300		0.33					1				47.33	0.33				2
7.01	319	0.31	0.31									50.16					
7.13	314							1.91				37.9					0.32
7.25	317							0.95				47.95					0.32
7.37	311					0.32		1.61				34.41					0.32
7.49	306	0.65						1.31				48.04					0.33
7.57	310							0.97				45.48					0.65
7.65	314							1.27				54.14					0.96
7.77	300							2.33				48.33					1
7.89	309							3.24				45.95					0.32
8.01	302							1.99				44.7		0.66			1.32
8.13	307							0.33				41.04					0.65
8.25	300							0.33				37		0.33			
8.37	300		0.33			0.33		0.33				33.33		0.33			
8.49	300							0.33				38.67		0.33			0.33
8.65	300							1				46.67					
8.77	301							0.33				65.45					
8.89	300		0.33			0.33		2				61.67					
9.01	300		0.33					0.67				62		0.33			0.67
9.09	301	0.33		0.33				1.66				58.47		1			
9.21	301		0.33					0.66				62.79		1.33			0.33
9.33	319	0.31										56.43		0.31			0.31
9.45	300		0.33					0.33				57.67		0.33			0.33
9.57	317	0.32					0.33	1.26				56.15		0.63			0.32
9.69	304		0.33			0.33		0.33				56.91		0.33			1.32
9.81	300									0.33		49		0.67			0.67
9.93	329					0.3		0.61				59.27					0.91
10.05	300							1	0.33			32.67					1
10.09	300							0.33				27	0.33	1			0.33

Appendix 6.2 (continued):

Depth	<i>Bolivina pseudoplicata</i>	<i>Bolivina pseudopunctata</i>	<i>Bolivina robusta</i>	<i>Bolivina spatulata</i>	<i>Bolivina striatula</i>	<i>Brizalina cancellaria</i>	<i>Buccella frigida</i>	<i>Bulimina elongata</i>	<i>Bulimina marginata</i>	<i>Buliminella elegantissima</i>	<i>Cassidulina cf. teretis</i>	<i>Cibicides lobatulus</i>	<i>Cibicides pseudoemgeria nus</i>	<i>Cibicides sp.</i>	<i>Cribronion subincertum</i>	<i>Dentalina spp.</i>	<i>Ephedium advenum</i>
0.35				3.67					0.33								2
0.43	0.67	5		1.67					2						0.33		2.67
0.55		0.67	1.33	5			0.67	2	1			1.33			1.67		4
0.67	0.33	1.33	2.33	3.99	1		2.33	1	1.33	1.66		1			1.99		4.98
0.79	0.66		3.61	1.97	0.66		1.97	2.62	1.31	3.61		0.33	0.33		1.97		2.95
0.91	0.33	1.67	1	2			2	0.67	0.67	2		0.33	0.67		1.33		7
1.01															0.33		2
1.05			0.65	0.65	0.33			0.33		0.65							5.54
1.17		0.9	0.3	1.8			2.4			0.9		0.3					4.8
1.29	0.33		1.33	2.99			2.66	0.66	0.33	0.33		0.33	0.66				4.98
1.41			1.33	2.33			3.67	0.33	0.33	2		0.67	0.67				3
1.53		1.29	0.97	2.58			4.19	1.29	0.32	0.65		0.32	0.97		6.45		7.1
1.65			1.33	4.32	1		1.33	0.66		0.66		0.66	0.33		3.32		5.65
1.77		0.32	1.94	6.47	0.32		0.65	0.32		0.97			0.65	0.97	4.21		6.8
1.89		0.33	0.33	2.28	0.33			0.33	0.33	0.98			1.3		3.26		6.51
2.03			0.66	1.98	0.66			0.33	1.98			0.66			1.98		3.3
2.15			1.59	5.08	1.27		0.32	0.63	1.27			0.63			2.22		4.44
2.27		1.66	1.99	2.99				0.66	1						2.33		5.65
2.39		0.65	1.31	0.65				0.98	0.65						1.96		6.54
2.57		0.32	0.65	1.62	1.95			0.32	1.62			0.32			0.65		5.19
2.65		0.66	0.99	2.65	0.66			0.33	0.99			0.33			2.32		1.99
2.77			1	2	0.33			0.33	0.33				1		1.33		4.33
2.89		0.32	0.63	2.21	1.58		0.32			0.95			0.32		1.89		4.42
3.03		0.33	0.66	1.31	0.33					1.64			0.33		0.33		8.2
3.15		0.62	1.55	3.72						0.93							7.12
3.27				1.67	0.33					1							6.33
3.39		0.32	1.9	1.59		0.32	0.32					0.32					3.49
3.57			0.62	2.49				0.62	0.31						0.31		3.74
3.65			1.44	1.72	0.29			0.29	0.29				0.29	0.29			4.89
3.77		0.33	2.33	3					0.33								4.33
3.89			1	4.32					0.33	1.33				0.33	0.33		4.32
4.04			0.63	2.21	0.63			0.32	0.63								3.15
4.15	0.3	0.61	1.52	2.73				0.3	0.3	0.3							3.33
4.27				0.97													4.53
4.39	0.67		0.33	0.67								0.32			0.32		7.67
4.57			0.32	0.96								0.32			2.25		5.14
4.65			0.63	1.58				0.32	1.26						2.21		5.68
4.77			0.83	1.38				0.28	0.28				0.28		3.59		4.97
4.89			0.61	1.52		0.3			0.3			0.91			0.91		3.03
5.03			0.66	2.96	0.33				0.33			0.66			1.32		4.28
5.11			0.65	1.62					0.65						0.65		5.5
5.23		0.64	0.32	2.24	0.64				0.32			0.32			1.92		6.73
5.35		0.32	0.65	1.29					0.65								6.8
5.47			1.33	2.33				0.67	0.67						2.33		7.67
5.57		0.29		1.77								0.29			2.06	0.29	4.42
5.61		0.65	0.33	0.33	0.33	0.33				0.33		0.65			1.86		1.95
5.73			0.31	1.24					0.31			0.31			1.86		1.86
5.85		0.33	1.33	0.67											1.33		3.33
5.97			0.33	2						0.33					0.33		2.33
6.29				0.61						0.31			0.31				3.67
6.41		0.32	0.63	0.63											0.95		4.43
6.57				1.31											2.3		3.93
6.65		0.33	0.67	1					0.33						0.67		3.33
6.77		0.32	0.97	2.26					0.32	0.32					0.97		4.84
6.89			0.67	2				0.33		1					1.67		5
7.01		0.31	0.63	2.82						0.31					1.25		2.19
7.13			0.64	0.64													5.1
7.25		0.32		1.89				0.32		0.63					1.89		1.89
7.37			0.96	2.25					0.32	0.32							3.54
7.49			0.65	1.31													5.88
7.57			0.32	0.97								0.32			0.65		3.55
7.65		0.32	0.32	0.96											3.18		2.87
7.77				1											1.67		3.33
7.89				2.27											1.94		5.5
8.01				1.32				0.33							1.32		4.3
8.13				1.3						0.33					3.26		1.95
8.25				0.67											1.67		1.33
8.37			0.33	1.33						0.33							1.33
8.49			0.33												3.67		2.67
8.65			0.67	1											2.67		1.33
8.77				1.33											1.66		2.99
8.89				1.67	0.33			0.33		0.33			0.33		2.33		3.67
9.01				1.33				0.67							1		4.33
9.09			0.33	1									0.33		3.99		1.99
9.21				2.33						0.33					6.98		1.66
9.33			1.25	2.82											7.52		2.51
9.45			1	2					0.33						16.33		2
9.57			0.32	0.32						0.32					10.09		2.52
9.69			0.66	1.64					0.33				0.33		7.57	0.33	2.3
9.81			0.67	1.33						0.33					6.67		2.67
9.93			0.3	1.52					1.22						9.42		1.82
10.05				1.67											4		2.33
10.09				1											3		5.33

Appendix 6.2 (continued):

Depth	Hanzawaia nipponica	Haynesina sp.	Heterolepa haldingeria	Hookinsina pacifica	Lagena acutirostrata	Lagena distoma	Lagena elongata	Lagena hispidula	Lagena hispida	Lagena perlucida	Lagena piscata	Lagena sp.	Lagena substriata	Lagena sulcata	Lagena wiesneri	Miliolinella circularis	Miliolinella sp.
0.35	0.33	4						1									
0.43	0.33	2						2									
0.55		5.33	0.33					1.33									
0.67		5.98		0.33				1.33		0.33							
0.79		4.59						1.31									
0.91		5						1.67		0.33							
1.01																	
1.05		1.95						0.33		0.33							
1.17		2.1						0.6		0.3						0.6	
1.29	1.33	1					0.33	1.99		0.33							
1.41		3.67						1.67		0.33	0.33						
1.53	1.29	7.1						4.84			0.32					0.32	
1.65	0.66	5.65		2.66				1.66		0.33	0.66				0.33		
1.77	0.32	4.85		2.59				2.59									
1.89		2.28		0.33				1.3									
2.03	0.33	6.27		2.64			0.33	1.65							0.33		
2.15	0.32	3.49		2.54				2.22	0.32								
2.27	0.33	4.65		2.99				2.99	0.33								
2.39		2.94		0.65				1.63			0.33						
2.57		1.3		1.3				2.6			0.32	0.32				0.33	
2.65	0.33	3.31		0.66				2.65									
2.77		3		1.33			0.67	1.67								0.33	
2.89		4.42		1.58				2.21			0.32						
3.03		2.95		1.64				0.98		0.66							
3.15		3.1		0.93				0.31		1.24	0.31						
3.27		1.33		1.33	0.33			1		1							
3.39		1.27		0.95				0.63		1.27						0.63	
3.57		2.8		1.56				2.49		1.25							
3.65	0.57	3.45		1.72				2.3		0.29							
3.77		7.67		3.33				2		2							
3.89		4.98		1.99				2.66									
4.04	0.32	3.15		3.15				1.89		0.95							
4.15		1.82		1.82				1.52		0.3							
4.27		2.27		0.97			0.97	0.32			0.32					0.32	
4.39	0.33	4		0.67				1.33		0.33							
4.57		1.61		1.93				1.29		0.32							
4.65	0.32	3.47		1.26				1.58		0.95							
4.77	0.28	2.49		2.49				0.55		0.28							
4.89		3.03		1.82				0.3		0.61							
5.03		2.3		1.32				1.64		0.33							
5.11		4.85		0.97				0.97		0.32							
5.23		2.56		0.64				0.96									
5.35		3.24		1.94			0.32	1.62		0.65							
5.47		3.33		0.67				1.67		1							
5.57		3.54		0.88				1.77		0.59	0.29						
5.61	0.33	1.3		0.98				0.65		0.33							
5.73		2.17		1.86			0.31	0.62	0.31	0.31							
5.85		1.33		1.67			0.33	2		0.33							
5.97		3.33		1.67		0.33	0.33	0.67		0.67		0.33				0.33	
6.29		1.22		1.22				1.22									
6.41		1.9		0.63				0.95		0.32						0.32	
6.57		2.3		2.3				1.31		0.66							
6.65	0.33	5		0.33				0.67		1.33							
6.77		3.55		1.94				1.29		0.32						0.65	
6.89		2.67		2.33				2.67		1							
7.01		1.88		2.51				2.82									
7.13		1.27		2.23			0.32	0.64								0.64	
7.25		1.89		1.58				0.63		0.32						0.32	
7.37		3.22		1.61				0.96									
7.49		2.61		1.31				0.98		0.65							
7.57		2.26		0.97				1.94				0.32					
7.65	0.32	4.14		1.91				2.55									
7.77		2.33		2.33				2									
7.89		1.62		0.97				0.97									
8.01		0.99		0.66				1.99				0.33				0.66	
8.13		2.28		2.61				2.28								0.33	
8.25		4.33		2				1.33		0.33						0.33	
8.37		1.67		0.33				0.67								0.67	
8.49		2.67		1.33				2				0.33				0.67	
8.65		4.33		2.33				2									0.33
8.77		2.33		1				1.66				0.33					
8.89		6		1.33				1.67		0.67							
9.01		5.33		2				2		0.33						1	
9.09	0.33	5.65		0.66			0.33	2.99		1.66						0.66	
9.21		2.33		2.33				1.99		0.33						0.66	
9.33		3.76		1.57			0.94	2.82		1.88						0.63	
9.45		4.67		3				3.33		1.33						0.67	
9.57		2.52		2.21			0.32	2.84		0.63						0.63	
9.69		2.63		2.63				2.96		1.32						0.66	
9.81	0.33	2.33		1.33				1		0.33							
9.93		4.26		4.56			0.3	3.34		2.13		0.61				0.3	
10.05		4.33		2				1.33		0.67						0.33	
10.09		3		0.33				1.33		0.33							

Appendix 6.2 (continued):

Depth	<i>Neoponides mira</i>	<i>Nonionella stella</i>	<i>Pararotalia nipponica</i>	<i>Planorbula mediterraneensis</i>	<i>Quinqueloculina akneriana</i>	<i>Quinqueloculina akneriana rotunda</i>	<i>Quinqueloculina bicostata</i>	<i>Quinqueloculina complanata</i>	<i>Quinqueloculina contorta</i>	<i>Quinqueloculina donghaiensis</i>	<i>Quinqueloculina elongata</i>	<i>Quinqueloculina granulocostata</i>	<i>Quinqueloculina amarkiana</i>	<i>Quinqueloculina poeyana</i>	<i>Quinqueloculina pseudoreticulata</i>	<i>Quinqueloculina sabulosa</i>	<i>Quinqueloculina seminula</i>
0.35		1			2.67	0.33					2.33						
0.43		2			1						2		2.33	0.67	0.33		
0.55	0.33	2			1.67	0.33					1.67		2				0.67
0.67	0.66	0.33		0.33	1						0.66		0.33				
0.79		0.98			2.95	0.33					1.97		1.64				1.97
0.91		0.33			2	1	0.67				2.33		1.67		0.33		2.33
1.01					10.67	0.67							5		1		2.33
1.05					8.79	0.98	0.33				0.33		6.84				3.58
1.17		0.9			12.31	1.5					1.5		3.6		0.3	1.2	4.5
1.29	0.33	0.66			13.95	0.66	1.99				4.98		4.98				1.66
1.41		0.67			13	0.67	2.33				4		6.33		0.33		3
1.53		0.97			2.58		0.97				3.55		0.97				1.61
1.65		1			8.97		1.33				1.66		4.98			0.66	3.32
1.77		1.94			2.27		1.62		1.62		1.62		1.29			0.32	1.29
1.89	0.65	1.3			14.01	0.33	0.98	0.33	0.65		2.61		9.45			0.98	3.26
2.03		0.33			9.24		1.65				0.99		7.59			1.65	4.95
2.15	0.32	1.59			10.16		2.86				0.95		3.81				1.9
2.27		0.33			13.62	0.33	3.32				2.33		5.32			1	0.66
2.39		0.33			14.71	0.33	1.96				0.98		5.56			2.29	1.63
2.57		1.3			21.43	0.32	3.57	0.32	0.32		2.6		6.49			2.6	0.65
2.65		1.99			14.57		2.32				1.99		2.65			1.32	2.65
2.77		1			19.33		3		0.33		4.67		3.67		0.33	1.67	2.33
2.89			0.32		18.3		1.89				3.15		3.47			0.95	2.84
3.03		0.66			15.74						1.97		3.93			1.64	2.3
3.15		0.62			8.98	0.31	0.93				2.48		6.19			1.55	2.48
3.27					15		0.67				2		5.33			1.33	4
3.39		0.32			18.73						2.86		9.52			1.27	3.49
3.57		0.31			12.46		0.31	0.31			2.8		2.8			0.62	0.62
3.65			0.29		18.39		0.57				1.44		4.02			0.86	2.3
3.77	0.33	0.67			6.33		0.33				1.33			0.33		0.33	1.67
3.89		0.33			14.62						1		2.33			0.33	2.99
4.04	0.32	0.63	0.32		21.45	0.32	0.63		0.32		0.63		3.47			0.95	4.73
4.15		1.21			21.52		0.3				2.12		9.7				9.39
4.27	0.32				25.89	0.32	0.32	0.32			1.29		11.97			0.65	6.15
4.39		0.33			15.33	0.33	2.33				1.33		6.67			0.33	2
4.57		0.32			9.97	0.32	1.93				0.32		3.86				3.54
4.65	0.32	1.26			12.3		1.58				1.26		2.21				0.95
4.77	0.28	0.55			9.67	0.28	1.1				1.93		4.42			0.55	2.76
4.89	0.3				23.94		1.52				0.91		5.15			0.61	5.15
5.03		0.33			18.75		1.64				1.32		4.61				3.95
5.11		0.32			19.09	0.65	1.29				0.65		7.12			0.32	3.56
5.23					24.68		0.96				2.56	0.32	5.13	0.32		0.64	1.28
5.35		0.65			22.65	0.97	2.27			0.32	0.97		4.53			0.65	2.91
5.47		0.33			15.67	0.67	1.33				1		3.33			0.67	0.67
5.57					14.75	0.29	1.47				2.06		3.54			0.29	2.36
5.61					25.41	0.98	1.3				2.93		6.19			0.65	5.54
5.73					27.64	0.31	0.31				3.11		6.21			0.62	2.8
5.85	0.33	0.33			36		1				1		5.67			0.33	1.33
5.97					28.67		1				1.33		7			0.67	2.33
6.29					38.23		0.92				3.06		5.5				2.45
6.41		0.32			26.58	0.32	0.32				3.16		7.91			0.32	1.58
6.57					19.67	0.66	0.98				1.31		5.25			0.33	1.97
6.65					12		1.33				1.67		3.67			0.33	2
6.77					7.74		0.97				1.94		1.94				1.29
6.89					11.33		0.67				1		3				1.33
7.01		0.31			11.91		0.31				3.76		3.76				1.57
7.13		0.32			26.11		0.64				1.91		4.78				3.5
7.25		0.63			22.71		0.63				1.58		1.89				2.84
7.37		0.64			28.3	0.64	1.93				2.89		3.22				1.93
7.49		0.33			16.99		1.31				1.31		2.29				0.65
7.57		0.32			25.81		0.65				1.29		2.26			0.65	0.32
7.65		0.64			11.78		0.96				0.96		1.91			0.32	0.96
7.77		0.67			18.33	0.67					1		2.67			0.33	1.33
7.89		0.32			17.48	0.32	1.94				0.65		2.27				1.29
8.01		0.66			11.59		2.32				2.32		1.32			0.33	0.66
8.13	0.33				24.76		0.65				1.3		2.93			0.33	3.26
8.25					28	0.33	1				1.33		5.33				5
8.37		0.33			41		1				1.33		4				4.33
8.49		0.67			26.67		1.33				1.67		4.67				2
8.65					19.33		1				1.67		4			0.33	1.67
8.77		0.66			6.64		1				1.33		1.33				0.33
8.89		0.33			4.67		1				1.33						0.67
9.01					2.67		1.67				0.67		1		0.33		1.33
9.09		0.66			3.65		1						1.99				1
9.21		0.66			1.33		0.66				0.66		0.33				0.33
9.33					2.19		1.57				0.63		0.94				0.63
9.45		0.33					0.33										
9.57		0.32			6.62		0.95				0.32		1.26			0.32	0.63
9.69		0.66			1.32		1.97				0.99						
9.81	0.33	0.33			10.67	1	1.67				0.33		3.33				1.33
9.93		0.3			0.3		0.91										
10.05		0.33			12.67	1.33	1				1.67		3.33				2.67
10.09		0.67			21.33	1	0.67						4.33		0.67		4.67

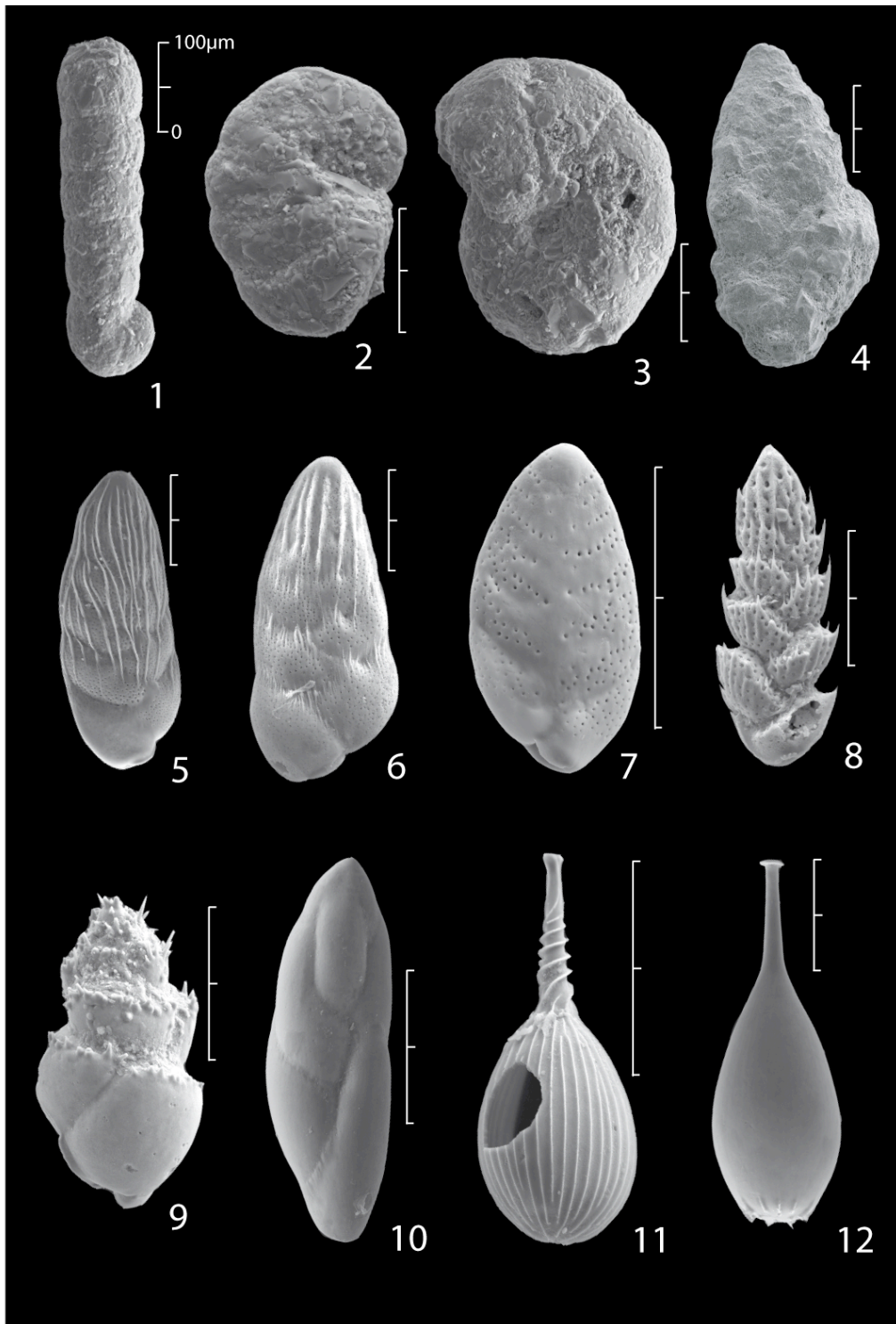
Appendix 6.2 (continued):

Depth	Quinqueloculina sp.	Quinqueloculina stalkerii	Quinqueloculina tiktoensis	Quinqueloculina venusta	Rosalina globularis	Rotalinoides ammetens	Spirillina sp.	Spiroloculina acescata	Spiroloculina communis	Spiroloculina laevigata	Spiroloculina lucida	Stainforthia complanata	Triloculina tricarinata	Triloculina trigonula	Unident.	Planktic foraminifera
0.35	2.33	1				0.33	0.33									
0.43					0.67		0.33									
0.55	0.33	1.33			0.33								0.33			0.33
0.67				0.33		0.33								0.33	0.66	1
0.79	1.64	0.98				0.33				0.33	0.33		0.33			0.66
0.91	0.67	2				3				0.33	0.33					0.67
1.01		1.33				41.67				1						
1.05		2.28	0.33			23.78				1.63	1.3					0.33
1.17		4.2				11.41	0.3			0.6	0.3		0.3			
1.29		1.99				8.64				0.66	0.66					1
1.41		2			0.33	2.67				0.67						0.33
1.53	0.97	1.61				2.58										0.97
1.65		2.66				1.99					0.33					1
1.77		1.29				2.27										2.59
1.89	0.33	1.63				1.3				0.33						0.65
2.03	1.32	0.99				1.65			0.66	0.33						0.99
2.15	0.63	0.32				0.95				0.32						
2.27	1	2.33				2.99			0.33		0.33					0.33
2.39	0.65	1.63				5.88										0.65
2.57	0.97	1.3		0.32		2.6				0.65						0.32
2.65	0.66	1.99				1.66		0.33		0.99						1.66
2.77	2.67	2		0.67		1.33										1
2.89	0.95	1.89	0.32	0.32		2.21	0.32								0.32	2.21
3.03		1.64	0.33	0.33		1.31				0.33			1.31	0.66		0.33
3.15	0.31	1.24		0.31		2.17					0.62			0.93	0.31	0.93
3.27	0.67	1.33				4.33				0.33	1		0.33	1	0.33	0.33
3.39	0.63	0.95	0.32			2.54								0.63		0.63
3.57	1.56	1.25		0.31		1.25			0.31			0.31		0.31	0.31	1.87
3.65	1.15	2.3	0.29			0.57					0.86		0.57	0.29		0.86
3.77	0.33	1				1					0.33			0.33		2.67
3.89	1.66	1.33	0.66							0.66				0.66		0.33
4.04	1.26	1.58				0.63	0.32				0.63		0.32	0.95		0.63
4.15	0.61	0.3				1.21								0.3		0.3
4.27	0.32	1.29				0.97			0.32		0.65		0.97			0.32
4.39	0.67	1.33												0.33		1
4.57	0.32	0.64				1.61	0.32				0.32			0.32		
4.65		0.95				0.32						0.32				
4.77						1.38				0.55						0.55
4.89	0.91							0.3		0.91						1.21
5.03		0.66				1.64				0.33						0.33
5.11		0.97				2.27				0.32						0.65
5.23		0.64				1.28				0.64	0.64					0.96
5.35	0.65					0.65				1.29						0.32
5.47						1				0.67			0.33			0.33
5.57	0.29	0.88		0.29		1.47				0.29	0.29					0.88
5.61	0.33	0.65		0.65						0.65						
5.73	0.31	0.31				1.55	0.31			0.93	0.93					
5.85						1.33				2						1
5.97						0.67				1.67				0.67		0.33
6.29		0.31				1.83				1.22						
6.41		0.32				2.53				1.27					0.32	0.63
6.57		0.66				1.31				0.98						0.33
6.65		0.33				2				0.67						0.33
6.77						2.26										0.97
6.89						2.67										0.33
7.01		0.63				0.94				0.63	0.63		0.31			
7.13		0.32				1.59	0.64			0.96			0.32			0.96
7.25		0.63				1.89	0.32								0.32	
7.37						0.96				1.61					0.64	
7.49						4.25				0.33						
7.57						3.23					0.32		0.32			0.65
7.65						3.18				0.32						0.64
7.77						4				0.33						0.67
7.89						4.53			0.32	0.65						
8.01						9.27				1.32						0.66
8.13		0.33				2.61				1.63	0.33		0.33			
8.25						3.33				1.33				0.67		0.33
8.37						2				1.33	0.33					
8.49		0.33				2				1	0.33		0.33	0.33		1
8.65		0.67				2.33				0.67						1
8.77		0.66				2.33				0.66	0.66					
8.89		0.67				2.33										0.67
9.01		1				1.33				0.67	0.33					0.33
9.09		1				1										1
9.21		0.66				1.99					0.33					1
9.33		0.94				2.19									0.31	1.25
9.45		0.33														0.33
9.57		0.95				0.95										1.26
9.69		0.33				2.3					0.33				0.33	0.66
9.81		1				3.67				0.67						0.67
9.93		0.61				1.52										1.82
10.05		1				14.67							0.33	0.33	0.33	0.33
10.09		0.33				8.33				0.67			2.33		0.33	

Plates

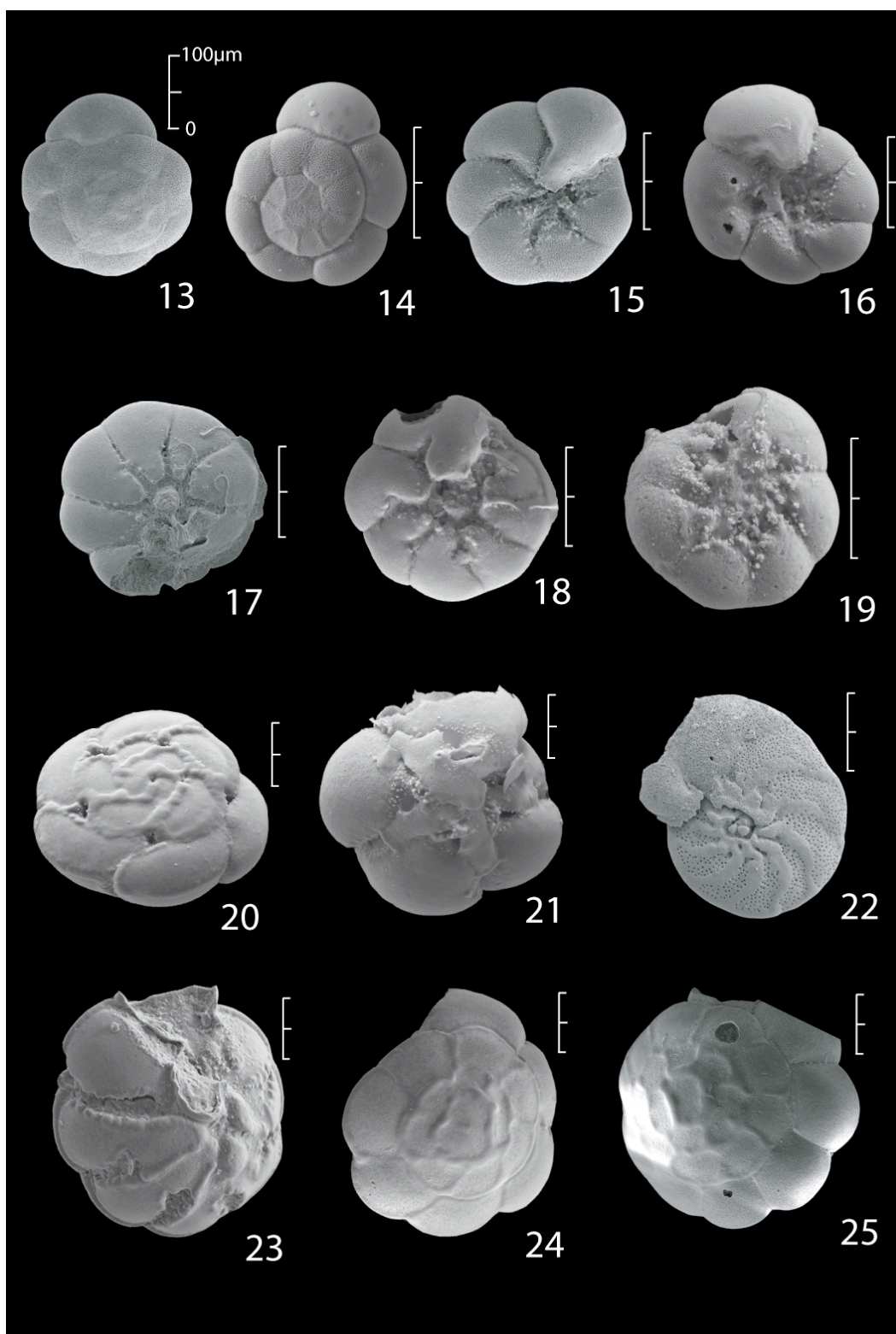
The following plates have been prepared using a Phillips XL30 environmental scanning electron microscope at magnifications of 80x to 800x. Specimens were gold coated and analysed in high vacuum mode with a secondary electron detector.

Plate 1



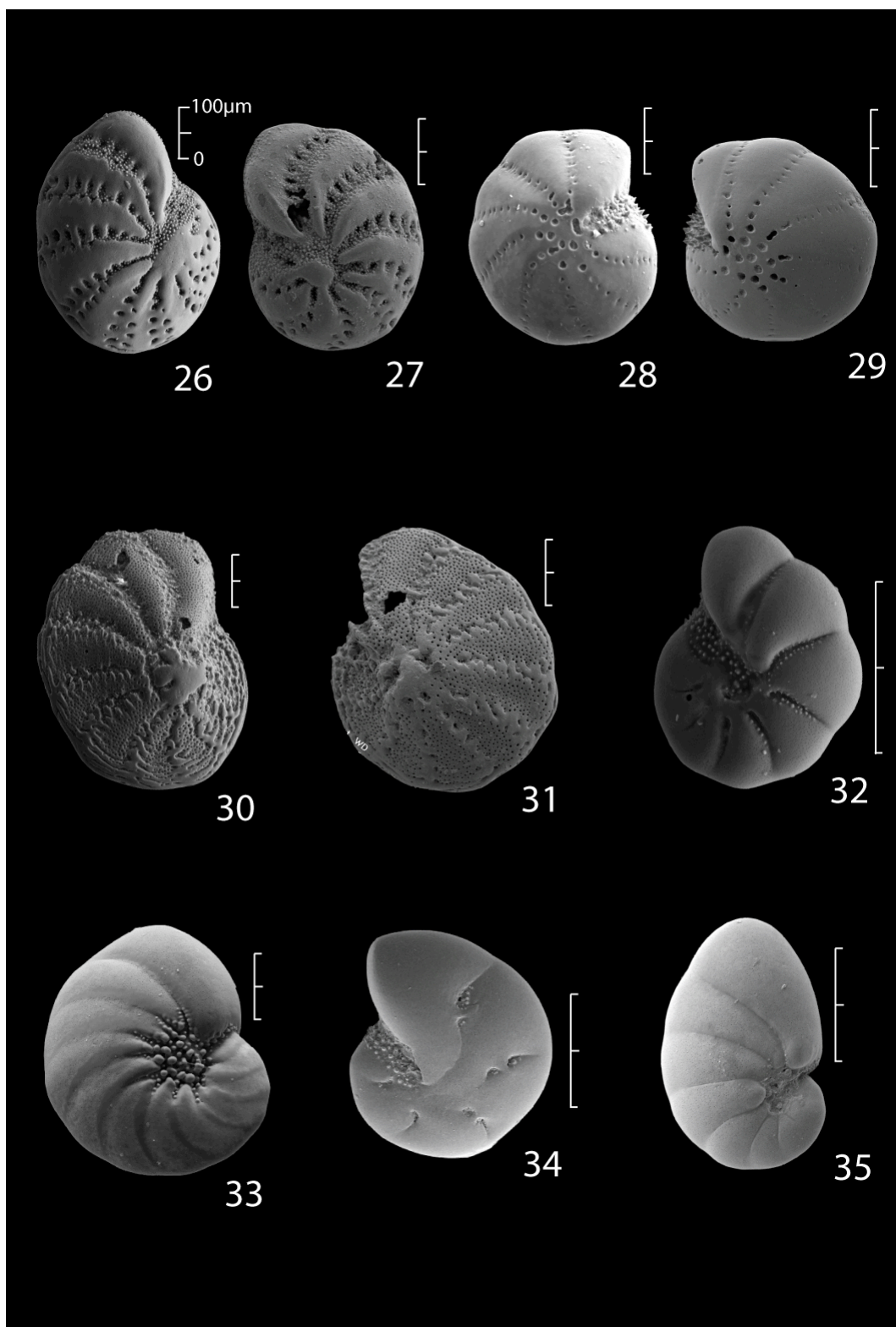
1. *Ammobaculites formosensis* Nakamura, 1937; 2. *Ammotium salsum* Cushman and Brönnimann, 1948; 3. *Haplophragmoides* spp.; 4. *Textularia foliacea* Heron-Allen & Earland, 1915; 5, 6. *Bolivina striatula* Lévi, 1957; 7. *Bolivina robusta* Brady, 1881; 8. *Brizalina* c.f. *canvallaria* Millet; 9. *Bulimina marginata* d'Orbigny, 1826; 10. *Fursenkoina compactiformis* McCulloch, 1977; 11. *Lagena substriata* Williamson, 1848; 12. *Lagena perlucida* Montagu, 1803

Plate 2



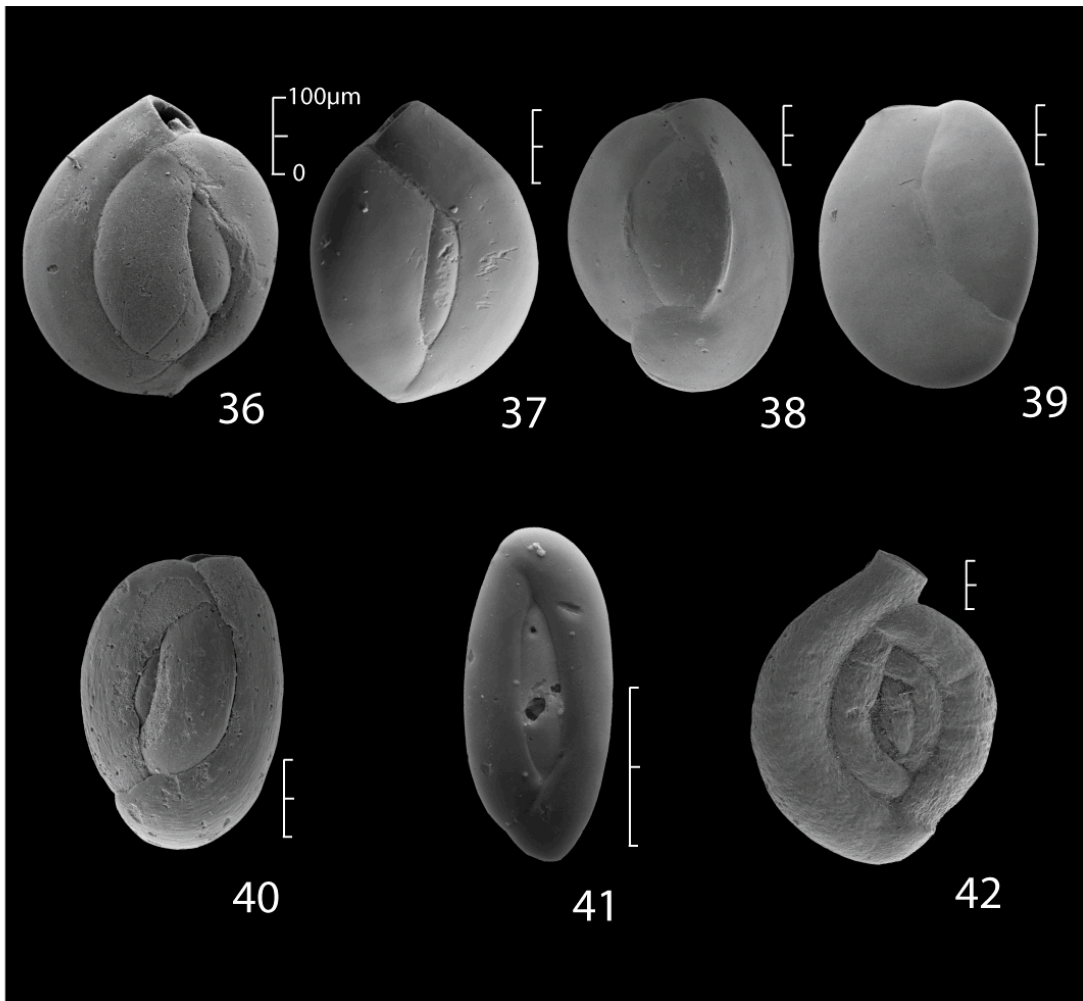
13. *Ammonia beccarii* Linné, 1758 c.f. morphotype T6 (Hayward *et al.*, 2004); **14.** *Ammonia beccarii* Linné, 1758; **15, 16.** *Ammonia beccarii* Linné, 1758 c.f. morphotype T6 (Hayward *et al.*, 2004); **17, 18.** *Ammonia beccarii* Linné, 1758 c.f. morphotype T4 (Hayward *et al.*, 2004); **19.** *Ammonia beccarii* Linné, 1758; **20, 21.** *Pararotalia nipponica* Asano, 1936; **22.** *Hanzawaia nipponica* Asano, 1944; **23, 24, 25.** *Rotalinoides annectens* Parker & Jones, 1865

Plate 3



26, 27. *Elphidium advenum* Cushman, 1922; **28, 29.** *Elphidium asiaticum* Polski, 1959; **30, 31.** *Elphidium hispidulum* Vacelet, Vasseur & Lévi, 1976; **32.** *Haynesina* sp.; **33.** *Florilus scaphus* Fichtel and Moll, 1798; **34.** *Cribrononion subincertum* Asano, 1950; **35.** *Nonionella stella* Cushman & Moyer, 1930

Plate 4



36, 37. *Quinqueloculina akneriana* d'Orbigny, 1846; **38, 39.** *Quinqueloculina lamarckiana* d'Orbigny, 1839; **40.** *Quinqueloculina seminula* Linné, 1758; **41.** *Quinqueloculina elongata* Natland, 1938; **42.** *Spiroloculina lucida* Cushman and Todd, 1944

References

- ALVE, E. & MURRAY, J. W. 1994. Ecology and taphonomy of benthic foraminifera in a temperate mesotidal inlet. *Journal of Foraminiferal Research*, 24, 18-27.
- AN, C. B., FENG, Z. D. & BARTON, L. 2006. Dry or humid? Mid-Holocene humidity changes in arid and semi-arid China. *Quaternary Science Reviews*, 25, 351-361.
- AN, Z., KUKLA, G., PORTER, S. & XIAO, J. 1991. Magnetic-susceptibility evidence of monsoon variation on the Loess Plateau of Central China during the last 13,000 years. *Quaternary Research*, 36, 29-36.
- AN, Z. S., PORTER, S., KUTZBACH, J., WU, X., WANG, S., LIU, X., LI, X. & ZHOU, W. 2000. Asynchronous Holocene optimum of the East Asian monsoon. *Quaternary Science Reviews*, 19, 743-762.
- AN, Z. S. 2000. The history and variability of the East Asian paleomonsoon climate. *Quaternary Science Reviews*, 19, 171-187.
- AN, Z. S. & XIAO, J. L. 1990. Study on the eolian dust flux over the Loess Plateau – an example. *Chinese Science Bulletin*, 35, 1627-1631.
- BAHR, A., WONG, H. K., YIM, W. W. S., HUANG, G., LUDMANN, T., CHAN, L. S. & THOMAS, W. N. R. 2005. Stratigraphy of Quaternary inner-shelf sediments in Tai O Bay, Hong Kong, based on ground-truthed seismic profiles. *Geo-Marine Letters*, 25, 20-33.
- BAKER, R. G. V., DAVIS, A. M., AITCHISON, J. C., FLOOD, P. G., MORTON, B. S. & HAWORTH, R. J. 2003. Comment on "Mid-Holocene higher sea level indicators from the south China coast" by W.W.-S. Yim and G. Huang. *Mar. Geol.* 182 (2002) 225-230 : a regional perspective. *Marine Geology*, 196, 91-98.
- BENDER, M. M. 1971. Variations in C-13/C-12 ratios of plants in relation to pathway of photosynthetic carbon dioxide fixation. *Phytochemistry*, 10, 1239

- BENZÉCRI, J.-P. 1973. *L'Analyse des Données. Volume II. L'Analyse des Correspondences*, Paris, Dunod.
- BERGER, A. 2009. Monsoon and general circulation system. *Chinese Science Bulletin*, 54, 1111-1112.
- BERGER, A. & LOUTRE, M. F. 1991. Insolation values for the climate of the last 10000000 years. *Quaternary Science Reviews*, 10, 297-317.
- BERKELEY, A., PERRY, C. T., SMITHERS, S. G., HORTON, B. P. & TAYLOR, K. G. 2007. A review of the ecological and taphonomic controls on foraminiferal assemblage development in intertidal environments. *Earth-Science Reviews*, 83, 205-230.
- BIRD, M. I., FIFIELD, L. K., TEH, T. S., CHANG, C. H., SHIRLAW, N. & LAMBECK, K. 2007. An inflection in the rate of early mid-Holocene eustatic sea-level rise: A new sea-level curve from Singapore. *Estuarine Coastal and Shelf Science*, 71, 523-536.
- BIRKS, H. J. B. 1995. Quantitative palaeoenvironmental reconstructions. In: MADDY, D. A. B., J.S. (ed.) *Statistical modelling of Quaternary science data*. Cambridge: Quaternary Research Association.
- BIRKS, H. J. B. 1998. D.G. Frey & E.S. Deevey review #1 - Numerical tools in palaeolimnology - Progress, potentialities, and problems. *Journal of Paleolimnology*, 20, 307-332.
- BLANCHON, P. & JONES, B. 1995. Marine-planation terraces on the shelf around Grand Cayman - a result of stepped Holocene sea-level rise. *Journal of Coastal Research*, 11, 1-33.
- BLANCHON, P., MOOSA, M. K., SOEMODIHARDJO, S., ROMIMOHTARTO, K., NONTJI, A., SOEKARNO & SUHARSONO 2002. Discovery of an early Holocene relict reef and shoreline off Grand Cayman. *Proceedings of the Ninth International Coral Reef Symposium, Bali, 23-27 October 2000. Volume 1.*, 223-229.
- BOND, G., KROMER, B., BEER, J., MUSCHELER, R., EVANS, M. N., SHOWERS, W., HOFFMANN, S., LOTTI-BOND, R., HAJDAS, I. & BONANI, G. 2001. Persistent solar influence on north Atlantic climate during the Holocene. *Science*, 294, 2130-2136.
- BRADY, H. B. 1884. Report on the Foraminifera dredged by H. M. S. 'Challenger' during the years 1873-76. *Voyage H. M. S. 'Challenger,' Zool.*, ix, 800 pp.
- BROECKER, W. S. 1994. Massive iceberg discharges as triggers for global climate-change. *Nature*, 372, 421-424.
- CAI, W., DAI, M., WANG, Y., ZHAI, W., HUANG, T., CHEN, S., ZHANG, F., CHEN, Z. & WANG, Z. 2004. The biogeochemistry of inorganic carbon and nutrients in the Pearl River estuary and the adjacent Northern South China Sea. *Continental Shelf Research*, 24, 1301-1319.
- CAI, W. J., GUO, X. H., CHEN, C. T. A., DAI, M. H., ZHANG, L. J., ZHAI, W. D., LOHRENZ, S. E., YIN, K. D., HARRISON, P. J. & WANG, Y. C. 2008. A comparative overview of weathering intensity and HCO₃⁻ flux in the world's major rivers with emphasis on the Changjiang, Huanghe, Zhujiang (Pearl) and Mississippi Rivers. *Continental Shelf Research*, 28, 1538-1549.
- CAI, Y. J., ZHANG, M. L., PENG, Z. C., LIN, Y. S., AN, Z. S., ZHANG, Z. F. & CAO, Y. N. 2001. The delta O-18 variation of a stalagmite from Qixing Cave, Guizhou Province and indicated climate change during the Holocene. *Chinese Science Bulletin*, 46, 1904-1908.
- CHAO, S. Y. 1998. Hyperpycnal and buoyant plumes from a sediment-laden river. *Journal of Geophysical Research-Oceans*, 103, 3067-3081.
- CHAO, W. C. & CHEN, B. 2001. The origin of monsoons. *Journal of the Atmospheric Sciences*, 58, 3497-3507.
- CHATFIELD, C. 1989. *The analysis of time series: an introduction*, London, Chapman and Hall.
- CHEN, C. T. A., LAN, H. C., LOU, J. Y. & CHEN, Y. C. 2003. The dry Holocene Megathermal in Inner Mongolia. *Palaeogeography Palaeoclimatology Palaeoecology*, 193, 181-200.
- CHEN, S. S., CHEN, L. F., LIU, Q. H., LI, X. & TAN, Q. Y. 2005. Remote sensing and GIS-based integrated analysis of coastal changes and their environmental impacts in Lingding Bay, Pearl River Estuary, South China. *Ocean & Coastal Management*, 48, 65-83.
- CHEN, X. H. & CHEN, Y. Q. D. 2004. Human-induced hydrological changes in the river network of the

- Pearl River Delta, South China. *GIS and Remote Sensing in Hydrology, Water Resources and Environment*, 289, 197-205.
- CHEN, Z. Y., SONG, B. P., WANG, Z. H. & CAI, Y. L. 2000. Late Quaternary evolution of the subaqueous Yangtze Delta, China: sedimentation, stratigraphy, palynology, and deformation. *Marine Geology*, 162, 423-441.
- CLIFT, P. D. & PLUMB, R.A. 2008. *The Asian Monsoon*, Cambridge, Cambridge University Press.
- COSFORD, J., QING, H. R., EGLINGTON, B., MATTEY, D., YUAN, D. X., ZHANG, M. L. & CHENG, H. 2008. East Asian monsoon variability since the Mid-Holocene recorded in a high-resolution, absolute-dated aragonite speleothem from eastern China. *Earth and Planetary Science Letters*, 275, 296-307.
- COSFORD, J., QING, H. R., MATTEY, D., EGLINGTON, B. & ZHANG, M. L. 2009. Climatic and local effects on stalagmite delta C-13 values at Lianhua Cave, China. *Palaeogeography Palaeoclimatology Palaeoecology*, 280, 235-244.
- CUI, J. X., ZHOU, S. Z. & CHANG, H. 2009. The Holocene warm-humid phases in the North China Plain as recorded by multi-proxy records. *Chinese Journal of Oceanology and Limnology*, 27, 147-161.
- DAI, S. B., YANG, S. L. & CAI, A. M. 2008. Impacts of dams on the sediment flux of the Pearl River, southern China. *Catena*, 76, 36-43.
- DALRYMPLE, R. W. 1992. Tidal depositional systems. In: WALKER, R. G. & JAMES, N.P. (eds.) *Facies models: Response to sea level change*. Canada: Geological Association of Canada.
- DAVIS, A. M., AITCHISON, J. C., FLOOD, P. G., MORTON, B. S., BAKER, R. G. V. & HAWORTH, R. J. 2000. Late Holocene higher sea-level indicators from the South China coast. *Marine Geology*, 171, 1-5.
- DIGGLE, P. J. 1990. *Time series: a biostatistical introduction*, Oxford, Oxford Science Publications.
- DING, Y. 2004. Seasonal march of the East-Asian summer monsoon. In: CHANG, C. P. (ed.) *East Asian Monsoon*. Singapore: World Scientific.
- DING, Z. L., RUTTER, N., HAN, J. T. & LIU, T. S. 1992. A coupled environmental system formed at about 2.5 ma in East-Asia. *Palaeogeography Palaeoclimatology Palaeoecology*, 94, 223-242.
- DIZ, P. & FRANCES, G. 2009. Postmortem processes affecting benthic foraminiferal assemblages in the Ria de Vigo, Spain: implications for paleoenvironmental studies. *Journal of Foraminiferal Research*, 39, 166-179.
- DODSON, J. R., TAYLOR, D., ONO, Y. & WANG, P. 2004. Climate, human, and natural systems of the PEP II transect. *Quaternary International*, 118, 3-12.
- DONG, L., SU, J., LI, Y., XIA, X. & GUAN, W. 2006. Physical processes and sediment dynamics in the Pearl River. *Environment in Asia Pacific Harbours*, 127-137.
- DONG, L., SU, J., WONG, L., CAO, Z. & CHEN, J. 2004. Seasonal variation and dynamics of the Pearl River plume. *Continental Shelf Research*, 24, 1761-1777.
- DUCHÉMIN, G., JORISSEN, F. J., ANDRIEUX-LOYER, F., LE LOC'H, F., HILY, C. & PHILIPPON, X. 2005. Living benthic foraminifera from "La Grande Vasière", French Atlantic continental shelf: Faunal composition and microhabitats. *Journal of Foraminiferal Research*, 35, 198-218.
- DYKOSKI, C. A., EDWARDS, R. L., CHENG, H., YUAN, D. X., CAI, Y. J., ZHANG, M. L., LIN, Y. S., QING, J. M., AN, Z. S. & REVENAUGH, J. 2005. A high-resolution, absolute-dated Holocene and deglacial Asian monsoon record from Dongge Cave, China. *Earth and Planetary Science Letters*, 233, 71-86.
- EDWARDS, R. J., WRIGHT, A. & VAN DE PLASSCHE, O. 2004. Surface distributions of salt-marsh foraminifera from Connecticut, USA: modern analogues for high-resolution sea level studies. *Marine Micropaleontology*, 51, 1-21.
- FATELA, F. 1994. *Contribution des Foraminifères benthiques profonds à la reconstitution des*

- paléoenvironnements du Quaternaire récent de la marge Ouest Ibérique (Marge Nord Portugaise, Banc de Galice)*. Doctorate thesis, Univsity of Bourdeaux.
- FATELA, F., MORENO, J., MORENO, F., ARAUJO, M. F., VALENTE, T., ANTUNES, C., TABORDA, R., ANDRADE, C. & DRAGO, T. 2009. Environmental constraints of foraminiferal assemblages distribution across a brackish tidal marsh (Caminha, NW Portugal). *Marine Micropaleontology*, 70, 70-88.
- FATELA, F. & TABORDA, R. 2002. Confidence limits of species proportions in microfossil assemblages. *Marine Micropaleontology*, 45, 169-174.
- FINKL, C. W. & KHALIL, S.M. 2005. Vibracore. In: SCHWARTZ, M. L. (ed.) *Encyclopedia of Coastal Science*. Netherlands: Springer.
- FLEITMANN, D., BURNS, S. J., MUDELSEE, M., NEFF, U., KRAMERS, J., MANGINI, A. & MATTER, A. 2003. Holocene forcing of the Indian monsoon recorded in a stalagmite from Southern Oman. *Science*, 300, 1737-1739.
- FU, C. B. 2003. Potential impacts of human-induced land cover change on East Asia monsoon. *Global and Planetary Change*, 37, 219-229.
- FYFE, J. A., SELBY, I. C., PLATER, A. J. & WRIGHT, M. R. 1999. Erosion and sedimentation associated with the last sea level rise offshore Hong Kong, South China Sea. *Quaternary International*, 55, 93-100.
- GALLOWAY, W. E. 1975. Process framework for describing the morphologic and stratigraphic evolution of deltaic depositional systems. In: BROUSSARD, M. L. *Deltas: models for exploration*. Houston: Houston Geological Society
- GASSE, F., JUGGINS, S. & KHELIFA, L. B. 1995. Diatom-based transfer-functions for inferring past hydrochemical characteristics of African lakes. *Palaeogeography Palaeoclimatology Palaeoecology*, 117, 31-54.
- GAUCH, H. G. & WHITAKE.RH 1972. Comparison of ordination techniques. *Ecology*, 53, 868
- GE, Q. S., WANG, S. W., WEN, X. Y., SHEN, C. M. & HAO, Z. X. 2007. Temperature and precipitation changes in China during the Holocene. *Advances in Atmospheric Sciences*, 24, 1024-1036.
- GIRAUDEL, J. L. & LEK, S. 2001. A comparison of self-organizing map algorithm and some conventional statistical methods for ecological community ordination. *Ecological Modelling*, 146, 329-339.
- GOLDSTEIN, S. T. & WATKINS, G. T. 1999. Taphonomy of salt marsh foraminifera: an example from coastal Georgia. *Palaeogeography Palaeoclimatology Palaeoecology*, 149, 103-114.
- GRIMM, E. C. 1987. CONISS – a FORTRAN-77 program for stratigraphically constrained cluster-analysis by the method of incremental sum of squares. *Computers & Geosciences*, 13, 13-35.
- GRIMM, E. C. 2004. TGView v.2.0.2.
- HAMILTON, S. & SHENNAN, I. 2005. Late Holocene relative sea-level changes and the earthquake deformation cycle around upper Cook Inlet, Alaska. *Quaternary Science Reviews*, 24, 1479-1498.
- HAMMER, O., HARPER, D. A. T. & RYAN, P. D. 2001. PAST: paleontological statistics software package for education and data analysis. *Palaeontologia Electronica*, 4, Unpaginated.
- HASLETT, S. K. 2001. The Palaeoenvironmental Implications of the Distribution of Intertidal Foraminifera in a Tropical Australian Estuary: a Reconnaissance Study. *Australian Geographical Studies*, 39, 67-74.
- HASSAN, G. S., ESPINOSA, M. A. & ISLA, F. I. 2009. Diatom-based inference model for paleosalinity reconstructions in estuaries along the northeastern coast of Argentina. *Palaeogeography Palaeoclimatology Palaeoecology*, 275, 77-91.
- HAUG, G. H., HUGHEN, K. A., SIGMAN, D. M., PETERSON, L. C. & ROHL, U. 2001. Southward migration of the intertropical convergence zone through the Holocene. *Science*, 293, 1304-1308.
- HAYWARD, B. W., HOLZMANN, M., GRENFELL, H. R., PAWLOWSKI, J. & TRIGGS, C. M. 2004.

- Morphological distinction of molecular types in *Ammonia* - towards a taxonomic revision of the world's most commonly misidentified foraminifera. *Marine Micropaleontology*, 50, 237-271.
- HILL, M. O. 1973. Diversity and evenness - unifying notation and its consequences. *Ecology*, 54, 427-432.
- HILL, M. O. & GAUCH, H. G. 1980. Detrended correspondence-analysis - an improved ordination technique. *Vegetatio*, 42, 47-58.
- HONG KONG ENVIRONMENTAL PROTECTION DEPARTMENT (HKEPD). 2007. <http://www.epd.gov.hk/epd/eindex.html> [Online]. [Accessed January 2009].
- HONG, Y. T., HONG, B., LIN, Q. H., SHIBATA, Y., HIROTA, M., ZHU, Y. X., LENG, X. T., WANG, Y., WANG, H. & YI, L. 2005. Inverse phase oscillations between the East Asian and Indian Ocean summer monsoons during the last 12,000 years and paleo-El Nino. *Earth and Planetary Science Letters*, 231, 337-346.
- HONG, Y. T., WANG, Z. G., JIANG, H. B., LIN, Q. H., HONG, B., ZHU, Y. X., WANG, Y., XU, L. S., LENG, X. T. & LI, H. D. 2001. A 6000-year record of changes in drought and precipitation in northeastern China based on a delta C-13 time series from peat cellulose. *Earth and Planetary Science Letters*, 185, 111-119.
- HORI, K., SAITO, Y., ZHAO, Q. H., CHENG, X. R., WANG, P. X., SATO, Y. & LI, C. X. 2001. Sedimentary facies and Holocene progradation rates of the Changjiang (Yangtze) delta, China. *Geomorphology*, 41, 233-248.
- HORTON, B. P. 1997. *Quantification of the indicative meaning of a range of Holocene sea-level index points from the Western North Sea*. Doctorate thesis, University of Durham.
- HORTON, B. P. 1999. The distribution of contemporary intertidal foraminifera at Cowpen Marsh, Tees Estuary, UK: implications for studies of Holocene sea-level changes. *Palaeogeography Palaeoclimatology Palaeoecology*, 149, 127-149.
- HORTON, B. P. & EDWARDS, R. J. 2005. The application of local and regional transfer functions to the reconstruction of Holocene sea levels, north Norfolk, England. *Holocene*, 15, 216-228.
- HORTON, B. P., EDWARDS, R. J. & LLOYD, J. M. 1999. A foraminiferal-based transfer function: Implications for sea-level studies. *Journal of Foraminiferal Research*, 29, 117-129.
- HORTON, B. P., LARCOMBE, P., WOODROFFE, S. A., WHITTAKER, J. E., WRIGHT, M. R. & WYNN, C. 2003. Contemporary foraminiferal distributions of a mangrove environment, Great Barrier Reef coastline, Australia: implications for sea-level reconstructions. *Marine Geology*, 198, 225-243.
- HORTON, B. P. & MURRAY, J. W. 2006. Patterns in cumulative increase in live and dead species from foraminiferal time series of Cowpen Marsh, Tees Estuary, UK: Implications for sea-level studies. *Marine Micropaleontology*, 58, 287-315.
- HU, C. Y., HENDERSON, G. M., HUANG, J. H., XIE, S., SUN, Y. & JOHNSON, K. R. 2008. Quantification of Holocene Asian monsoon rainfall from spatially separated cave records. *Earth and Planetary Science Letters*, 266, 221-232.
- HUANG, G. 2000. Holocene record of storms in sediments of the Pearl River estuary and vicinity. Doctorate thesis: University of Hong Kong.
- HUANG, G. & YIM, W. W. S. 1998. Holocene foraminiferal distribution in the Pearl River Estuary and vicinity. In: MORTON, B. (ed.) *3rd International Conference on the Marine Biology of the South China Sea*. Hong Kong: Hong Kong University Press.
- HUANG, R. H., ZHOU, L. T. & CHEN, W. 2003. The progresses of recent studies on the variabilities of the East Asian monsoon and their causes. *Advances in Atmospheric Sciences*, 20, 55-69.
- HUANG, Z., ZONG, Y. & ZHANG, W. 2004. Coastal inundation due to sea level rise in the Pearl River Delta, China. *Natural Hazards*, 33, 247-264.
- HUANG, Z., ZONG, Y., & HE, R. 1982. On the depositional facies of the Zhujiang (Pearl) Delta based on fossil diatoms. *Acta Oceanologica Sinica*, 7, 744-750 (In Chinese).
- HUANG, Z. & ZONG, Y. 1982. Grain size parameters and sedimentary facies of the Quaternary

- sequences in the Zhujiang (Pearl) Delta, China. *Tropical Geography*, 2, 82-90 (In Chinese).
- HUGHEN, K. A., BAILLIE, M. G. L., BARD, E., BECK, J. W., BERTRAND, C. J. H., BLACKWELL, P. G., BUCK, C. E., BURR, G. S., CUTLER, K. B., DAMON, P. E., EDWARDS, R. L., FAIRBANKS, R. G., FRIEDRICH, M., GUILDERSON, T. P., KROMER, B., MCCORMAC, G., MANNING, S., RAMSEY, C. B., REIMER, P. J., REIMER, R. W., REMMELE, S., SOUTHON, J. R., STUIVER, M., TALAMO, S., TAYLOR, F. W., VAN DER PLICHT, J. & WEYHENMEYER, C. E. 2004. Marine04 marine radiocarbon age calibration, 0-26 cal kyr BP. *Radiocarbon*, 46, 1059-1086.
- JACKSON, S. T. & WILLIAMS, J. W. 2004. Modern analogs in Quaternary paleoecology: Here today, gone yesterday, gone tomorrow? *Annual Review of Earth and Planetary Sciences*, 32, 495-537.
- JAVAUX, E. J. & SCOTT, D. B. 2003. Illustration of modern benthic foraminifera from Bermuda and remarks on distribution in other subtropical/tropical areas. *Palaeontologia Electronica*, 6, 1-29.
- JENNINGS, A. E., NELSON, A. R., SCOTT, D. B. & ARAVENA, J. C. 1995. Marsh foraminiferal assemblages in the Valdivia estuary, south-central Chile, relative to vascular plants and sea-level. *Journal of Coastal Research*, 11, 107-123.
- JIAN, Z. M., HUANG, B., KUHN, W. & LIN, H. L. 2001. Late quaternary upwelling intensity and east Asian monsoon forcing in the South China Sea. *Quaternary Research*, 55, 363-370.
- JIAN, Z. M., WANG, L. J., KIENAST, M., SARNTHEIN, M., KUHN, W., LIN, H. L. & WANG, P. X. 1999. Benthic foraminiferal paleoceanography of the South China Sea over the last 40,000 years. *Marine Geology*, 156, 159-186.
- JIANG, W. Y., GUO, Z. T., SUN, X. J., WU, H. B., CHU, G. Q., YUAN, B. Y., HATTE, C. & GUIOT, J. 2006. Reconstruction of climate and vegetation changes of Lake Bayanchagan (Inner Mongolia): Holocene variability of the East Asian monsoon. *Quaternary Research*, 65, 411-420.
- JONES, V. J. & BIRKS, H. J. B. 2004. Lake-sediment records of recent environmental change on Svalbard: results of diatom analysis. *Journal of Paleolimnology*, 31, 445-466.
- JONES, V. J. & JUGGINS, S. 1995. The construction of a diatom-based chlorophyll a transfer function and its application at three lakes on Signy Island (maritime Antarctic) subject to differing degrees of nutrient enrichment. *Freshwater Biology*, 34, 433-445.
- JUGGINS, S. 2003. C2 v.1.5.0.
- KIM, J. M. & KENNETT, J. P. 1998. Paleoenvironmental changes associated with the Holocene marine transgression, Yellow Sea (Hwanghae). *Marine Micropaleontology*, 34, 71-89.
- KIM, J. M. & KUCERA, M. 2000. Benthic foraminifer record of environmental changes in the Yellow Sea (Hwanghae) during the last 15,000 years. *Quaternary Science Reviews*, 19, 1067-1085.
- KONDOH, A., HARTO, A., ELEONORA, R. & KOJIRI, T. 2004. Hydrological regions in monsoon Asia. *Hydrological Processes*, 18, 3147-3158.
- KOVACH, W. L. 1995. Multivariate data analysis. In: MADDY, D. A. B., J.S. (ed.) *Statistical modelling of Quaternary science data*. Cambridge: Cambridge University Press.
- KUMAR, V. & MANIVANNAN, V. 2001. Benthic foraminiferal responses to bottom water characteristics in the Palk Bay, off Rameswaram, southeast coast of India. *Indian Journal of Marine Sciences*, 30, 173-179.
- LAMB, A. L., WILSON, G. P. & LENG, M. J. 2006. A review of coastal palaeoclimate and relative sea-level reconstructions using delta C-13 and C/N ratios in organic material. *Earth-Science Reviews*, 75, 29-57.
- LAU, K. M. & YANG, S. 1997. Climatology and interannual variability of the east Asian summer monsoon. *Advances in Atmospheric Sciences*, 14, 141-162.
- LAWS, R. A. 1983. Preparing strewn slides for quantitative microscopical analysis - a test using calibrated microspheres. *Micropaleontology*, 29, 60-65.

- LEE, E., CHASE, T. N. & RAJAGOPALAN, B. 2008. Highly improved predictive skill in the forecasting of the East Asian summer monsoon. *Water Resource Research*, 44.
- LEGENDRE, P. & LEGENDRE, L. 1998. *Numerical ecology*, Amsterdam, Elsevier.
- LEGRANDE, A. N. & SCHMIDT, G. A. 2009. Sources of Holocene variability of oxygen isotopes in paleoclimate archives. *Climate of the Past*, 5, 441-455.
- LEPŠ, J. & ŠMILAUER, P. 2003. *Multivariate analysis of ecological data using CANOCO*, Cambridge, Cambridge University Press.
- LI, C. C., LEI, Y. P., HE, W. & DAI, Z. J. 2001. Land-ocean interaction in modern delta formation and development: A case study of the Pearl River delta, China. *Science in China Series B-Chemistry*, 44, 63-71.
- LI, C. X., CHEN, G., YAO, M. & WANG, P. 1991. The influences of suspended-load on the sedimentation in the coastal zones and continental shelves of China. *Marine Geology*, 96, 341-352.
- LI, P., QIAO, P., ZHENG, H. FANG G. & HUANG, G. 1990. *The environmental evolution of the Pearl River Delta in the last 10,000 years*. China Ocean Press (In Chinese)
- LI, Q. Y. & YIM, W. W. S. 1988. Foraminiferal thanatocoenoses in surficial sea-floor sediments of Hong Kong. *Acta Micropalaeontologica Sinica*, 5, 221-236.
- LI, S. 1988. Distribution of agglutinated Foraminifera in bottom sediments of the Zhujiang River Estuary. *Oceanologia et Limnologia Sinica*, 19, 187-196.
- LI, X., WAI, O., LI, Y., COLES, B., RAMSEY, M. & THORNTON, I. 2000. Heavy metal distribution in sediment profiles of the Pearl River estuary, South China. *Applied Geochemistry*, 15, 567-581.
- LI, X. D., ZHU, Y. F. & QIAN, W. H. 2002. Spatiotemporal variations of summer rainfall over eastern China during 1880-1999. *Advances in Atmospheric Sciences*, 19, 1055-1068.
- LI, Z., SAITO, Y., MATSUMOTO, E., WANG, Y. J., TANABE, S. & VU, Q. L. 2006. Climate change and human impact on the Song Hong (Red River) Delta, Vietnam, during the Holocene. *Quaternary International*, 144, 4-28.
- LIEW, P. M., LEE, C. Y. & KUO, C. M. 2006. Holocene thermal optimal and climate variability of East Asian monsoon inferred from forest reconstruction of a subalpine pollen sequence, Taiwan. *Earth and Planetary Science Letters*, 250, 596-605.
- LIU, H., LIN, Z., QI, X., ZHANG, M. & ZHANG, Z. A. D., M. In press. Multiple analysis of variation of the East Asian Monsoon during the Holocene. *Quaternary International*. doi:10.1016/j.quaint.2009.02.017
- LIU, J. P., MILLIMAN, J. D., GAO, S. & CHENG, P. 2004. Holocene development of the Yellow River subaqueous delta, North Yellow Sea. *Marine Geology*, 209, 45-67.
- LIU, X. D. & YIN, Z. Y. 2002. Sensitivity of East Asian monsoon climate to the uplift of the Tibetan Plateau. *Palaeogeography Palaeoclimatology Palaeoecology*, 183, 223-245.
- LIU, X. Q., HERZSCHUH, U., SHEN, J., JIANG, Q. F. & XIAO, X. Y. 2008. Holocene environmental and climatic changes inferred from Wulungu Lake in northern Xinjiang, China. *Quaternary Research*, 70, 412-425.
- LO, C. P. 1996. Environmental impact on the development of agricultural technology in China: The case of the dike-pond ('jitang') system of integrated agriculture-aquaculture in the Zhujiang Delta of China. *Agriculture Ecosystems & Environment*, 60, 183-195.
- LOUBERE, P. & GARY, A. 1990. Taphonomic process and species microhabitats in the living to fossil assemblage transition of deeper water benthic foraminifera. *Palaios*, 5, 375-381.
- LOUBERE, P., GARY, A. & LAGOE, M. 1993. Sea-bed biogeochemistry and benthic foraminiferal bathymetric zonation on the slope of the northwest Gulf-of-Mexico. *Palaios*, 8, 439-449.
- LUDMANN, T., WONG, H. & WANG, P. 2001. Plio-Quaternary sedimentation processes and neotectonics of the northern continental margin of the South China Sea. *Marine Geology*, 172, 331-358.
- LUNT, D. J., FLECKER, R., VALDES, P. J., SALZMANN, U., GLADSTONE, R. & HAYWOOD, A. M. 2008. A

methodology for targeting palaeo proxy data acquisition: A case study for the terrestrial late Miocene. *Earth and Planetary Science Letters*, 271, 53-62.

- MAHER, B. A. 2008. Holocene variability of the East Asian summer monsoon from Chinese cave records: a re-assessment. *Holocene*, 18, 861-866.
- MAHER, B. A. & HU, M. Y. 2006. A high-resolution record of Holocene rainfall variations from the western Chinese Loess Plateau: antiphase behaviour of the African/Indian and East Asian summer monsoons. *Holocene*, 16, 309-319.
- MAHER, L. J. 1972. Nomograms for computing 0.95 confidence limits of pollen data. *Review of Palaeobotany and Palynology*, 13, 85-&.
- MALMGREN, B. A. & NORDLUND, U. 1997. Application of artificial neural networks to paleoceanographic data. *Palaeogeography Palaeoclimatology Palaeoecology*, 136, 359-373.
- MANLY, B. F. J. & CHOTKOWSKI, M. 2006. Two new methods for regime change analyses. *Archiv Fur Hydrobiologie*, 167, 593-607.
- MAO, Q. W., SHI, P., YIN, K. D., GAN, J. P. & QI, Y. Q. 2004. Tides and tidal currents in the Pearl River estuary. *Continental Shelf Research*, 24, 1797-1808.
- MARTIN, R. E. 1999. Taphonomy and temporal resolution of foraminiferal assemblages. In: GUPTA, B. K. S. *Modern Foraminifera*. Dordrecht: Kluwer Academic Publishers. 281-298.
- MASLIN, M. A. & BURNS, S. J. 2000. Reconstruction of the Amazon Basin effective moisture availability over the past 14,000 years. *Science*, 290, 2285.
- MILLIMAN, J. D. 1991. Flux and fate of fluvial sediment and water in coastal seas. *Ocean Margin Processes in Global Change*, 69-89.
- MILLIMAN, J. D. & MEADE, R. H. 1983. World-wide delivery of river sediment to the oceans. *Journal of Geology*, 91, 1-21.
- MINGRAM, J., SCHETTLER, G., NOWACZYK, N., LUO, X. J., LU, H. Y., LIU, J. Q. & NEGENDANK, J. F. W. 2004. The Huguang maar lake - a high-resolution record of palaeoenvironmental and palaeoclimatic changes over the last 78,000 years from South China. *Quaternary International*, 122, 85-107.
- MOSIMANN, J. E. 1965. Statistical methods for the pollen analyst: multinomial and negative multinomial techniques. In: KUMMEL, B. & RAUP., D. (ed.) *Handbook of Paleontological Techniques*. San Francisco: Freeman.
- MURRAY, J. W. 1991. *Ecology and palaeoecology of benthic Foraminifera*. New York: Longman Scientific & Technical
- MURRAY, J. W. 2000. The enigma of the continued use of total assemblages in ecological studies of benthic foraminifera. *Journal of Foraminiferal Research*, 30, 244-245.
- MURRAY, J. W. 2001. The niche of benthic foraminifera, critical thresholds and proxies. *Marine Micropaleontology*, 41, 1-7.
- MURRAY, J. W. 2006. *Ecology and applications of benthic foraminifera*. Cambridge: Cambridge University Press
- MURRAY, J. W. 2007. Biodiversity of living benthic foraminifera: How many species are there? *Marine Micropaleontology*, 64, 163-176.
- MURRAY, J. W. & ALVE, E. 1999. Natural dissolution of modern shallow water benthic foraminifera: taphonomic effects on the palaeoecological record. *Palaeogeography Palaeoclimatology Palaeoecology*, 146, 195-209.
- NEFF, U., BURNS, S. J., MANGINI, A., MUDELSEE, M., FLEITMANN, D. & MATTER, A. 2001. Strong coherence between solar variability and the monsoon in Oman between 9 and 6 kyr ago. *Nature*, 411, 290-293.
- NG, S. L. & SIN, F. S. 2003. A diatom model for inferring sea level change in the coastal waters of Hong Kong. *Journal of Paleolimnology*, 30, 427-440.

- OWEN, R. B. 2005. Modern fine-grained sedimentation - spatial variability and environmental controls on an inner pericontinental shelf, Hong Kong. *Marine Geology*, 214, 1-26.
- PATTERSON, R. T., GUILBAULT, J. P. & CLAGUE, J. J. 1999. Taphonomy of tidal marsh foraminifera: implications of surface sample thickness for high-resolution sea-level studies. *Palaeogeography Palaeoclimatology Palaeoecology*, 149, 199-211.
- PEARSON, K. 1901. On lines and planes of closest fit to systems of points in space. *Philosophical Magazine*, 6, 2, 559-572.
- PETIT, J. R., JOUZEL, J., RAYNAUD, D., BARKOV, N. I., BARNOLA, J. M., BASILE, I., BENDER, M., CHAPPELLAZ, J., DAVIS, M., DELAYGUE, G., DELMOTTE, M., KOTLYAKOV, V. M., LEGRAND, M., LIPENKOV, V. Y., LORIUS, C., PEPIN, L., RITZ, C., SALTZMAN, E. & STIEVENARD, M. 1999. Climate and atmospheric history of the past 420,000 years from the Vostok ice core, Antarctica. *Nature*, 399, 429-436.
- PHLEGER, F. B. 1960. Ecology and distribution of recent Foraminifera. *Ecology and distribution of recent Foraminifera.*, pp. viii, 297.
- PORTER, S. C. 2001. Chinese loess record of monsoon climate during the last glacial-interglacial cycle. *Earth-Science Reviews*, 54, 115-128.
- PORTER, S. C. & AN, Z. S. 1995. Correlation between climate events in the north-Atlantic and China during last glaciation. *Nature*, 375, 305-308.
- PORTER, S. C. & ZHOU, W. J. 2006. Synchronism of Holocene East Asian monsoon variations and North Atlantic drift-ice tracers. *Quaternary Research*, 65, 443-449.
- PRIESTLEY, M. B. 1981. *Spectral analysis and time series*. London: Academic Press.
- QIAN, W., KANG, H. S. & LEE, D. K. 2002. Distribution of seasonal rainfall in the East Asian monsoon region. *Theoretical and Applied Climatology*, 73, 151-168.
- RACCA, J. M. J., GREGORY-EAVES, I., PIENITZ, R. & PRAIRIE, Y. T. 2004. Tailoring palaeolimnological diatom-based transfer functions. *Canadian Journal of Fisheries and Aquatic Sciences*, 61, 2440-2454.
- RACCA, J. M. J. & PRAIRIE, Y. T. 2004. Apparent and real bias in numerical transfer functions in palaeolimnology. *Journal of Paleolimnology*, 31, 117-124.
- RAMAGE, C. S. *Monsoon meteorology*, New York, Academic Press.
- REIMER, P. J., BROWN, T. A. & REIMER, R. W. 2004. Discussion: Reporting and calibration of post-bomb C-14 data. *Radiocarbon*, 46, 1299-1304.
- ROSSI, V. & HORTON, B. P. 2009. The application of a subtidal foraminifera-based transfer function to reconstruct holocene paleobathymetry of the Po delta, northern Adriatic Sea. *Journal of Foraminiferal Research*, 39, 180-190.
- SAIDOVA, K. M. 2007. Benthic foraminiferal assemblages of the South China Sea. *Oceanology*, 47, 653-659.
- SAITO, Y. 2005. Characteristics and recent environmental changes of large river deltas in Asia. In: Proceedings of International Symposium on Long-term variations in the Coastal Environments and Ecosystems, 2005 Matsuyama, Japan. Ehime University.
- SAITO, Y., YANG, Z. S. & HORI, K. 2001. The Huanghe (Yellow River) and Changjiang (Yangtze River) deltas: a review on their characteristics, evolution and sediment discharge during the Holocene. *Geomorphology*, 41, 219-231.
- SALIEGE, J. F. & FONTES, J. C. 1984. Experimental-determination of isotopic fractionation of C-13 and C-14 during natural processes. *International Journal of Applied Radiation and Isotopes*, 35, 55-62.
- SCHAFFER, C. T. 2000. Monitoring nearshore marine environments using benthic foraminifera: Some protocols and pitfalls. *Micropaleontology*, 46, 161-169.

- SCOTT, D. B., TAKAYANAGI, Y., HASEGAWA, S. & SAITO, T. 2000. Illustration and taxonomic reevaluation of some Neogene foraminifera described from Japan. *Palaeontologia Electronica*, 3, Unpaginated.
- SCOTT, D. B. & MEDIOLI, F.S. 1986. Foraminifera as sea-level indicators. In: VAN DE PLASSCHE, O. (ed.) *Sea-Level Research: A Manual for the Collection and Evaluation of Data*. Norwich: Geo Books.
- SERANDREI-BARBERO, R., ALBANI, A. D. & BONARDI, M. 2004. Ancient and modern salt marshes in the Lagoon of Venice. *Palaeogeography Palaeoclimatology Palaeoecology*, 202, 229-244.
- SHI, Y. F., KONG, Z. Z., WANG, S. M., TANG, L. Y., WANG, F. B., YAO, T. D., ZHAO, X. T., ZHANG, P. Y. & SHI, S. H. 1994. The climatic fluctuation and important events of holocene megathermal in China. *Science in China Series B-Chemistry*, 37, 353-365.
- SIMPSON, G. L. 2007. Analogue methods in palaeoecology: Using the analogue package. *Journal of Statistical Software*, 22.
- STUIVER, M. & REIMER P.J. AND REIMER THE, R. 2005. CALIB v.5.10.
- SU, J. 2004. Overview of the South China Sea circulation and its influence on the coastal physical oceanography outside the Pearl River Estuary. *Continental Shelf Research*, 24, 1745-1760.
- TA, T. K. O., NGUYEN, V. L., TATEISHI, M., KOBAYASHI, I., TANABE, S. & SAITO, Y. 2002. Holocene delta evolution and sediment discharge of the Mekong River southern Vietnam. *Quaternary Science Reviews*, 21, 1807-1819.
- TAO, S. Y. & CHEN, L.X. 1987. A review of recent research on the East Asian summer monsoon in China. In: CHANG, C. P. & KRISHNAMURTI, T.N. (ed.) *Monsoon meteorology*. Oxford: Oxford University Press.
- TELFORD, R. J., ANDERSSON, C., BIRKS, H. J. B. & JUGGINS, S. 2004. Biases in the estimation of transfer function prediction errors. *Paleoceanography*, 19.
- TELFORD, R. J. & BIRKS, H. J. B. 2005. The secret assumption of transfer functions: problems with spatial autocorrelation in evaluating model performance. *Quaternary Science Reviews*, 24, 2173-2179.
- TER BRAAK, C. J. F. 1986. Canonical correspondence-analysis - a new eigenvector technique for multivariate direct gradient analysis. *Ecology*, 67, 1167-1179.
- TER BRAAK, C. J. F. 1987. *Unimodal models to relate species to environment*. Doctorate thesis, University of Wageningen.
- TER BRAAK, C. J. F. 1995. Nonlinear methods for multivariate statistical calibration and their use in paleoecology - a comparison of inverse (k-nearest neighbors, partial least-squares and weighted averaging partial least-squares) and classical approaches. *Chemometrics and Intelligent Laboratory Systems*, 28, 165-180.
- TER BRAAK, C. J. F. 1996. *Unimodal models to relate species to environment*, Wageningen, DLO-Agricultural Mathematics Group.
- TER BRAAK, C. J. F. 2006. CANOCO v.4.55.
- TER BRAAK, C. J. F., JUGGINS, S. & BIRKS, H. J. B. A. V., H. 1993. Weighted averaging partial least-squares regression (WA-PLS) - definition and comparison with other methods for species-environment calibration. *Multivariate Environmental Statistics*, 6, 525-560.
- TER BRAAK, C. J. F. & JUGGINS, S. 1993. Weighted averaging partial least-squares regression (WA-PLS) - an improved method for reconstructing environmental variables from species assemblages. *Hydrobiologia*, 269, 485-502.
- TER BRAAK, C. J. F. & ŠMILAUER, P. 2002. *CANOCO reference manual and CanoDraw for Windows users guide: software for Canonical Community Ordination (version 4.5)*, New York, Microcomputer Power.
- TOBIN, R., SCOTT, D. B., COLLINS, E. S. & MEDIOLI, F. S. 2005. Infaunal benthic foraminifera in some North American marshes and their influence on fossil assemblages. *Journal of Foraminiferal Research*, 35, 130-147.

- TRENBERTH, K. E., STEPANIAK, D. P. & CARON, J. M. 2000. The global monsoon as seen through the divergent atmospheric circulation. *Journal of Climate*, 13, 3969-3993.
- WALLER, H. O. 1960. Foraminiferal biofacies off the south china coast. *Journal of Paleontology*, 34, 1164-1182.
- WAN, S. M., LI, A. C., CLIFT, P. D. & JIANG, H. Y. 2006. Development of the East Asian summer monsoon: Evidence from the sediment record in the South China Sea since 8.5 Ma. *Palaeogeography Palaeoclimatology Palaeoecology*, 241, 139-159.
- WANG, B. & DING, Q. H. 2006. Changes in global monsoon precipitation over the past 56 years. *Geophysical Research Letters*, 33, L06711.
- WANG, B., WU, R. G. & LI, T. 2003. Atmosphere-warm ocean interaction and its impacts on Asian-Australian monsoon variation. *Journal of Climate*, 16, 1195-1211.
- WANG, L., SARNTHEIN, M., ERLLENKEUSER, H., GRIMALT, J. O., GROOTES, P., HEILIG, S., IVANOVA, E., KIENAST, M., PELEJERO, C. & PFLAUMANN, U. 1999a. East Asian monsoon climate during the Late Pleistocene: high-resolution sediment records from the south China Sea. *Marine Geology*, 156, 245-284.
- WANG, L. J., SARNTHEIN, M., ERLLENKEUSER, H., GROOTES, P. M., GRIMALT, J. O., PELEJERO, C. & LINCK, G. 1999b. Holocene variations in Asian monsoon moisture: a bidecadal sediment record from the South China Sea. *Geophysical Research Letters*, 26, 2889-2892.
- WANG, P. 1980. *Papers on Marine Micropaleontology*, Beijing, Ocean Press.
- WANG, P. 1985. *Marine Micropaleontology of China*, Beijing, Ocean Press.
- WANG, P. 1997. Marine micropaleontology in China - Introduction. *Marine Micropaleontology*, 32, 1-2.
- WANG, P. & BIAN, Y. 1985. Foraminifera and Ostracoda in bottom sediments of the Bohai Gulf and their bearing on Quaternary paleoenvironments. In: WANG, P. (ed.) *Marine micropaleontology of China*. 133-150.
- WANG, P., HONG, X. & ZHAO, Q. 1985a. Living Foraminifera and Ostracoda: distribution in the coastal area of the East China Sea and the Huanghai Sea. In: WANG, P. (ed.) *Marine Micropaleontology of China*.
- WANG, P., ISHIZAKI, K. & SAITO, T. 1992. Distribution of Foraminifera in estuarine deposits: a comparison between Asia, Europe and Australia. *Centenary of Japanese micropaleontology*, 71-83.
- WANG, P. & LIPPS, J. H. 2005. Micropaleontology of the South China Sea. *Marine Micropaleontology*, 54, 1-3.
- WANG, P., MIN, Q. & BIAN, Y. 1985b. Distribution of Foraminifera and Ostracoda in bottom sediments of the northwestern part of the south Huanghai (Yellow) Sea and its geological significance. In: WANG, P. (ed.) *Marine Micropaleontology of China*. Beijing: Ocean Press.
- WANG, P., MIN, Q., BIAN, Y. & HUA, D. 1985d. Characteristics of foraminiferal and ostracod thanatocoenoses from some Chinese estuaries and their geological significance. In: WANG, P. (ed.) *Marine Micropaleontology of China*. Beijing: Ocean Press.
- WANG, P. & MURRAY, J. W. 1983. The use of foraminifera as indicators of tidal effects in estuarine deposits. *Marine Geology*, 51, 239-250.
- WANG, P. & QIUBAO, M. & BIAN, Y. 1985c. Foraminiferal biofacies in the northern continental shelf of the South China Sea. In: WANG, P. (ed.) *Marine Micropaleontology of China*. Beijing: Ocean Press.
- WANG, P., ZHANG, J., ZHAO, Q., MIN, Q., BIAN, Y., ZHENG, L. & CHENG, X. A. C., R. 1988. *Foraminifera and Ostracoda in the bottom sediments of the East China Sea*, Unknown publisher.
- WANG, P. 2009. Global monsoon in a geological perspective. *Chinese Science Bulletin*, 54, 1113-1136.
- WANG, P., CLEMENS, S., BEAUFORT, L., BRACONNOT, P., GANSEN, G., JIAN, Z. M., KERSHAW, P. &

- SARNTHEIN, M. 2005a. Evolution and variability of the Asian monsoon system: state of the art and outstanding issues. *Quaternary Science Reviews*, 24, 595-629.
- WANG, Y., CHENG, H., EDWARDS, R., AN, Z., WU, J., SHEN, C. & DORALE, J. 2001. A high-resolution absolute-dated Late Pleistocene monsoon record from Hulu Cave, China. *SCIENCE*, 294, 2345-2348.
- WANG, Y., CHENG, H., EDWARDS, R. L., HE, Y. Q., KONG, X. G., AN, Z. S., WU, J. Y., KELLY, M. J., DYKOSKI, C. A. & LI, X. D. 2005b. The Holocene Asian monsoon: Links to solar changes and North Atlantic climate. *Science*, 308, 854-857.
- WANG, Y., CHENG, H., EDWARDS, R. L., KONG, X. G., SHAO, X. H., CHEN, S. T., WU, J. Y., JIANG, X. Y., WANG, X. F. & AN, Z. S. 2008. Millennial- and orbital-scale changes in the East Asian monsoon over the past 224,000 years. *Nature*, 451, 1090-1093.
- WEBSTER, P. J. 1987. The Elementary Monsoon. In: FEIN, J. S. A. S., P.L (ed.) *Monsoons*. Washington: Wiley and Sons.
- WEBSTER, P. J. 2006. The coupled monsoon system. In: WANG, B. (ed.) *The Asian Monsoon*. Netherlands: Springer.
- WEBSTER, P. J., MAGANA, V. O., PALMER, T. N., SHUKLA, J., TOMAS, R. A., YANAI, M. & YASUNARI, T. 1998. Monsoons: Processes, predictability, and the prospects for prediction. *Journal of Geophysical Research-Oceans*, 103, 14451-14510.
- WENG, Q. 2007. A historical perspective of river basin management in the Pearl River Delta of China. *Journal of Environmental Management*, 85, 1048-1062.
- WONG, L. A., CHEN, J., XUE, H., DONG, L. X., SU, J. L. & HEINKE, G. 2003. A model study of the circulation in the Pearl River Estuary (PRE) and its adjacent coastal waters: 1. Simulations and comparison with observations. *Journal of Geophysical Research-Oceans*, 108.
- WOODROFFE, S. A. 2006. *Holocene relative sea-level changes in Cleveland Bay, North Queensland, Australia*. Doctorate thesis, University of Durham.
- WOODROFFE, S. A. 2009. Recognising subtidal foraminiferal assemblages: implications for quantitative sea-level reconstructions using a foraminifera-based transfer function. *Journal of Quaternary Science*, 24, 215-223.
- WU, C. Y., REN, J., BAO, Y. & LEI, Y. P. A. S., H.Y. 2007. Long-term morphological modeling study on the evolution of the Pearl River Delta, network system, and estuarine bays since 6000 yr B.P. *Geological Society of America Special Paper*, 426, 199 - 214.
- XIANG, R., YANG, Z., SAITO, Y., FAN, D., CHEN, M. H., GUO, Z. & CHEN, Z. 2008. Paleoenvironmental changes during the last 8400 years in the southern Yellow Sea: Benthic foraminiferal and stable isotopic evidence. *Marine Micropaleontology*, 67, 104-119.
- XUE, C. T., ZHU, X. H. & LIN, H. M. 1995. Holocene sedimentary sequence, foraminifera and ostracoda in west coastal lowland of Bohai Sea, China. *Quaternary Science Reviews*, 14, 521-530.
- YANCHEVA, G., NOWACZYK, N. R., MINGRAM, J., DULSKI, P., SCHETTLER, G., NEGENDANK, J. F. W., LIU, J. Q., SIGMAN, D. M., PETERSON, L. C. & HAUG, G. H. 2007. Influence of the intertropical convergence zone on the East Asian monsoon. *Nature*, 445, 74-77.
- YANG, S. Y., YIM, W. W. S. & HUANG, G. Q. 2008. Geochemical composition of inner shelf quaternary sediments in the northern South China Sea with implications for provenance discrimination and paleoenvironmental reconstruction. *Global and Planetary Change*, 60, 207-221.
- YIM, W. W.-S. 1994. Offshore quaternary sediments and their engineering significance in Hong-Kong. *Engineering Geology*, 37, 31-50.
- YIM, W. W.-S. 1999. Radiocarbon dating and the reconstruction of late Quaternary sea-level changes in Hong Kong. *Quaternary International*, 55, 77-91.
- YIM, W. W.-S. 2001. Stratigraphy of quaternary offshore sand and gravel deposits in the Hong Kong SAR, China. *Quaternary International*, 82, 101-116.

- YIM, W. W.-S. & HE, X. X. 1988. Holocene Foraminifera in Hong Kong and their palaeoenvironmental significance. *Centre of Asian Studies Occasional Papers and Monographs*, 77, 787-809.
- YIM, W. W.-S., HILGERS, A., HUANG, G. & RADTKE, U. 2008. Stratigraphy and optically stimulated luminescence dating of subaerially exposed Quaternary deposits from two shallow bays in Hong Kong, China. *Quaternary International*, 183, 23-39.
- YIM, W. W.-S. & HUANG, G. 2002. Middle Holocene higher sea-level indicators from the south China coast. *Marine Geology*, 182, 225-230.
- YIM, W. W.-S., HUANG, G., FONTUGNE, M., HALE, R., PATERNE, M., PIRAZZOLI, P. & THOMAS, W. 2006. Postglacial sea-level changes in the northern South China Sea continental shelf: Evidence for a post-8200 calendar yr BP meltwater pulse. *Quaternary International*, 145, 55-67.
- YIM, W. W.-S., IVANOVICH, M. & YU, K. F. 1990. Young age bias of radiocarbon-dates in pre-Holocene marine deposits of Hong-Kong and implications for Pleistocene stratigraphy. *Geo-Marine Letters*, 10, 165-172.
- Yim, W. W.-S. & Tovey, N.K. 1995. Desiccation of inner continental shelf sediments during Quaternary low sea-level stands. *Geoscientist* 5/4, 34-35.
- YU, F. 2009. *Reconstruction of the East Asian monsoon variability since the mid-Holocene from the Pearl River estuary, southern China*. Doctorate thesis, Durham University.
- YUAN, D. X., CHENG, H., EDWARDS, R. L., DYKOSKI, C. A., KELLY, M. J., ZHANG, M. L., QING, J. M., LIN, Y. S., WANG, Y. J., WU, J. Y., DORALE, J. A., AN, Z. S. & CAI, Y. J. 2004. Timing, duration, and transitions of the Last Interglacial Asian Monsoon. *Science*, 304, 575-578.
- ZHANG, D. & LU, L. H. 2007. Anti-correlation of summer/winter monsoons? *Nature*, 450, E7-E8.
- ZHANG, J., YU, Z., WANG, J., REN, J., CHEN, H., XIONG, H., DONG, L. & XU, W. 1999. The subtropical Zhujiang (Pearl River) Estuary: Nutrient, trace species and their relationship to photosynthesis. *Estuarine Coastal and Shelf Science*, 49, 385-400.
- ZHANG, M. L., YUAN, D. X., LIN, Y. S., QIN, J. M., BIN, L., CHENG, H. & EDWARDS, R. L. 2004. A 6000-year high-resolution climatic record from a stalagmite in Xiangshui Cave, Guilin, China. *Holocene*, 14, 697-702.
- ZHANG, P. Z., CHENG, H., EDWARDS, R. L., CHEN, F. H., WANG, Y. J., YANG, X. L., LIU, J., TAN, M., WANG, X. F., LIU, J. H., AN, C. L., DAI, Z. B., ZHOU, J., ZHANG, D. Z., JIA, J. H., JIN, L. Y. & JOHNSON, K. R. 2008. A Test of Climate, Sun, and Culture Relationships from an 1810-Year Chinese Cave Record. *Science*, 322, 940-942.
- ZHANG, Q., XU, C. Y., ZHANG, Z., CHEN, Y. D. & LIU, C. L. 2009. Spatial and temporal variability of precipitation over China, 1951-2005. *Theoretical and Applied Climatology*, 95, 53-68.
- ZHANG, S., LU, X. X., HIGGITT, D. L., CHEN, C. T. A., HAN, J. T. & SUN, H. G. 2008. Recent changes of water discharge and sediment load in the Zhujiang (Pearl River) Basin, China. *Global and Planetary Change*, 60, 365-380.
- ZHAO, J. X., WANG, Y. J., COLLERSON, K. D. & GAGAN, M. K. 2003. Speleothem U-series dating of semi-synchronous climate oscillations during the last deglaciation. *Earth and Planetary Science Letters*, 216, 155-161.
- ZHENG, Z. 1998. Paleoenvironments in China during the Last Glacial Maximum and Holocene Optimum. *Episodes*, 21, 152-158.
- ZHOU, M., WU, C., LI, S., WANG, X. & LIU, Q. 2006. Geographical and economical setting of the Pearl River estuary. *Environment in Asia Pacific Harbours*, 113-125.
- ZHU, Z., DENG, Q., ZHOU, H., OUYANG, T., KUANG, Y., HUANG, N. & QIAO, Y. 2002. Water pollution and degradation in Pearl River Delta, South China. *Ambio*, 31, 226-230.
- ZONG, Y. 2004. Mid-Holocene sea-level highstand along the southeast coast of China. *Quaternary International*, 117, 55-67.
- ZONG, Y. & HORTON, B. P. 1999. Diatom-based tidal-level transfer functions as an aid in reconstructing Quaternary history of sea-level movements in the UK. *Journal of Quaternary*

- Science*, 14, 153-167.
- ZONG, Y., HUANG, G., SWITZER, A. D., YU, F. & YIM, W. W. S. 2009a. An evolutionary model for the Holocene formation of the Pearl River delta, China. *Holocene*, 19, 129-142.
- ZONG, Y., LLOYD, J., LENG, M., YIM, W. & HUANG, G. 2006. Reconstruction of Holocene monsoon history from the Pearl River Estuary, southern China, using diatoms and carbon isotope ratios. *Holocene*, 16, 251-263.
- ZONG, Y., YIM, W. W. S., YU, F. & HUANG, G. 2009b. Late Quaternary environmental changes in the Pearl River mouth region, China. *Quaternary International*, 206, 35-45.
- ZONG, Y., YU, F., HUANG, G., LLOYD, J. & YIM, W.W.-S. Submitted a. The history of water salinity in the Pearl River estuary, China, during the Late Quaternary. *Journal of Quaternary Science*.
- ZONG, Y., YU, F., LLOYD, J., HUANG, G. & YIM, W.W.-S. Submitted b. Diatoms in the Pearl River estuary, China and their suitability as water salinity indicators for coastal environments. *Marine Micropaleontology*.